FLOX/METHANE

PUMP-FED ENGINE STUDY

by

J. E. Colbert, S. A. Mosier, and T. E. Bailey

Prepared for

NATIONAL AERONAUTICS AND SPACE ADMINISTRATION

FINAL REPORT

FLOX/METHANE
PUMP-FED ENGINE STUDY

by

J. E. Colbert, S. A. Mosier, and T. E. Bailey

PRATT & WHITNEY AIRCRAFT
FLORIDA RESEARCH AND DEVELOPMENT CENTER
BOX 2691, WEST PALM BEACH, FLORIDA 33402

Prepared for

NATIONAL AERONAUTICS AND SPACE ADMINISTRATION

10 May 1969

Contract NAS3-7950

NASA Lewis Research Center
Cleveland, Ohio
L. H. Gordon, Project Manager
Liquid Rocket Technology Branch

FOREWORD

iii

ABSTRACT

An experimental program was conducted to demonstrate the feasibility of using the flox/methane propellant combination in a flight-type pump-fed rocket engine. Components from RL10A-1 oxygen/hydrogen engines were modified and the suitability of the modifications was verified in component tests; the program culminated with nine demonstration firings of the integrated engine system. The data acquired definitely established that a flight-qualified flox/methane engine can be developed using existing technology.

CONTENTS

ILLUSTRATIONS

ILLUSTRATIONS (Continued)

x

ILLUSTRATIONS (Continued)

ILLUSTRATIONS (Continued)

TABLES

SECTION I

SUMMARY

The flox/methane pump-fed engine study was conducted to demonstrate the feasibility of using the space-storable flox/methane propellant combination in pump-fed upper stage rocket engines. The objective was accomplished by conducting demonstration firings of a modified RL10A-1 oxygen/hydrogen engine; the RL10A-1 was the first production model of the RL10 engine and produced a nominal vacuum thrust of 15,000 lb$_f$ at a chamber pressure of 300 psia. RL10 oxygen/hydrogen engines utilize the expander cycle, i.e., the fuel vaporized in convectively cooling the thrust chamber is expanded through a turbine to provide driving energy for the pumps. Although the properties of methane as a working fluid do not approach those of hydrogen, its high specific heat and relatively low critical pressure make it a good convective coolant and turbine working fluid, and therefore it is well suited for use in this type of cycle.

One of the primary program constraints was that hardware modifications incorporated to permit operation of the engine with flox/methane be held to a minimum. Early cycle analyses based on this premise dictated that the operating chamber pressure of the flox/methane RL10 should be 250 psia, and component modifications were established accordingly. In the fuel system, modifications to the major components were required to compensate for the six-fold increase in density encountered in converting from hydrogen to methane. Oxidizer system modifications were limited initially to those changes required to achieve fluorine compatibility; however, engine testing experience showed a requirement for drastic changes to oxidizer control valve characteristics to provide acceptable system starting characteristics, and a significantly modified valve was incorporated.

Nine engine demonstration tests were conducted; during the first three tests, thrust chamber damage was encountered because of a starting transient problem. In the final build of the engine, major problems were overcome and six tests were conducted. Unfortunately, the partial failure of a turbine modification during the first of the six firings prevented the attainment of sustained operation at the 250-psia chamber pressure level. At the time of the failure, repair of the engine was not within the remaining scope of the program effort. Therefore, various control and orifice modifications were made to rebalance the cycle so that testing could be continued and the maximum possible amount of information could be obtained. A total of 120 seconds of engine operation was attained on the build, with 65 seconds of that time at chamber pressures above 200 psia. The good condition of the hardware following those tests produced a high degree of confidence that satisfactory operation at the 250-psia chamber pressure design point could have been achieved with correction to the turbine or further changes to the existing components to adjust the cycle balance.

1

Selected components were modified and/or tested in advance of the assembly of a complete engine system. During both component and engine testing, the only components with which durability problems were consistently encountered were the injector and thrust chamber. To approach the desired level of injector performance (a 95% characteristic exhaust velocity efficiency at the optimum mixture ratio of 5.75), it was necessary to use mechanical swirlers to promote oxidizer atomization and mixing. Because previous experience with swirlers in fluorine and flox had been poor, development of a configuration with adequate durability was necessary. Also, injectors modified to provide high performance were prone to rapid thermal erosion of the oxidizer element tips. This problem was completely eliminated by a more extensive modification of the RL10 injector than initially envisioned, substitution of a nickel oxidizer plate for the normal stainless steel plate. The final configuration was tested only in an engine system, and data were limited to low mixture ratios; however, extrapolation of the results indicates that the performance level at a mixture ratio of 5.75 would satisfy the target goal of 95% efficiency.

Problems encountered with the RL10 tubular wall thrust chamber were attributed to the large coolant passages, which were orginally designed for hydrogen. These large passages caused difficulties for two reasons: (1) the coolant velocities were low and (2) the internal tube volume was excessive. To increase coolant velocities in the critical heat transfer areas, blocking inserts were used to decrease the tube flow areas. The large internal volume of the tubes produced the severest operational problem encountered during the engine testing. Because of the quantity of methane that could accumulate in the tubes and the extreme density reduction that occurred with the initial rise in chamber pressure (heat flux), a transient interruption in the coolant flow occurred and subsequent chamber damage resulted. This was the starting transient problem referred to in the above summary of engine tests. The coolant flow interruption was ultimately overcome by incorporating chamber modifications that reduced the internal tube volume and by controls changes that reduced the rate of the chamber pressure increase. All of the other engine components operated essentially as predicted by the initial analyses, and no other problems of a continuing nature were encountered.

In summary then, the basic objective of the program was achieved, and in instances where major problems were encountered, they were due to the use of modified components. The modified units were at best a compromise from the optimum configuration. The data acquired during the engine firings definitely proved that the development of a flight-type pump-fed flox/methane engine is a practical goal and that all of the technology required is available, i.e.:

1. Oxidizer — Use of the existing fluorine design, materials, and handling procedures for the engine allowed the completion of the

2

program with minimal flox corrosion or burnout problems.

2. Fuel — No methane handling or material compatibility problems were encountered.

3. Turbopump — No turbopump problems were encountered that could be attributed to the propellant combination. The fuel-cooled bearings and gears were in perfect condition, proving that methane can be used as a gearbox coolant. This will simplify engine design by eliminating the need for a separate lubricant.

4. Expander Cycle — The expander cycle was shown to be well-suited to the propellants. The availability of sufficient starting power to provide a self-bootstrapping capability was demonstrated repeatedly.

SECTION II

INTRODUCTION

Technology investigations relative to the application of space-storable propellant combinations have been in progress for a number of years. In past efforts, attention has been directed primarily to the problems of pressure-fed engine systems operating at chamber pressures of approximately 100 psia. Pratt & Whitney Aircraft conducted experimental studies of the flox/light hydrocarbon fuel class of space storables for such systems under Contracts NAS3-4195, NAS3-6296, and NAS3-10294 (References 1, 2 and 3). The particular advantage of this class over systems using hydrazine or diborane is that the fuels can be used for active thrust chamber cooling to permit reliable long duration operation.

Recent studies of future space mission requirements have indicated an advantage for pump-fed space-storable engine systems operating at moderately high chamber pressures over pressure-fed systems. Some of the advantage is realized in terms of envelope. Figure 1 shows delivered specific impulse as a function of chamber pressure for a fixed thrust level flox/methane engine with the exit diameter held constant. As shown in figure 1, a gain of over 20 seconds in specific impulse is possible in the same envelope if pump-fed systems are used instead of pressure-fed systems. Figure 1 also includes a typical operating point for a pressure-fed earth-storable system for comparison. Flox/methane engines operating at pump-fed chamber pressure levels provide specific impulse performance levels over 100 seconds higher than pressure-fed earth-storable systems having the same envelope.
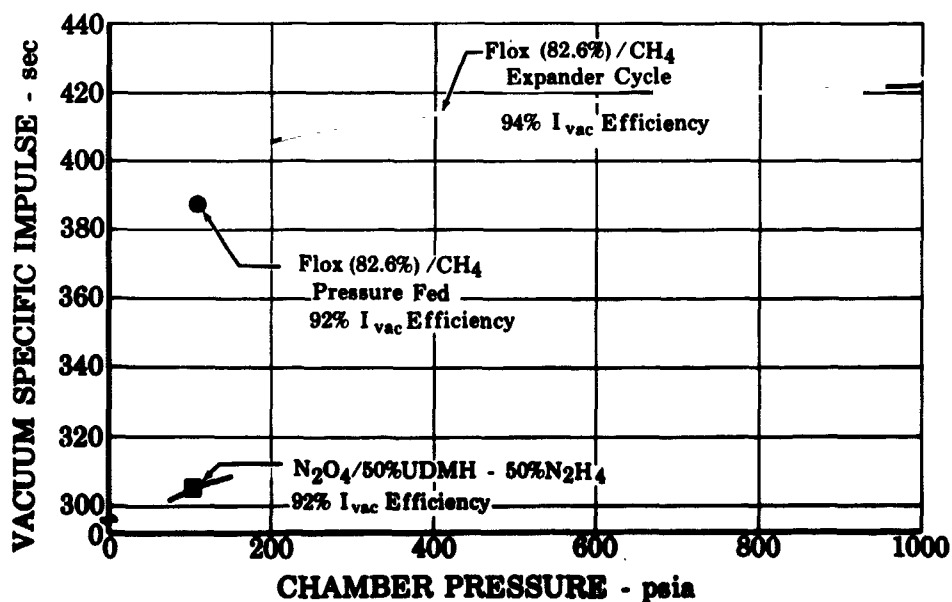
Figure 1. Delivered Performance — Constant Exit Diameter

FD 24524B

5

Methane is an attractive fuel for space-storab'e pump-fed engines because it is a good regenerative coolant and makes a good turbine working fluid. In combination with flox (82.6% fluorine and 17.4% oxygen), it has the highest theoretical impulse of the flox/light hydrocarbon propellants, and the liquid temperature range of the combination is high enough to be practical for long lerm space storage.

The flox/methane pump-fed engine study described herein was undertaken to demonstrate the feasibility of a flight-type pump-fed engine system using that propellant combination. To achieve the objective, an oxygen/hydrogen RL10A-1 engine was modified and tested with flox and methane. Use of the RL10A-1, the first production model of the RL10 engine, facilitated accomplishment of the program because delivered engines that had been replaced with later, higher performance models were made available for modification by the Government. Also, engines of the same model had been modified and tested successfully with fluorine/hydrogen in a propulsion system research program conducted under Contract NASw-754 (Reference 4). Oxidizer flow system components modified for fluorine compatibility under that program were also made available by the Government and were used essentially without change in the flox/methane engines.

Engine cycle studies conducted before the program was undertaken showed that because of fuel pump and turbine efficiency losses encountered when modifications were made to adjust for the extreme difference in density between hydrogen and methane, the engine would be power-limited to operation at a chamber pressure below its normal 300-psia design level. The studies indicated that at a mixture ratio of 5.75 (the theoretically optimum mixture ratio for flox and methane), an acceptable chamber pressure for the expander cycle engine with modified components would be 250 psia. Component and engine system modifications were therefore targeted for operation at that level. Important operating parameters predicted for the flox/methane engine are compared in Table I with those for the basic RL10A-1 engine and the fluorine/hydrogen modified engine tested under Contract NASw-754.

TABLE I.   RL10 ENGINE CONFIGURATIONS

	RL10A-1	Fluorine Demonstrator	Methane Demonstrator
Fuel	H_2	H_2	CH_4
Oxidizer	O_2	F_2	82.6% Flox
Mixture Ratio	5.0	5 to 13	5.75
Chamber Pressure - psia	300	300	250
Thrust — lb.	15,000	15,000	13,000

6

The results obtained in the experimental program are presented in the following sections of this report. Because the primary objective of the program was to demonstrate engine feasibility, engine system testing is described first (Section III), followed by discussion of the modification and/or tests of major subassemblies that were accomplished on the component level before an engine was assembled. The section numbers and headings under which the components are grouped are Section IV — "Injectors and Thrust Chamber," Section V — "Turbopump Modification and Test," and Section VI — "Valves and Controls." In those instances where component performance data were obtained in both component and engine testing, a discussion of all results is contained in the component section to facilitate analysis and comparison.

SECTION III

ENGINE FEASIBILITY DEMONSTRATION

A. GENERAL

As noted in the introduction, the approach taken to achieve the program objective of demonstrating the feasibility of a pump-fed engine using the space storable propellant combination of liquid flox (82.6% fluorine — 17.4% oxygen mixture) and liquid methane was to modify the flight qualified RL10 upper stage oxygen/hydrogen engine and to conduct demonstration firings of the modified system using those propellants.

An important requirement for the program was that only minimum modifications were to be made to components. Cycle studies completed before the program was undertaken indicated that this would be possible, and defined the nature of necessary changes. Methane is an excellent working fluid for cooling and for turbine power in the expander cycle; however, it is not as good as hydrogen in components sized for the lower density fuel and subjected to minimum modifications. As a result, the studies showed that with flox/methane the engine would be power limited at a chamber pressure of 250 psia, which would produce a thrust level of approximately 13,000 lb_f.

Modification and/or test of important components was accomplished in separate tasks preceding engine assembly and test. Before test engines were assembled initially, and as testing progressed, cycle performance calculations were repeated using estimated characteristics based on information from the experimental effort to establish final system trim requirements and control settings. The results of these analyses are presented in Appendix C.

In the first engine test, a serious transient coolant flow slowdown problem was discovered, but the engine bootstrapped, and indications that components were operating essentially as expected were obtained. Therefore, the system testing program was directed toward development of techniques to overcome the transient cooling problem. The necessary hardware and procedural changes were developed and satisfactory engine starts were demonstrated. Thus the feasibility of a flox/methane pump-fed engine was demonstrated. Extensive steady-state data at the predicted operating chamber pressure were not obtained because of program limitations, but the results were adequate to provide confidence that, if additional testing were possible within the scope of the program, target operating conditions could have been achieved.

B. ENGINE DESCRIPTION

1. BASIC ENGINE

The oxygen/hydrogen RL10A-1 engine has a vacuum thrust rating of 15,000 pounds at 300 psia chamber pressure. It operates at a nominal

oxygen/hydrogen mixture ratio of 5, and has a nozzle expansion ratio of 40. The engine uses an expander cycle in which a portion of the energy imparted to the fuel as it regeneratively cools the thrust chamber is utilized to drive the propellant pumps. The simplified propellant flow schematic presented in figure 2 shows the essential features of the cycle and identifies major engine components.
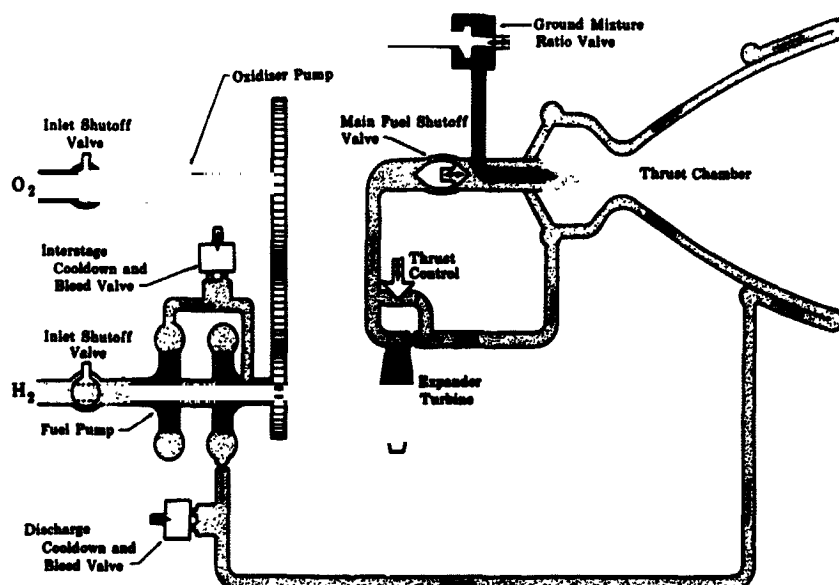
Figure 2. RL10A-1 Propellant Flow Schematic   **FD 8520A**

Fuel is supplied to the engine through an inlet shut-off valve mounted on the two-stage centrifugal fuel pump. Valves at the pump interstage and discharge provide for overboard discharge of fuel during cooldown and fuel bleed to prevent pump stall during acceleration. From the pump, fuel passes through the thrust chamber jacket where it is vaporized and heated; before reaching the injector it is expanded through a turbine which provides the turbopump driving power. Thrust is held constant by a feedback control that senses chamber pressure and regulates turbine bypass flow (and therefore turbopump speed) to maintain the pressure at the desired level.

The oxidizer flow path is through a ball type inlet valve, single-stage centrifugal pump, a flow control valve, and the injector, into the thrust chamber.

2. ENGINE MODIFICATION FOR FLOX/METHANE SERVICE

To adapt the RL10A-1 oxygen/hydrogen engine for operation with flox and methane as the propellants, changes to fuel system components were necessary to compensate for the higher density of methane as compared to hydrogen, and oxidizer components required modification to assure chemical compatibility with flox. Thrust chamber modifications were re-

10

quired for cooling with the more dense methane, and injector modifications were necessary for both performance and durability reasons.

RL10A-1 oxidizer flow system components, inlet valve, pump, and flow control valve, had been modified for compatibility with liquid fluorine in the hydrogen/fluorine propulsion system research program conducted under Contract NASw-754 (Reference 4) ; the modified parts were made available to the flox/methane engine study as Government-furnished equipment. Fuel component modifications were unique and were accomplished under the contract; assemblies that were changed were the pump, turbine, thrust control, injector, and thrust chamber.

In addition to the changes to major components, the engine system was modified by eliminating ignition system parts not required with the hypergolic propellant combination, and minor changes were made to permit alteration of sequencing. Changes in sequencing were largely established on the basis of experimental results as the program progressed and will be discussed later.

C. TEST HARDWARE

One basic engine assembly, designated S/N FX-153 in accordance with the experimental engine numbering system used at the Florida Research and Development Center, was used for the demonstration testing. Four separate builds of the engine were completed in the course of the effort. One modified fuel pump-turbine assembly and one set of major fuel valves were used, and the same oxidizer inlet shutoff valve was incorporated in all builds. However, thrust chambers, injectors, oxidizer pumps, and oxidizer flow control valves were changed between builds as shown in table II. Descriptions of the parts are given in the appropriate component section. Miscellaneous small components such as solenoid valves were obtained from the Government-furnished engines that served as sources for the major parts that were modified. These components were used following successful completion of functional checks to verify integrity and operation.

An operating schematic for the flox/methane RL10 engine is shown in figure 3; a pre-test photograph of the engine is presented in figure 4. The engine was operated as a completely integrated system. Control of starting transient and steady-state propellant scheduling, mixture ratio, and chamber pressure were accomplished entirely by engine system components. Where adjustments were made during test, remote electro-mechanical drives were used. Test firing events were sequenced by a digital sequencer which automatically programed electrical signals to the engine-mounted helium solenoid valves. Several control overrides were added to permit variation of the standard oxygen/hydrogen start and shutdown sequences without making hardware changes.

TABLE II. MAJOR COMPONENTS USED IN DEMONSTRATION ENGINE ASSEMBLIES

Engine Build No.	Oxidizer Pump Assembly	Thrust Chamber Assembly	Injector Assembly	Oxidizer Control Valve
1	C71Y002 Modified for chemical compatibility with flox	JP 97 Nozzle fins and 3-in. spiral chamber inserts	IP 764 Modified RL10A-1 part. Incorporated minimum (0.008-in.) fuel gaps - no outer row oxidizer swirlers	C51Y002 Modified for chemical compatibility with flox
2	C71Y002 Modified for chemical compatibility with flox	JP 88 Nozzle fins and 3-in. spiral chamber inserts	3K 2945 Modified RL10A-3 part. Incorporated nickel swirlers in all oxidizer injection elements	C51Y002 Modified for chemical compatibility with flox
3	C71Y001 Modified for chemical compatibility with flox	JP 42 Nozzle fins, 11-in. spiral chamber inserts, and silver-filled combustion chamber	AAF11-1 Modified RL10A-3 part. Incorporated a nickel spudplate with nickel swirlers in all oxidizer injection elements	C51Y002 Modified for chemical compatibility with flox
4	C71Y001 Modified for chemical compatibility with flox	JP 88 Nozzle fins, 11-in. chamber fins, and nickel-plated combustion chamber	AAF11-2 Cooling Holes added to outer periphery	C52Y001 Scheduled opening valve

Figure 3. Flox/Methane Engine Operating Schematic

FD 23765F.

13

Oxidizer Inlet Valve

Oxidizer Pump

Discharge
Cooldown Valve

Turbine Discharge

Fuel Inlet Valve

Fuel Pump

Interstage Cooldown
Valve

Thrust Control

Turbine Inlet
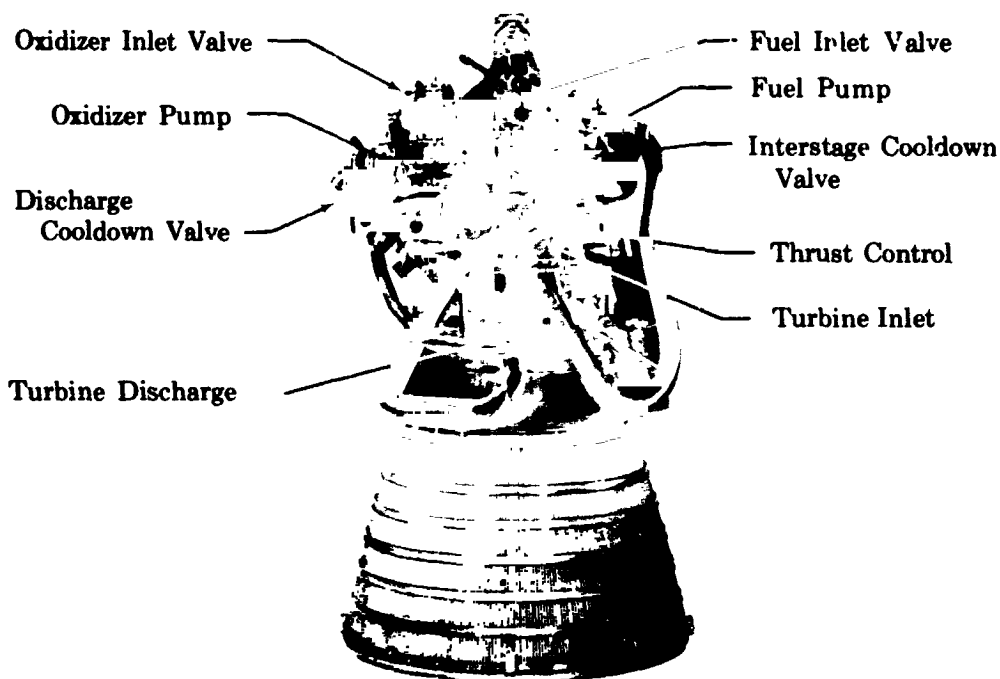
Figure 4. Pretest Photograph of Flox/Methane Engine FX-153, Build No. 3   FD 25709

D. TEST SUMMARY

Nine engine feasibility firings were made for an accumulated total time of 186 seconds. All of the tests were conducted under simulated altitude conditions in the 15,000 lb thrust firing bay of the Liquid Propellant Research Facility at the Florida Research and Development Center. A detailed description of the facility, its propellant supply system, altitude simulation system, and data acquisition system, is presented in Appendix A.

Individual tests are summarized in Appendix D. With only a few exceptions, major components performed as intended. The major development effort in the engine test program was directed to the solution of a system problem which resulted from the change in fuel density. The problem was one of a coolant flow reduction coincident with the rapid increase in chamber pressure that occurred when full oxidizer flow was initiated during the start transient. The typical result of the coolant slowdown was extensive thrust chamber tube damage. The loss of coolant also contributed to injector failures and made it difficult to assess component durability separately. Damage occurred in the initial firing attempt of each of the first three engine builds (tests No. E-1 through E-3), causing removal of the engine from the test stand for repair in each instance. Detailed review and interpretation of data made it possible to establish a combination of hardware and start sequence changes for the fourth build that proved reasonably successful and 6 tests (E-4 through E-9) were con-

ducted on that assembly. The fourth build was the final one that could be completed within the scope of the contract, so refinements could not be investigated and, because there was some deterioration of hardware, data could not be obtained over a complete range of steady-state operating conditions.

The causes of and solutions for the coolant flow reduction problem are described in the following discussion of engine operation. Because a knowledge of the sequence of events during engine start and operation is necessary to permit explanation, a description is provided as introduction. Component problems encountered are presented here as they affected system testing; more complete discussions of the problems on the component level and all discussion of component performance are presented in the appropriate component sections of the report, Section IV, V, or VI.

E. ENGINE OPERATION

1. OPERATING SEQUENCE

a. Engine Conditioning

Immediately prior to the engine start, a sequenced 35 second fuel preflow was used to temperature condition the fuel pump. The cooldown fuel was discharged through the normally open pump interstage and discharge cooldown valves.* The flox pump was pre-cooled with liquid nitrogen which was supplied at the pump inlet, flowed through the engine oxidizer system, and was discharged through the injector. Because the cooldown nitrogen was discharged into the chamber, a heated nitrogen purge was used to maintain the cooling jacket temperature at an acceptable level during the cooldown period. The purge through the jacket was in a direction opposite to the normal fuel flow. Temperatures approximately 200°R above ambient were maintained at the coolant outlet manifold and approximately ambient temperature was maintained at the coolant inlet manifold (purge outlet).

b. Engine Start

After engine conditioning, a sequenced electrical start signal opened solenoid valves to supply helium pressure to simultaneously (1) open the main fuel shutoff valve, (2) open the flox inlet valve, and (3) step the pump cooldown valves to an intermediate position.

When the main fuel shutoff valve opens, fuel enters the cooling jacket and is vaporized by the residual heat in the chamber. This supplies the power required to begin acceleration of the turbopump. During this period, a low flowrate of flox passes through the prechilled pump, through a bypass

* *Flow through the jacket is prevented by the normally closed main fuel shutoff valve during the prestart period.*

15

system in the oxidizer control valve, and into the combustion chamber. As the engine accelerates and a preset oxidizer pump differential pressure is attained, the oxidizer control valve opens to the flow area required for steady-state operation.

The intermediate position assumed by the fuel pump cooldown valves allows a relatively high fuel flowrate to be maintained during the pump acceleration period. This is required to prevent pump stall when the engine is operated with hydrogen. Normally, the fuel valves are closed by fuel pump discharge pressure when a given level is attained.

Prior to the first methane test, it was anticipated that the stall problem would not be severe with methane, and therefore a somewhat different sequencing of the cooldown valves might be used. During the initial cold flow tests, it was verified that fuel pump stall would not be encountered during the acceleration transient if the valves were fully closed, so the adjustment was made. To avoid the necessity of physical changes to the valves, an override helium pressure was provided to permit full closing of either one or both cooldown valves independent of the level of pump discharge pressure.

c. Steady-state Mixture Ratio and Thrust Control Adjustment

Engine thrust is regulated by the thrust control, and steady-state mixture ratio is controlled by adjusting the flow area of the oxidizer flow control valve. The adjustments for both valves are usually set and locked during ground acceptance test of delivery engines; however, to facilitate changes of engine operating point during test, remotely controlled electrical drives were provided on both components.

d. Engine Shutdown

Engine shutdown was programed with a lagging fuel flow so that jacket cooling would be maintained while the flox system was purged. At the sequenced shutdown signal the flox inlet valve closed and a gaseous helium purge was activated at the flox pump inlet. A separate gaseous helium purge was used for the injector oxidizer cavity; it was controlled by a check valve which closed as chamber pressure increased after start and opened automatically as chamber pressure decreased during shutdown.

The main fuel shutoff valve and fuel inlet valve were closed 1 second later than the oxidizer valve. When the flox flow was stopped during engine shutdown, the pump power requirement decreased approximately 25%. To prevent a sudden acceleration of the pump, a thrust control override was added. This consisted of a three-way solenoid operated valve in the thrust control servo supply line which could be used to vent the line and open the thrust control to maximize the turbine bypass flow. This vent system was energized at shutdown to prevent overspeed when flox flow was stopped.

16

2. EXPERIMENTAL TESTING

a. Build No. 1

The problem of coolant flow reduction during the starting transient was revealed in the first test, which was conducted primarily for facility checkout after the minor modifications necessary to accommodate the flox/ methane engine had been made. Details of the operating cycle for this initial build are given in Appendix C. As explained in Appendix C and in Section V, cold flow tests conducted before the first firing revealed that the fuel pump head coefficient was greater than predicted, and it was necessary to add a fuel pump discharge orifice. The components incorporated in the engine were identified in table II; because the test was for facility checkout, a non-optimum injector was used.

Important occurrences during the test can best be illustrated by reference to figure 5. Turbopump rotation started 1.3 sec after the main fuel shutoff valve was opened; this was approximately 1 sec longer than is typical for hydrogen fueled RL10 engines. As the engine accelerated, the oxidizer flowrate was restricted to a low value by the mixture ratio control valve; when the oxidizer pump pressure rise reached 140 psi, the valve opened and allowed full oxidizer flow. This point is shown by the rapid rise in chamber pressure at 2.7 sec. The 1.4 sec interval between the start of rotation and the opening of this valve was approximately 10 times that encountered in an oxygen/hydrogen RL10 transient. However, the engine did reach design speed, which proved that sufficient power was available in the cycle.

Although a reset system in the thrust control reacted to limit the acceleration, the chamber pressure overshot to a peak value of 330 psia (at approximately 3.3 sec). This overshoot is greater than normal and apparently was caused by slower reaction of the engine system with flox/ methane than with oxygen/hydrogen. Also, a tendency toward thrust control bypass piston sticking was indicated. Following the overshoot, a slight overcorrection reduced the chamber pressure to 220 psia (at 4.5 sec), followed by a slight overacceleration to 280 psia (at 4.9 sec).

The system appeared to be controlling at 260 psia chamber pressure at 5.7 sec, when the oxidizer pump discharge pressure suddenly decreased without a change in turbopump speed. When this occurred, the thrust control sensed the lower chamber pressure and accelerated the turbopump in an attempt to increase the flow. The oxidizer pump did not recover for approximately 3 sec. During this time, the turbopump started to decelerate; the system finally stabilized at 175 psia chamber pressure and a mixture ratio of 3.0 for the remainder of the test.

17
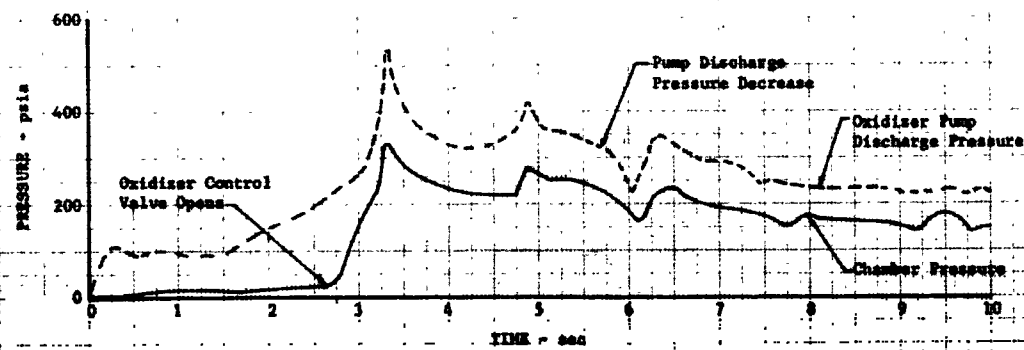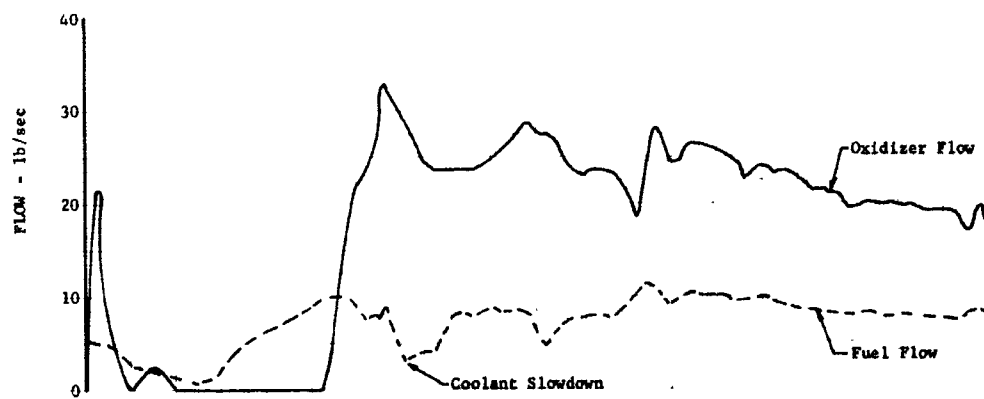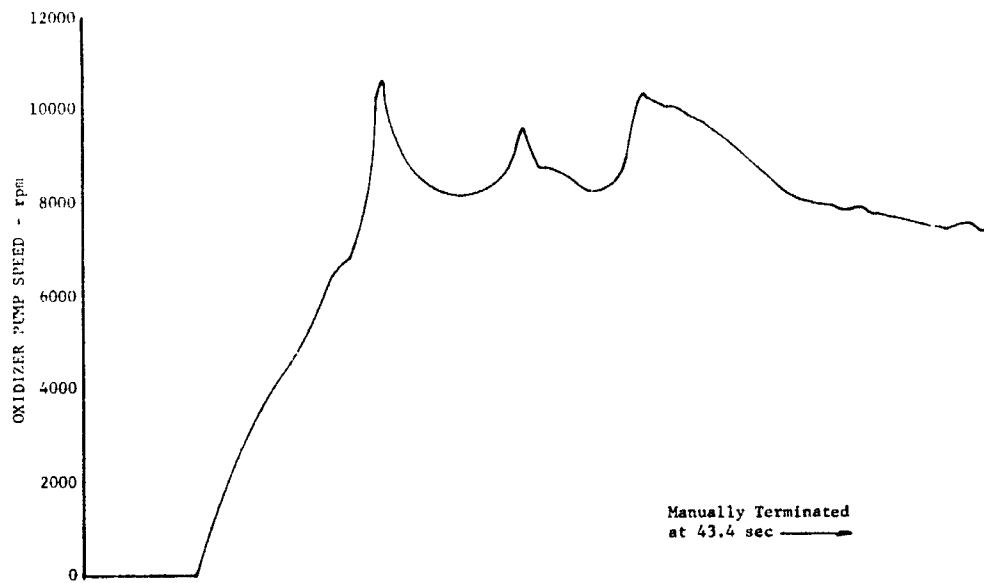
Figure 5.   Starting Transient for Engine Test No. E-1   DF 68963

The stabilization of the engine at low chamber pressure in the latter portion of the test was indicative of a lack of power caused by fuel leakage upstream of the turbine (i.e., in the cooling jacket). Review of data showed that coolant tube leakage started at some time during the first 8 seconds of the firing. The exact time of failure cannot be unequivocally established; however, the sharp decrease in turbopump speed shown at 6.2 seconds in figure 5 could be an indication that it occurred at that point. The data indicated that the failure was located upstream of the nozzle throat. Unfortunately, the oxidizer inlet shutoff valve failed to close for 50 seconds after fuel shutoff, and, as a result, approximately 10 gallons of flox were dumped into the hot chamber. This caused extensive chamber and injector damage*, which made it difficult to assess physically where tube failures had occurred during the test, but all areas that were predicted to be minimum margin points were relatively intact after shutdown.

It was conjectured that the tube failures during the test were related to the sudden expansion of the methane within the jacket during the first chamber pressure spike. This expansion would have caused a temporary coolant flow slowdown, thereby reducing cooling. However, the jacket would have had to be relatively intact for the turbopump to reaccelerate as it did at 4.3 and 5.7 sec. It was thus reasoned that the tubes were weakened or eroded during the flow slowdown, and that they failed during the last period of high speed turbopump operation.

Following test No. E-1, the corrective action required for all problems except the coolant slowdown and the delay in pump rotation was obvious. The oxidizer inlet shutoff valve was subjected to bench tests to investigate the cause of its failure to close. The valve demonstrated a tendency to stick, but the resistance did not appear to be enough to prevent valve closing. A separate helium actuation pressure for closing was added at the valve actuator, and the problem did not recur. As described in Section V, the oxidizer pump pressure decrease was traced to ingestion of gas from instrumentation and purge lines. Relocation of lines and purge valves corrected this problem, and it was not encountered again.

Although the cause of slow turbopump rotation was not immediately identified, it was ultimately traced to an interference between the oxidizer pump gearbox housing and the driven gear on the oxidizer pump shaft. The problem was overcome when a different pump was incorporated for build 3. The most difficult problem, therefore, was alleviation of the coolant flow reduction, and the bulk of the remaining effort on the program was directed to this end.

It is difficult to summarize concisely the changes made to overcome the starting problem in sufficient detail to explain the limitations under which they were made and the logic behind them. Therefore, for the pur-

* There was no nozzle damage except at the bottom of the engine, where it was obvious, that there had been a stream of liquid oxidizer.

19

poses of the discussion here, only the nature of the changes and the net result obtained will be described. A chronological sequence that more specifically explains changes, reasons therefor, and results achieved, is presented in Appendix D.

b. Build No. 2

The first approach taken to overcome coolant slowdown was to alter start sequencing using existing valves. The servo supply flow to the thrust control was increased to improve its response, and the oxidizer flow control valve was adjusted to increase starting flowrate and to delay the start of full oxidizer flow. These changes were not effective, and a coolant flow slowdown with resulting thrust chamber and injector damage was encountered in the test conducted on the second engine build, test No. E-2.

c. Build No. 3

The starting oxidizer flowrate was restored to its original level for test No. E-3 on build No. 3, and a system to maintain the thrust control open throughout the transient, with provision for manual reactivation to feedback control during the test, was added. This latter alteration was made to eliminate the contribution of the automatic thrust control action to the coolant flow slowdown. However, the slowdown and related thrust chamber damage were still encountered.

During test No. E-3, the injector, which was of an improved design incorporating a nickel oxidizer spudplate for greater durability, was undamaged. Additionally, there was no delay in the start of turbopump rotation. This resulted, as noted above, from the replacement of oxidizer pump S/N C71Y002 with S/N C71Y001. The replacement was made because of increased secondary seal leakage in the oxidizer pump S/N C71Y002 after removal from storage following tests No. E-1 and E-2. When the pump was completely disassembled to investigate the seal problem, signs of interference between the pump housing and gear of pump S/N C71Y002, were found. The interference, which apparently was responsible for the delay, occurred only with rearward shaft loading as explained in Section V, and was not detectable in normal pump torque checks.

d. Build No. 4

In build No. 4 of the engine, two significant component changes were made. These were in the thrust chamber and the oxidizer flow control valve. Modifications to the thrust chamber to improve cooling were somewhat different but accomplished with the same intent as in previous units, i.e., to improve cooling in the combustion chamber and tube transition region (Refer to Section IV). The major difference was that during modification and repair (the thrust chamber was the unit damaged during test No. E-2), filler rods were added in the coolant tubes at the end of the

20

nozzle to reduce volume. The oxidizer flow control valve was changed to a different design that had provisions for a more gradual, scheduled opening. The valve is described in Section VI.

(1) Test No. E-4

The higher response thrust control was retained for build No. 4, and with one exception, the starting sequence for test No. E-4 was identical to that of test No. E-3, i.e., open thrust control to be manually activated when the engine stabilized after the start transient. The change consisted of delaying the opening of the oxidizer inlet valve by 0.200 sec to obtain the fuel lead required to establish coolant flow into the jacket before the start of oxidizer flow through the scheduled control valve.

Engine behavior during the start transient of test No. E-4 is illustrated by the plot of important operating parameters presented in figure 6. The scheduled oxidizer control valve produced a relatively gradual rise in chamber pressure during the initial phase of the start, but the turbopump acceleration rate was greater than predicted, and the chamber pressure increase became exponential rather than linear later in the transient. Some of the increased acceleration rate was attributed to the higher turbine inlet temperature (as compared with test No. E-3) maintained throughout the start transient. Turbine temperature histories for the two starts are compared in figure 7. The high temperature in test No. E-4 was the result of the increased residual heat provided by the greater mass of the cooling jacket (due to the filler inserts) and also by the higher oxidizer flow provided by the scheduled oxidizer control valve throughout the starting period. A fuel slowdown was noted at the point of maximum chamber pressure increase, but its magnitude was minor compared to that encountered in Test No. E-3. This verified that a small jacket volume and an extended chamber pressure ramp were desirable to prevent chamber damage during the starting period.

The engine stabilized at the design chamber pressure of 250 psia for 1.5 seconds at a mixture ratio of 3.6, after which the turbopump slowly decelerated. The reduced speed resulted in an oxidizer pump discharge pressure too low to keep the spring-loaded oxidizer control valve in its full open position. (It was predicted that the oxidizer control valve would not seat if the engine operated at a mixture ratio below 4.5, but cycle studies showed that, if all components operated as predicted, this would be achieved.) As the valve closed from the full open position it created a higher flow restriction, and therefore a reduction in mixture ratio, which further reduced speed. When the thrust control was activated at 5.5 seconds there was a temporary increase in rpm, but it was not sufficient to seat the oxidizer control valve and the system continued to decelerate. The test was manually terminated at 13.8 seconds; no hardware damage was found during the post-test inspection.
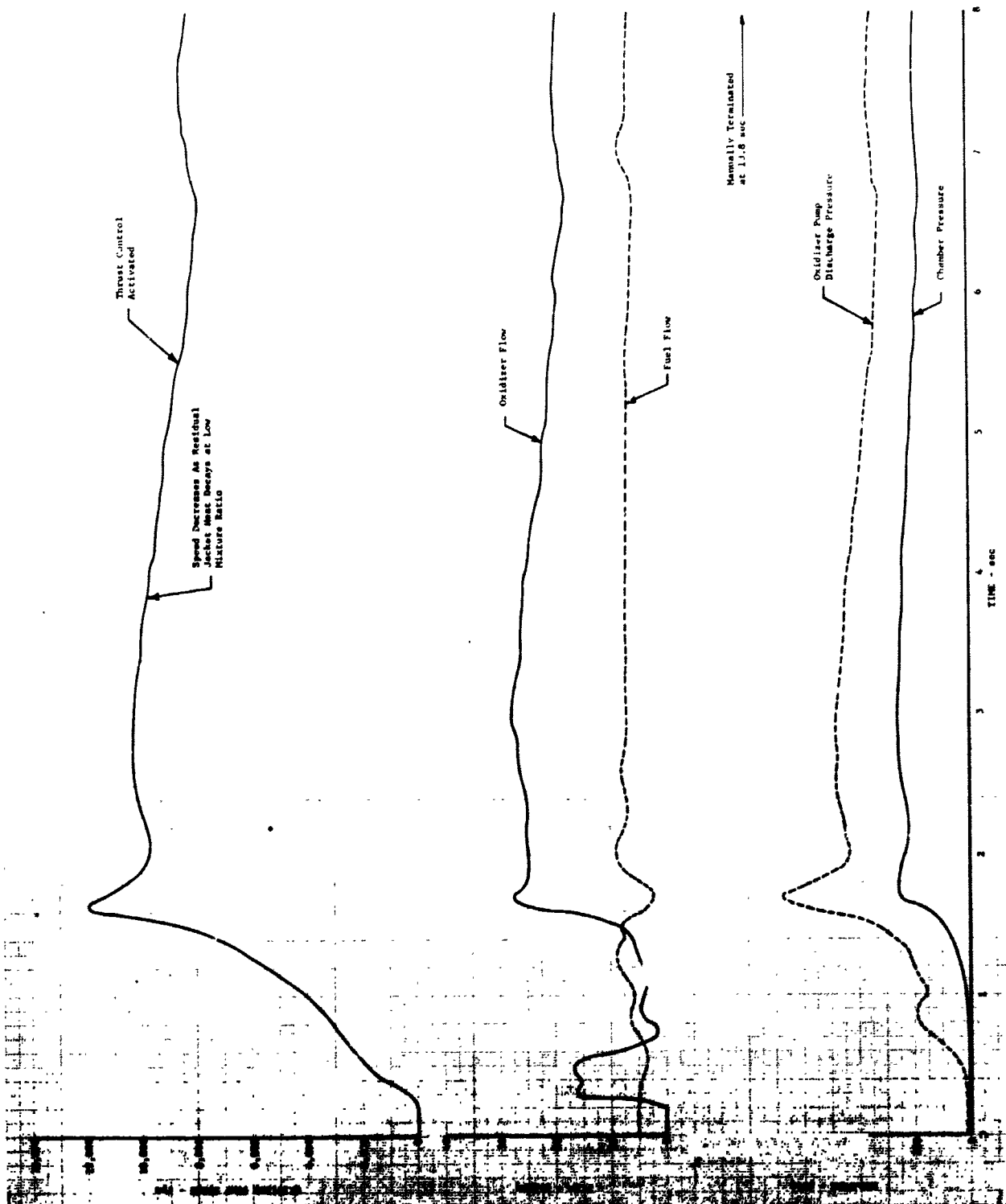
Figure 6. Starting Transient for Engine Test No. E4

DF 68967
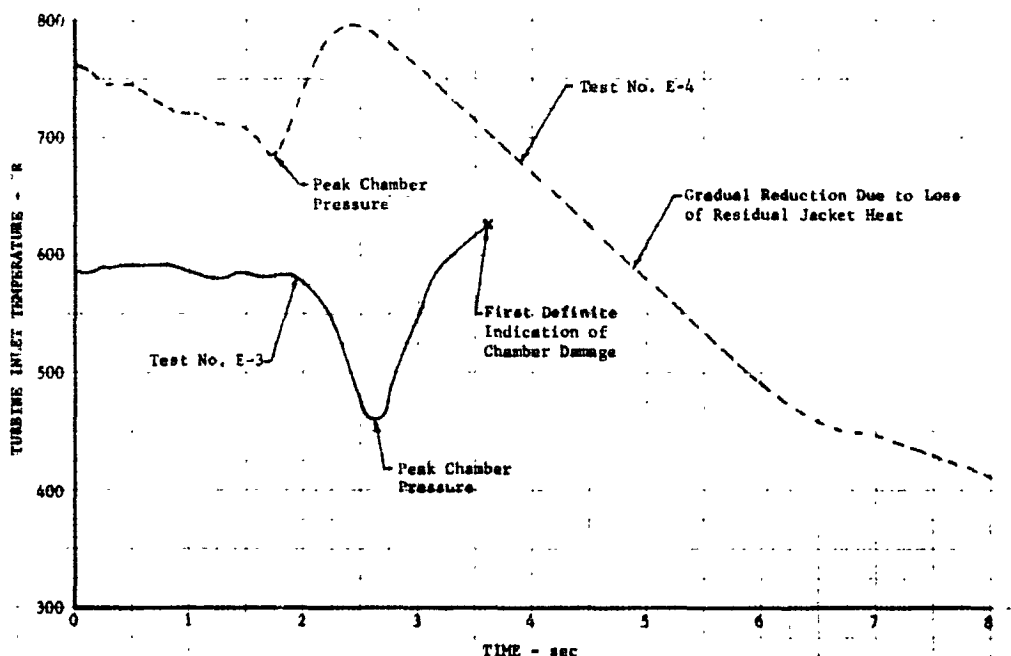
Figure 7. Turbine Inlet Temperature Comparison, Tests E-3 and E-4   DF 68959

(2)   Test No. E-5

Following the successful demonstration of start, adjustments were made to the thrust control sequencing, and the oxidizer flow control valve reference pressure was changed to a lower level source in an effort to assure that the valve would seat during the next test. A second firing, E-5, was made with the configuration, but the desired chamber pressure was not achieved. The data obtained in this test made it apparent that the turbine stator area was greater than desired.

When the turbine stator area variance was discovered through analysis of data, the remaining scope of effort permitted under the program was insufficient to allow removal of the engine from the test stand for inspection, reoperation, and rebuild. Therefore, it was necessary to proceed on the assumption that the turbine area had changed without establishing the mode of failure*. To balance the cycle and increase mixture ratio with the greater turbine area, it was decided to increase the flow resistance in the fuel system. The most readily available means for accomplishing this was to decrease the size of the fuel pump discharge orifice. Cycle calculation results for the system with the reduced diameter orifice are presented in Appendix

---

* As described in Section V, post-test inspection revealed that the change resulted from failure of welds made at the stator vane trailing edges where the vanes were deformed to reduce area.

28

C. In addition to providing a higher steady-state mixture ratio balance, a high flow restriction at this point has a stabilizing influence which tends to reduce coolant slowdowns.

(3) Test No. E-6

Four tests, E-6 through E-9, were completed with the smaller orifice installed. In test No. E-6 the sequencing used in test No. E-5 was retained, but when used with the increased fuel system resistance it produced a fuel pressure overshoot that caused rupture of the first stage fuel pump housing. It had been recognized that, because of the reduction in impeller diameter and resultant increase in area subjected to pump discharge pressure, the maximum pressure capability of the housing would be reduced. A limit of 850 psia had been estimated from the calculated housing stress and the 0.2% yield strength of housing material at 200°R. At the time of rupture the first-stage discharge pressure was 900 psia. Further discussion of the failure is given in Section V. Replacement of the first stage housing was readily accomplished on the test stand, and testing was continued.

(4) Test No. E-7 through E-9

A satisfactory start was obtained in test No. E-7, but steady-state chamber pressure was approximately 200 psia. Mild erosion of welds at tube fin inserts had been noted after test No. E-6, because of the loss of coolant flow when the fuel pump housing ruptured. Minor leakage through the eroded areas apparently increased during test No. E-7 (See Section IV) and caused a reduction of power. To compensate for this, a bypass was added around the oxidizer flow control valve to increase mixture ratio. In test No. E-8, a coupling set up between the flow control valve and thrust control caused 1 Hz cycling of the system, so the thrust control was made inoperative by venting the chamber pressure sense system, and test No. E-9 was made. The start was good and stable operation was achieved for approximately 3 seconds, as shown in figure 8, after which flox depletion caused oxidizer pump head rise to decrease, with a corresponding reduction in chamber pressure. The test was terminated at 11.6 seconds to complete the program.

F. STEADY-STATE OPERATION

Table III summarizes engine operating pressure and temperature levels at important stations in the system for those portions of tests in which steady-state operation was achieved. Thrust chamber and injector performance and efficiency data were obtained during both engine and component tests; therefore, to facilitate comparison, data from both types of tests are analyzed in Section IV — Injectors and Thrust Chambers. Performance data for turbopump components are presented in Section V.
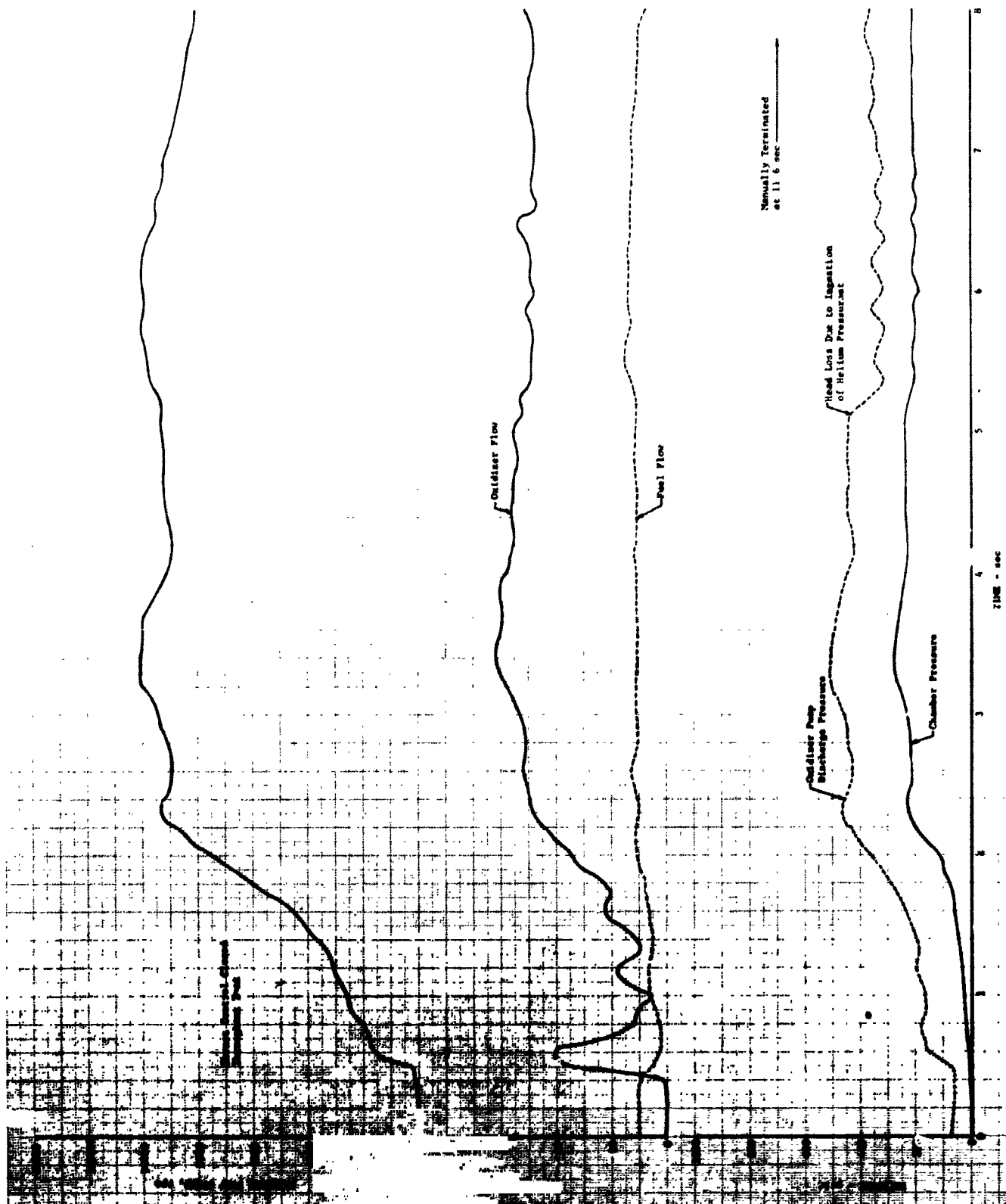
Figure 8. Starting Transient for Engine Test No. E-9

TIME - sec

Oxidizer Flow

Fuel Flow

Manually Terminated
at 11.6 sec

Head Loss Due to Ingestion
of Helium Pressurant

Oxidizer Pump
Discharge Pressure

Chamber Pressure

TABLE III. LOX/METHANE ENGINE PARAMETERS

Test No.	E-1	E-1	E-1	E-2	E-3	E-4	L-4	F-5	E-5	E-5	E-7	E-7	E-8	E-9	E-9
Engine Build No.	1	1	1	2	3	4	4	4	4	4	4	4	4	4	4
Engine Mixture Ratio [2]	2.97	2.99	2.41	2.83	4.43	3.58	2.91	3.00	3.24	4.33	4.33	4.68	5.49	5.05	5.57
Chamber Pressure, psia [2]	182.8	184.4	152.9	204.6	186.1	245.7	159.9	252.6	237.7	236.9	238.4	208.4	229.7	236.1	202.7
Delivered Impulse, $lb_f\text{-}sec/lb_m$ [2]	343.8	347.1	340.7	311.8	342.1	376.4	370.5	365.7	376.1	377.4	376.3	376.3	330.8	347.7	340.7
Oxidizer System — Pump Flowrate, lb/sec	19.62	19.61	15.56	24.30	22.13	25.35	16.05	25.52	23.97	25.35	25.54	22.39	29.25	27.65	24.57
Inlet Pressure, psia	75.8	76.3	83.4	72.9	77.3	68.7	86.8	106.3	109.0	103.9	103.2	114.6	101.6	118.1	131.5
Inlet Temperature, °R	152.2	152.9	149.3	158.0	152.6	151.7	155.7	149.5	158.1	164.9	166.2	150.5	155.7	161.6	158.3
Discharge Pressure, psia	246.8	246.3	228.7	314.5	282.1	446.8	292.4	549.2	475.8	478.7	482.8	388.2	506.4	441.8	359.1
Speed, rpm	6601	6574	6001	7940	7226	9743	7189	1C,556	9654	9922	10,013	8302	9215	9213	7870
NPSH, ft	100.3	100.2	11>.3	88.0	101.0	89.5	113.6	151.6	146.7	126.6	123.6	164.2	137.6	156.4	183.2
Injector Inlet Pressure, psia	199.9	201.8	167.1	246.7	209.1	291.4	197.1	288.1	268.6	295.2	297.7	260.4	276.2	280.3	234.1
Inlet Temperature, °R	155.7	156.2	154.7	161.1	156.8	158.4	159.4	158.4	159.0	171.9	173.4	152.8	157.5	161.5	162.5
Fuel System — Pump Flowrate, lb/sec [1]	6.60	6.56	6.46	8.42	5.00	7.08	5.53	8.50	7.40	5.85	5.90	4.78	5.33	5.48	4.41
Inlet Pressure, psia	62.4	62.6	61.4	63.4	65.6	74.4	65.6	73.0	72.7	77.4	77.3	72.0	73.7	71.4	66.8
Inlet Temperature, °R	202.8	202.7	203.1	203.4	203.9	203.5	203.3	203.3	203.0	210.0	210.0	209.0	223.6	211.1	211.0
Discharge Pressure, psia	480.1	476.8	406.1	660.3	558.4	961.5	555.8	1127.4	948.6	986.0	1000.4	711.7	841.7	867.6	645.5
Speed, rpm	13,981	13,924	12,710	16,817	15,305	20,636	15,227	22,358	20,446	21,015	21,208	17,584	19,517	19,514	16,669
NPSH, ft	253.3	253.5	247.3	257.3	273.0	317.4	269.1	309.5	309.6	311.1	310.9	285.0	142.0	270.3	246.1
Coolant Jacket [2] Inlet Pressure, psia	407.9	405.0	337.4	538.1	518.3	890.2	510.4	1014.0	868.6	760.3	774.1	560.9	653.2	668.9	506.0
Inlet Temperature, °R	218.0	217.2	216.9	218.5	217.8	224.5	212.6	224.5	221.0	230.2	230.6	221.4	240.6	226.0	223.6
Exit Pressure, psia	384.6	381.1	316.0	496.8	394.0	707.9	445.1	830.9	740.8	631.2	640.1	474.9	506.4	533.6	417.6
Exit Temperature, °R	491.3	486.1	430.1	772.2	733.6	690.9	365.7	651.8	516.4	717.0	729.5	618.1	1009.4	899.8	719.4
Turbine [2] Inlet Pressure, psia	369.0	365.5	303.2	447.6	364.2	641.9	420.2	766.6	692.2	581.3	588.2	438.3	470.5	496.7	389.1
Inlet Temperature, °R	452.8	467.8	430.2	737.8	716.9	687.5	358.7	655.8	518.3	707.6	720.2	603.2	1000.4	892.5	701.2
Injector [2] Manifold Pressure, psia	198.3	199.3	165.6	242.0	209.4	307.4	189.7	324.8	296.4	284.3	287.4	235.2	259.4	267.3	226.4
Inlet Temperature, °R	400.8	418.9	388.9	638.3	638.5	651.1	324.0	617.1	494.4	662.7	678.7	537.9	873.5	798.0	636.7

(1) Includes gearbox coolant and cooldown valve leakage.
(2) In test No. 1, 2, 3, 8, and 9 these data are not representative because of coolant tube failures.

G. HARDWARE CONDITION

The total firing duration accumulated in the six tests of build No. 4 was 120.2 seconds. With the exceptions of the change in the turbine flow area and the relatively minor damage sustained by the thrust chamber in this build, all other engine components were in excellent condition at the conclusion of the test program. Figure 9 presents a post-test photograph of FX-153 build No. 4 after the completion of testing. The carbon deposits on the nozzle exterior are caused by normal diffuser blowback during the start and shutdown transients.

Figure 9. Flox/Methane Engine FX-153 After Test E-9   FE 80376

The occurrence of thrust chamber damage has previously been described. Most of the damage consisted of minor tube erosion just upstream of the throat. A few areas closer to the injector also showed some erosion of welds used for installation of fins to improve cooling, but the leaks in these areas could only be detected by pressure checks using a bubble solution. Three tests of approximately 77 seconds total duration were made after the

27

first indication of tube leaks. Therefore, at least a portion of the observed damage at the completion of the program was due to partial reduction of coolant flow because of leakage from previously failed tubes.

H. CONCLUDING REMARKS

The good condition of the engine hardware following the last series of six tests verified that a flight-type pump-fed rocket engine can be operated with flox/methane propellants. Although several problems were encountered, these were caused primarily by the use of modified components which were, at best, serious compromises from optimized designs.

The most serious problem encountered during the engine demonstration was chamber damage resulting from a coolant surge during starting. The severity of the surge problem was due to the large coolant volume contained in the chambers which were originally designed for hydrogen. In spite of this, the control sequence developed for the last test series reduced the surge to an acceptable level. Chambers designed specifically for methane should greatly reduce, and possibly eliminate, the expansion surge, allowing significantly more control flexibility and faster engine acceleration.

Based on the results obtained, it is believed that a full scale engine development program can be undertaken using available technology because:

1. By using the technology available at the start of this program, no handling or compatibility problems were experienced with either flox or methane.

2. The turbopump modification was extremely straightforward and no unpredictable turbopump failures were experienced. The practicability of using gear-driven centrifugal turbopumps employing methane for bearing and gearbox lubrication was unequivocally established.

3. The satisfactory operation of the expander cycle demonstrated its applicability for use with methane as the turbine drive fluid. Development of an engine based on this cycle would eliminate one major unknown which was not investigated, that of carbon deposition in the turbines of cycles employing fuel rich combustion products for the drive fluid.

SECTION IV

INJECTORS AND THRUST CHAMBERS

A. GENERAL

Modification and testing of the injector and thrust chamber were initiated in advance of engine system testing. The objectives were to achieve a combustion performance target of 95% characteristic exhaust velocity efficiency (referenced to theoretical shifting equilibrium) at the theoretical optimum mixture ratio of 5.75, and to establish a thrust chamber configuration that would have adequate durability when regeneratively cooled with methane. As in the case of all components, the effort was guided by the restrict :., that changes to basic RL10 hardware be held to a minimum.

In initial tests uncooled workhorse copper thrust chambers, rather than RL10 tubular thrust chambers, were used with the injectors. The heat sink chambers were employed to obtain experimental heat flux data that could be used to guide modification of the cooled chambers. Pressure-fed tests of modified RL10 thrust chambers were made with overcooling as injector development continued, and the final configurations of both the injector and the thrust chamber were evaluated in engine tests.

The engine tests in which the final injector and thrust chamber designs were used were limited to low mixture ratios because it was not possible, within the scope of the program, to correct a turbine area change that occurred. However, a c* efficiency of 96.7% was obtained at a mixture ratio of 4.68, and extrapolation of performance data to higher mixture ratios indicates that the injector had the capability for providing 95% characteristic exhaust velocity efficiency at r=5.75.

It was determined that modifications to the thrust chamber were required not only to improve cooling in critical areas, but also to reduce the jacket volume for the benefit of the engine system. The final thrust chamber accumulated six firings and 120 seconds of engine operation. Some tube leaks developed in areas where modifications were made but the assembly had been subjected to unusual transients as system operating techniques were developed. It is therefore believed that its durability would be adequate under less stringent operating conditions, and that, with only minor further improvement, it would have withstood the conditions that were imposed.

B. INJECTORS

1. DESCRIPTION

a. Basic Injector

All injectors used in the test program were modified RL10 parts, the external features of which are shown in figure 10. The injector has 216

injection elements, each of which consists of an oxidizer tube (or spud),
and a concentric fuel annulus. The elements are arranged in concentric
rows and inject in a direction perpendicular to the 15-degree conical face.
The porous faceplate is fabricated from Rigimesh* and is transpiration
cooled by the fuel. A cross section sketch showing construction features of
the injector and its internal manifolding scheme is presented in figure 11.
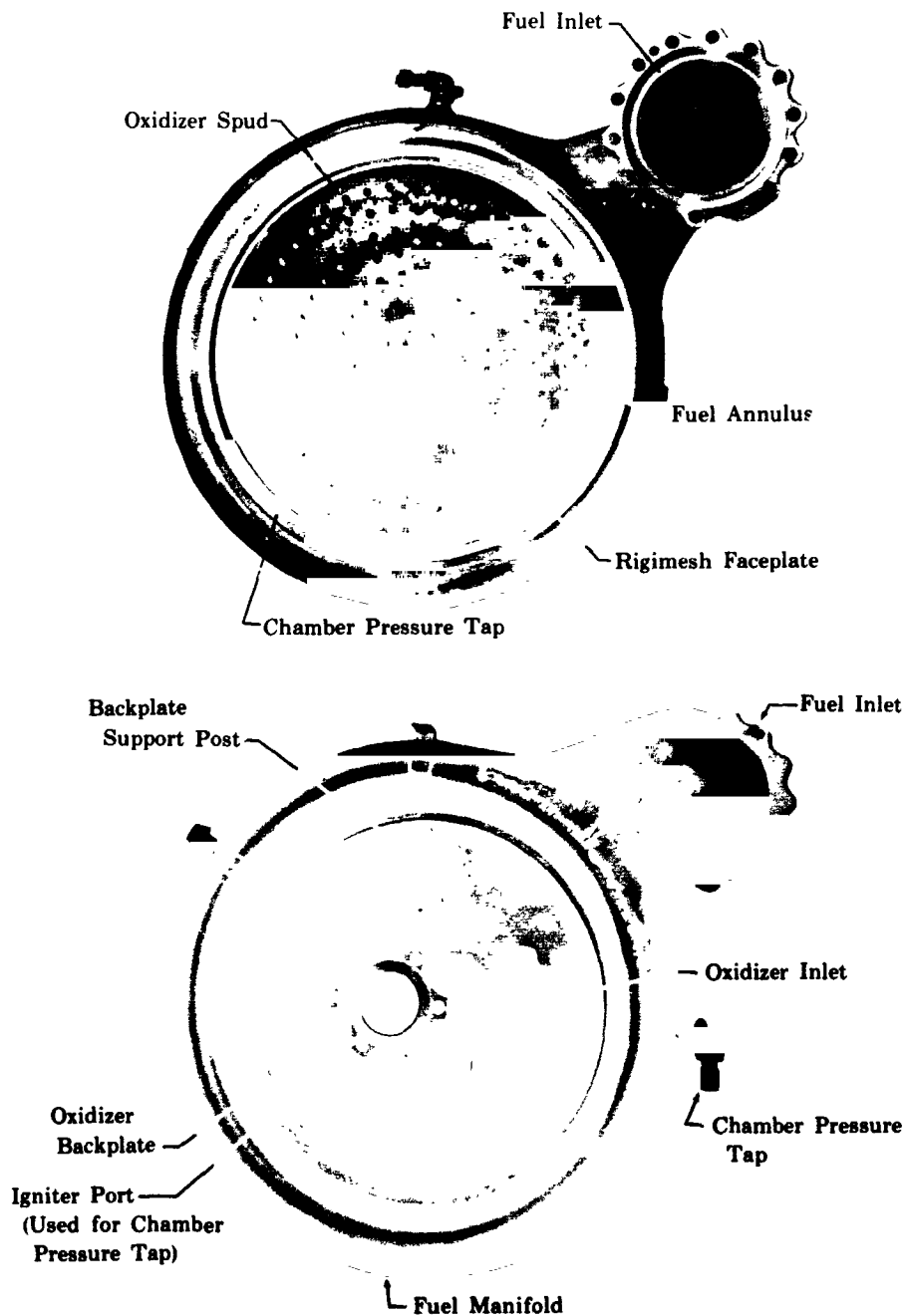
Figure 10.   RL10 Injector External Features   FD 12777A

* Rigimesh is a registered trade name for a sintered wire mesh material made by Aircraft
  Porous Media Incorporated, Glen Cove, N.Y.
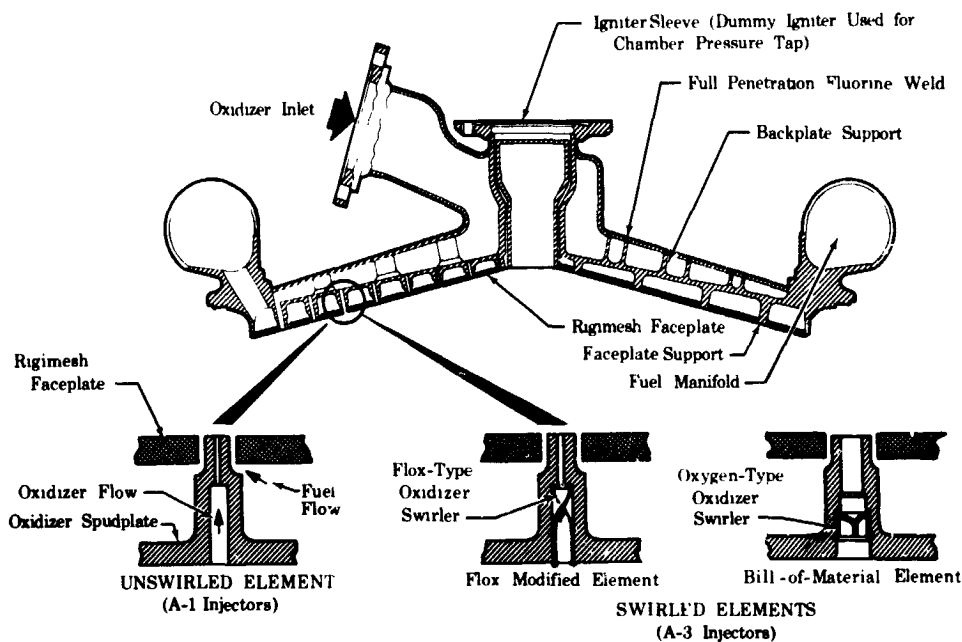
Figure 11. RL10 Injector Cross Section Showing Manifolding and
Element Configuration

FD 25713A

The same basic injector design has been used in all production RL10
engine models, the RL10A-1, RL10A-3, RL10A3-1, and RL10A-3-3; changes
made to the injector between models have been limited to details of the
injection elements. In the initial model, the RL10A-1, oxidizer spud passages
were straight bores, and all rows of elements were the same size. In advancing
to the A-3 models swirlers were added to the intermediate concentric rows
of elements (i.e., all but the innermost and outermost rows) to improve
atomization and mixing. Use of swirlers in the outer row was avoided so
that spray impingement on the thrust chamber walls would not be encoun-
tered, and the straight passages were retained in the inner row in view of
its small diameter. The swirlers provided a 2.5% improvement in perform-
ance in the first of the A-3 models. Further improvements were achieved
in later versions by tailoring injection dimensions to improve radial distri-
bution of mass flow and mixture ratio.

b. Modifications for Flox/Methane Service

Prior to the start of the pump-fed engine study, RL10 injectors had
been tested with fluorine and hydrogen in the Contract NASw-754 hydro-
gen/fluorine propulsion system research program and with flox and liquefied
petroleum gases (at 100 psia chamber pressure) in the Contract NAS3-4195
investigation of flox and light hydrocarbon fuels as rocket propellants. Both
Bill-of-Material and modified injectors were tested with fluorine and hydro-
gen, and modified parts were tested with flox and light hydrocarbons. In
both programs, reasonable durability was demonstrated by A-1 model injec-
tors, but problems attributed to nonsuitability of the oxygen swirler design
for fluorine service were encountered with A-3 type units. The oxygen and
fluorine type swirlers are compared in figure 11.

31

The fact that Bill-of-Material RL10A-1 injectors were successfully tested with fluorine in the Contract NASw-754 program proved the compatibility of the basic RL10 injector design with fluorine. Therefore, it is not mandatory to make any changes for fluorine or flox service; however, when injectors were modified in that program, improved welding techniques for full penetration were used in making of backplate attaching welds as a matter of good fluorine construction practice.

Fuel side modifications in both of the early programs were essentially limited to installation of new faceplates to reduce the fuel orifice dimensions.

The experience in the use of RL10 injectors in the earlier programs provided a starting point for the injectors tested in the flox/methane engine study; in fact, testing was started with parts previously modified and tested with fluorine and hydrogen. However experimental evaluation demonstrated the need for additional changes. Because these were made in an evolutionary fashion during injector development, they are best described in the context of injector testing and therefore are discussed in the following paragraphs.

2. INJECTOR DEVELOPMENT

In the course of injector development directed toward the achievement of 95% characteristic exhaust velocity efficiency, seven modified injectors were tested. Because of the earlier experience that showed A-3 type injectors subject to durability problems, the effort was started using A-1 type parts. Initial results showed that these could not be modified sufficiently to provide the desired performance level, and therefore it was necessary to develop a swirler type unit to achieve both durability and performance. Two of the injectors evaluated were RL10A-1 units, and the remainder were RL10A-3 types.

The injector configurations tested are summarized in table IV. Initial tests were conducted using uncooled pressure-fed thrust chambers, and testing progressed to pressure-fed cooled thrust chambers and engine systems. Measured and derived performance data obtained in the testing are presented in tables V through X. The tables provide a reference for the following discussion of injectors by type.

TABLE IV. INJECTOR CONFIGURATIONS

Injector S/N	RL10 Model	Fuel Gaps, in. Inner(1)	Intermediate	Outer	Rigimesh Flow Rating, scfm	Oxidizer Orifice Diameters, in. Inner(1)	Intermediate	Outer	Modifications to Bill-of-Material Configuration(2)
HK 713	A-1	0.012	0.008	0.008	120	0.074	0.074	0.074	Faceplate replaced only to provide minimum gap.
KH 707	A-1	0.008	0.008	0.008	120	0.074	0.074	0.074	Faceplate replaced only to provide minimum fuel gaps.
IF 764	A-3	0.018	0.013	0.015	120	0.067	0.085	0.085	Installed 0.010-in. thick stainless steel swirlers in intermediate rows. Outer row metering orifices removed and spuds drilled out to 0.085-in.
RY 14	A-3	--	0.013	0.012	120	--	0.085	0.093	Inner row removed and welded closed. Installed 0.010-in. thick stainless steel swirlers in all rows. Outer row drilled out to 0.093-in.
IF 763-1	A-3	--	0.009	0.009	120	--	0.085	0.117	Inner row removed and welded closed. Installed 0.010-in. thick stainless steel swirlers in all rows. Outer row drilled out to 0.117-in.
IF 763-2	A-3	--	0.009	0.009	120	--	0.085	0.117	Thin swirlers replaced with 0.037-in. thick nickel swirlers.
3K 2945	A-3	--	0.015	0.012	60	--	0.085	0.117	Oxidizer side same as IF 763 Fuel faceplate porosity reduced.
AAF11-1	A-3	--	0.012	0.015	120	--	0.085	0.101	Replaced stainless steel oxidizer plate with nickel plate. Nickel swirlers (0.037-in.) in all spuds.
AAF11-2	A-3	--	0.012	0.015	120	--	0.085	0.101	Twenty-six 0.010-in. diameter fuel holes added near the outer circumference, and outer row fuel annuli increased from 0.15-in. to 0.020-in. in their outer semicircle.

(1) Refers to inner ring of six elements; in later modifications these were sealed closed. Outer refers to the ring of 48 elements nearest the chamber wall. Intermediate refers to the 162 elements not covered under the previous designations.

(2) Modifications listed are in addition to replacing the faceplate (to reduce the fuel gaps), and using improved weld techniques when replacing oxidizer backplate after incorporation of changes.

TABLE V. UNCOOLED THRUST CHAMBER PERFORMANCE TESTS—MEASURED DATA

Test No.	Injector S/N	Flow Concentration, %	Chamber Pressure, psia	Oxidizer Flow, lb$_m$/sec	Fuel Flow, lb$_m$/sec	Oxidizer Injector Inlet Temperature, R	Oxidizer Injector Inlet Pressure, psia	Fuel Injector Inlet Temperature, R	Fuel Injector Inlet Pressure, psia	Net Thrust, lb$_f$	Ambient Pressure, psia
1-USL	NK 713	79.0	251.6	28.63	5.97	151.3	278.2	515.7	339.0	9203.	14.6
2-USL	NK 713		Test Terminated Prematurely								
3-USL	NK 707		Test Terminated Prematurely								
4-USL	NK 707	77.0	243.4	26.90	6.37	168.6	266.2	525.1	341.4	8788.	14.6
5-USL	NK 707	77.0	236.7	27.91	5.33	152.7	260.0	514.4	306.1	8460.	14.6
6-USL	NK 707	77.0	225.8	28.27	4.65	153.1	247.7	512.3	279.0	7997.	14.6
7-USL	NK 707		Test Terminated Prematurely								
8-USL	NK 707	82.4	272.6	28.52	7.66	155.0	297.1	521.4	394.1	9947.	14.8
9-USL	NK 707	82.4	258.6	29.63	6.00	153.6	283.0	520.9	337.1	9312.	14.8
10-USL	NK 707	82.4	268.2	29.00	6.88	153.8	290.7	522.1	369.1	9741.	14.8
11-USL	NK 707	82.4	258.4	30.37	5.86	152.1	286.7	518.3	333.3	9367.	14.8
12-USL	NK 707	82.4	261.7	31.06	5.65	153.7	288.6	520.4	329.7	9419.	14.8
13-USL	NK 707	82.4	257.3	32.86	5.35	149.3	287.2	520.4	330.2	9314.	14.8
14-USL	IF 764	82.9	261.1	28.20	6.48	153.7	283.5	508.3	296.9	9530.	14.7
15-USL	IF 764	82.9	252.4	29.03	5.16	152.8	276.1	516.5	277.3	9130.	14.7
16-USL	IF 764	82.9	259.1	28.70	5.78	151.3	282.9	511.4	289.2	9451.	14.7
17-USL	IF 764	82.9	250.4	29.15	5.03	144.6	275.0	520.8	274.1	9047.	14.7
18-USL	IF 764	82.9	258.6	28.95	5.64	151.0	283.0	516.2	284.8	9181.	14.7
19-USL	RY 14	80.5	259.6	27.57	6.92	161.6	284.4	515.7	327.0	9639.	14.9
20-USL	RY 14	82.1	229.5	28.78	4.84	155.3	257.1	506.2	268.0	8120.	14.8

TABLE VI. UNCOOLED THRUST CHAMBER PERFORMANCE TESTS—DERIVED DATA

Test No.	Mixture Ratio	Thrust Total Pressure, psia	Vacuum Thrust, lb$_f$	Fuel/Oxid. Mom. Ratio	$c*_{P_c}$, ft/sec	$c*_F$, ft/sec	$C_{F_{vac}}$	I_{vac}, lb$_f$-sec/lb$_m$	$\eta_{c*}(P_c)$, %	η_{c*_F}, %	$\eta_{c_{F_{vac}}}$, %	$\eta_{I_{vac}}$, %
1-USL	4.79	243.9	10,541	4.76	6332	6397	1.552	305.4	89.24	90.16	98.62	88.01
4-USL	4.23	236.1	10,126	5.71	6375	6393	1.540	305.2	90.86	91.14	97.91	88.90
5-USL	5.24	229.4	9,790	3.96	6200	6172	1.534	295.5	88.42	88.02	97.19	85.94
6-USL	6.08	218.6	9,335	3.03	5964	5928	1.534	284.3	86.49	85.97	97.05	83.94
8-USL	3.73	264.2	11,229	6.87	6557	6530	1.536	313.0	95.74	95.34	97.21	93.06
9-USL	4.94	250.4	10,664	4.10	6309	6272	1.529	299.9	89.54	89.02	97.05	86.90
10-USL	4.21	260.1	11,093	5.49	6509	6468	1.532	309.8	93.97	93.37	97.80	91.16
11-USL	5.19	250.3	10,699	3.73	6284	6181	1.535	296.0	87.75	87.39	97.23	85.32
12-USL	5.64	253.3	10,771	3.09	6062	6006	1.527	287.7	85.37	84.79	96.73	82.78
13-USL	6.14	249.2	10,664	2.73	5856	5842	1.537	279.8	83.48	83.27	97.38	81.30
14-USL	4.35	253.2	10,869	3.29	6557	6553	1.542	314.2	94.41	94.35	97.56	92.12
15-USL	5.62	244.9	10,470	2.17	6436	6410	1.535	307.1	90.93	90.56	97.24	88.42
16-USL	4.97	251.6	10,791	2.57	6553	6555	1.542	313.9	93.14	93.18	97.68	90.90
17-USL	5.79	243.0	10,306	2.01	6508	6462	1.535	304.8	90.37	89.99	97.23	87.87
18-USL	5.13	250.9	10,720	2.41	6516	6489	1.534	310.7	92.40	92.02	97.23	89.89
19-USL	3.98	251.8	10,997	6.21	6596	6675	1.568	319.5	94.83	96.56	99.39	94.28
20-USL	5.95	221.8	9,469	3.81	5925	5929	1.533	282.8	83.98	83.90	97.37	81.84

TABLE VII. PRESSURE-FED COOLED THRUST CHAMBER PERFORMANCE TESTS—MEASURED DATA

Test No.	Injector S/N	Flow Concentration, %	Chamber Pressure, psia	Oxidizer Flow, lbm/sec	Fuel Flow, lbm/sec	Oxidizer Injector Inlet Temperature, °R	Oxidizer Injector Inlet Pressure, psia	Fuel Injector Inlet Temperature, °R	Fuel Injector Inlet Pressure, psia	Net Thrust, lbf	Ambient Pressure, psia	Diffuser Pressure, psia
1-CA	IF 763-1	82.6	267.8	28.07	6.59	150.3	284.3	397.5	281.2	3816	14.8	1.6
2-CA	IF 763-1	81.8	252.5	27.69	5.31	150.2	270.7	457.0	300.2	3278	14.9	1.0
3-CA	IF 763-2	82.9	266.3	27.66	7.10	156.6	313.5	428.6	356.9	4029	14.7	1.0

TABLE VIII. PRESSURE-FED COOLED THRUST CHAMBER PERFORMANCE TESTS—DERIVED DATA

Test No.	Mixture Ratio	Throat Total Pressure, psia	Vacuum Thrust, lbf	$c^*(P_c)$, ft/sec	$C_{F_{vac}}$	I_{vac}, lbf-sec/lbm	$\eta_{c^*}(P_c)$, %	$\eta_{C_F vac}$, %	$\eta_{I vac}$, %
1-CA	4.26	260.0	13,508	6765	1.856	390.2	90.07	97.67	95.79
2-CA	5.22	245.4	12,576	6709	1.832	382.1	95.34	96.10	91.60
3-CA	3.89	258.4	13,267	6692	1.835	381.7	98.13	96.70	94.90

TABLE IX. ENGINE DEMONSTRATION TESTS—MEASURED DATA

Test No.	Engine Build No.	Injector S/N	Flow Concentration, %	Chamber Pressure, psia	Oxidizer Flow, lbm/sec	Fuel Flow, lbm/sec	Oxidizer Injector Inlet Temperature, °R	Oxidizer Injector Inlet Pressure, psia	Fuel Injector Inlet Temperature, °R	Fuel Injector Inlet Pressure, psia	Net Thrust, lbf	Ambient Pressure, psia	Diffuser Pressure, psia
E-1(1)	1	IF 764	82.6	182.8	19.62	6.60	155.7	199.9	400.8	198.3	-188	14.6	0.7
			82.6	184.4	19.61	6.56	156.2	201.8	418.9	199.3	-27	14.6	0.7
			82.6	152.9	15.56	6.46	154.7	167.1	388.9	165.6	-1545	14.6	0.6
E-2(1)	2	3K 2945	82.6	204.6	24.30	8.42	161.1	246.7	638.3	242.0	945	14.9	0.8
E-3(1)	3	AAF11-1	82.5	186.1	22.13	5.00	156.8	209.1	638.5	209.4	-22	14.8	0.9
E-4	4	AAF11-2	82.5	245.7	25.35	7.08	158.4	291.4	651.1	307.4	2848	14.7	1.1
			82.5	159.9	16.05	5.53	159.4	197.1	324.0	189.7	-1176	14.7	0.7
E-5	4	AAF11-2	82.5	252.6	25.52	8.50	158.4	288.1	617.1	324.8	3079	14.7	1.1
			82.5	237.7	23.97	7.40	159.0	268.6	494.4	296.4	2464	14.7	1.0
E-7	4	AAF11-2	82.5	236.9	25.35	5.85	171.9	295.2	662.7	284.3	2457	14.6	1.1
			82.5	238.4	25.34	5.90	173.4	297.2	678.7	287.4	2506	14.6	1.1
			82.5	208.4	22.39	4.78	152.8	260.4	537.9	235.2	970	14.6	0.9
E-8(2)	4	AAF11-2	82.5	229.7	29.25	5.33	157.5	276.2	873.5	259.4	2012	14.7	1.0
E-9(1)	4	AAF11-2	82.5	236.1	27.65	5.48	161.9	280.3	798.0	267.3	2209	14.7	0.9
			82.5	202.7	24.57	4.41	162.5	234.1	636.7	226.4	624	14.7	0.8

(1) Data unrepresentative because of tube leaks.

(2) Transient data.

TABLE X. ENGINE DEMONSTRATION TESTS—DERIVED DATA

Test No.	Engine Mixture Ratio[1]	Chamber Mixture Ratio	Throat Total Pressure, psia	Vacuum Thrust, lb_f	c^* (P_c), ft/sec	$C_{F_{vac}}$	I_{vac}, lb_f-sec/lb_m	η_{c^*} (P_c), %	$\eta_{C_{F_{vac}}}$, %	$\eta_{I_{vac}}$, %
E-4	3.58	3.67	238.6	12,142	6649	1.82	376.4	97.85	96.31	94.24
	2.91	2.99	15'.6	7,934	6508	1.83	370.5	97.96	97.79	95.80
E-5	3.00	3.06	244.9	12,379	6501	1.81	365.7	97.36	96.71	94.16
	3.24	3.32	230.5	11,736	6647	1.82	376.1	98.64	96.93	95.61
E-7	4.33	4.46	230.3	11,713	6677	1.82	377.4	96.33	95.60	92.10
	4.33	4.46	231.8	11,764	6670	1.82	376.3	96.22	95.44	91.84
	4.68	4.86	202.6	10,160[2]	6757	1.79	376.3	96.74	92.61	89.60

(1) Includes gearbox coolant and cooldown valve leakage.

(2) Thrust Data Questionable.

a. RL10A-1 Type Injectors

Two RL10A-1 type injectors, S/N HK 713 and S/N HK 707, were tested. These were the first tests of the program and were conducted in pressure-fed uncooled thrust chambers so that experimental heat flux as well as injector performance data could be obtained. The tests were limited to a 2.5 to 4.0 second duration because the chambers were uncooled, and one mixture ratio data point was obtained in each firing.

As indicated in table IV, the two A-1 injectors were essentially identical; the only reason that two were tested was that a test mishap caused damage to injector S/N HK 713 during its second firing* and performance data could not be obtained over the desired mixture ratio range. Injector S/N HK 707 was substituted and 11 firings were made over a mixture ratio range from 3.7 to 6.1.

Both injector S/N HK 713 and injector S/N HK 707 were obtained in the modified condition as GFE from the Contract NASw-754 hydrogen/ fluorine research program. The important modification made in each case under that program was replacement of the faceplate with a part having smaller diameter fuel holes. The fuel annulus gap width in the modified injectors was 0.008 inch.

Reduction of fuel gap was the approach taken in the earlier programs to improve mixing. In the RL10A-1 injector the propellants are injected in straight concentric streams, and mixing is effected by the shear forces between the oxidizer and the fuel streams. Thus, reducing the fuel gap increased the fuel velocity and the fuel-to-oxidizer injection momentum ratio.

* *The injector oxidizer purge regulator malfunctioned during the start transient, permitting fuel to enter the oxidizer manifold before oxidizer flow started. When oxidizer was introduced, combustion started in the manifold, destroying the injector.*

At the nominal mixture ratio of 5.75, the c* efficiency indicated for injector S/N HK 707 with flox/methane was approximately 84.5%, well below the target of 95%. The injection momentum ratio was calculated for each of the firings, and the plot of c* efficiency vs momentum ratio presented in figure 12 was constructed. Based upon the momentum ratio to c* efficiency relationship shown, a momentum ratio of 6.2 would be required at a mixture ratio of 5.75 to achieve 95% c* efficiency. The 0.008-inch fuel annulus width of injector HK 707 provided a momentum ratio of 3.1 at the nominal mixture ratio; to achieve the higher level, a gap width of 0.004 inch would have been required.
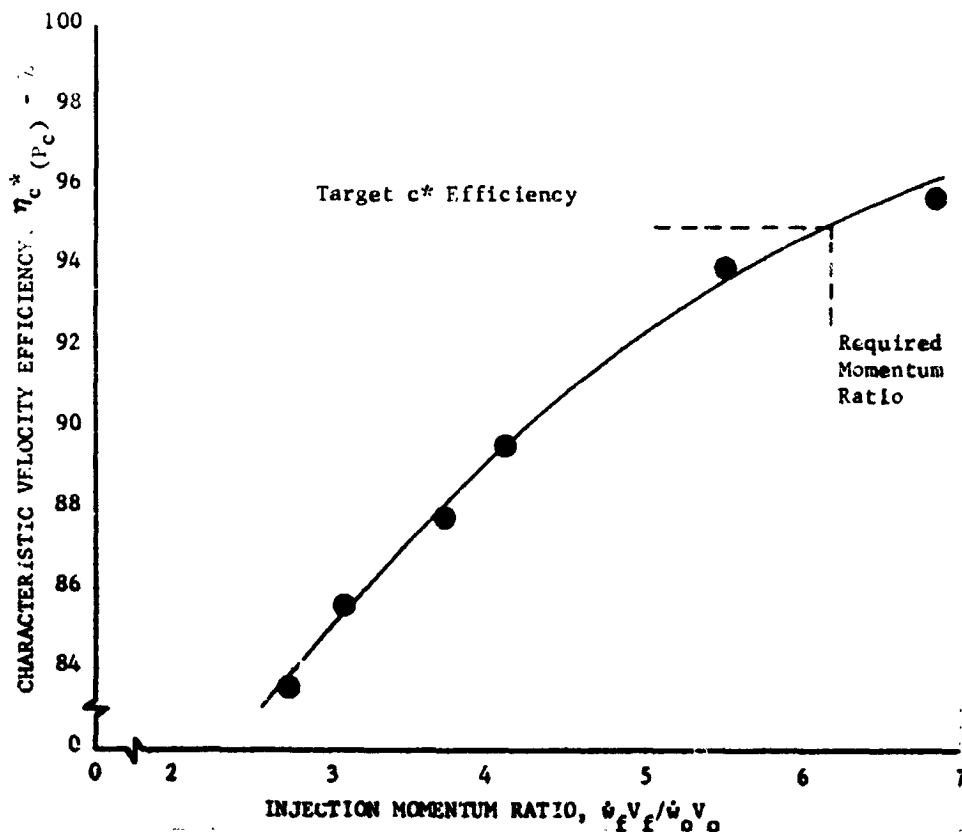
Figure 12. Variation in Characteristic Velocity Efficiency With Injection Momentum Ratio (Injector S/N HK 707)

DF 69051

It was not considered practical to attempt the incorporation of 0.004-inch gap fuel annuli in an RL10 injector. Because the face of the injector is conical, the installation of a finite thickness fuel plate incorporating such small clearances is impossible without distorting the oxidizer spuds. In addition, uneven thermal growth during est operation could cause the clearance space at some spuds to be closed for at least a portion of the circumference, with loss of cooling in the areas of contract and resulting spud tip erosion. This latter phenomena was noticed to some extent in injector S/N HK 707 with 0.008-inch fuel gaps. The injector was in generally good condition following 11 tests for a total of 35 seconds, but spuds touched the Rigimesh face at a few locations, and minor tip erosion was noted. The post-test condition of the injector is shown in figure 13. The carbon deposits on the Rigimesh face are typical. Because further modification of RL10A-1 type injectors was not practical, attention was directed to the A-3 type. This effort is described in paragraph b following.

Typical Hotspots
Caused by
Tangent Spuds
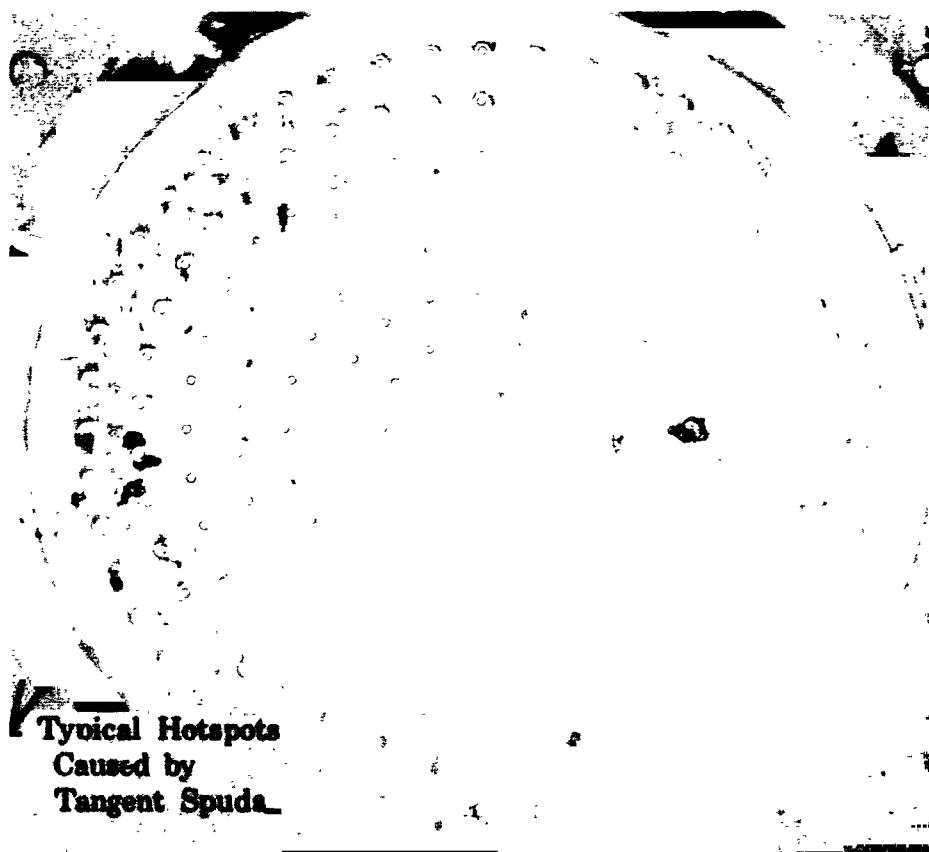
Figure 13. Injector S/N HK 707 After Test No. 1 -USL   *FD 16051A*

An important effect noted during the initial test series was that of flox mixture composition on performance. The method of flox mixture preparation at FRDC is described in Appendix A. Flox mixtures were

made in batches by weight and, for the initial firings, samples were taken for analysis during propellant transfer operations immediately preceding testing. The samples were retrieved and analyzed following the test. One of the two batches used in testing of the A-1 injectors was found to be of 77% rather than 82.6% concentration when analyzed; the other batch contained 82.4% fluorine. Figure 14 displays c* efficiency vs mixture ratio for injector S/N HK 707 for each of the two flox concentrations. There is an obvious difference in performance and further, there is a 2% difference in c* efficiency at the optimum mixture ratio for each concentration (5.5 for 77% and 5.7 for 82.4% fluorine). To provide better control of concentration for further tests, sampling at both the time of mixing and prior to test was instituted, and a tolerance of ±0.5% on the 82.6% concentration was specified for all mixes.
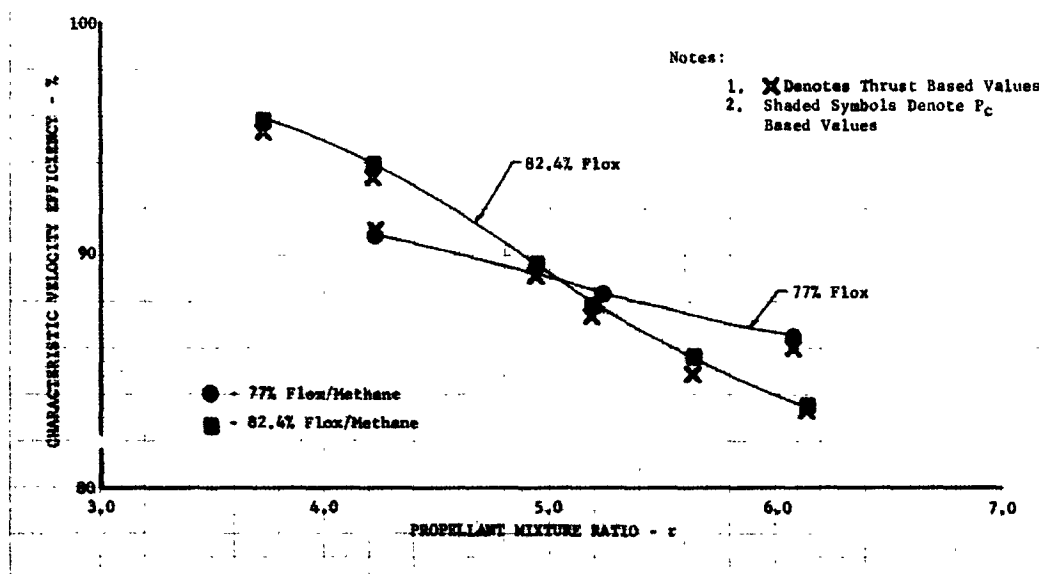
Figure 14. Comparison of Injector S/N HK 707 Characteristic Exhaust DF 69052
Velocity Efficiencies at Different Flox Concentrations

One other result worthy of note can be seen in figure 14. The uncooled thrust chambers had low expansion ratio ($\epsilon_e = 3.25$), 15-degree half-angle nozzles for which the thrust coefficient could be calculated with confidence and for which any chemical kinetic effects could be neglected. It was, therefore, possible to calculate c* efficiency from thrust measurements as well as chamber pressure measurements. Values calculated both ways are included in the plot, and the excellent agreement between them is obvious. This confirms the validity of measurements and of the method of calculating combustion momentum losses.

b. RL10A-3 Type Injectors

Five RL10A-3 type injectors, serial numbers IF 764, RY 14, IF 763, 3K 2945, and AAF 11, were tested. As in the instance of the RL10A-1 type injectors, fuel injection gap widths were varied. In addition, numbers of swirlers, swirler design, and radial mass flow and mixture ratio distribution were varied. Changes were made progressively and, in accordance with the minimum change restriction, were limited in each step to the items felt necessary to achieve performance and durability.

(1) Injector Development

(a) INJECTOR S/N IF 764

For the first RL10A-3 type injector, the Bill-of-Material oxidizer swirlers were replaced with 0.010-inch thick twisted stainless steel ribbons having straight axial extensions, as shown in figure 11. The swirlers were inserted from the rear of the spud plates and fixed in place by tack welding the ends of the extensions at the spud entrances. As in the oxygen/hydrogen units, swirlers were installed in the intermediate rows only. The inner concentric row of six elements was retained without change; the orifices of the outer row elements were drilled to the same diameter as the intermediate rows (0.085-inch). In view of the fact that a performance improvement was expected because of the improved atomization and mixing provided by the swirlers, and to avoid possible durability problems, fuel gap widths were increased over those of A-1 injectors S/N HK 713 and HK 707. The gaps were sized to provide uniform, mixture ratio distribution and therefore varied from row-to-row to match the different types of oxidizer elements (table IV).

Injector IF 764 was subjected to five uncooled pressure-fed thrust chamber tests to obtain data over a mixture ratio range from 4.35 to 5.79. The condition following test was considered excellent as shown in figure 15*. The only variance noted was minor erosion on some of the straight passage outer row spuds; the intermediate spuds containing swirlers were in excellent condition.

Performance data obtained indicated that at the desired mixture ratio of 5.75, the c* efficiency provided by the injector would be between 90 and 91%. This represented a significant gain over the performance of the A-1 type injector, but was still below the 95% target, so a necessity for further changes was indicated.

---

* Following test, the injector was retained in its modified condition. It was used in the first engine test conducted to check out stand modifications and, as described in Section III, was damaged because of an oxidizer inlet shutoff valve malfunction.
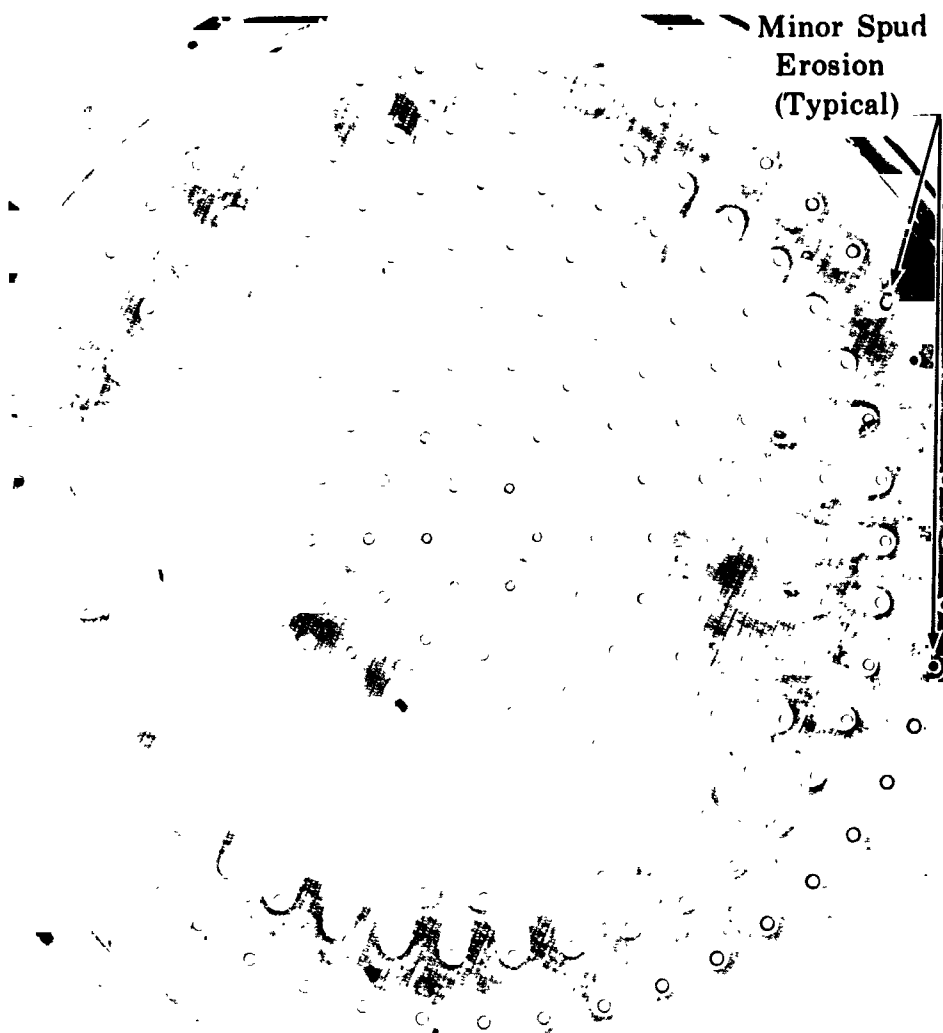
Figure 15. *Injector S/N IF 764 After Uncooled Testing*   FD 29199

(b) INJECTORS S/N RY 14

To achieve even further performance improvement over that realized with S/N IF 764, swirlers were installed in the outer as well as intermediate rows of injector S/N RY 14, and the innermost row of six elements was eliminated. The swirlers used in the outer row were two turns per inch, rather than five turns per inch, to reduce the spray angle so that oxidizer would not impinge on the thrust chamber wall. The outer row oxidizer orifice diameters were increased to improve the mass distribution uniformity, but the extent of this modification was limited because of modifications previously made to this injector during its use in the oxygen/hydrogen development program. The outer row fuel gaps were decreased to 0.012-inch diameter to provide a uniform mixture ratio profile.

41

Injector S/N RY 14 had been reoperated frequently during use in the RL10 oxygen/hydrogen engine development program, and apparently some of the reoperations compromised its integrity. Because of this, the injector was damaged during its two flox/methane tests and the results were nonrepresentative.

(c) INJECTOR S/N IF 763

Injector S/N IF 763 was initially modified (IF 763-1 in table IV) to include the same features as RY 14, but the outer row oxidizer orifice diameter was increased to improve radial mass flowrate distribution, and fuel annulus widths were reduced to 0.009 to improve mixing. The part sustained damaged in its first two tests (1-CA and 2-CA), and, during subsequent repair, 0.037-inch thick nickel swirlers with the same numbers of turns per inch were substituted for the 0.010-inch thick stainless steel parts used originally. The injector was designated IF 763-2 after the second change.

The injector was subjected to three tests in pressure-fed cooled chambers after its first modification. In the first two tests, the chamber was overcooled, i.e., the jacket flow was in excess of regenerative flow and a portion was discharged overboard at the jacket discharge while the required amount was passed through the injector. The test arrangement is described in Appendix A. Control problems aggravated by the excessive volume of the coolant jacket for methane resulted in chamber damage during the start transients and both tests were limited to a few seconds duration. The tests were sufficiently long, however, to reveal a problem of swirler durability.

Swirler damage was typically found at the three outer rows of elements. In most cases the swirlers were completely missing. They were consumed by reactions as indicated by traces of carbon deposited on the backplate and spudplate in the area of damage, as shown in figure 16. It is conjectured that, during transients, combustion products back-flowed into the oxidizer dome through outer row spuds causing swirler reactions. The products of the reactions were expelled from the oxidizer cavity through the next two adjacent inner rows of spuds, causing damage to the swirlers in those rows. The backflow problem persisted even though a high pressure-high volumetric flowrate helium purge was added at the oxidizer manifold.

With 0.37-inch nickel swirlers substituted for the 0.010-inch thick stainless steel swirlers, injector S/N IF 763 was tested in a pressure-fed cooled thrust chamber with separate cooling. The separate cooling scheme, which is also described in Appendix A, is one in which liquid coolant is supplied to the jacket at any desired flowrate and gaseous fuel is supplied to the injector. Difficulties were encountered in the single test conducted

42

and thrust chamber damage resulted for reasons that will be explained in later paragraphs. The injector was also damaged, but, even though spud erosion occurred, the nickel swirlers were intact. The nickel swirler design was therefore retained in future units. Although the extent of testing of injector S/N IF 763 was limited because of the problems noted above, sufficient data were obtained to indicate that it provided a significant improvement, somewhat over 2%, in c* efficiency, over S/N IF 764.

Figure 16. Deposits on Spudplate as a Result of Swirler Reaction   *FD 29200*

(d) INJECTOR S/N 3K 2945

Injector S/N 3K 2945 duplicated the revised (nickel swirler) configuration of S/N IF 763-2 except that more conservative (larger) fuel gaps were used, 0.015 in intermediate rows and 0.012 in the outer row. A faceplate having one-half the standard scfm porosity was incorporated so that a greater percentage of the fuel would be injected through the fuel gaps. This was done to maintain the momentum ratio as high as possible with the larger gaps.

Injector S/N 3K 2945 was tested in the engine system and was damaged as a result of the coolant transient surge problem encountered. However, evidence of a spud tip erosion problem was noted and it was decided to institute a change to correct it in the next unit.

(e) INJECTOR S/N AAF 11

The change made in injector S/N AAF 11 to overcome spud tip erosion was to change the oxidizer spudplate material from stainless steel to nickel. It was expected that nickel would provide the necessary durability at elevated

temperatures in the fluorine environment. Nickel swirlers 0.037-inch thick were used as they were in S/N IF 763-2 and S/N 3K 2945. Two configurations of the injector are shown in table IV, S/N AAF 11-1 and S/N AAF 11-2. After the initial tests of S/N AAF 11-1, signs of nonuniform heat flux were evident from the carbon formation on the thrust chamber wall. To minimize any effects of possible oxidizer stream misdirection, 26 0.010-inch diameter fuel holes were drilled near the outer circumference of the injector face in suspect areas. In addition, outer row fuel annuli were electro-discharge machined to increase the gap in the outer semicircle from 0.015 to 0.020 inch. The identification was changed to AAF 11-2 after this change.

The change to nickel in the spudplate provided excellent durability, as evidenced by the fact that the injector was in like-new condition following seven engine firings (E-3 through E-9) for a total of 134 seconds at mixture ratios that reached as high as 6.8 for short periods. A post-test photo of the injector is presented in figure 17. There was no damage to either the swirlers or the spuds, even though, as can be seen in the photograph, there were some uncarboned areas of the faceplate near several elements, which indicated contact between the spud and the faceplate. In injectors with stainless steel spudplates, premature spud erosion would surely have resulted.
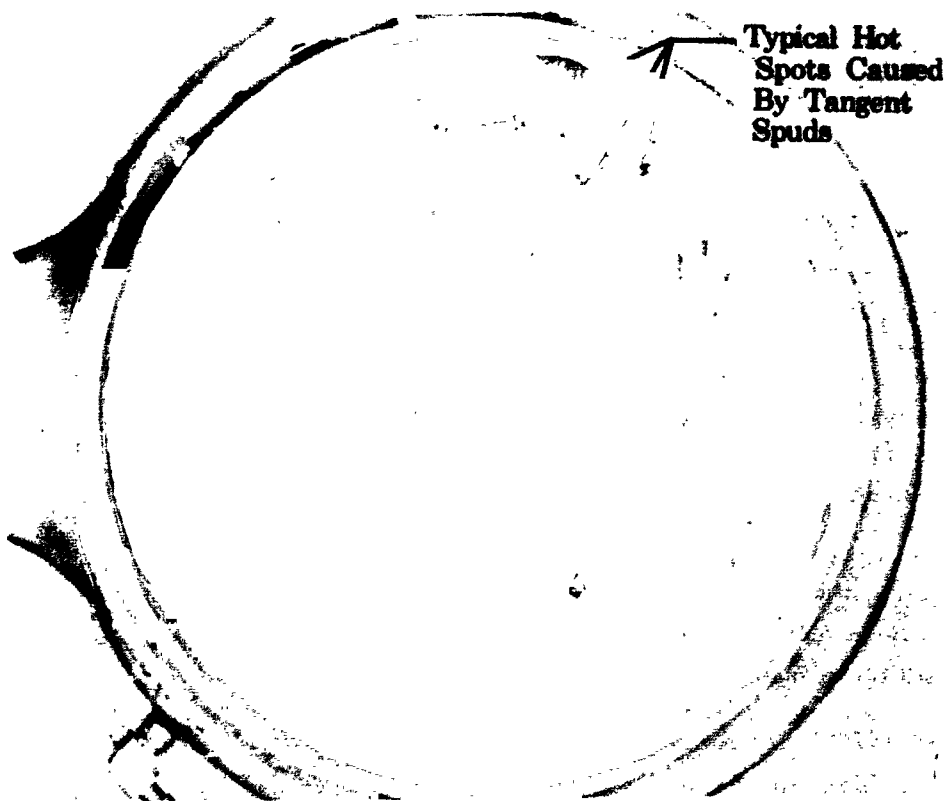
Figure 17. Injector S/N AAF 11 After Six Engine Firings   FD 29198

3. PERFORMANCE SUMMARY

a. Characteristic Exhaust Velocity

Characteristic exhaust velocity efficiency data for the injectors tested are summarized ir figure 18. The performance improvements realized by progression from the A-1 injector (S/N HK 707) to an injector with swirlers in intermediate rows (S/N IF 764), 'nd finally to swirlers in all rows (S/N IF 763 and AAF 11) are at once obvious. The lower performance of injector AAF 11 compared to IF 763 is attributed to the larger fuel gaps it contained, which reduced momentum ratio. One data point is shown for injector S/N RY 14 and, although the gap widths for it and S/N AAF 11 were similar (table IV), a significant difference in performance was noted between them, with S/N RY 14 providing much lower efficiency. This difference is attributed to uneven mass flow distribution in injector S/N RY 14. The mass flow per unit area distributions of injectors IF 763 and AAF 11 were tailored to be radially uniform for high efficiency. In the case of injector S/N RY 14, the area mass flow in the outer row was 22% less than the mass flow of the inner rows. The radial variations of mass flow per unit area determined from water flow calibration of those three injectors are compared in figure 19.

As can be seen in figure 18, the performance efficiency of all injectors decreased with increasing mixture ratio. Unfortunately, the data obtained with the highest performance injectors was limited to low mixture ratios; however, the plot of absolute characteristic exhaust velocity level in figure 20 shows that injectors S/N IF 763 and S/N AAF 11 both demonstrated peak characteristic velocities at low mixture ratios that were above 95% of the maximum theoretical (i.e., at r = 5.75). The extrapolated efficiency of injector AAF 11 was above 95% at a mixture ratio of 5.75.
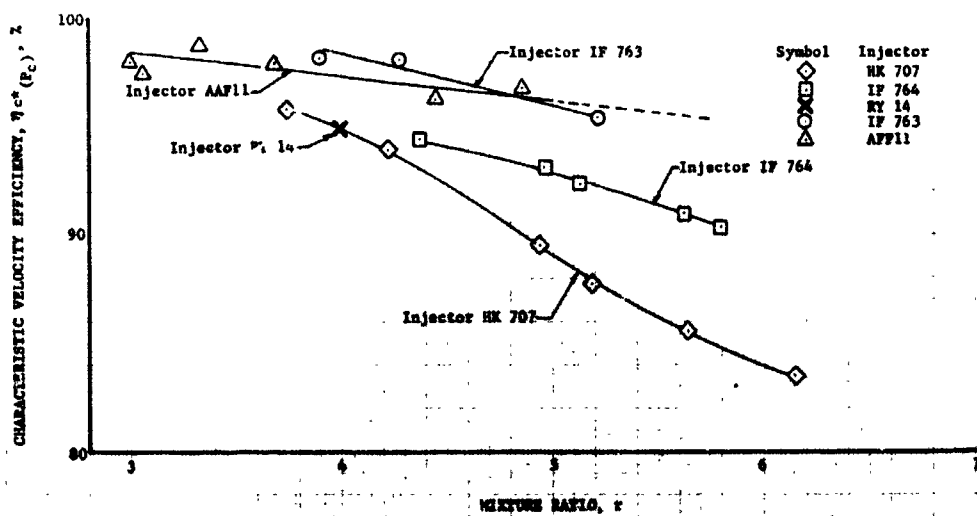
Figure 18. Charactcristic Exhaust Velocity Efficiency Summary   DF 69112
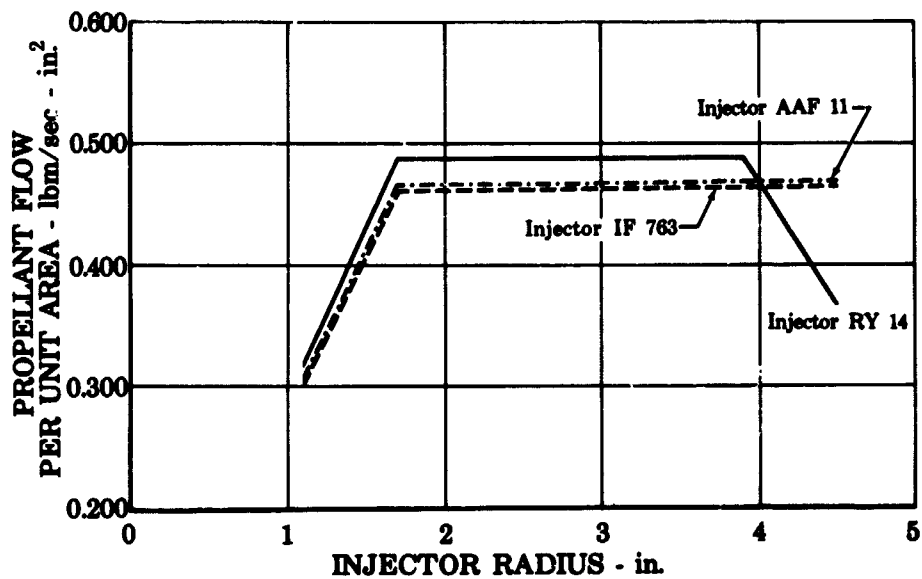
Figure 19. Variation in Injector Mass Flow Distribution (Based   FD 25710
on Water Flow Calibrations)
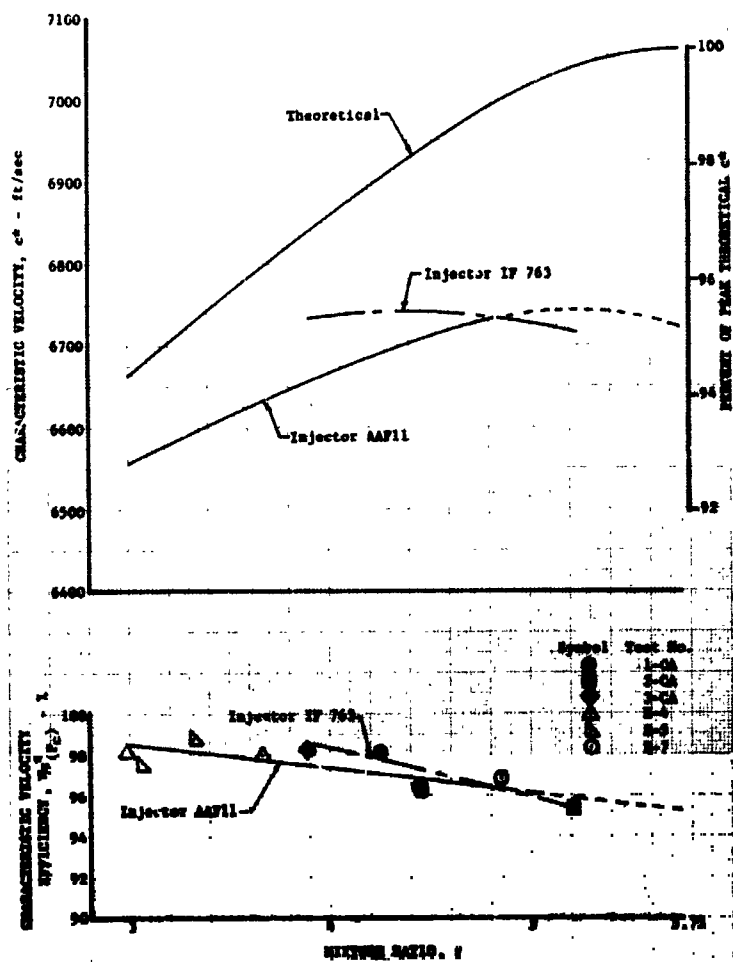
Figure 20. Characteristic Exhaust Velocities, Injectors S/N IF 763   DF 69065
and S/N AAF 11

b. Vacuum Specific Impulse

Figure 21 displays the vacuum specific impulse efficiency obtained with the two highest performing injectors. The absolute value of impulse that these efficiencies would provide when referenced to the standard normal boiling point liquid propellant inlet conditions is also shown. Both injectors produced maximum impulse at a mixture ratio below the theoretical optimum. Based on the standard propellant inlet conditions, the maximum specific impulse demonstrated with the area ratio of 40 nozzles was 384 seconds (injector S/N IF 763).
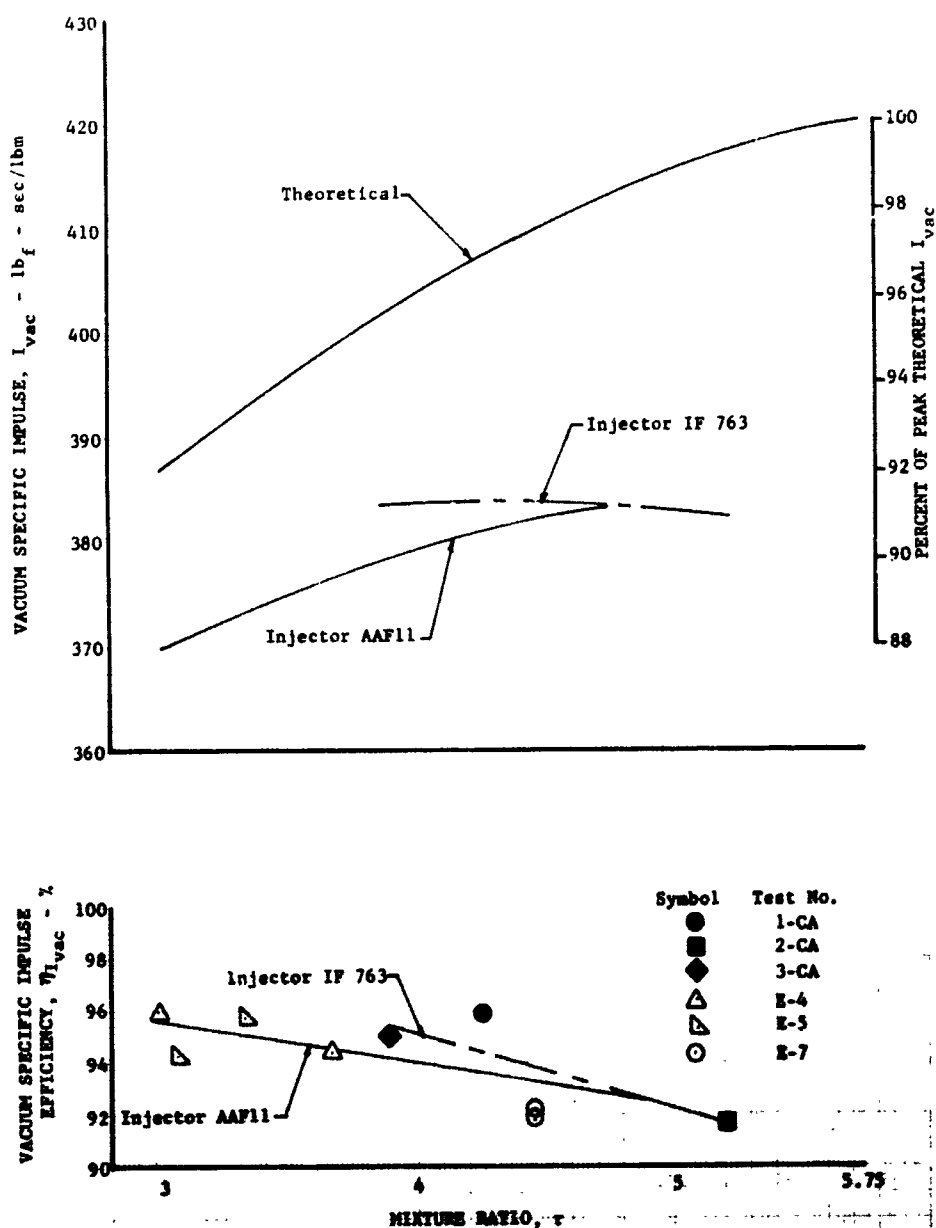
Figure 21. Vacuum Specific Impulse, Injectors S/N IF 763 and S/N AAF 11   DF 69064

Vacuum thrust coefficient efficiencies for the thrust chamber are presented in figure 22. The dropoff that occurs with increasing mixture ratios is a.tributed to two phenomena: (1) kinetic losses, and (2) a decrease in the theoretical C_F due to mixture ratio variations within the exhaust gases. Theoretical thiust coefficient losses due to kinetics have not been calculated for flox/methane at the conditions of the tests. Low chamber pressure flox/methane data (References 2 and 3) indicated that the kinetic losses predicted by the present methods are from three · five times higher than the experimental losses. A NASA funded program (Reference 5) is now in progress at the United Aircraft Corporation Research Laboratories to identify the important rate limited reactions and to generate a correlation with available experimental data. With respect to mixture ratio variations, the possibility of C_F efficiency losses because of nonuniform mixture ratio profiles was established in Reference 6, but the magnitude of such losses cannot be determined without specific knowledge of the mass flow-mixture ratio distribution.
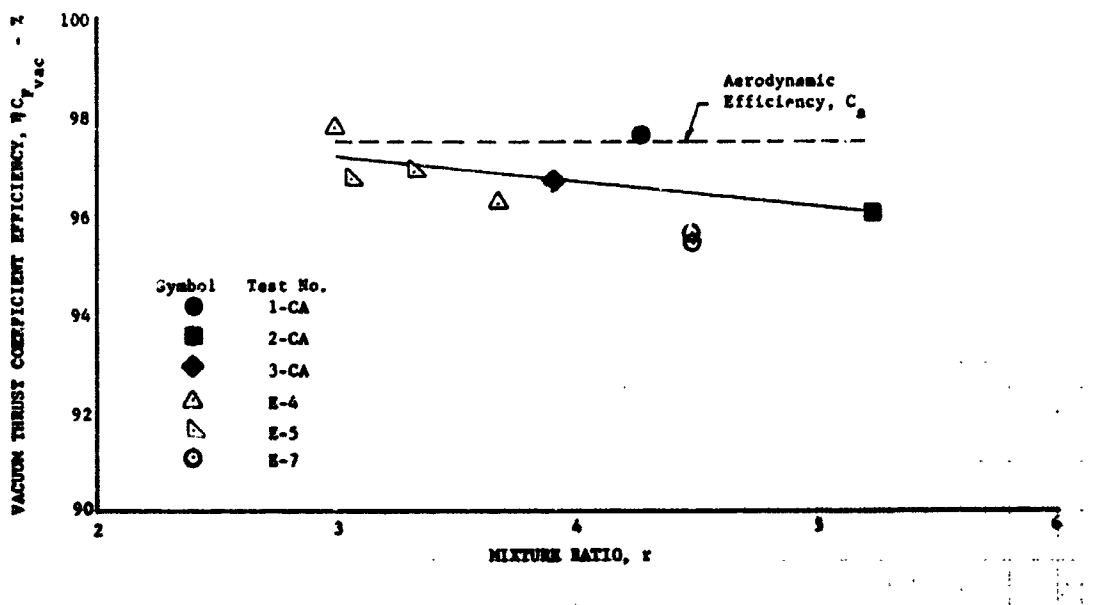
Figure 22. Experimental Vacuum Thrust Coefficient Efficiency   DF 68970

C. THRUST CHAMBERS

Because of the large density differences between hydrogen and methane, it was recognized that cooli g passage modifications would be required to permit operation of RL10 thrust chamber with regenerative cooling in flox/methane demonstration test engines. However, experience in testing with flox and light hydrocarbon fuels under Contracts NAS3-4195 and NAS3-62f6 had shewn that actual heat fluxes would vary from theoretika'

values because of carbon deposition on thrust chamber walls. Therefore, initial injector evaluation tests were made in instrumented uncooled thrust chambers to obtain experimental heat flux data before modification of the cooled thrust chambers was attempted.

Significant reductions from theoretical heat flux levels because of carbon deposition were found in uncooled thrust chamber testing, but wide circumferential variations were noted. Therefore, a conservative approach was dictated for the modification of cooled thrust chambers. Cooled chambers were modified to improve cooling in areas shown by analysis to be critical, and were tested. However, transient problems that caused tube failures were encountered in both pressure-fed thrust chamber and pump-fed engine tests. Thrust chamber damage was encountered consistently until additional changes were made to reduce coolant jacket volume in areas where the basic design was satisfactory from a heat transfer standpoint. The steps that led to the development of a suitable thrust chamber configuration are described in the following paragraphs.

1. UNCOOLED CHAMBERS

a. Test Hardware

Three series of uncooled pressure-fed tests were conducted using heat sink copper thrust chambers with low-expansion ratio nozzles. The copper thrust chamber assembly consisted of three major components, a chamber, a circumferential instrumentation ring, and an adapter ring. An exploded view showing the parts is presented in figure 23.

The chamber section was machined from high purity oxygen-free copper and consisted of an RL10 contour combustion section and a 3.25 expansion ratio, 15-degree half-angle conical nozzle. A constant wall thickness of 0.75-inch was selected to provide an acceptable combination of run duration capability and thermocouple response. Instrumentation on the chamber section initially consisted of one longitudinal row of 28 chromel-alumel thermocouples embedded in outer surface, but for the third series of uncooled tests two rows of circumferential outer wall thermocouples were added. These were used to obtain circumferential profile data near the throat. Thermocouples were distributed as shown in figure 24. The axial spacing was established based on expected temperature gradients, closest spacing being used in the region where highest thermal gradients were expected. This was done so that heat flux profiles could be determined with accuracy using an inverse two-dimensional conduction calculation procedure. To provide the adiabatic boundary condition assumed in the calculations, the chamber was wrapped with fiberglass insulation.
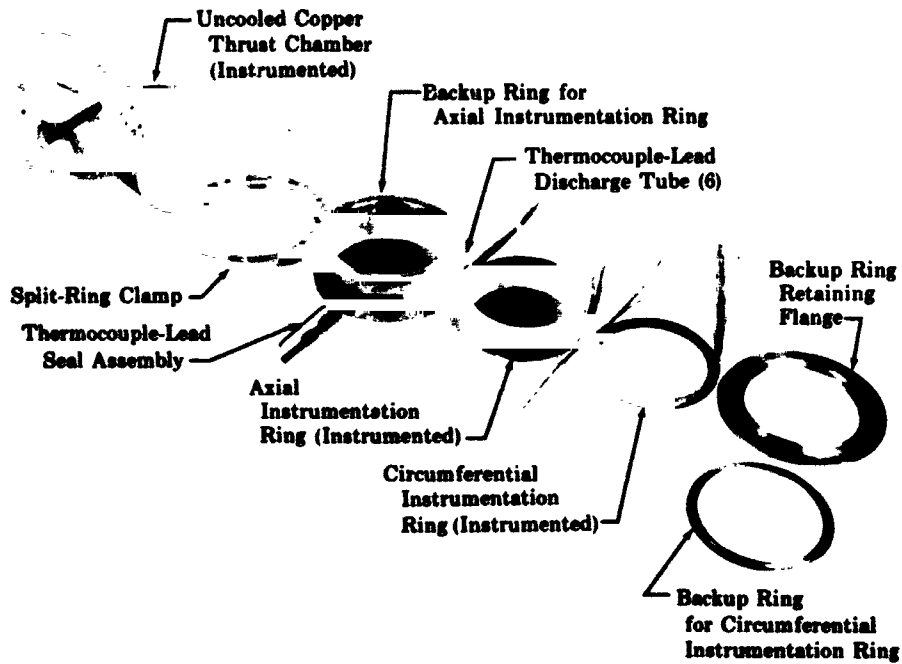
Figure 23. Exploded View of Uncooled Copper Thrust Chamber and   FD 15710
          Instrumentation Ring Assembly
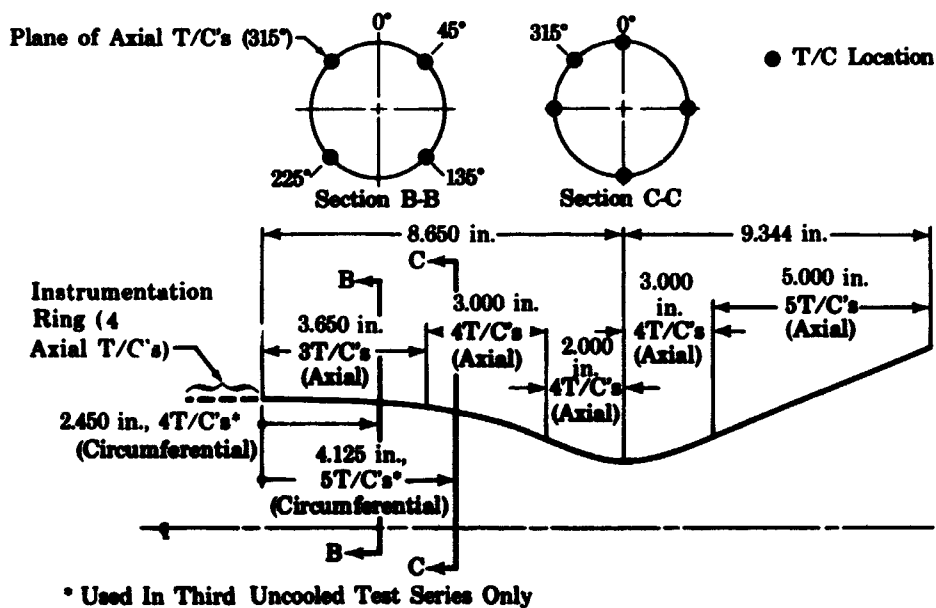
Figure 24. Location of Axial and Circumferential Skin Thermocouples   FD 15518C
          on Uncooled Thrust Chamber

The instrumentation ring was installed next to the injector so that the circumferential heat flux profile at that station could be determined. It was fabricated from high-purity oxygen-free copper and contained 48 isolated segments for which radial one-dimensional heat flux could be determined. Thirty-one of the segments were equally spaced over a 90-degree arc and seventeen were distributed equally over remaining circumference as shown in figure 25. The segments were created by milling pairs of 0.375-inch deep slots the length of the ring (0.50 inch) to isolate sections 0.26-inch wide. The machined segments were insulated circumferentially from one another and axially from the adapter ring with spacers fabricated from a silica glass fiber phenolic-resin laminate. A chromel-alumel thermocouple was installed in each segment, 0.12-inch from the inner surface of the ring, to provide the temperature data required for heat flux determination.
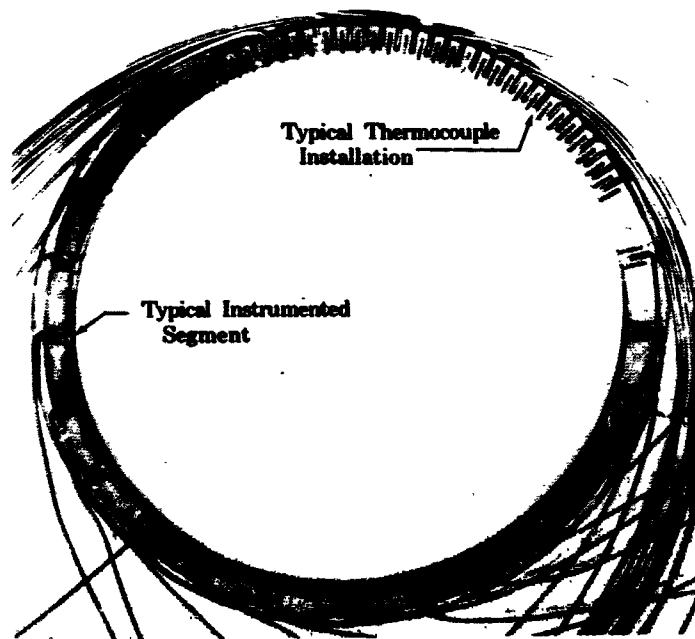
Figure 25. Circumferential Instrumentation Ring   FD 17380A

The adapter ring was provided to permit assembly of the instrumentation ring to the injector and thrust chamber. As shown in figure 26, it consisted of an inner copper cylinder that contained axially spaced thermocouples to provide continuity of longitudinal thermal data from the circumferential instrumentation ring to the chamber, and an outer steel backup ring with attaching flanges.
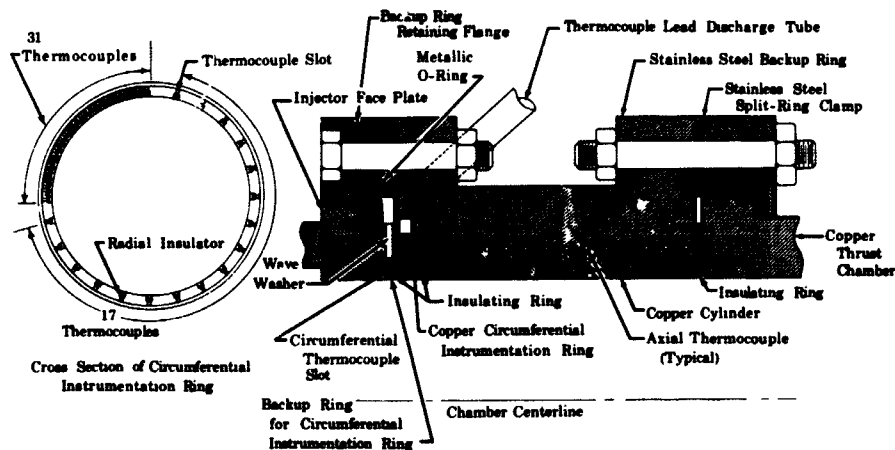
Figure 26. *Arrangement of Circumferential Instrumentation*   *FD 14535C*
            Ring and Adapter

b. Test Experience

Twenty sea-level exhaust tests (d‹ ⁿ ted 1-USL through 20-USL in Appendix D) were made with the uncooled thrust chamber. Two RL10A-1 type injectors (S/N HK 713 and S/N HK 707) and two RL10A-3 type injectors (S/N IF 764 and S/N RY 14) were used in the testing. After all tests a characteristic carbon layer was deposited on the chamber walls and injector faceplate. Figure 27 shows the deposits on the chamber after the last uncooled test series.

Figure 27. *Carbon Deposits in Uncooled Thrust Chamber*   *FE 64994*
          After Test Series No. 3

52

c. Heat Transfer

Longitudinal heat flux profiles and combustion side wall temperatures were calculated from experimental time-temperature data at the chamber outer surface using inverse two-dimensional transient conduction equations. The method used in processing uncooled thrust chamber data is presented in Reference 7. Data obtained from the circumferentially-instrumented ring (one dimensional heat flux) were treated as a special case of the two-dimensional application.

Combustion side film coefficients predicted using the Bartz short form (Reference 8) are compared with experimentally-determined longitudinal film coefficients in table XI. The experimental film coefficients in the combustion section were consistently between 20 and 50% of the predicted values, with the maximum film coefficient occurring at, or slightly upstream of, the throat. A graphic comparison of predicted and experimentally determined longitudinal film coefficients obtained with injector S/N IF 764 for three different mixture ratios is presented in figure 28.
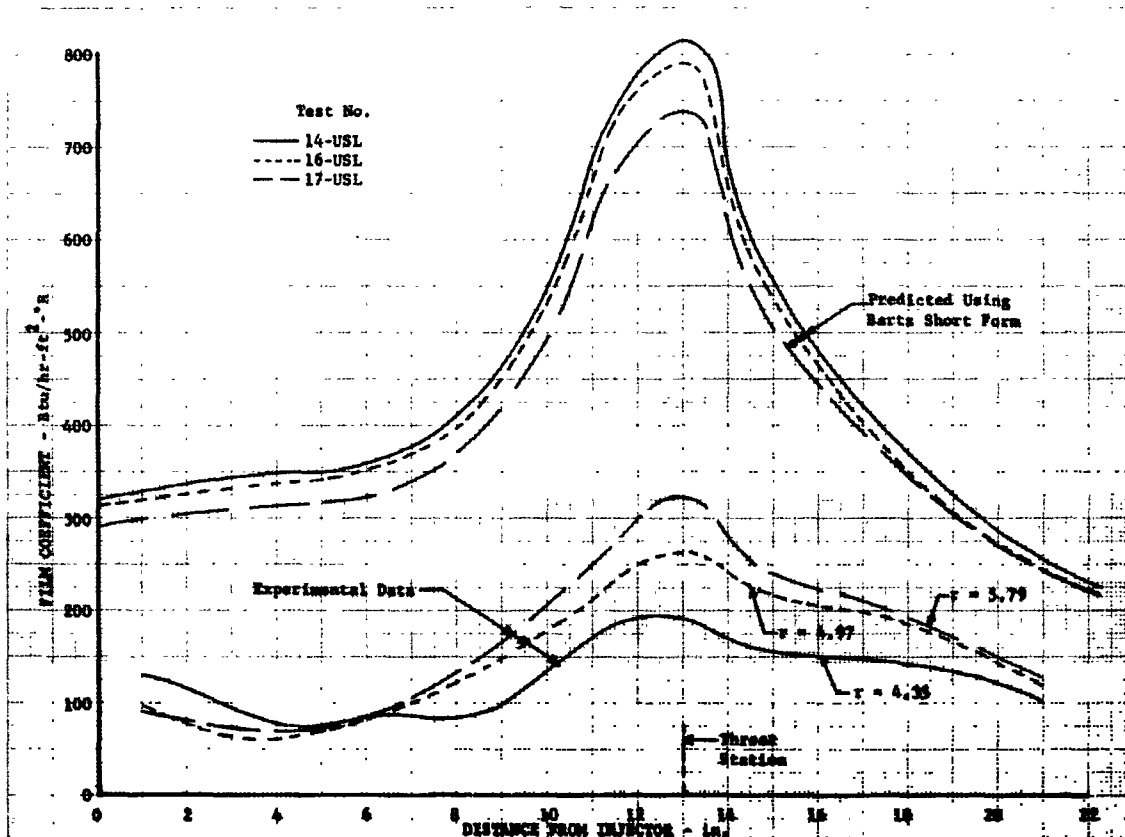
*Figure 28. Comparison of Measured and Experimental Heat Flux   DF 69053
            For Injector S/N IF 764*

TABLE XI. COMBUSTION-SIDE EXPERIMENTAL AND THEORETICAL FILM COEFFICIENTS

1* - Experimental film coefficients derived from rest data (Btu/hr-ft²-°R)

2* - Theoretical film coefficients derived from Bartz short-form analysis (Btu/hr-ft²-°R)

3* - Data not available; thermocouple not utilized, or erroneous instrumentation.

TABLE XI. COMBUSTION-SIDE EXPERIMENTAL AND THEORETICAL FILM COEFFICIENTS (CONTINUED)

1* - Experimental film coefficients derived from rig test data (Btu/hr-ft²-°R)

2* - Theoretical film coefficients derived from Bartz short-form analysis (Btu/hr-ft²-°R)

3* - Data not available; thermocouple not utilized, or erroneous instrumentation.

Figure 29 shows the circumferential heat flux variation measured with two injectors, S/N HK 707 and S/N IF 764, each at a mixture ratio near the theoretical optimum of 5.75. Although the coefficients determined from circumferential instrumentation in the radial plane of the longitudinal thermocouples agree favorably with the values obtained from the longitudinal instrumentation (within 4%, 107 to 103 btu/hr-ft²-sec), a circumferential variation of nearly 100% was found for both injectors.
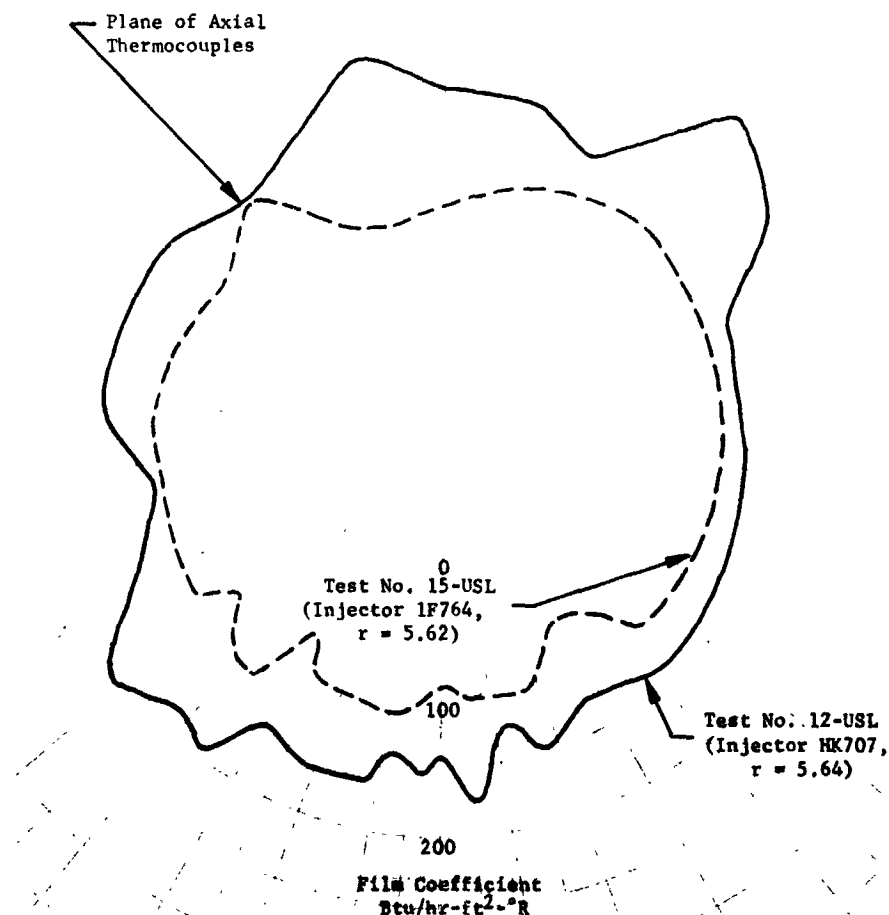
Figure 29. Circumferential Heat Flux Variation in Uncooled Chambers: DF 69061
Data Taken 1.08 Inches from Injector Face

2. COOLED CHAMBERS

Extensive heat transfer analyses of the RL10 thrust chamber operating with flox/methane were made to identify possible problem areas so that suitable modifications could be incorporated. Experimental heat flux data from uncooled tests were taken into account, and experimental results from independently conducted methane heated tube tests were used to determine coolant side coefficients. (See figure 30.)
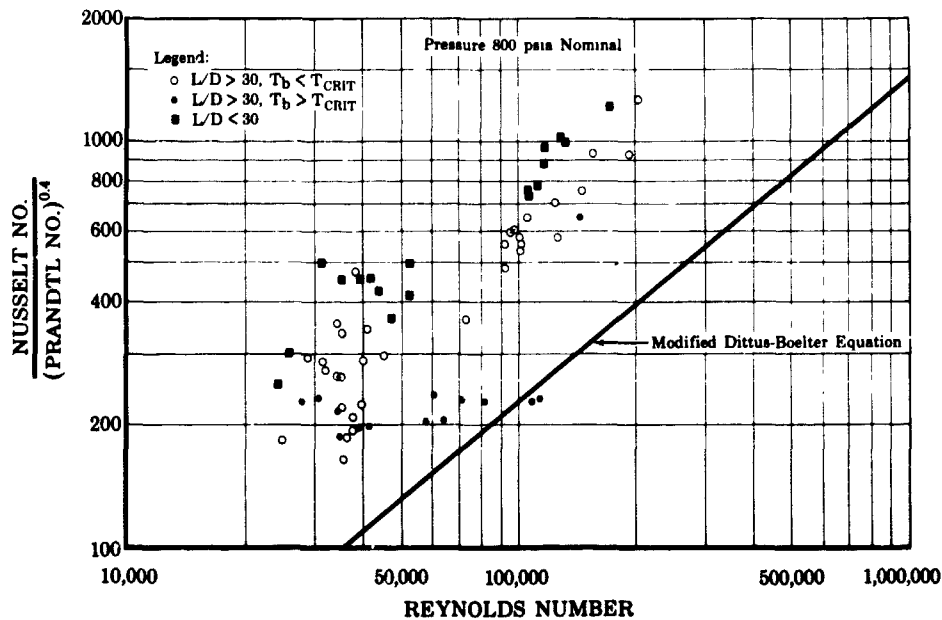
Figure 30. Results of Methane Heated Tube Tests at Supercritical Pressure   FD 12554

The combustion side film coefficients determined experimentally in uncooled tests were significantly below theoretical, and calculations based on those coefficients indicated that the chamber could be adequately cooled without modification. However, the large circumferential variations indicated that values approaching the Bartz coefficients could reasonably be expected to occur. A conservative approach was warranted, and therefore the initial modifications were based on analyses using the theoretical combustion coefficients. The modifications are discussed after the following brief description of the basic thrust chamber.

a. Chamber Description

As depicted in figure 31, the RL10 thrust chamber is an assembly consisting of 180 "long tubes" and an equal number of "short tubes." The long tubes extend from the injector to the exit plane. The short tubes are interleaved between the long tubes in the nozzle at a point approximately one-third of the distance from the throat, and extend to a turnaround manifold at the nozzle exit. The jacket inlet manifold is located at the start of the short tubes. During engine operation, fuel enters the short tubes at the inlet manifold and flows parallel to the exhaust gases to the turnaround manifold. Then it enters the long tubes and flows counter to the exhaust gases to the collector manifold, where it is routed to the turbine.

The tubes have a wall thickness of 0.013 inch and are fabricated from AISI 347 stainless steel tubing. The long tubes are "double-tapered" and the short tubes are "single-tapered." In the "double-tapered" long tubes, the tube diameter increases progressively from the throat section to either

end, giving the tube a venturi shape. The "single-tapered" short tubes increase in diameter from the part inlet manifold to the nozzle exit section. The chamber is formed by furnace brazing the tube bundle and a reinforcing jacket is used to strengthen the combustion chamber and throat region. The dimensions of the chamber are shown in figure 32.
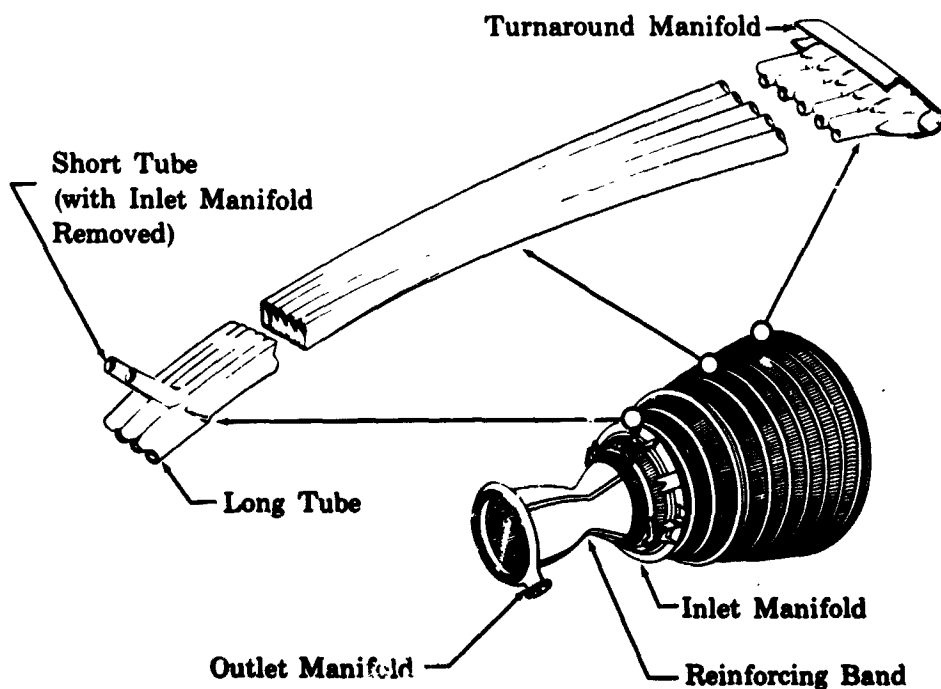
Figure 31. RL10 Thrust Chamber Configuration   FD 25671
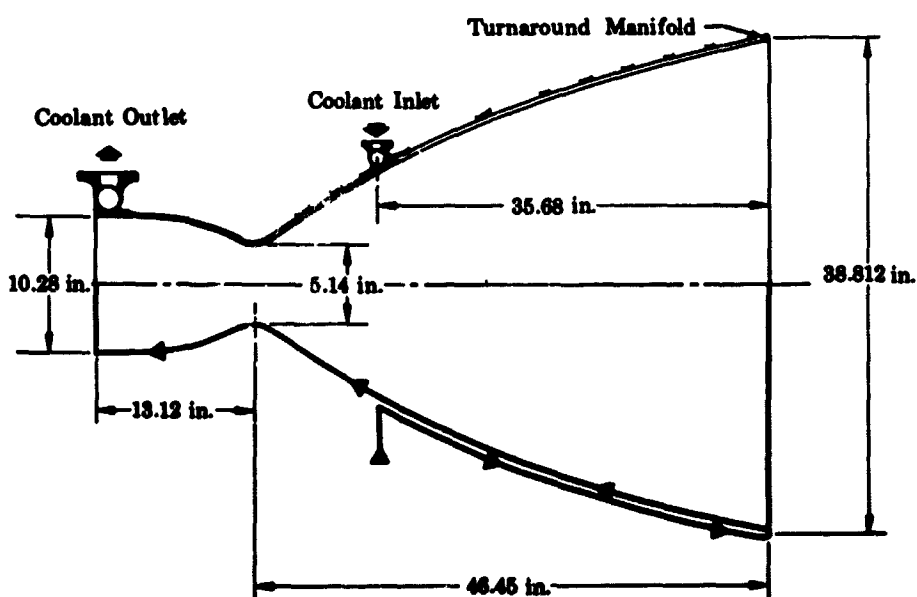
Figure 32. RL10 Thrust Chamber Contour   FD 25658

b. Modifications

Analyses indicated that there were two potential failure areas in the RL10 thrust chamber it it were to be tested with flox/methane without modification: (1) in the long tubes at the transition section where a tube cross-section area increase is necessary to compensate for the termination of the short tubes; and (2) in the combustion region near the injector. In both of these regions coolant velocities were too low to provide film coefficients adequate for local heat fluxes. Two different modifications were tried in each of these regions as described below.

(1) Transition Area Modifications

The first modification tried in the transition region was applying a high-conductivity silver-braze material to fill the root area between tubes The filler material provided a conduction path into the root zone to reduce crown temperatures. The calculated effect of braze addition on tube wall temperature distribution is shown in figure 33. The diagram on the left shows wall temperature isotherms predicted in the transition region in the Bill-of-Material configuration. The diagram on the right shows the predicted temperature distribution with braze addition. A reduction of crown temperature from 2492 R to 1630°R was indicated by calculations, but in actual application it was found that the filler braze was subject to erosion and that other techniques for modification were required.
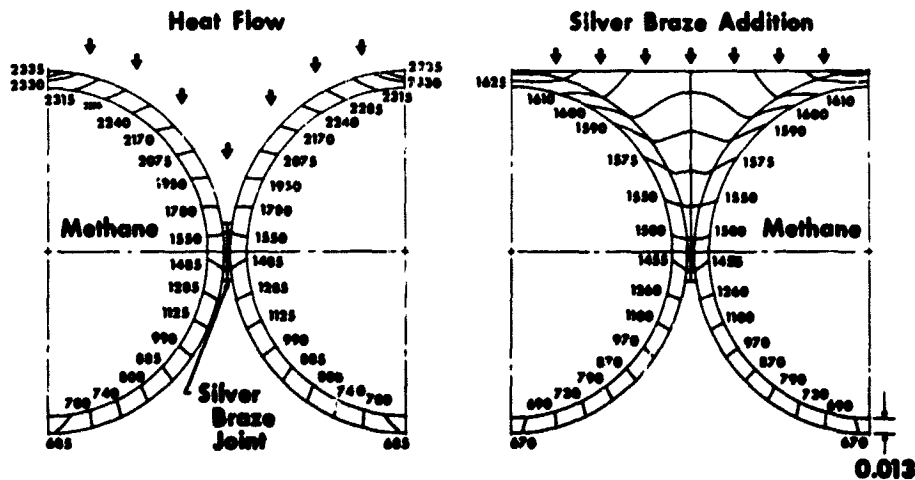
Figure 33. Effect of Filler Braze on Temperature Distribution in Tube Walls   GS 7905

The second and more effective modification in the transition region consisted of incorporated cooling fins in the long tubes. The fins were 9-inches long and were fabricated from 0.060-inch thick stainless steel. They were welded into the tubes to radially bisect the tube flow area, and a small pressure equalizing gap was left at the outer crown. A sketch show-

58

ing the modification is presented in figure 34. This alteration improved tube durability in three ways: (1) the coolant side film coefficient was increased because of the higher coolant velocities caused by the flow area blockage; (2) the heat transfer rate to the coolant was increased because of the larger conduction area provided by the fins; and (3) hoop stress at the tube crown was reduced because of the increased wall thickness produced by the welding operation.
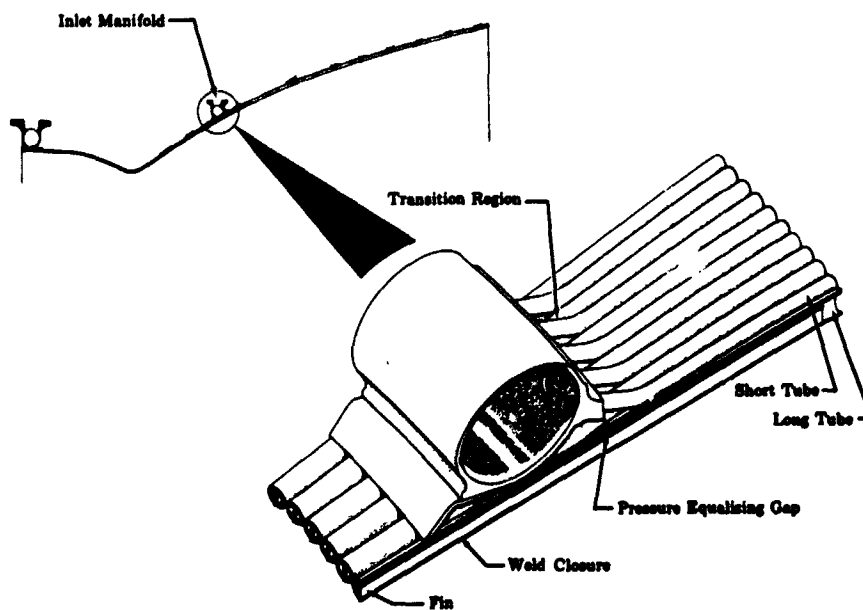
Figure 34. Fin Installation in RL10 Chamber Nozzle   *FD 23713*

(2) Combustion Chamber Modifications

The first modification used in the combustion chamber region consisted of installing twisted copper inserts in the tubes to reduce coolant flow area and increase the coolant side film coefficient. The inserts were installed through holes drilled in the coolant discharge manifold, and were held in place by stainless steel extensions that were welded to the outlet manifold. (See figure 35.) The inserts were fabricated from 0.090-inch square copper bar stock, which was twisted to assure that there would be no extended areas of direct contact with the tube wall. The length of these inserts was varied between 3 and 8 inches in different thrust chambers. In two chambers, the insert length was extended to 11 inches by the addition of smaller diameter copper wire.

The second, and more effective, combustion area modification involved the use of fins similar to those used in the transition region. The fins extended from the discharge manifold to a point 1 inch upstream of the throat (for a total length of 11.2 inches). They were fabricated from 0.060-inch thick stainless steel plate and were of the appropriate height to

provide the same blocking area as the inserts. Thus, in addition to providing the same coolant velocity as the inserts they produced further improvements due to the fin conduction and the increased wall thickness.

The use of silver braze filler was also tried in the combustion chamber area of a number of chambers, but operational problems resulted in damage to those chambers and the utility of the approach was not established.
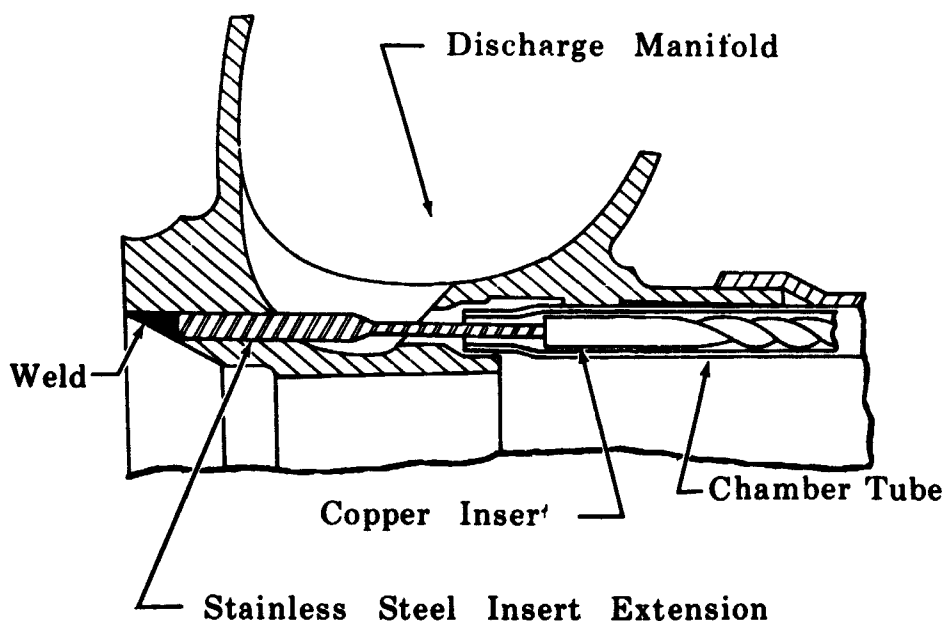
Figure 35. Tube Insert Installation in Combustion Chamber   *FD 18413A*

c. Chamber Instrumentation

A number of coolant bulk temperature thermocouples were installed in the modified cooled thrust chambers tested to provide additional data on heat transfer. Typical coolant tube thermocouple installations are shown in figure 36. Because the thrust chambers were completed assemblies as received, installation of the thermocouples was difficult and the number used was limited accordingly.

d. Test Experience

Three over-cooled pressure-fed thrust chamber tests and nine pump-fed engine tests were made using five thrust chambers, one of which was modified twice. Modifications incorporated in the various units are summarized in table XII.
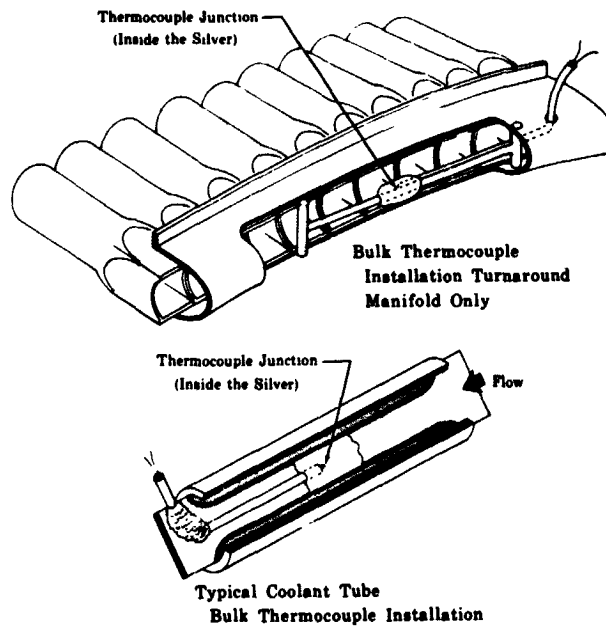
Figure 36. Thermocouple Installation in Cooled Thrust Chamber   FD 12881C

TABLE XII.   COOLED THRUST CHAMBER MODIFICATIONS

Test No.	Chamber S/N	Cooling Mode	Modifications
1-CA, 2-CA	KD 115	Supplemental Cooled	8-inch inserts in tubes of combustion section. Silver braze in tube transition area.
3-CA	HF 318	Separately Cooled	11-inch inserts in tubes of combustion section. Silver braze in tube transition area.
E-1	JP 97	Regenerative (Engine)	3-inch inserts in tubes of combustion section. Fins in long tube transition area.
E-2	JP 88	Regenerative (Engine)	3-inch inserts in tubes of combustion section. Fins in long tubes of transition area.
E-3	JP 42	Regenerative (Engine)	11-inch inserts in tubes of combustion section. Silver and nickel plating in combustion area. Fins in long tube transition area.
E-4 through E-9	JP 88	Regenerative (Engine)	Rebuilt with 11-inch fins installed in tubes of combustion section. Fins in long tube transition area. 26-inch long rods inserted in all nozzle tubes.

61

(1) Pressure-Fed Tests

The first two pressure-fed tests of cooled thrust chambers were made in supplementary cooled mode, i.e., liquid fuel in excess of the amount required for combustion was fed to the cooling jacket. The excess coolant was bled overboard after passing through the cooling jacket with the remainder being supplied to the injector. Control system difficulties experienced in those tests resulted in chamber damage. Prior to the third pressure-fed test, the system was modified to supply the injector from a separate source and thus eliminate the need for two control valves downstream of the cooling jacket. This scheme provided satisfactory control. However, during the steady-state portion of the test, 17 tubes failed in the transition region, permitting the coolant flow to be diverted from the combustion section cooling tubes into the nozzle and causing damage to the tubes in combustion section. Detailed analysis of the affected area in the transition region revealed the failure to be a result of the high coolant flow, which allowed low coolant temperatures to be maintained well into the low area ratio portion of the nozzle.

Figure 37 shows the effect of coolant temperature on wall margin* in the failed area. Because the pressure at the failure point was not directly measured, the margins are presented for both the jacket inlet and outlet pressure levels. Thermocouple data indicated that with the amount of overcooling used, the coolant bulk temperature at the location of failure would be dangerously close to 340°R, the point of minimum tube wall margin. The dramatic change in margin in this region of bulk temperature is due to the wide variation in coolant properties near the critical temperature (343°R). At regenerative cooling flowrates, this condition would not have been encountered because the critical region would have been traversed in the lower heat flux regions further out in the nozzle.

(2) Engine Tests

During the engine tests a severe transient cooling problem was encountered. As detailed in Section III, the relatively large internal volume of the cooling tubes allowed a significant quantity of high density methane to accumulate in the tubes during the engine start. When the chamber pressure, and therefore heat flux, increased rapidly during the transient, a large decrease in the coolant density occurred. This caused a surge or, in some cases, a complete inlet flow reversal. The reduced cooling velocities during this period resulted in tube failures.

---

* *Wall margin is defined as the difference between the predicted tube operating temperature and the temperature at which the calculated tube hoop stress equals the 0.2% yield stress of the m r'erial.*
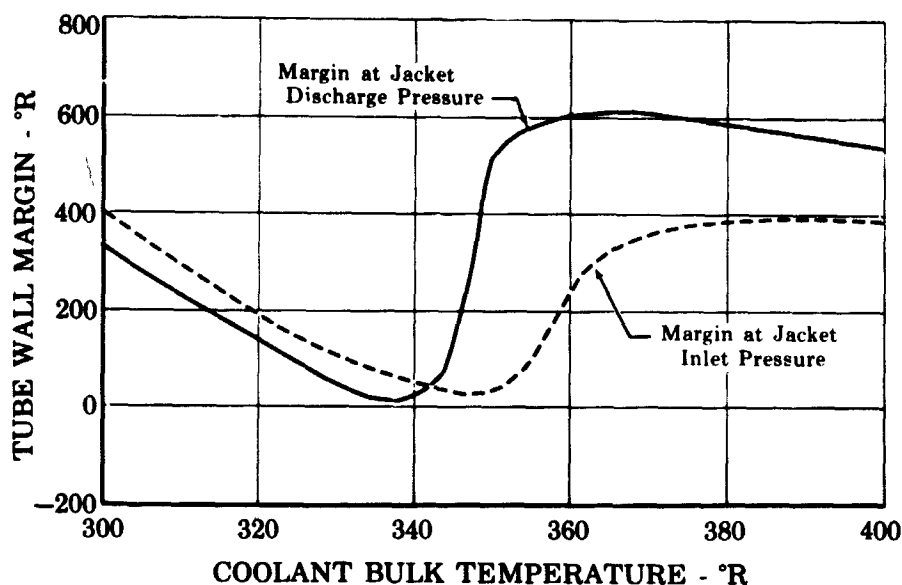
Figure 37. Predicted Variation in Tube Wall Margin With Coolant   FD 25628
Bulk Temperature at Point of Failure in Test No. 3-CA

The surge problem was resolved by a system change and a thrust chamber change in combination. The system alteration was a controls change that reduced the rate of oxidizer introduction into the chamber and therefore the rate of change of heat flux; the chamber was modified to reduce coolant tube volume as well as to improve heat transfer in the problem areas.

RL10 thrust chamber tubes, sized for hydrogen, have an aggregate internal volume of almost 0.7 ft^3. This volume is equivalent to approximately 18 pounds of liquid methane. To reduce this volume, the final chamber tested, S/N JP 88, was modified by insertin 0.187-inch diameter stainless steel rods into each of the nozzle tube . The rods were inserted through the turn-around manifold and extended 2 inches into the tubes as shown in figure 38. In addition to reducing the chamber volume by almost 25%, the additional mass of the rods provided residual heat capable of heating 4 pounds of liquid methane to 400°R (with the jacket at the temperature typically experienced at engine start). The combination of reduced chamber pressure rise-rate and reduced cha nber volume had the desired effect. The coolant flow upset was significantly reduced and it was possible to proceed with engine testing.

Because of the possible stability problems that could be encountered with bulk-boiling, the engine cycle was configured to maintain cooling jacket pressures sufficiently high so that this situation would be avoided. (Refer to Appendix C.) The jacket pressure was either maintained above the critical pressure (673 psia) throughout, or the inlet pressure was sufficiently high so that the coolant critical temperature (343°R) was exceeded at pressures above critical. Because of the change in turbine area during

test No. E-4, the engine operated with jacket inlet pressures below the critical value for about 9 seconds. No signs of instability were noted and no chamber damage was encountered. Brief periods of subcritical pressure operation were also encountered in tests No. E-7 through E-9. No coolant flow instabilities were indicated. However, the slight chamber damage existing at the start of test E-7 increased during that test. The increased damage was probably caused by the weakened condition of the chamber at the start of the test, but the possibility of tube-to-tube fluctuations due to boiling cannot be definitely eliminated. Although the lack of inlet or outlet flow instability indicated that the system was at least marginally stable with bulk-boiling, it is felt that subcritical pressure operation should be avoided unless extensive dynamic analyses are completed to assure that stability can be maintained. The work reported in Reference 3 showed that an RL10 chamber could be cooled with bulk-boiling methane; however, extensive chamber modifications were required to minimize tube-to-tube feedback.
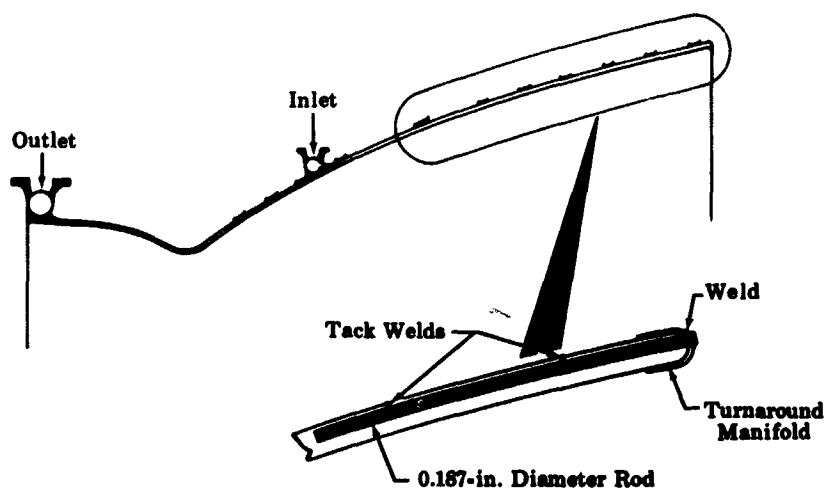
Figure 38.   Rod Installation in Chamber JP88 Nozzle   FD 25627

e.   Heat Transfer

Because of the limited amount of detailed information that could be obtained, heat transfer analyses for the cooled thrust chambers consisted primarily of comparing the experimental coolant energy rise profile to that predicted using theoretical gas film coefficients. Figure 39 compares the coolant energy rise determined from coolant bulk temperature measurements with the theoretical rise based on two different percentages of the Bartz coefficients, 250% in the nozzle region downstream of the inlet manifold and 25% in the regions upstream of the inlet manifold.

Reviewing the data obtained, it was found that the overall coolant energy rise (heat transfer rate) was approximately 90% of the theoretical value. The experimental value is based on inlet and outlet manifold temperatures and thus provides an integrated average value for the thrust chamber. The 10% reduction is slightly less than that measured in flox/ methane tests at low chamber pressure (100 psia) as reported in References 2 and 3.

The unique indication of figure 39 is that the heat transfer rate downstream of the transition region is approximately 2.5 times higher than the theoretical value. Based on the data from test 3-CA, in which the thrust chamber was most extensively instrumented, approximately 80% of the heat transfer occurred in the nozzle downstream of the throat. While the bulk temperature thermocouples used were subject   ome conduction errors because of the method of installation, and there were also circumferential heat flux variations, these factors could not reasonably explain a difference of this magnitude This result is also substantiated by the fact that when the high indicated value of nozzle heat transfer is subtracted from the well defined overall heat transfer rate, the resulting chamber heat flux is shown to be about 25% of theoretical, which compares favorably with that calculated using experimental film coefficients obtained in the uncooled tests.
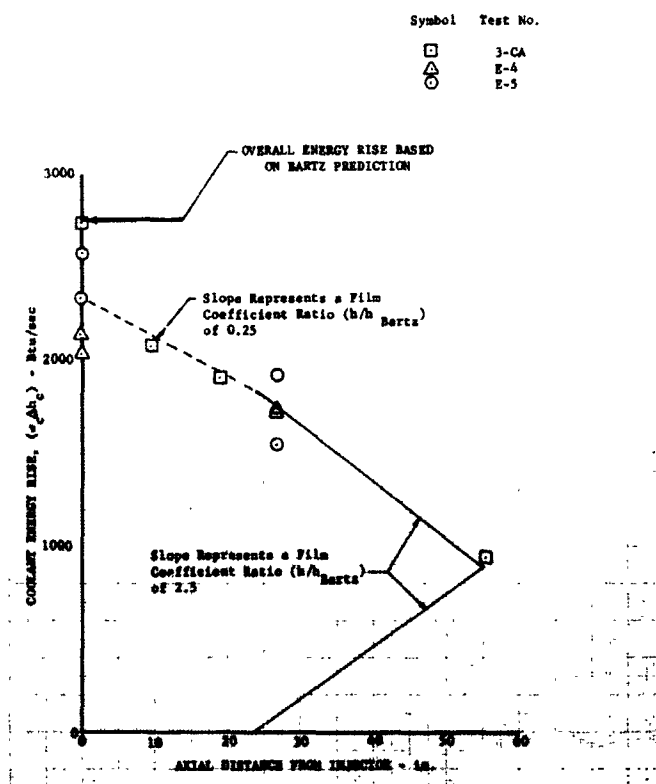
Figure 39. Coolant Energy Rise   *DF 68969*

SECTION V

TURBOPUMP MODIFICATION AND TEST

A cut-away sketch of the RL10A-1 turbopump is presented in figure 40. The assembly consists of a two-stage centrifugal fuel pump mounted on a common shaft with a two-stage impulse turbine, and a single stage oxidizer pump that is gear driven from the turbine-fuel pump shaft. Changing to methane made it necessary to modify the fuel pump and turbine to compensate for the great difference in the density of the hydrocarbon fuel as compared to hydrogen (methane density is 26 lb/ft^3, hydrogen is 4 lb/ft^3). With alterations to the fuel pump and a change in gear ratio, cycle requirements could be satisfied while retaining RL10A-1 oxidizer pump geometry; therefore the only modifications required to the oxidizer pump were those necessary to achieve chemical compatibility with liquid fluorine. Fortunately, RL10A-1 oxidizer pumps modified for fluorine service in the fluorine/hydrogen propulsion system research program conducted under Contract NASw-754 were available for use in this program.

Detailed descriptions of basic configuration, modifications, and test experience with the various elements of the turbopump (fuel pump, oxidizer pump, turbine, and gear train) are presented in this section of the report.

A. FUEL PUMP

1. PUMP DESCRIPTION

The RL10A-1 fuel pump, which is mounted on a common shaft with the turbine, is a two-stage centrifugal unit with rear shrouded impellers mounted back-to-back for thrust unbalance minimization. The first-stage impeller has 50-degree swept vanes and the second-stage impeller incorporates radial vanes. A three-bladed axial flow inducer is mounted forward of the first stage impeller. Recovery of velocity head is accomplished through straight conical diffusers at the discharges of the volute collectors. The first stage volute and diffuser are contained in the fuel pump housing; the second stage impeller cavity and flow passages are located in the forward end of the gearbox drive housing. The shaft is supported by two ball bearings, one mounted between the impellers and one at the turbine end of the shaft. The bearings are not lubricated, but are cooled by fuel bled from the inlet of the second-stage fuel pump impeller. Net thrust loads are controlled by selection of pump impeller and turbine rotor disk areas.

There are four dynamic seals on the common pump-turbine shaft. All of these are of the spring-loaded face seal type with piston rings for axial sealing. The stationary nosepieces are silver impregnated carbon, rubbing on chrome plated rotating surfaces. One seal is located between the two pump impellers to prevent leakage from the second to first stage.

67

Two seals in series, with an interseal bleed back to the first stage inlet, are used between the second stage impeller inlet and the gearbox, and there is a seal between the gearbox and the turbine.
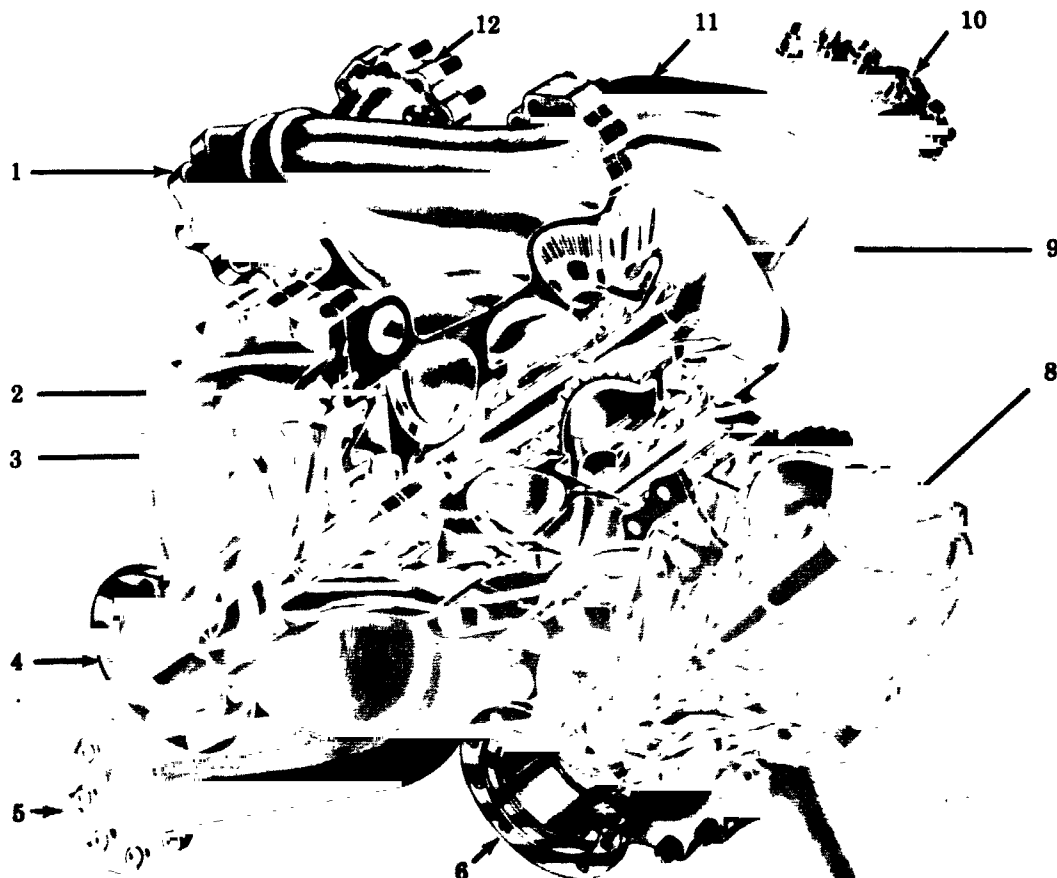
1. THRUST CONTROL MOUNT
2. 2ND-STAGE IMPELLER
3. 1ST-STAGE IMPELLER
4. FUEL PUMP INLET
5. PUMP DISCHARGE TO SECOND STAGE
6. OXIDIZER PUMP INLET
7. OXIDIZER PUMP DISCHARGE
8. MAGNETIC SPEED PICKUP
9. TURBINE
10. TURBINE DISCHARGE
11. TURBINE BYPASS FROM THRUST CONTROL
12. TURBINE INLET

Figure 40. RL10A-1 Turbopump Assembly   FD 3261A

2. *Modifications*

Because of the significantly higher liquid density of methane as compared to hydrogen, fuel pump head rise and volumetric flow requirements

for the modified engine are reduced drastically. The primary approach for meeting the revised head rise requirement with minimum effect on the remainder of the system was to reduce fuel pump diameter. However, a modest reduction in pump speed was also effected by using a reduced oxidizer pump gear ratio.

The modified pump is compared to the standard RL10 hydrogen pump in figure 41. The modified impellers were sized at 4.25 inch-diameter for both stages, based on a head coefficient of 0.495 and a shaft speed of 19,926 rpm. Filler plates were added to the bearing support to fill the voids left by the reduced diameter impellers, and thereby to' maintain smooth flow passages that would reduce possible head losses. No changes were made to the bearings, seals, or the fuel distribution system for gearbox cooling.
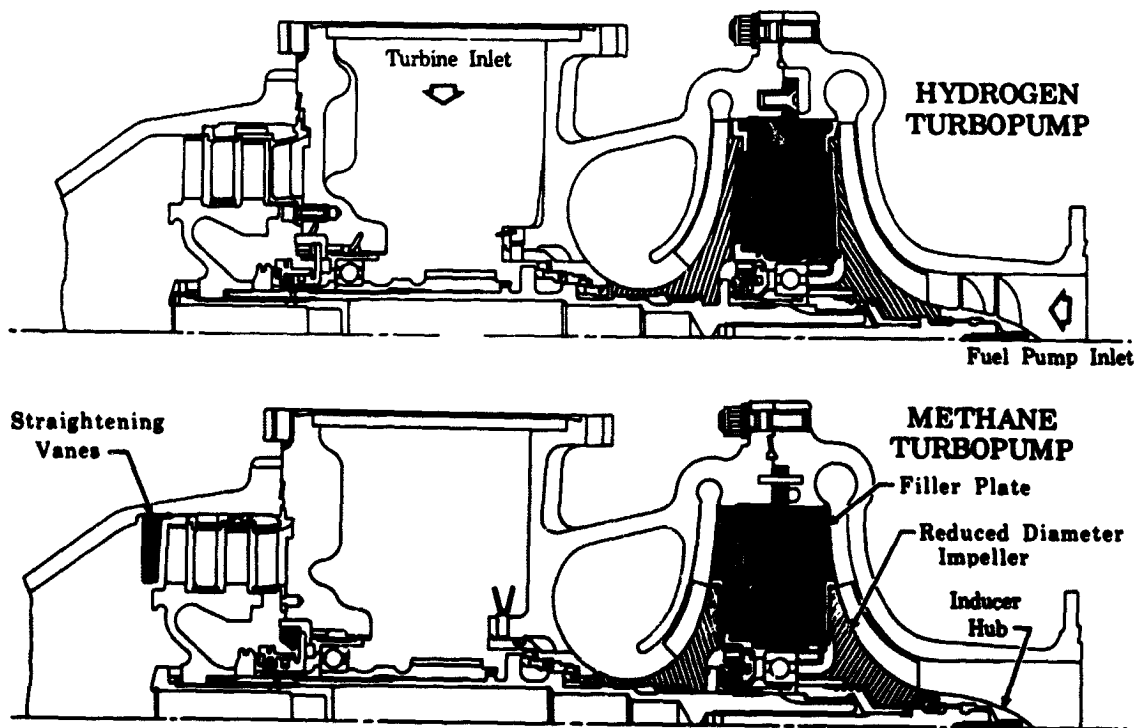
Figure 41. Comparison of Hydrogen and Methane
         RL10 Turbopump Assembly

FD 14533B

It was necessary to remove the inducer blading because of increased stress levels resulting from the increased fluid density and operation at low flow coefficients. Pump NPSH capability was affected only slightly because of the compensating effect of the six-fold reduction in pump volumetric flow. Figure 42 shows the first-stage impeller, inducer hub, and bearing support of the partially-assembled modified fuel pump.
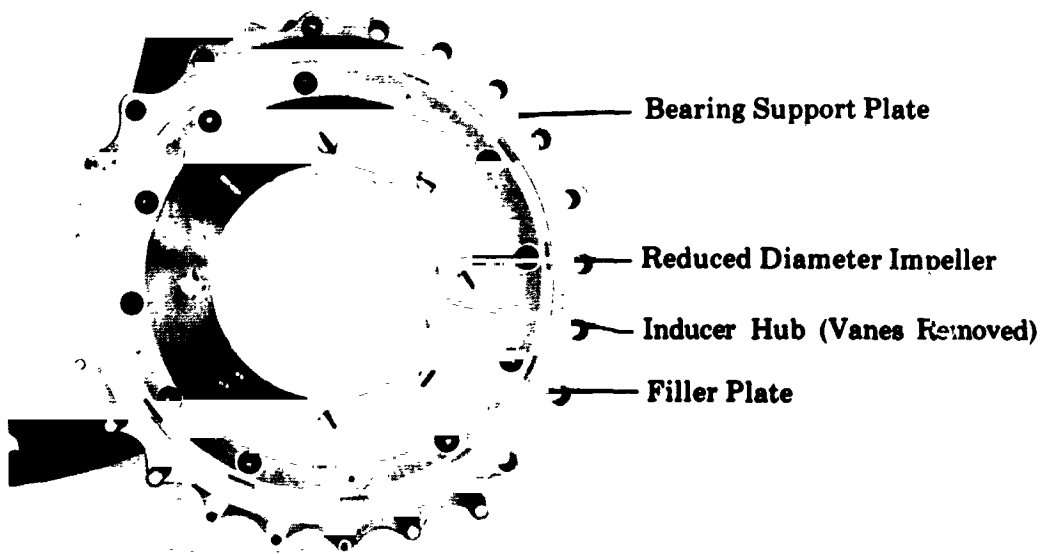
Figure 42. First Stage of Modified Methane Pump   FD 23837A

3. Testing

Preliminary data on fuel pump operating characteristics were obtained during engine cold flow tests made before the first hot firing. Figure 43 displays pump pressure rise vs flow, corrected to design point operating speed. Two conclusions were drawn from the cold flow data: (1) the head coefficient was approximately 0.55, rather than 0.495, resulting in 10% greater pressure rise than predicted; and (2) the slope of the pressure rise vs flow curve in the region of the design point was positive. Operation in regions where the pump characteristic curve has a positive slope is undesirable from the standpoint of system stability. To obtain more favorable characteristics (since excess pressure rise was available) a 0.586-in. diameter orifice was installed downstream of the fuel pump. During the last engine test series the engine cycle balance was adjusted by reducing the discharge orifice diameter to 0.495 inches (see Section III). The head/flow characteristics for the pump and orifice combinations, also presented in figure 43, show the negative slope achieved in the design point region when restrictions were added.

Fuel pump efficiencies were calculated from measurements of temperature rise across the pump made during hot firing tests. The demonstrated efficiencies are presented in figure 44. These efficiencies are in the range of 30 to 34%, or approximately 60% of the level that is predicted using Worthington similarity curves; the low efficiency is attributed to the non-

70

optimum configuration of the highly modified pump and was predicted
before testing. Pumps designed specifically for these conditions should have
an efficiency closer to the "Worthington" value.
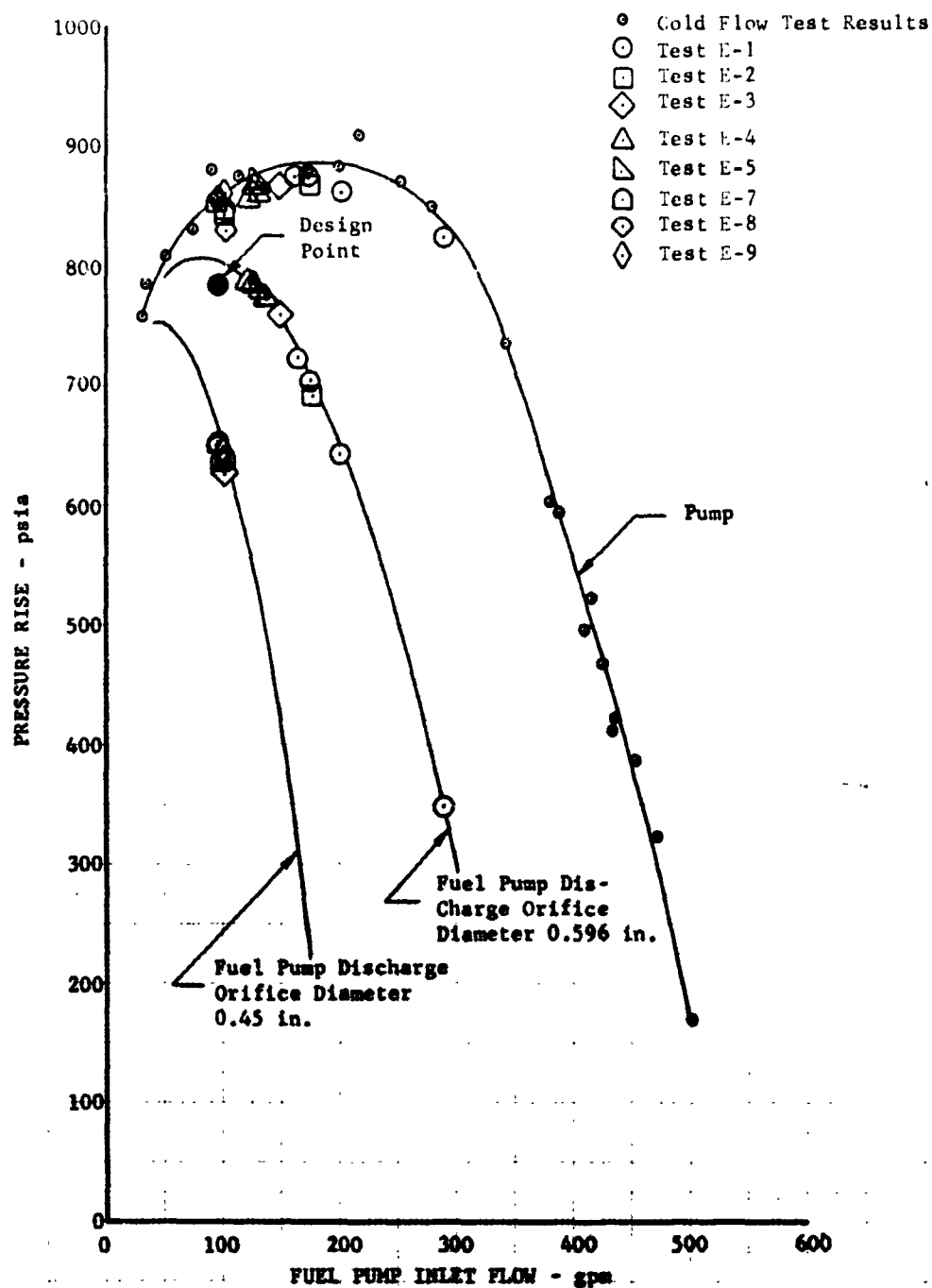
Figure 43. *Pressure Rise Characteristics of Methane Modified RL10A-1 Fuel Pump; 20,000 rpm*

DF 68972
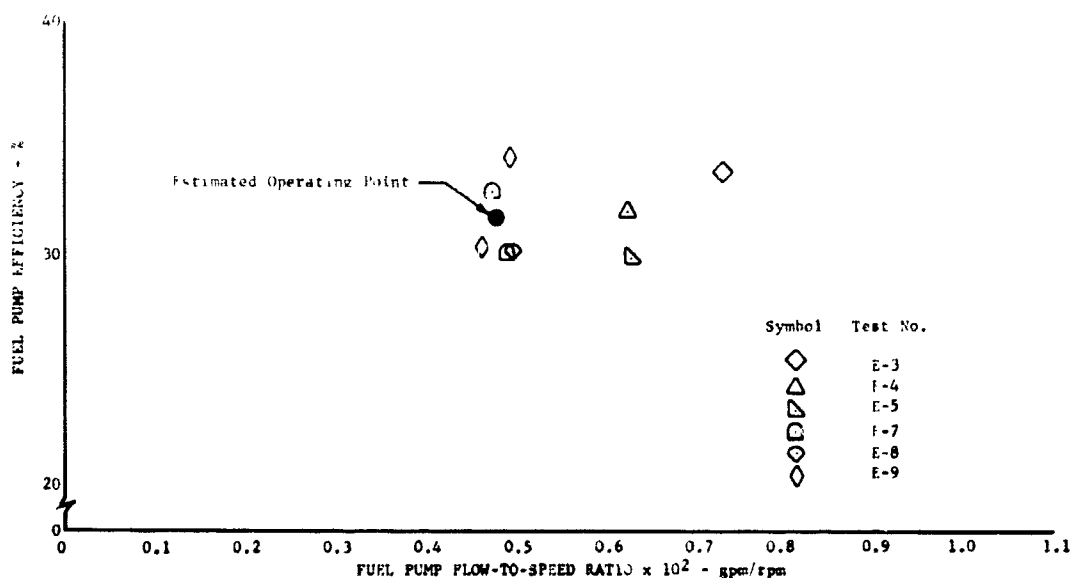
Figure 44. Variation in Efficiency With Flow-to-Speed Ratio for Methane Modified RL10A-1 Fuel Pump

DF 68971

The durability of the modified fuel pump was considered completely satisfactory. In test No. E-6 a stress failure of the inlet housing was experienced because of a pump overspeed during the start transient (refer to Section III). The increased loading of the housing resulting from impeller diameter reduction (which increased the area upon which discharge pressure acted) had been recognized, and an 850 psia limit had been estimated from the calculated housing stress and the 0.2% yield strength of the housing material at 200°R. The rupture occurred during a pump overspeed when the first-stage discharge pressure was 900 psia and therefore was not unexpected. The failure occurred in the form of a single crack emanating from the vicinity of the cutwater and extending circumferentially approximately 180 degrees around the housing. Following this occurrence, engine control modifications were made to eliminate the overspeed, and no further fuel pump malfunctions were experienced.

B. OXIDIZER PUMP

1. PUMP DESCRIPTION

Details of the RL10A-1 oxidizer pump assembly are shown in figure 45. The assembly has three main housings: an inducer housing, impeller housing, and gearbox housing. The gearbox housing flange mates the oxidizer pump to the fuel turbopump assembly which provides driving power through a reduction gear train. The pump is a single-stage centrifugal unit

72

having a fully shrouded impeller and shrouded axial inducer. Labyrinths are incorporated at the inducer shroud to minimize flow recirculation. Radial blades are used on both the front and rear impeller shrouds to reduce thrust loads on the shaft. The pump shaft is supported by a ball bearing located in the impeller housing behind the dynamic seals, and a roller bearing located in the gearbox housing. The drive gear is located between the bearings, both of which are cooled by fuel which is tapped off of the first stage housing, approximately at the midpoint of the impeller.
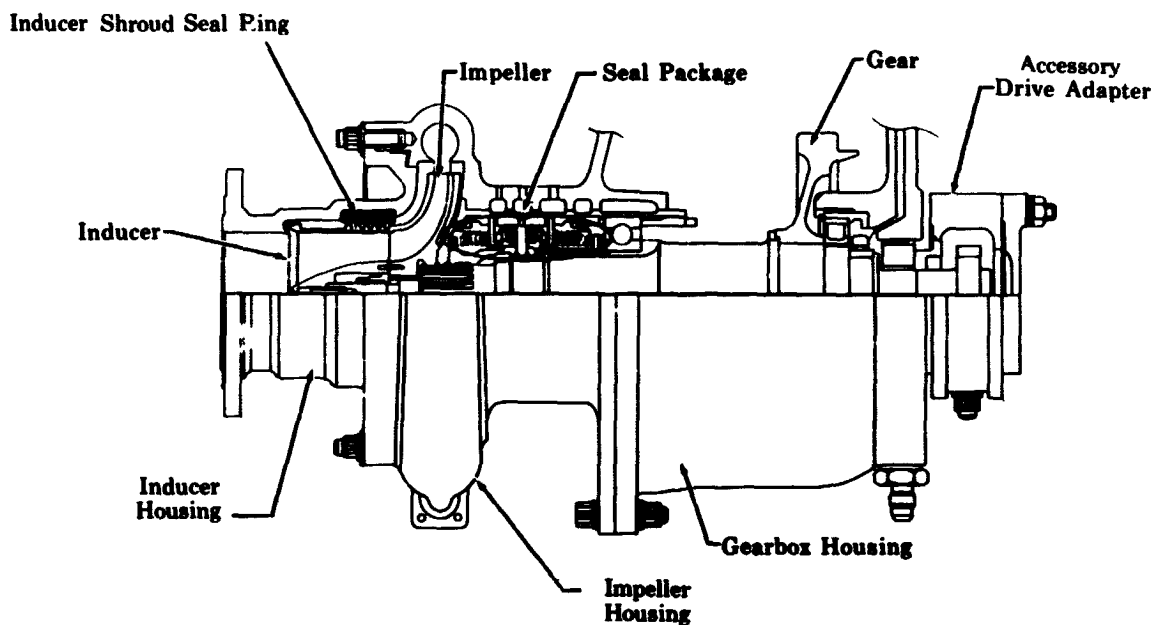
Figure 45. RL10A-1 Oxidizer Pump   *FD 11043A*

Because fuel is used to cool the gearbox, effective shaft sealing between the impeller cavity and the gearbox is mandatory. The shaft seal package used consists of four seals, two bellows type face seals and two split ring seals. These are shown more clearly in the enlarged sketch of the seal package presented in figure 46. The bellows type seals are used in the primary seal positions at both the pump and gearbox. The split ring seals are used behind the bellows types as secondary seals. Vent ports provide for overboard discharge of propellants from the cavities between primary and secondary seals at both sides. An additional port is provided in the cavity between the two secondary seals. This port is vented during flight, but low pressure (9-13 psig) helium is supplied to it to provide isolation during engine ground test.
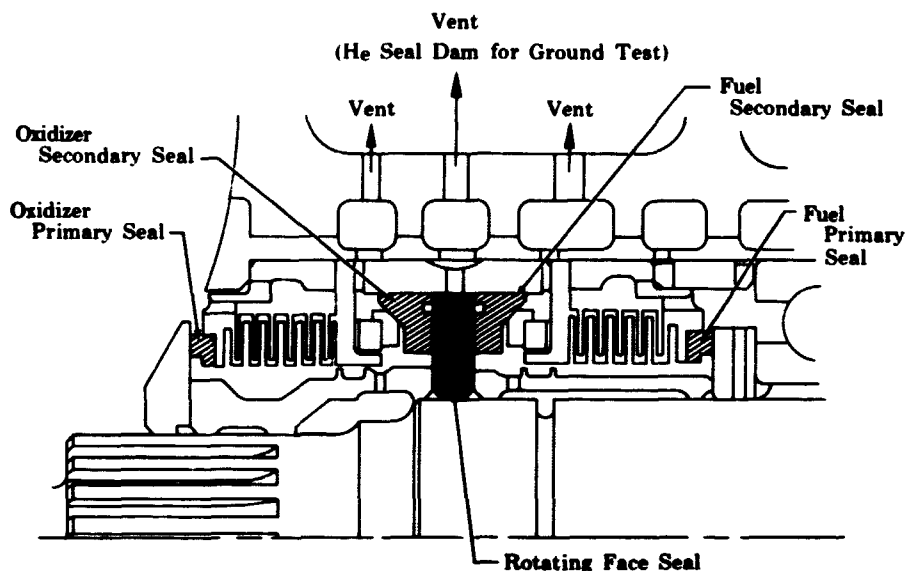
Figure 46. RL10 Oxidizer Pump Seal Arrangement   FD 11042C

2. MODIFICATIONS

The results of preliminary engine cycle studies indicated that, when intended modifications to the fuel pump and gearing were made, the RL10A-1 oxidizer pump geometry would be suitable for flox-methane operation of the engine. Therefore the only modifications required for the oxidizer pump were those necessary to make the assembly chemically compatible with liquid flox. Such modifications had been incorporated in two RL10A-1 oxidizer pumps used in fluorine-hydrogen engine demonstration testing under Contract NASw-754, and these pumps were available. The two pumps, identified as S/N C71Y001 and C71Y002, were therefore transferred to the flox-methane pump-fed engine program.

Details of the compatibility modifications incorporated in the pumps are fully discussed in Reference 4. The basic rotating elements of the pump were fabricated from compatible materials and therefore were retained essentially without change. The bearings and gear are located in areas not normally exposed to fluorine and were also retained. The cast aluminum inducer and impeller housings, which are exposed to fluorine, were changed to forgings in order to avoid possible cleaning and porosity problems. The carbon inducer shroud seal ring was eliminated and, when the change from castings to forgings was made, the volute cross section area was reduced so that efficient performance would be maintained at the lower volumetric flow rates in the fluorine modified engine. The steel sleeve normally installed in the housing bore to accept shaft seals and spacers was replaced with two sleeves, aluminum at the impeller cavity, and steel at the gearbox end. The OD of the aluminum sleeve was electron beam welded at the surface of the impeller cavity to prevent liquid fluorine from entering the sleeve-housing interface.

74

As used in fluorine/hydrogen demonstration test engines, the modified pumps incorporated 3.914 inch diameter RL10A-3 impellers rather than 3.826 inch diameter RL10A-1 impellers. The shaft seal materials employed in the primary and secondary fluorine seal positions were a titanium carbide-nickel cermet. Kentanium K-162B*, and aluminum oxide. The Kentanium K-162B was used for the rotating mating rings on the shaft; alumina was used in solid form for secondary seal split rings and as a flame-sprayed coating on the primary seal nosepiece. Primary seal bellows were changed from machined beryllium copper to welded stainless steel.

The Kentanium K-162B-aluminum oxide material combination was proved in the initial phase of a seal material investigation conducted under the fluorine/hydrogen propulsion research program. The investigation continued after engine demonstration tests had been accomplished and in the course of this effort other materials were proved. For the flox/methane engine program, advantage was taken of later results in making a selection. Materials chosen for shaft seals included a Kentanium K-162B mating ring rotating on a K-162B nosepiece in the primary fluorine seal, aluminum oxide split rings on a Kentanium K-162B secondary fluorine seal mating ring (which is common for the secondary gearbox seal), and boron nitride split rings for the secondary gearbox seal. The hard chrome mating ring of the primary gearbox seal was retained, but the nosepiece carbon was changed to Purebon 658RC**grade, which is compatible with gaseous, but not liquid, fluorine.

Pump testing experience was also gained in the later phases of the shaft seal material investigation, and this defined other minor changes to improve the durability of the pump in liquid fluorine service. Changes incorporated in the oxidizer pump for the flox/methane engine program were: (1) Inco 718 seal bellows were used so that permanent set problems encountered with stainless steel parts could be avoided; and (2) the impeller front shroud blading was removed and the rear shroud was scalloped to 3.3 inch diameter to increase the shaft thrust load and prevent possible unloading of the primary seal by forward movement of the pump shaft. Impellers of the nominal RL10A-1 diameter, 3.826 inches, were used.

3. Testing

Although the pump modifications had been proved in liquid fluorine testing, the fact that the material combinations used for the primary and secondary flox seals relied upon the formation of nickel fluoride lubricating films at the seal rubbing surfaces to reduce friction made it desirable to conduct seal rig and pump tests with the oxidizer containing 17.4 percent

* K-162B is a designation of the Kennametal Company, Latrobe, Pa.

** Purebon 658RC is a carbon grade designation of the Pure Carbon Corp., St. Mary's, Pennsylvania.

oxygen before committing the pumps to engine use. A 31.8 minute seal rig test was conducted at the P&WA Florida Research and Development Center, and a 34 minute and two 5 minute tests of pump assemblies were conducted at NASA-LeRC Plumbrook Station.

a. Seal Rig Test

The seal rig test in liquid flox was conducted without incident using the test rig and operating techniques that had been employed for the original fluorine seal evaluations (see Appendix A and Reference 4). Operating conditions were: primary seal preload 14 lbs, secondary seal preload 8 lbs, liquid flox pressure 145 psia, shaft speed 11,000 rpm, atmospheric oxidizer and fuel seal vent cavity pressures, helium seal dam pressure 35 psia. No abnormalities were disclosed in the post-test inspection of the seal package; measured seal wear, shown in table XIII, was perfectly acceptable. The variation in cumulative flox leakage over the period of the test is shown in figure 47. Average flox leakage was 23.3 lb_m/hr.

TABLE XIII. FLOX PUMP SEAL WEAR*

Seal Location	Primary Flox Seal	Secondary Flox Seal
Mating ring wear, in.	0.0001	0.0001
Nosepiece/split ring wear, in.	0.0002	0.0001

Measured after 31.8-minute rig test.
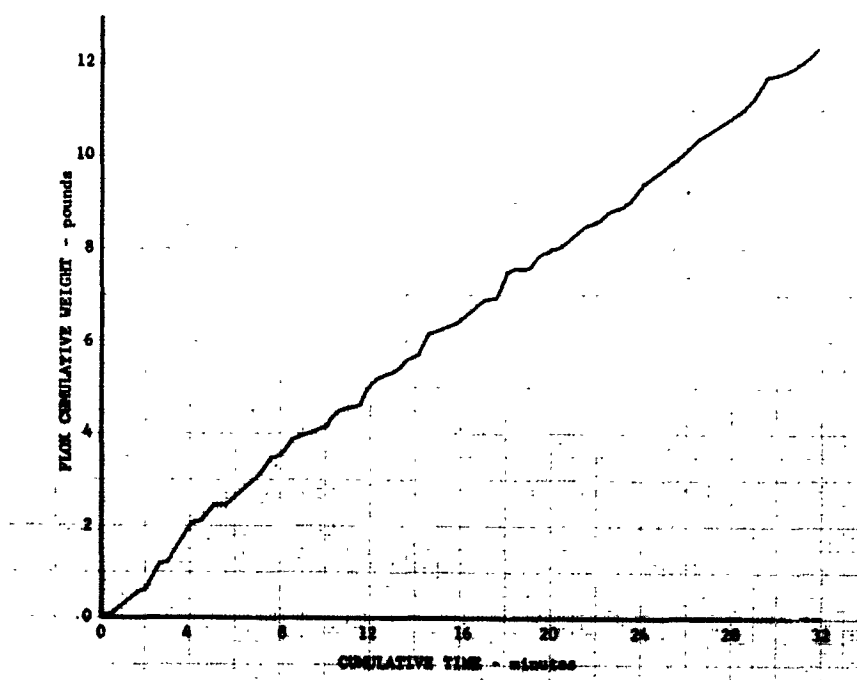
Figure 47. Variation in Cumulative Flox Leakage With Operating Time   DF 68907

b. Pump Loop Tests

A 34 minute test of pump S/N C71Y002 was conducted to verify the integrity of a modified pump in liquid flox and to permit acquisition of head rise and efficiency data.

Performance data obtained during four flow executions from 80 to 210 gpm at 9950 rpm with inlet pressures of 15, 25, and 35 psig are presented in figure 48. The pump was found to be in generally good condition during disassembly and inspection following the 34 minute test, but one discrepancy was noted. The K-162B primary flox seal mating ring had developed a hairline radial crack.
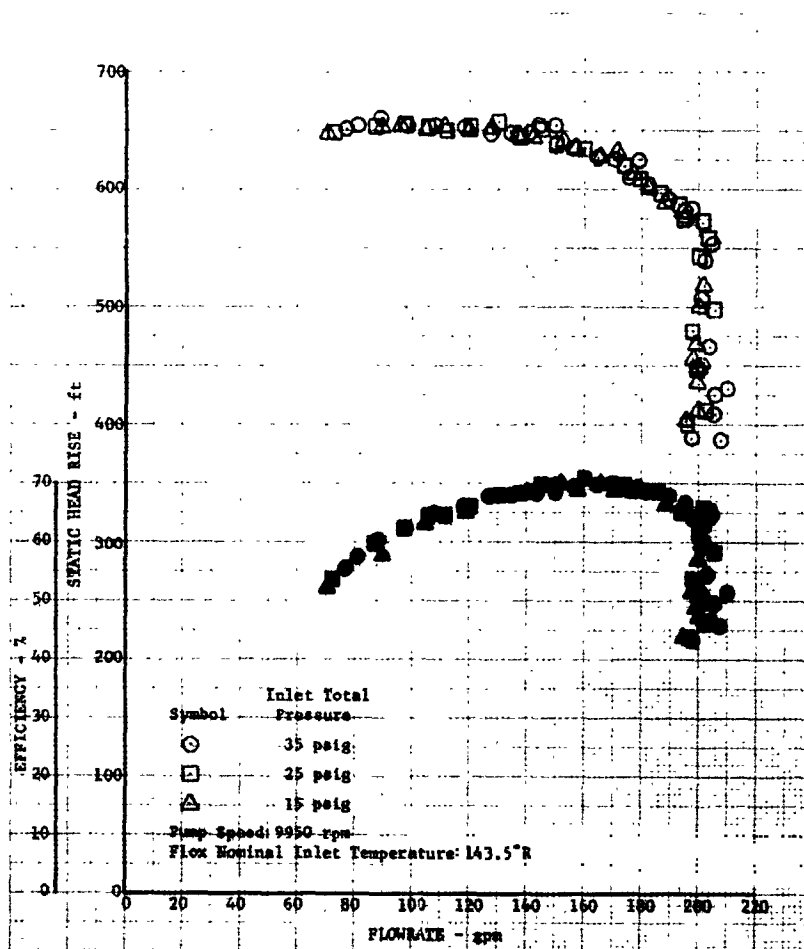
Figure 48. Performance Data From 34-Minute Flox Pump Performance   **DF 68908**
and Durability Demonstration (Pump S/N C71Y002)

No explanation for the mating ring discrepancy was found. Based on vent pressure measurements, seal performance during the entire test period was consistent; therefore it was assumed that the crack was present before testing started. The measured wear of the primary flox seal was approximately five times that expected based on results of seal rig testing, but was

still acceptable; the wear at the secondary seal was normal. The increased wear rate of the primary seal is attributed to the presence of the crack in the mating ring.

Because of past history with K-162B mating rings and the fact that pump S/N C71Y002 performed satisfactorily with the damaged mating ring, it was decided that the configuration was acceptable and that a material change was not required. The interference fit of the mating ring on the oxidizer shaft, measured at assembly, was 0.0011 inch. This was less than the maximum interference fit of 0.0012 inch that had been used successfully in fluorine pumps tested under Contract NASw-754 and therefore did not appear to be a factor. However, to reduce the possibility of recurrence, the maximum allowable interference fit between the mating ring and the shaft was reduced from 0.0012 to 0.0010 inch.

Following completion of the 34 minute test, both pumps available to the program, S/N C71Y001 and C71Y002, were assembled in the same configuration and subjected to 5 minute liquid flox checkout tests prior to their certification for engine use. No discrepancies were noted during these tests and the calibrated post-test seal leakage was well within established limits. Performance data obtained during the 5 minute tests of the two pumps in flow excursions from 80 to 210 gpm at 9950 rpm with a 35 psig inlet pressure are presented in figures 49 and 50.

c. Engine System Tests

Pump S/N C71Y002, which had accumulated a total of 39 minutes of component testing, was used for the first two engine firings. During engine test No. E-1 a temporary reduction in oxidizer pump head was experienced at 5.7 seconds into the 43.4 second test. This was an effect resembling inlet cavitation, but the net positive suction pressure at the time of the occurrence was 40 psi, and satisfactory operation of the pump at this level had been demonstrated previously. The problem was attributed to gas ingestion at the inlet due either to purge gas leakage or vaporization of flox in the inlet instrumentation taps. For the remaining engine tests the purge shutoff valves and the inlet instrumentation transducers were moved closer to the engine to minimize the line volume between them and the engine connections, and no further head loss problems were experienced.

Figure 50. *Performance Data From Flox Pump Checkout Test: Pump S/N .71Y002*

DF 68909

Inlet Total Pressure: 35 psig
Pump Speed: 9950 rpm
Flox Nominal Inlet Temperature: 143.5°R

Figure 49. *Performance Data From Flox Pump Checkout Test: Pump S/N C71Y001*

DF 68910

Inlet Total Pressure: 35 psig
Pump Speed: 9950 rpm
Flox Nominal Inlet Temperature: 143.5°R

Prior to the third engine build using pump S/N C71Y002, a standard preassembly check of the turbopump seals revealed higher-than-normal leakage rates across both the secondary flox and secondary gearbox seals (refer to figure 46). The pump was disassembled and it was found that the common rotating mating ring between the secondary seals had developed a single radial hairline crack. Leakage levels had been acceptable in checks made between engine builds No. 1 and 2 and at engine disassembly following build No. 2. It was therefore established that the seal had cracked during the storage period between builds.

As in the instance of the primary fluorine seal, a room temperature interference fit between the K-162B mating ring and the inconel shaft was specified at the secondary seal location because of differences in expansion properties. It is surmised that the failure resulted from a combination of the residual stresses caused by the interference fit and thermal cycling during two pump component tests, 6 engine cold flows, and 2 engine hot firing tests (41.3 minutes total test duration). Although leakage rates during helium calibration were measurably high because of the crack, the problem was not serious enough to have caused any difficulties during an engine test.

Following discovery of the mating ring failure in pump S/N C71Y002, the second pump, S/N C71Y001, was substituted for later engine tests. Pump S/N C71Y002 was reassembled with a new mating ring, but was not required for further use.

This failure and the similar failure of the primary mating ring in the pump loop tests indicate that the amount of ring/shaft interference is a critical item with K-162B rings. This is definitely an area which should be further investigated if this material is used in future engine programs.

C. TURBINE

1. DESCRIPTION

Turbopump power is supplied by a two-stage partial admission impulse turbine. The first and second rotor stages are machined from a single piece of aluminum and the blades are shrouded to minimize blade tip leakage. The first stage turbine stator has fixed vanes over an admission arc of approximately 135 degrees. The second stage stator is a full admission type. Adjustment of turbine inlet area is a standard procedure in the assembly of oxygen/hydrogen engines. Individual passages between vanes are closed with plugs as required, and finer adjustment is provided by a vernier gate at one end of the admission arc, as shown in figure 51.
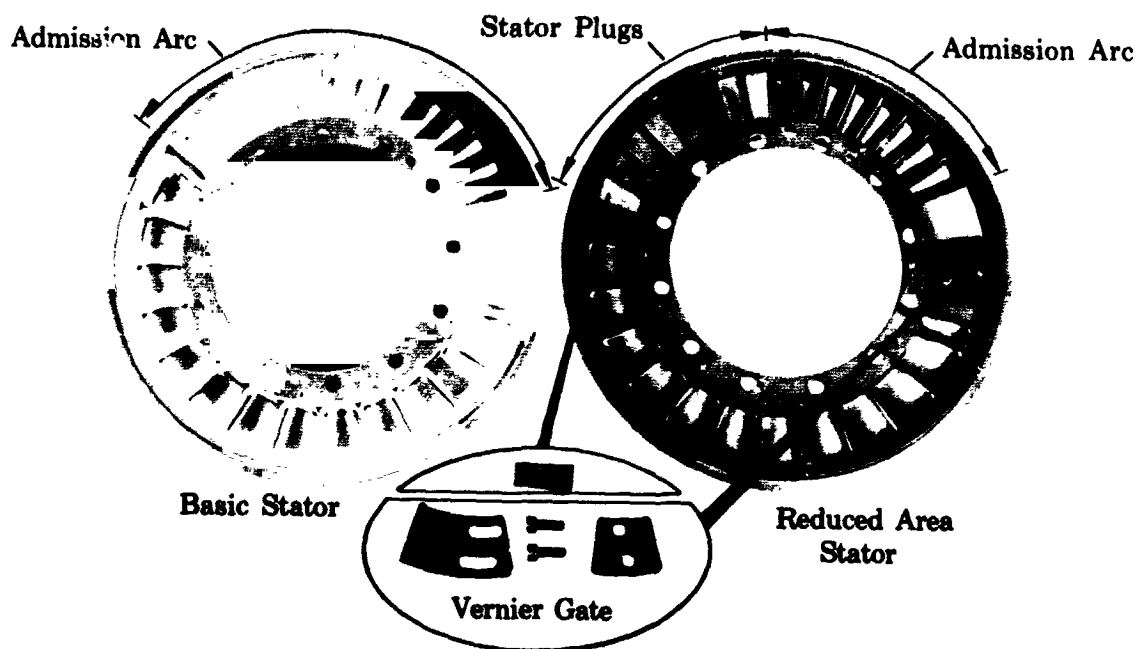
Figure 51. RL10A-1 1st-Stage Turbine Stator Area Reduction   *FD 12763A*

2. MODIFICATION

A significant reduction of the RL10 turbine first-stage stator area was necessary to maintain adequate pressure ratios across the stator with methane. The standard method of stator area reduction, insertion of stator vane plugs, was used, but because of the extent of reduction required and the inherent loss of efficiency as the arc of admission is decreased, a second technique was also utilized. This second technique was reduction of the vane trailing edge gap, which achieves some of the required area reduction without changing the arc of admission. To reduce the trailing edge gap, the aft portions of the vanes were cut at their inner and outer attaching points, the trailing edges were bent to the desired positions, and the inner and outer edges were welded in the new position. To further maximize the admission arc, a sealant was used on stator vane plugs to prevent leakage around them. The inlet area measured in bench flow tests following modification was 0.471 in.^{2} compared to 1.145 in.^{2} for normal oxygen/hydrogen operation.

Development experience with the oxygen/hydrogen RL10 showed that a swirl or vortex in the turbine exhaust housing, caused by turbine operation off the peak efficiency point (optimum U/C), caused a pressure loss and reduced cycle power. Therefore, to eliminate the loss of cycle power

81

in flox methane demonstration engines, stationary straightening vanes were installed at the exit of the second-stage turbine rotor. These are shown in figure 52, which is an exploded view of modified methane pump and turbine parts.
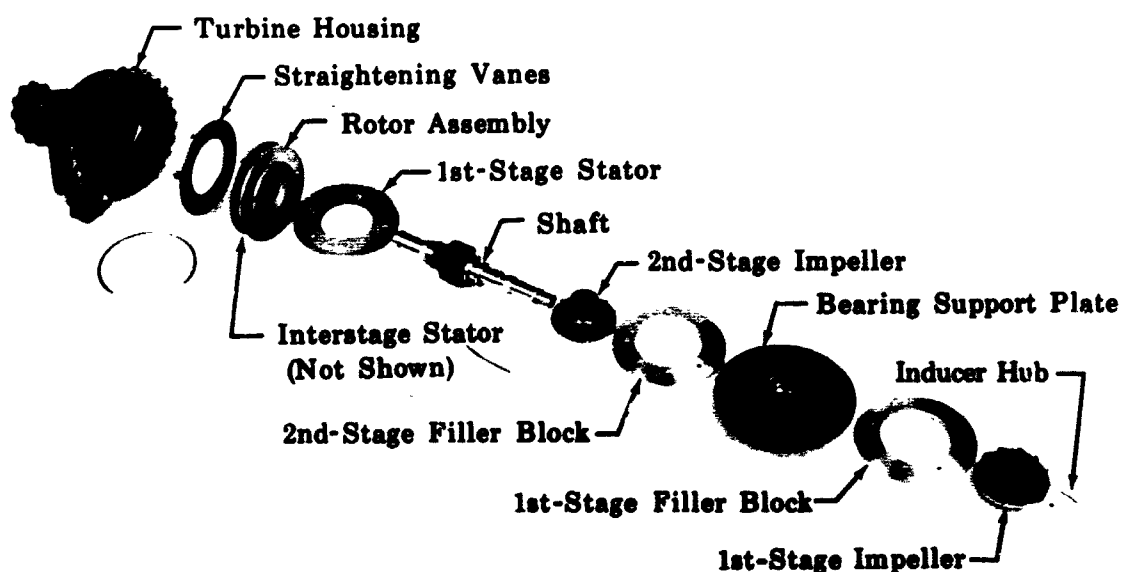
Figure 52. Methane Modified RL10A-1 Fuel Pump and Turbine Parts   *FD 23838A*

3. TESTING

In the first three builds of engine FX-153 the turbine operated essentially as expected. During tests No. E-4 and E-5 the cycle balanced at lower than predicted steady-state mixture ratios, a condition symptomatic of component failures that reduce the fuel side flow restriction. Sufficient steady-state data to identify the point of reduced restriction were not available until after test No. E-5, but when they were obtained it was established that the turbine inlet flow area had increased. The program was nearing completion at that point in time and the remaining scope was insufficient to permit cessation of testing and removal of the engine from the test stand for turbine disassembly and inspection. It was therefore necessary to accept the turbine area change and to proceed without immediately establishing the mode of failure. The turbine area, calculated from engine data, was 0.57 inch; orifice and control changes were made to compensate for the change and balance the cycle for the remainder of testing.

Teardown inspection after test No. E-9 provided visual confirmation that the turbine flow area had increased and permitted the cause to be ascertained. The failure was associated with the trailing edge modification made to reduce the stator area. Several of the weld joints holding the vanes in their relocated positions had cracked, permitting the affected blades to deform and thereby allowing the area to increase. Figure 53 is a post-test photograph of the first-stage turbine stator showing cracked trailing edge welds. The weld failures can only be explained in light of the relatively poor welding characteristics of the AMS 4130 (high silicon content) aluminum used in the stator.

Typical Weld Failures

Deformed Blades
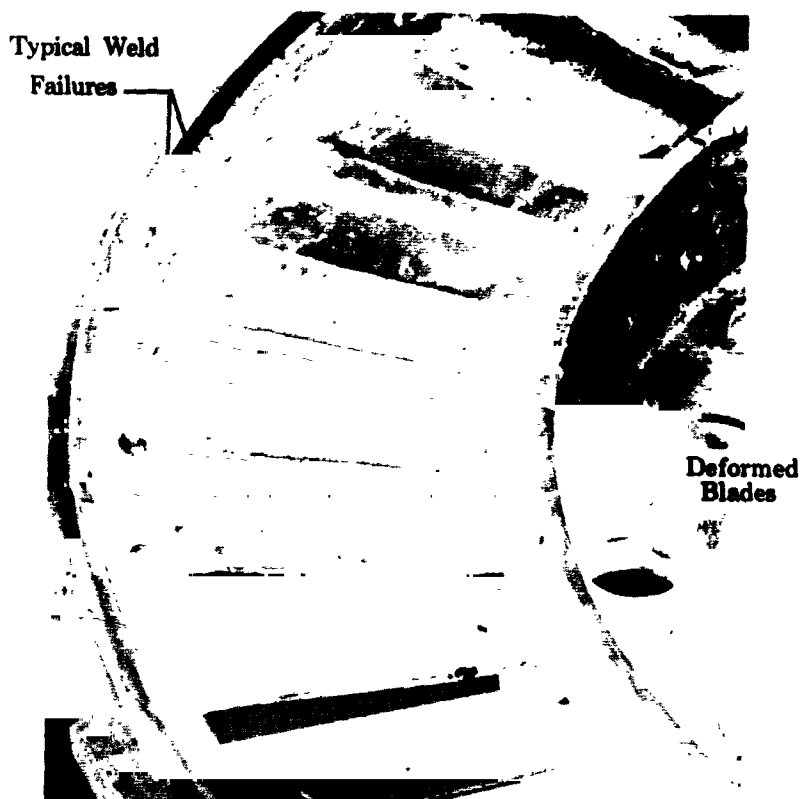
Figure 53. Post-Test Condition of 1st-Stage Turbine Stator   **FD 25343**

Turbine efficiency data obtained during the steady-state portions of the longer duration tests are presented in figure 54. The maximum demonstrated efficiency was 51%, which was approximately 5% lower than that for unmodified RL10 turbines, but is about 5% higher than was originally predicted based on oxygen-hydrogen RL10 data for reduced admission areas. The improvement is attributed to the use of stationary straightening vanes and reduced trailing edge gaps. Significantly higher efficiencies could be achieved in a turbine designed specifically to operate at these conditions.
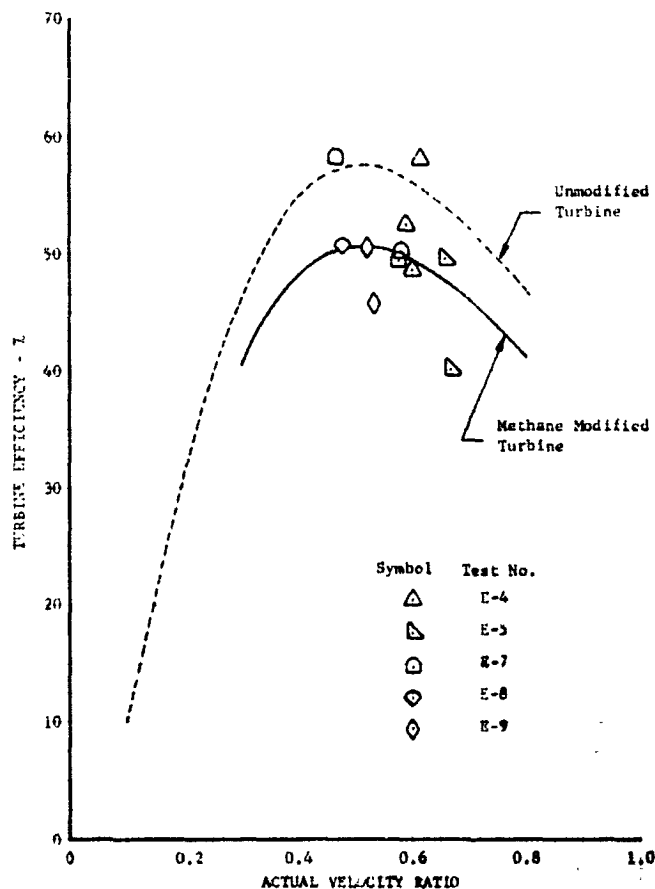
Figure 54. Efficiency of Methane Modified RL10A-1 Turbine   **DF 68973**

D. GEAR TRAIN

Turbine power is transmitted to the oxidizer pump through a spur gear mounted on the common turbine/fuel pump shaft, an idler gear located in the gearbox housing, and a gear on the oxidizer shaft. The bearings (ball and roller) and spur gears are not lubricated but are cooled by fuel tapped off of the fuel pump and distributed through a system of internal passages (see Reference 9). The overall gear ratio of the standard RL10A-1 engine turbopump is 2.5. To permit a reduction of fuel pump speed without making changes to the oxidizer pump geometry necessary, RL10A-4 gearing, which provides an overall ratio of 2.118, was used in the flox/methane demonstrator.

The calculated fuel flowrate required to cool the bearings and gears in the hydrogen application is 0.01 lb_m/sec, based on the heat generated at RL10 design conditions. With no modifications to the passages, the methane flowrate was approximately 0.2 lb_m/sec. Post-test inspection of the turbopump assemblies did not reveal any wear problems, indicating

that the cooling afforded by the methane was adequate and probably could be reduced. This is a significant result because it assures that the complication of separate lubricating or coolant supply systems will not be necessary in methane engine designs.

The only problem experienced because of the gear train was a delay in the start of turbopump rotation in the first two engine tests. In tests No. E-1 and E-2 there was a period of approximately 1 second between the opening of the propellant valves and the start of turbopump rotation, whereas a hesitation of 0.25 seconds is more typical of the RL10 oxygen/hydrogen engine. The greater delay was traced to insufficient clearance between the hub of the spur gear on the oxidizer pump shaft and the gearbox housing of oxidizer pump S/N C71Y002. The low clearance was evidenced by galling of the housing surface, and caused binding when a rearward shaft loading was applied. Apparently, the pressure resulting from initiation of oxidizer flow provided sufficient rearward loading to cause rubbing. The binding was not revealed in pre- and post-firing static torque checks which are made with the pump installed on the engine but with essentially no axial load. The galling at the housing surface was not visible at disassembly to the component level, but was found when the pump was completely disassembled for investigation of secondary seal leakage. No hesitation problems were encountered with pump S/N C71Y001, and the housing of S/N C71Y002 was machined to provide the proper clearance. However, as noted above, the original unit was not required for further service.

SECTION VI

VALVES AND CONTROLS

There are seven major valves in the propellant flow streams of the RL10A-1 engine. (Refer to figure 2.) The fuel system incorporates a fuel inlet shutoff valve, two fuel pump cooldown valves, a thrust control, and a main fuel shutoff valve. Oxidizer flow is controlled by the oxidizer inlet shutoff valve and the oxidizer flow control valve. Except for the thrust control and the oxidizer flow control valve, all of these valves are actuated for at least some part of their function by helium gas pressure that is controlled by electrically operated solenoid valves. The solenoid valves respond to electrical signals from the vehicle control system or, in the case of the flox/methane engine, from the test facility sequencer.

Only the two oxidizer valves and the thrust control required modification for use on the flox/methane engine. All other valves were used without physical change from their RL10A-1 Bill-of-Material configuration.

A. FUEL VALVES

1. GENERAL

Four of the fuel-side valves (fuel inlet shutoff, fuel pump interstage cooldown, fuel pump discharge cooldown, and main fuel shutoff) did not require any changes from their RL10 configurations, which are described in detail in Reference 9. Preparation of these valves consisted only· of vacuum baking (to remove moisture that could freeze during operation) and bench calibration testing to verify satisfactory sealing and operation. The functional checks consisted of applying the applicable actuation pressures and checking for proper valve movement. During the engine tests, all of these valves operated as programed and no requirements for changes were revealed. After each test the valves were inspected, subjected to bench tests, vacuum-baked, and stored for use on the next assembly.

The fifth valve in the fuel system is the thrust control. Because of the great difference in density of methane and hydrogen and also because scheduling of the starting transient proved to be extremely critical, several thrust control modifications were required.

2. THRUST CONTROL

a. Description

The thrust control is a servo operated variable position valve that references chamber pressure and controls the amount of fuel that bypasses the turbine; this regulates the turbine power and hence turbopump speed.

A schematic diagram of the valve is presented in figure 55. The amount of bypass flow is determined by the position of the sliding bypass valve. The bypass valve position is established by the balance of forces resulting from the differential between the turbine discharge pressure (acting on the bottom of the valve) and the servo chamber pressure and the springs. Continuous flow to the servo chamber is supplied from the heat exchanger discharge line through a fixed choked orifice An increase in combustion chamber pressure moves the bellows carriage downward against the springs to open the shear orifice and reduce the servo chamber pressure. As the servo chamber pressure decreases, the net force on the bypass valve changes, and the bypass valve piston moves to increase the bypass area. As the bypass area increases, the quantity of fuel bypassing the turbine increases, thus reducing the turbine power output. The bypass valve travel is transmitted to the bellows carriage through the feedback spring, thus balancing the forces on the carriage and returning the servo valve lever to an equilibrium position. Conversely, a decrease in the chamber pressure allows the bellows carriage to move upward and closes the shear orifice. Servo chamber pressure then increases and the resulting force differential moves the bypass valve piston to decrease the bypass area.
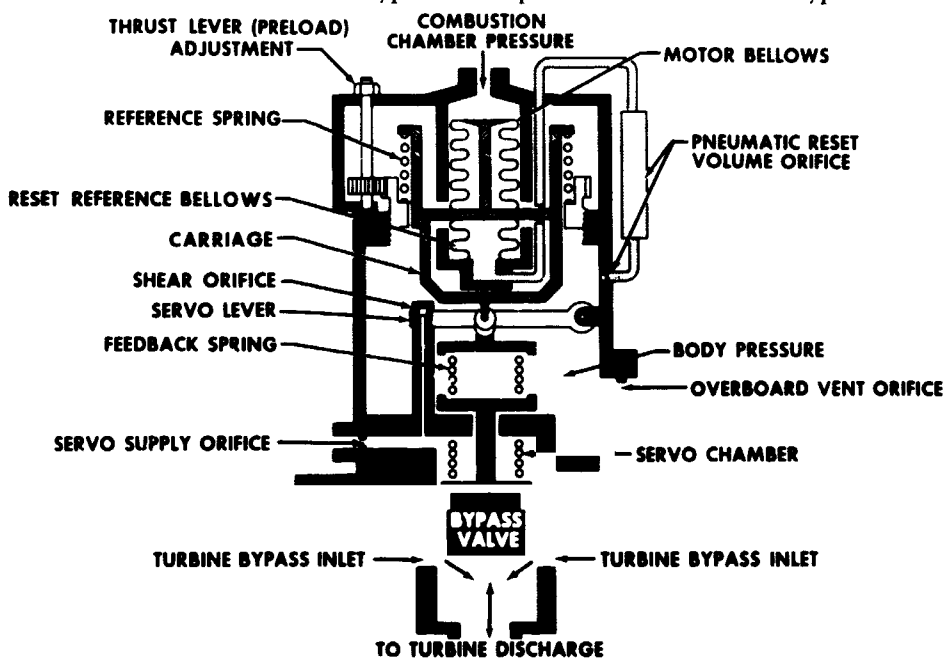
Figure 55. Thrust Control Schematic   FD 3212D

The forces on the thrust control carriage, which positions the servo lever, consist of combustion chamber pressure acting through the motor bellows, the pressure acting through the reset bellows, and the reference spring and feedback spring loads. The chamber pressure at which the valve controls is set by the preload on the reference spring. The preload is adjustable, and the adjustment is normally set and locked during engine acceptance test. However, for the flox/methane engines, an electromechanical drive was provided to allow remote adjustment during engine tests.

The control also incorporates a lead-lag reset feature that senses the time rate-of-change of chamber pressure and reacts to prevent system overshoot or undershoot. It affects the pressure differential acting on the reset bellows area during transient conditions. The reset bellows internal pressure is supplied from the body through the pneumatic reset volume orifice into the reset bellows. (See figure 55.) Because of the restriction created by the reset volume orifice, rapid changes in chamber pressure react on the motor bellows before the pressure within the reset reference bellows can adjust. The resulting imbalance on the reference carriage allows changes to the position of the servo lever before the preset value of chamber pressure is reached.

b. Modifications

Prior to the first engine test, the only changes made to the RL10 Bill-or-Material configuration were resizing of the servo supply and body vent orifices to compensate for the higher methane density and installation of a mechanical stop to limit the control bypass area. The bypass area was limited to approximately 25% of the turbine area to prevent extensive overcorrection that might produce high speed pump stall. Setting the control for operation at a 250-psia chamber pressure, compared to 300 psia for the oxygen/hydrogen RL10, was accomplished with the reference spring preload adjustment.

c. Test Experience

The modified valve functioned as expected in bench tests. Examination of data from the first engine test (No. E-1) revealed that steady-state control was adequate, but that the response desired during the starting transient was not obtained, and that more than normal chamber pressure variation was encountered during that period. This sluggishness appeared to be caused by two factors: (1) the flox/methane system is basically less responsive than an oxygen/hydrogen system and (2) the thrust control piston had a minor tendency to stick. Operation of the thrust control piston was well within acceptable limits for an oxygen/hydrogen system, but when used in the slow response methane system, undesirable system overcorrections occurred. To improve the control response, larger servo inlet and body discharge orifices were installed prior to test No. E-2. These larger orifices increased the flow through the servo system and improved the valve's ability to limit thrust undershoot.

In the first two engine tests, the thrust control anticipated an overshoot and began to open the turbine bypass at a chamber pressure of approximately 220 psia because of the lead-lag feature. However, the chamber pressure overshot to a maximum of 330 psia, followed by rapid deceleration toward the 250-psia set point, because of the slower system response. This deceleration occurred almost simultaneously with the

89

initial coolant slowdown resulting from expansion of methane within the jacket (as explained in Section III), and contributed to the severity of chamber damage encountered on those tests.

The design and testing of a new faster reacting thrust control was not within the scope of this contract; therefore, for the third engine test, a new starting procedure was devised to avoid the overshoot. A three-way solenoid valve had been incorporated into the servo chamber supply line to vent the line to ambient pressure (rather than to supply coolant at jacket discharge pressure) to reduce power during shutdown. For the third test, the system was used to deactivate the thrust control at a high bypass position during the start transient. With reduced servo supply pressure, the bypass piston began to open when the turbine discharge pressure was approximately 35 psia, and the engine was accelerated with the turbine bypass full open. This reduced the rate of acceleration and also prevented system overshoot and subsequent rapid deceleration. The mechanical stop was changed to further limit the travel of the bypass piston so that a bypass area consistent with a steady-state chamber pressure of 235 psia at a mixture ratio of 5.4 would be obtained. During the first test using this procedure (test No. E-3), the control performed as expected, and the system accelerated to the predicted chamber pressure of approximately 230 psia with minimum overshoot.

Several variations of this procedure were used during the subsequent engine tests, and satisfactory thrust control characteristics were demonstrated in all tests except No. E-8. During that test, a feedback loop was established between the thrust control and the marginally seated oxidizer control valve. The resulting system changes that occurred as the oxidizer valve changed positions produced more upset than the thrust control could compensate, and a 1-Hz cycling between 200- and 250-psia chamber pressure resulted. Normally, there is insufficient power to reaccelerate the system after the oxidizer valve has become unseated; however, a bypass line installed around the oxidizer control valve prior to this test evidently changed the system enough to allow reacceleration.

B. OXIDIZER VALVES

As discussed in Section III, there are two valves in the RL10 oxidizer flow system: the inlet shutoff valve and the oxidizer control valve. Oxidizer valves used on the flox/methane engines were assemblies that had previously been modified for fluorine use and tested in the Contract NASw-754 hydrogen/fluorine propulsion system research program (Reference 4). Before being used on flox/methane engines, they were rebuilt, and those additional modifications deemed advisable based on the previous experience were incorporated. During the initial engine demonstration tests, minor changes were made to the oxidizer control valve to provide an altered starting transient. However, because of the discovery of a

serious problem of coolant flow slowdown during the start transient, changes in scheduling that were not within the capability of the valve were required, and it was necessary to substitute a more extensively modified version that provided a scheduled opening.

1. INLET SHUTOFF VALVE

The oxidizer inlet shutoff valve is a normally closed, ball-type valve that is actuated by helium pressure through a spring-loaded piston. Linear motion of the actuating piston is changed to rotary motion by a rack and pinion arrangement to provide the required 90-degree ball rotation (figure 56). The valve mounts directly on the oxidizer pump inlet flange, and its inlet flange is the engine-vehicle (engine-test stand) oxidizer interface.
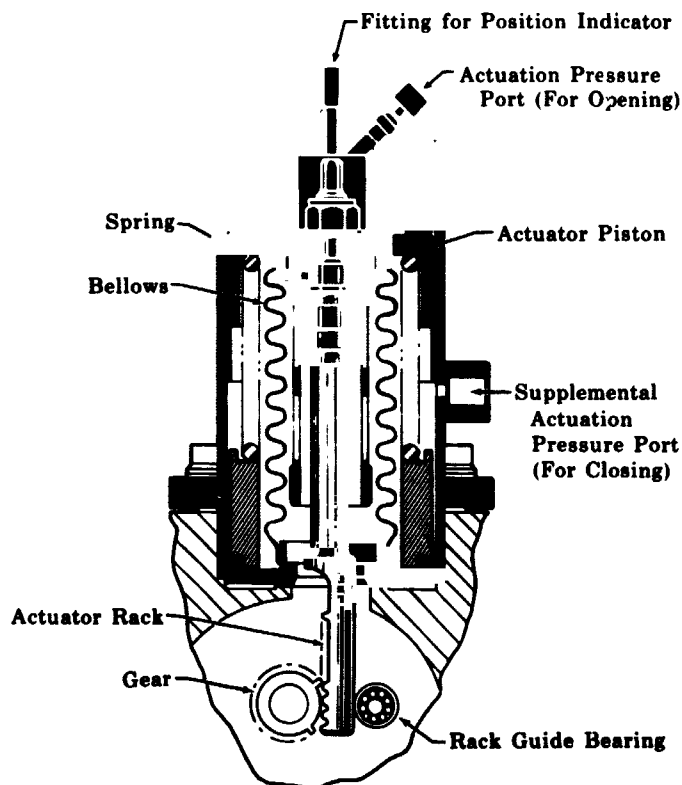
Figure 56. Oxidizer Inlet Valve Actuator FD 17309A

a. Modifications for Fluorine Service

Prior to its use on fluorine/hydrogen engines, extensive changes were made to the oxygen inlet valve design to achieve compatibility. These are described in complete detail in Reference 4 and are summarized below:

1. Replacement of cast aluminum housings with machined parts to avoid possible cleaning and porosity problems.

2. Substitution of soft aluminum seals for Teflon static seals between housing sections.

3. Elimination of dry film lubricants on actuator parts. (The gear and rack were gold plated to reduce friction: other parts were used without coatings.)

4. Replacement of the three-ply actuator bellows with a single-ply bellows to avoid possible contamination in the event of a bellows ply failure. (The attachment of the actuator rod was also altered to facilitate cleaning.)

5. Replacement of the Teflon dynamic ball seal with metal-to-metal seals. The single Teflon seal in the standard valve was replaced with two metal-to-metal seals, one at either end of the valve, to assure zero through leakage. An overboard vent was provided to relieve pressure between the seals. A cross section sketch comparing the revised seal arrangement with the original configuration is presented in figure 57. Valve balls with slightly better than usual sphericity tolerance (0.0003 inch as compared to 0.0005 inch) were used to improve sealing with the nonresilient materials.
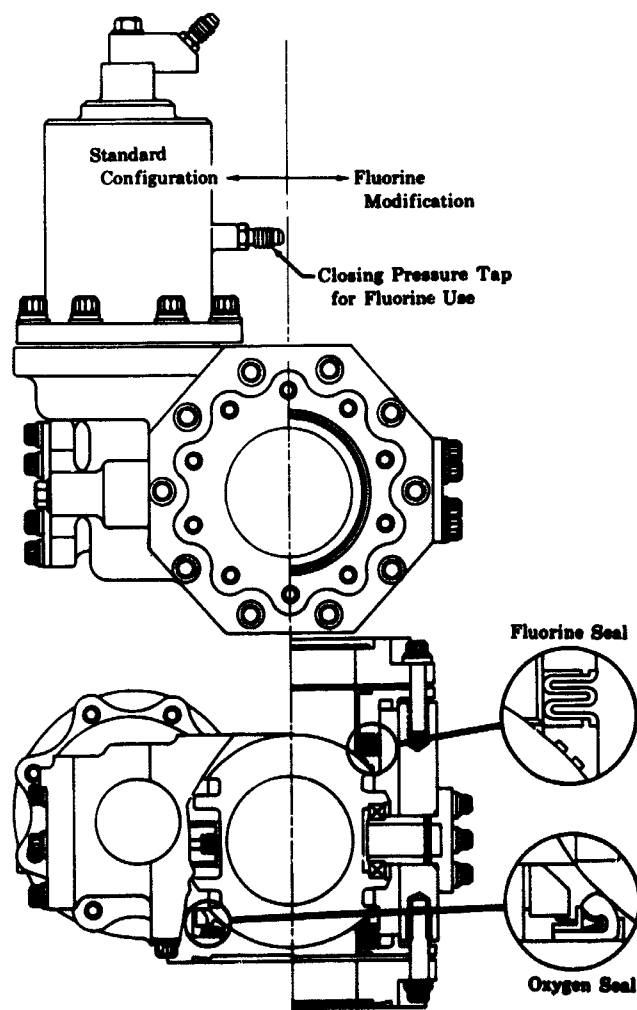
Figure 57. Oxidizer Inlet Shutoff Valve   *FD 13722*

92

The performance of the modified valves in fluorine/hydrogen engine testing was satisfactory; however, some potential problem areas were revealed. Therefore, during the process of refurbishing the valves for this program, additional modifications were made to further improve them. The initial modification, refurbishment, and incorporation of the later changes were accomplished by the supplier of the original oxygen valves, Parker Aircraft Company.

The changes incorporated during valve refurbishment for the flox/methane engine are shown in the bottom view of figure 58; these included (1) redesigned ball seals, (2) remachining of the body static seal grooves to obtain sharp-edged interlocking serrations, and (3) redesigned inlet and outlet flanges to include the ball seals, thereby eliminating two static seals.

The original design of the metal-to-metal seal shown in the top view of figure 58 featured a bellows-loaded contoured nosepiece grooved to achieve a labyrinth effect. The stationary nosepiece was stainless steel, coated with gold to reduce friction and to provide a "soft" contact surface. For the flox/methane engine, the ball seal configuration was changed from a three land labyrinth seal to a single land seal because etching of the ball had occurred in the areas under the labyrinth grooves after exposure to fluorine. Apparently fluorine (liquid or gas) trapped in these grooves was not removed by normal purging. The fluorine reacted slowly with atmospheric moisture that leaked into the grooves, producing hydrofluoric acid that attacked (etched) the hardcoat surface of the aluminum ball. The use of a single land seal facilitated purging and eliminated the post-test etching problem.

Modifications to the static seal grooves were made to reduce the difficulties encountered in making the joints of the originally modified valves leak tight. As can be seen in figure 58, square-edged serrations had been provided in areas where soft aluminum gaskets were used. To maintain a flightweight configuration to the greatest possible extent, the bolt loadings of the original design had been maintained in the modified design. Unfortunately, the loading was not adequate to prevent delayed leakage characteristics resulting from continued creep of the aluminum gaskets. With comparable bolt loadings, the sharp-edged interlocking serrations incorporated for this program increased the unit load on the gaskets, permitting greater initial plastic deformation and thereby decreasing the tendency for gasket creep.

Primary Seal

Typical Static Seal

Secondary Seal

Ball Seal

**Original Modification for
Fluorine/Hydrogen Engine**

Secondary Seal

Typical Static Seal

Secondary Seal

Ball Seal

**Configuration for
Flox/Methane Engine**
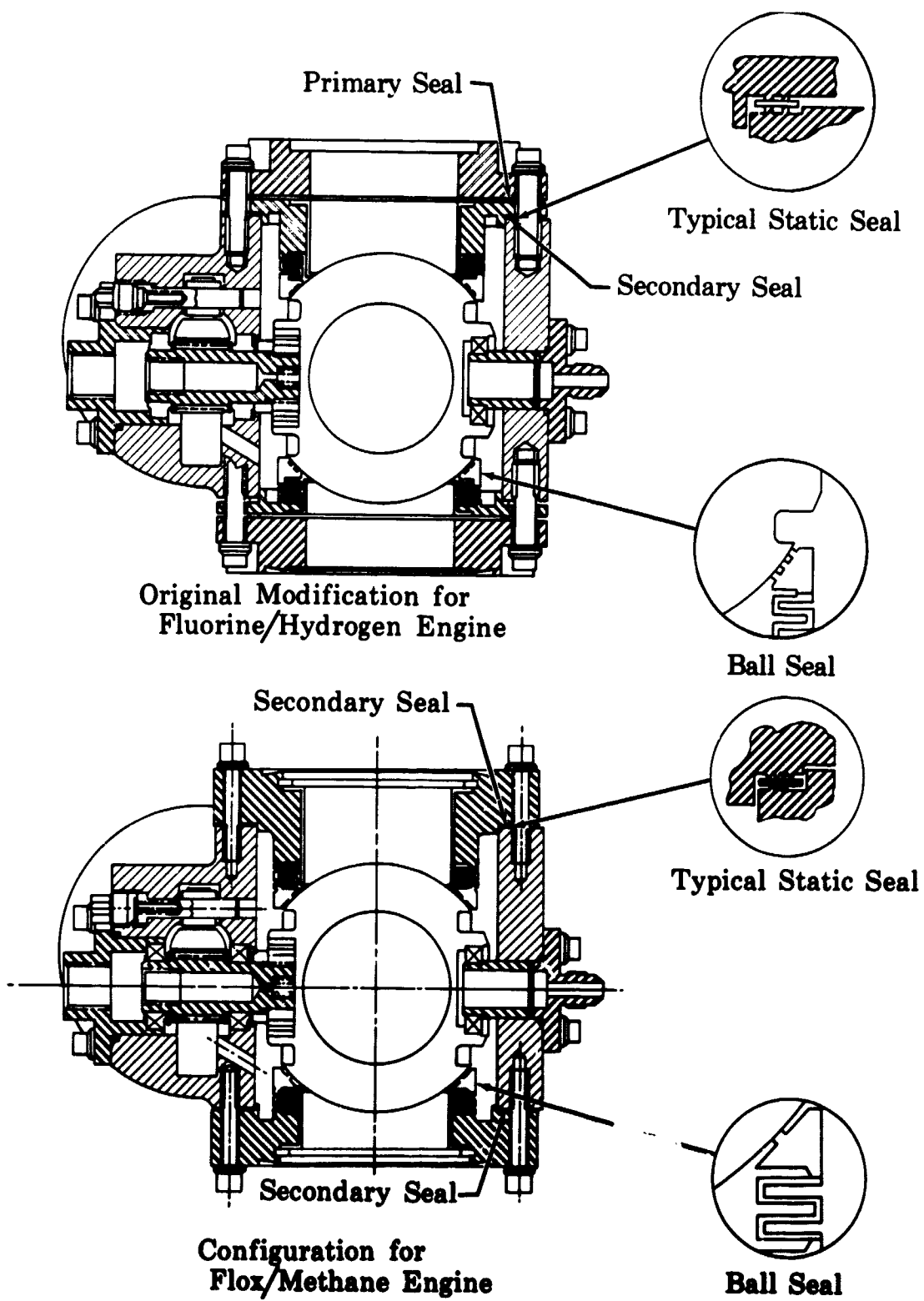
*Figure 58.   Oxidizer Inlet Shutoff Valve Showing Original Fluorine
Configuration and Improved Configuration*

FD 25663

b. Test Experience

(1) Component Testing

Three valves were refurbished to meet the combined requirements of both this program and a concurrent fluorine hydrogen engine demonstration conducted under Contract NAS3-7991 (Reference 10). Because the same facility was used for testing of engines in both programs, conflicts of usage requirements were avoided, and it was possible to schedule valve assignments so as always to meet engine demands while maintaining an available backup unit.

Upon receipt from the supplier, the refurbished valves were subjected to standard RL10 leakage and response tests. The results are presented in tables XIV and XV. In bench tests, gaseous helium was supplied to the valve inlet port at the maximum specification working pressure of 130 psia, and leakage was measured (by water displacement for a 15-minute period) at the vent and discharge ports. Tests were conducted with the valve at ambient temperature and at 140°F (submerged in liquid nitrogen). Table XIV shows that zero through leakage was demonstrated in the closed position by all valves at both test temperatures. The specification limit for through leakage in the RL10 Bill-of-Material valve is 1500 std cc of helium per minute through the single seal; however, much lower values are usually demonstrated. For the modified valves, the leakage values shown represent the leakage of a single seal for the closed position and the leakage of two seals for the open position. The measured leakage of the modified valves was less than the specification limit under all conditions.

TABLE XIV. TEST RESULTS FOR MODIFIED OXIDIZER INLET SHUTOFF VALVES

Valve Position	Valve Temperature	Helium Leakage, std cc/min					
		S/N C41Y013		S/N C41Y014		S/N C41Y015	
		Through	Vent	Through	Vent	Through	Vent
Closed	Ambient	0	32	0	16	0	32
	140°R	0	267	0	130	0	210
Open	Ambient	—	750	—	273	—	190
	140°R	—	1000	—	595	—	200

Two of the valves were subjected to response tests at both ambient and liquid nitrogen temperatures; the third valve was tested only at LN_2 temperature. The tests were made at inlet pressures up to the maximum working pressure (130 psia). Measured response times (in milliseconds) are given in Table XV. In instances where tests were made at both temperatures, ambient response was equal to, or better than, the reduced temperature response; however, acceptable actuation was demonstrated under all conditions.

95

TABLE XV. OXIDIZER SHUTOFF VALVE RESPONSE

Valve S/N	Valve Position	Valve Temperature	Valve Response Time, ms
C41Y013	Opening	Ambient	95 ± 10
	Closing		74 + 5
	Opening	140°R	186 ± 10
	Closing		123 + 5
C41Y014	Opening	Ambient	122 ± 5
	Closing		77 ± 5
	Opening	140°R	125 ± 10
	Closing		125 ± 10
C41Y015	Opening	Ambient	—
	Closing		—
	Opening	140°R	100 ± 10
	Closing		95 ± 10

(2) Operation During Engine Tests

Of the three valves that were refurbished, only one was required for the flox/methane engine testing. All flox/methane engine tests were accomplished with the same inlet valve, S/N C41Y013. The valve was cleaned, detail passivated, final-assembled, and assembly-passivated prior to use on the engine, but was not subjected to liquid fluorine flow tests.* One incident marred the otherwise satisfactory performance of the valve. On the first engine firing (Test No. E-1), the valve did not close for a period of 50 seconds after the helium supply was vented at engine shutdown.

Bench tests of the valve after removal from the engine revealed that it operated somewhat erratically, and minor etching of the ball flow passage by acid reaction was observed. This indicated the presence of moisture, and other indications of moisture within the system were found. To check the possibility that moisture caused the problem, the valve was dried in a vacuum oven, after which it operated normally and was considered satisfactory for use on other engine assemblies. The continuous gaseous nitrogen purges used to prevent system contamination had a moisture content below 1 ppm for at least 48 hours preceding the test; therefore, the source of the moisture was not determined. In later tests, higher purge flowrates were maintained, and the moisture problem did not recur. To provide assurance that the valve would close without difficulty, a positive closing pressure was supplied to the supplemental helium actuation pressure port (figure 56) in the same manner as for units used in fluorine/hydrogen RL10A-1 engine firings (Reference 4). Helium pressure was maintained at this port for 500 ms after venting the main actuation

* The integrity of the modified valve design had been proved in liquid fluorine flow testing under Contract NASw-754 (Reference 4); therefore, duplication of that testing was not considered necessary.

96

pressure port. This provided a sustained positive pressure for valve closure, and no difficulties were encountered during the remaining tests.

2. OXIDIZER CONTROL VALVE

a. Valve Description

The RL10 oxidizer flow control valve is a spring-loaded poppet-type valve that schedules oxidizer flow during the starting transient and also contains an adjustment to set mixture ratio during steady-state operation. The oxidizer starting flow scheduling includes an initial low volume flow for pump temperature conditioning followed by a delayed, but rapid, transition to full flow. When full oxidizer flow starts, rapid increases in chamber pressure occur. These produce increases in turbine back pressure and in required turbine power. Sequencing of the oxidizer flow transition is therefore important in the RL10 because, if the changes occur at a point where the excess power available for acceleration is not adequate, the engine cycle will not bootstrap.

Two configurations of the oxidizer flow control valve were used in flox/methane engine tests: a Bill-of-Material valve modified to obtain fluorine compatibility and a highly modified scheduled opening version that provided a more gradual transition flow. The major components of these two valves are compared in figure 59.
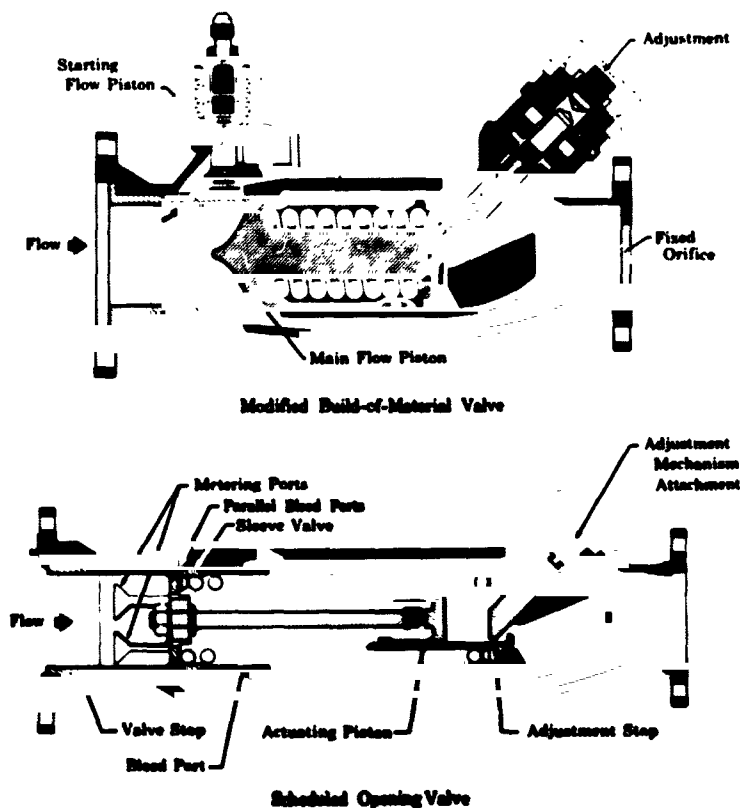
Figure 59.   Modified Oxidizer Flow Control Valves

FD 18412A

97

(1) Bill-of-Material Valve

The operation of the fluorine modified Bill-of-Material valve can best be explained by reference to the top sketch in figure 59. The main flow piston is spring-loaded in the closed position, and a bypass around the main piston permits an initial low oxidizer flowrate to precool the pump and to provide heating for cycle acceleration. During engine start, the piston remains in the closed position until oxidizer pump pressure rise increases to a level where the pressure differential acting on it overcomes the spring preload. At that point, the piston starts to move to the open position, and oxidizer flow to the thrust chamber is increased. The transition from bypass to main flow is very rapid because the axial travel of the piston is small. The piston traverses from the closed to the open position with a 60-psi increase in oxidizer pump pressure rise. Sensitivity to pump pressure rise rather than discharge pressure is achieved by venting the cavity behind the piston to the oxidizer pump inlet. Maximum travel is limited by an adjustable stop. This stop is normally adjusted and locked during acceptance tests; however, during the flox/methane engine tests an electromechanical drive was used to permit mixture ratio variations.

Very few changes to the Bill-of-Material oxidizer flow control valve were necessary to achieve fluorine compatibility. All basic valve parts are stainless steel and the main housing sections are assembled using silver braze. Thus, all these items were retained without alteration. In the oxygen version, the main flow and starting flow pistons are Teflon coated to reduce friction, and a Teflon piston ring is used to reduce leakage around the main piston. Chrome plate was substituted for the Teflon coatings, and the piston ring was changed to beryllium copper. The only other change was to replace the existing spring with one having a higher rate. This was done to obtain greater preloads so that the opening point of the piston could be delayed.

(2) SCHEDULED OPENING VALVE

As discussed in Section III, engine test experience with the modified Bill-of-Material valve showed that a more gradual transition from bypass to full flow would be desirable. A similar requirement had been recognized for fluorine/hydrogen modified RL10A3-3 engines being evaluated under a concurrent program (Contract NAS3-7991), and valve modifications to effect scheduled opening were made as part of that effort.

A scheduled opening valve from the fluorine/hydrogen program was made available for the flox/methane engine to expedite engine testing. Operation of the scheduled opening valve is similar to that of the modified Bill-of-Material valve, but the starting flow piston is eliminated, and the main flow piston is in the form of a ported sleeve. Bypass flow is provided through a series of bleed ports in the main piston. (See figure 59.) The piston actuating force is provided by the differential between the oxidizer

pump discharge pressure acting on the front side of the actuating piston and the oxidizer pump inlet pressure acting on the rear side. The axial travel of the piston is significantly longer than the Bill-of-Material valve, and a 300-psi change in pump pressure rise is required to make the piston traverse the full span. The sleeve ports are configured to provide a linear increase in oxidizer flowrate with piston movement.

b. Preparation

(1) Modified Bill-of-Material Valve

The modified Bill-of-Material valve was accepted for use on the flox/methane engine without change. It was calibrated with LN_2 and cleaned and fluorine-passivated for service in liquid flox. The LN_2 calibration of flow resistance at different piston stop settings is shown in figure 60. This calibration provided data to establish the initial setting of the piston stop for engine testing. No changes were made until, as discussed in Section III, data from the engine tests indicated the desirability of changes in the bypass flowrate and the poppet cracking pressure for engine test No. E-2. These were minor changes and required only alterations in the bypass orifice size and the piston spring preload.

(2) Scheduled Opening Valve

The scheduled opening valve had been used in fluorine/hydrogen tests of a modified RL10A3-3 engine after flow calibration in liquid nitrogen, cleaning, and fluorine passivation. It was therefore accepted for use on the flox/methane engine without further preparation. Figure 61 shows the valve flow resistance-piston stop calibration for this valve. Two curves are shown; one based on LN_2 bench calibrations, and the other based on fluorine/hydrogen engine test data. The difference in the two calibrations is probably due to differences in instrumentation locations during the bench tests and the engine tests; however, with the Bill-of-Material valves, the bench calibration data usually corroborate the engine data. The calibration based on the engine tests was considered to be representative of installed performance and was used to determine the initial flox/methane engine settings.

99

Figure 60. *Oxidizer Flow Control Valve S/N C51Y002 Full Open   DF 69054
Adjustment Calibration*

Figure 61. *Oxidizer Flow Control Valve S/N C52Y001 Full Open   DF 69050
Adjustment Calibration*

c. Test Experience

(1) Modified Bill-of-Material Valve

The modified Bill-of-Material valve was used in three flox/methane engine tests for a total of 65.5 seconds. No problems were encountered with valve integrity, and its function was as expected. It was removed from the engine only after test experience demonstrated that characteristics different from those that the valve could provide were required for satisfactory engine starting.

(2) Scheduled Opening Valve

The scheduled opening valve was used in Build 4 of Engine FX-153, which was subjected to 6 firings for a total of 120.2 seconds. The integrity of the part was completely satisfactory but one operational problem was encountered.

It was recognized that a high differential pressure (approximately 360 psi) across the actuating piston would be required to seat the sleeve of the scheduled opening valve. Cycle analysis showed that, at some mixture ratios, the estimated oxidizer pump differential pressure was less than that required for seating the valve. (Refer to Appendix C.) However, because a high spring rate was desirable to slow the chamber pressure ramp it was decided not to alter the spring supplied with the valve, and additional pressure differential was attained by venting the reference cavity to a low pressure ejector system rather than to normal pump inlet pressure. Cycle analysis indicated that with 10-psia ejector pressure, the oxidizer pump discharge pressure - ejector pressure differential would be sufficient to seat the valve at mixture ratios above 4.5.

During the first engine test with the scheduled opening valve, test No. E-4, a slight delay in opening was noted. This delay was attributed to limited ejector system capacity, which prevented the reference cavity from being pumped-down at a satisfactory rate. In subsequent tests, the reference cavity was vented to the exhaust diffuser system which provided increased pumping capacity. This change did not substantially improve the valve response and it was ultimately determined that the slow decay of the cavity pressure was caused by restrictions at the reference cavity vent. All other aspects of the valve's operation were normal as indicated in the test discussions presented in Appendix D.

APPENDIX A

TEST FACILITIES AND PROPELLANT HANDLING

A. TEST FACILITIES

Experimental testing in the Flox/Methane Pump-Fed Engine Study was conducted at Pratt & Whitney Aircraft's Florida Research and Development Center and at NASA Lewis Research Center's Plumbrook Station. Firing tests, including pressure-fed uncooled sea level and cooled altitude thrust chamber tests, and pump-fed engine tests, were conducted at the Florida Research and Development Center, as was the single seal rig test that was made. Tests of liquid flox pumps were made at NASA's Plumbrook Station.

1. FLORIDA RESEARCH AND DEVELOPMENT CENTER

a. Liquid Propellant Research Facility

(1) General

The Liquid Propellant Research Facility (LPRF) is used for all testing operations at the Florida Research and Development Center requiring significant quantities of liquid fluorine or flox. The LPRF (figure 62) has four separate horizontal firing bays for 1000-, 5000-, 15,000-, and 50,000-lb thrust, a component test loop, and an injector water flow calibration bench. (See figure 63.) The 5000- and 15,000-lb thrust bays are connected to a continuous steam-driven ejector system for altitude simulation. Supersonic exhaust diffusers located at the two firing positions expel the combustion products into a common crossover duct. After leaving the crossover duct the gases are cooled in a tube-in-shell water-cooled heat exchanger and then pumped through two-stages of steam ejectors. Combustion products are passed through a scrubber-condenser that condenses the steam and removes all but trace concentrations of hydrogen fluoride before they are discharged to the atmosphere. The capability of the ejector system to maintain exhaust pressure below 1.5 psia during hot testing assured full expansion in the 15,000-lb thrust cooled chambers used in the program.
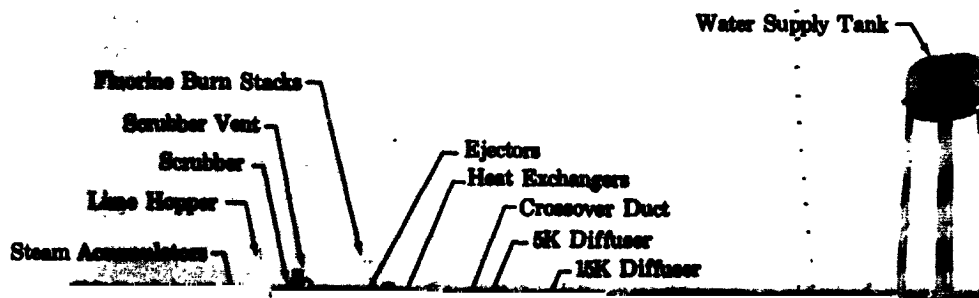
Figure 62. Liquid Propellant Research Facility
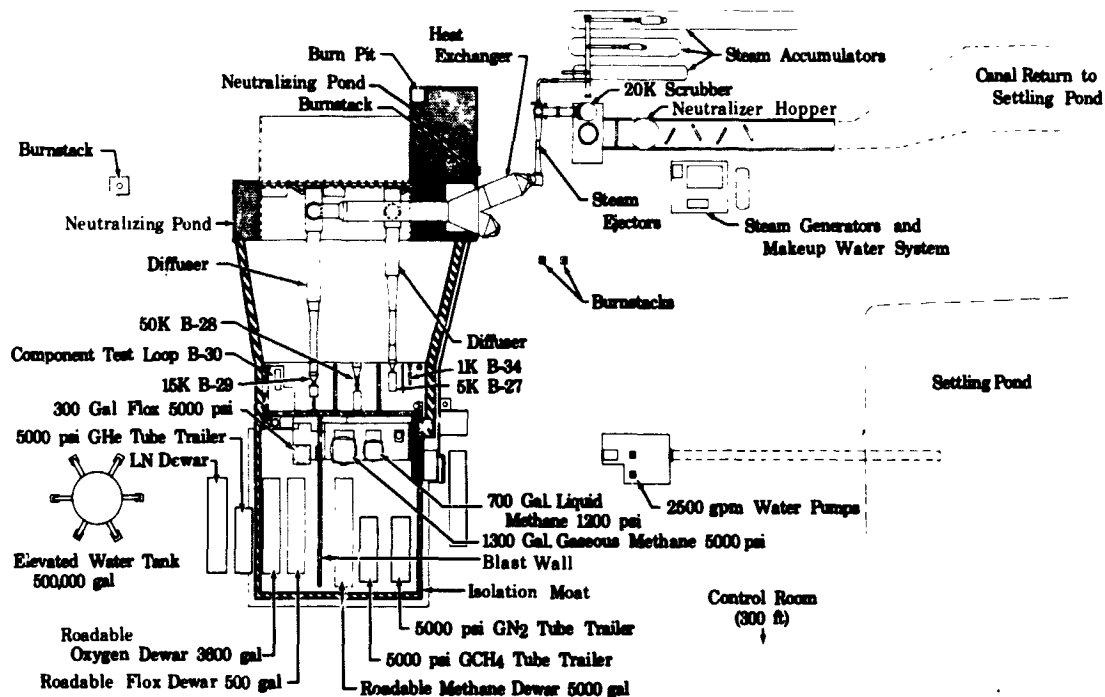
Figure 63. *Liquid Propellant Research Facility Schematic*   FD 12808C

(2)   Propellant Supply System

All flox/methane thrust chamber and engine tests conducted under the program were made in the 15,000-lb firing bay; however, four different flow configurations were used in performing the tests.

(A)   UNCOOLED PRESSURE-FED THRUST CHAMBERS

The propellant flow path for uncooled pressure-fed sea level thrust chamber tests is shown in figure 64. Ambient temperature gaseous methane was supplied from a 700-gallon high pressure run tank. Because chamber heat transfer considerations limited the run duration to four seconds, a continuous pressurizing system was not required and the tank served as a fixed volume blowdown system. Fuel flowrate was controlled by a single servo-operated control valve; a flow orifice and a choked venturi were used to provide redundant flowrate measurements. Liquid flox was supplied from a 300-gallon, 5000-psi tank through a liquid-nitrogen-jacketed run line with a flow nozzle and a cavitating venturi for measurement, and a single servo-operated valve for control.

104

Instrumentation List

No.[1]	Parameter	Recording and Readout Mode[2]		
		Digital Recorder	Oscillograph	Strip Chart
1	Methane Run Tank Pressure	1		1
2	Methane Orifice Upstream Pressure	1		
3	Methane Orifice Differential Pressure	2	1	1
4	Methane Orifice Downstream Temperature	1		
5	Methane Supply Line Pressure	1	1	
6	Methane Inlet Venturi Upstream Pressure	2	1	
7	Methane Injector Inlet Temperature	1		
8	Methane Injector Manifold Pressure	1	1	
9	Methane Run Valve Position	1	1	
10	Flox Run Tank Pressure	1		1
11	Flox Nozzle Upstream Pressure	1		
12	Flox Nozzle Differential Pressure	2	1	1
13	Flox Nozzle Downstream Temperature	1		
14	Flox Supply Line Pressure	1	1	
15	Flox Supply Line Temperature	1		
16	Flox Inlet Venturi Upstream Pressure	2	1	1
17	Flox Injector Inlet Temperature	1		
18	Flox Injector Manifold Pressure	1	1	
19	Flox Run Valve Position	1	1	
20	Chamber Pressure (Injector Face Static)	2	1	1
21	...ust	2	1	
22	Instrumentation Ring Temperature - Circumferential	33		
23	Instrumentation Ring Temperature - Axial	6		
24	Chamber Outer Skin Temperature	21		

(1) Numbers refer to locations shown on schematic.

(2) Numbers indicate quantity of records of parameters, either redundant or at different locations.

FD 25689A
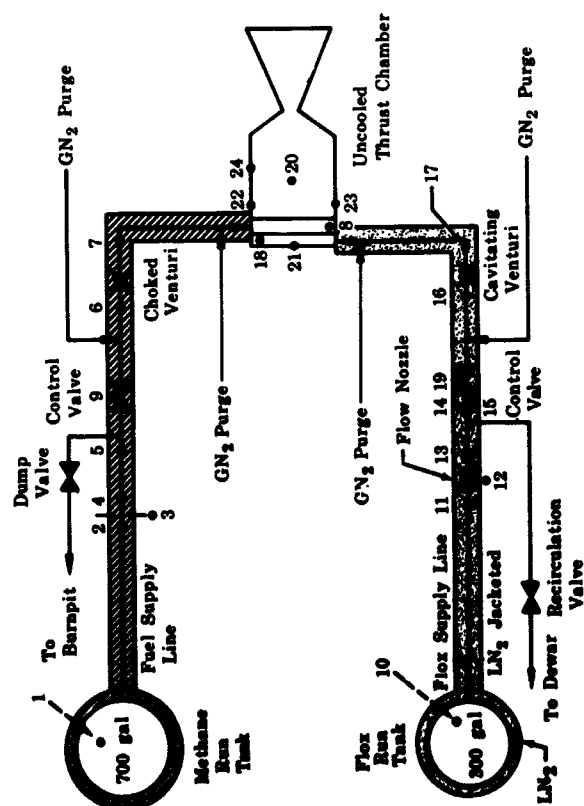
Figure 64. Propellant Flow Schematic for Uncooled Sea Level Tests

(B)   PRESSURE-FED COOLED THRUST CHAMBERS

Two types of pressure-fed cooled thrust chamber tests were conducted; separately cooled tests and supplemental cooled tests. In separately cooled tests, liquid methane for jacket cooling and gaseous methane for injection and combustion were supplied from separate sources. During supplemental cooled tests, liquid methane was supplied to the cooling jacket at a flowrate greater than that required for regenerative cooling and the desired flowrate of gaseous methane for the injector was tapped off at the jacket discharge. The flow schematics for these systems are shown in figures 65 and 66. They both permitted overcooling of the thrust chamber.

For cooled thrust chamber testing, liquid flox was supplied from the same system used for the uncooled tests. Liquid methane was supplied from a 700-gallon vacuum jacketed tank; the tank was pressurized with gaseous hydrogen and a single servo-operated valve was used for flow control. A turbine meter was used for liquid methane flow measurement in both types of tests. In the supplemental cooled tests, two servo-operated control valves were used; one maintained the discharge pressure, the other regulated the amount of fuel tapped off to supply the injector. As shown in figure 66, redundant instrumentation was used to measure the dump flow and the injector flow. For the separately cooled tests, ambient temperature gaseous methane was supplied from a 1300 gallon, 5000 psi run tank. Because the chamber was actively cooled, longer run durations than for the uncooled tests were planned, and high pressure roadable tube trailers were used to supply gaseous methane to the 1300 gallon tank. A single servo-operated control valve was provided in the coolant discharge line to maintain jacket exit pressure.

(C)   ENGINES

A schematic of the facility propellant supply configuration used during engine tests is shown in figure 67. Because of the large volume-low inlet pressure requirements, propellants for the engine tests were supplied from roadable Dewars. The fuel was supplied from a 5000 gallon, 70 psia vacuum-jacketed vessel through a vacuum jacketed run line. Liquid flox was supplied from a 500-gallon, 150-psia roadable Dewar connected to a liquid-nitrogen-jacketed line.

106

Instrumentation List

No.[1]	Parameter	Recording and Readout Mode[2]			
		Digital Recorder	O-Graph	Strip Chart	Meter
1	Methane Run Tank Pressure	1	1		
2	Methane Flowmeter Downstream Pressure	1	1	1	
3	Methane Flowmeter Downstream Temperature	2	1	1	
4	Methane Flow (Turbine Meter)	1			
5	Methane Jacket Inlet Pressure	1		1	
6	Methane Jacket Inlet Temperature	1			
7	Methane Jacket Discharge Temperature	1			
8	Methane Jacket Discharge Pressure	1	1	1	
9	Methane Run Tank Pressure				
10	Mixture Ratio				
11	Methane Orifice Upstream Pressure	1	1	1	
12	Methane Orifice Differential Pressure	2	1		
13	Methane Orifice Upstream Temperature	1			
14	Methane Venturi Upstream Pressure	2	1		
15	Methane Injector Inlet Pressure	1	1		
16	Methane Injector Inlet Temperature	1			
17	Methane Injector Manifold Pressure	1			
18	Flox Run Tank Pressure	1		1	
19	Flox Flow Nozzle Downstream Temperature	1	1		
20	Flox Flow Nozzle Upstream Pressure	2	1		
21	Flox Flow Nozzle Differential Pressure				
22	Methane Dump Valve Position	1	1		
23	Flox Injector Inlet Temperature	2			
24	Flox Injector Venturi Upstream Pressure		1		
25	Flox Injector Inlet Pressure	1	1		
26	Oxidizer Run Valve Position	1	1		
27	Jacket Fuel Valve Position	1	1		
28	Fuel Injector Valve Position	1			
29	Chamber Pressure (Injector Face Static)	2	1	1	
30	Coolant Tube Fuel Bulk Temperature	12			
31	Thrust	2	1	1	
32	Diffuser Half-Shell Pressure	4	1		
33	Oxidizer Purge Pressure	1			
34	Oxidizer Purge Regulator Pressure				
35	Flox Plumbing Inlet Temperature	1	1	:	
36	Fuel Inlet Venturi Temperature	1			
37	Flox Stand Cooldown Pressure		1	1	1

[1] Numbers refer to locations shown on schematic.
[2] Numbers indicate quantity of records of parameters, either redundant or at different locations.

FD 25690A

Figure 65. Propellant Flow Schematic for Separately Cooled Tests

107

Instrumentation List

No. [1]	Parameter	Recording and Readout Mode [2] Digital Recorder	O-Graph	Strip Chart	Meter
1	Methane Run Tank Pressure	1	1	1	
2	Methane Flowmeter Downstream Pressure	1		1	
3	Methane Flowmeter Downstream Temperature	1		1	
4	Methane Flow (Turbine Meter)	2	1	1	
5	Methane Jacket Inlet Pressure	1	1		
6	Methane Jacket Inlet Temperature	1	1	1	
7	Methane Jacket Discharge Temperature	1		1	
8	Methane Jacket Discharge Pressure	1			
9	Methane Overboard Discharge Orifice Upstream Pressure				
10	Methane Overboard Discharge Orifice Differential Pressure	2	1	1	
11	Methane Orifice Upstream Pressure	1	1		
12	Methane Orifice Differential Pressure	2	1	1	
13	Methane Orifice Downstream Temperature	1	1		
14	Methane Venturi Upstream Pressure	2	1		
15	Methane Injector Inlet Pressure	1	1		
16	Methane Injector Inlet Temperature	1	1		
17	Methane Injector Manifold Pressure	1			
18	Flox Run Tank Pressure	1			
19	Flox Flow Nozzle Downstream Temperature	1			
20	Flox Flow Nozzle Upstream Pressure	2	1	1	
21	Flox Flow Nozzle Differential Pressure	1			
22	Methane Dump Valve Position	1			
23	Flox Injector Inlet Temperature	2	1		
24	Flox Injector Venturi Upstream Pressure	1	1	1	
25	Flox Injector Inlet Pressure	1	1		
26	Oxidizer Run Valve Position	1			
27	Jacket Fuel Valve Position	1			
28	Fuel Injector Valve Position	2	1	1	
29	Chamber Pressure (Injector Face Static)	14			
30	Coolant Tube Fuel Bulk Temperature	2	1	1	
31	Thrust	4	1		
32	Diffuser Half-Shell Pressure	1			
33	Oxidizer Purge Pressure				
34	Oxidizer Purge Regulator Pressure				
35	Methane Overboard Discharge Orifice Temperature	1	1		
36	Fuel Inlet Venturi Temperature	1	1	1	
37	Flox Stand Cooldown Pressure	1	1	1	
38	Flox Plumbing Inlet Temperature				
39	Mixture Ratio				1

(1) Numbers refer to locations shown on schematic.
(2) Numbers indicate quantity of records of parameters, either redundant or at different locations.
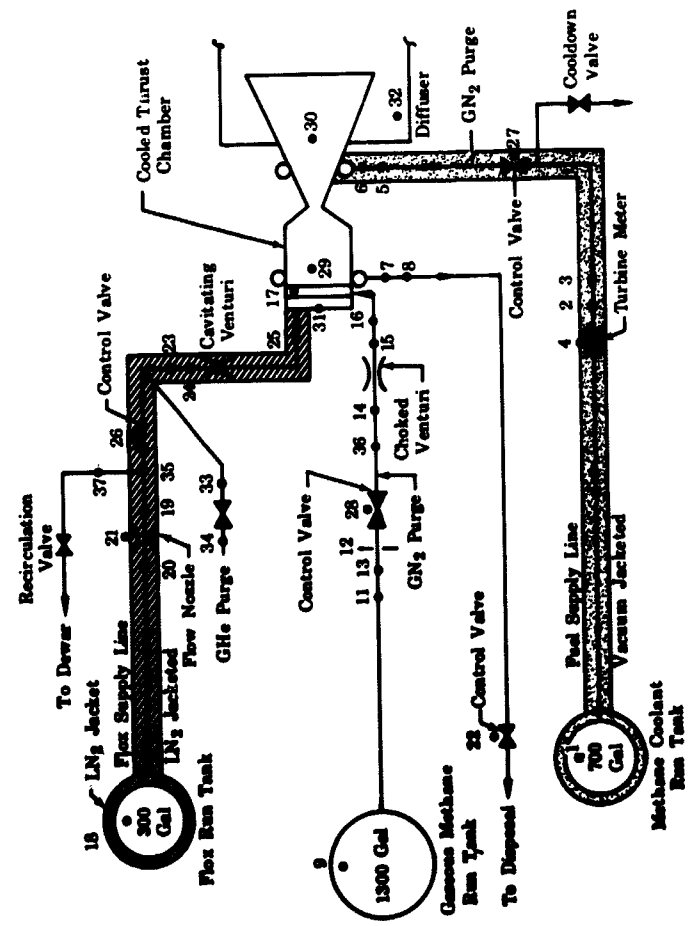
FD 25691A
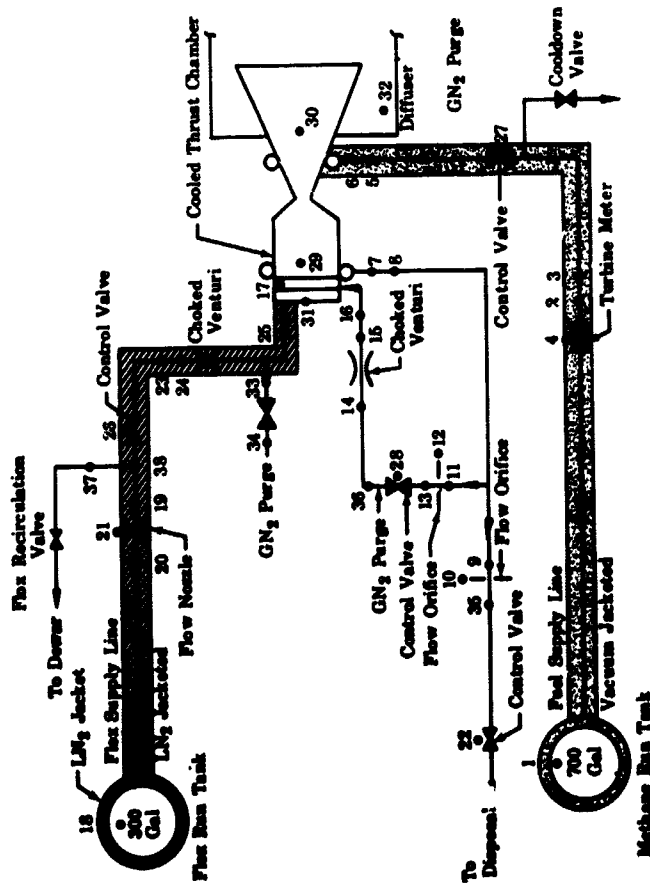

Figure 66. Propellant Flow Schematic for Supplemental Cooling Tests

Figure 67. Test Facility Flow Schematic for Engine Tests

FD 25692A

(3)   Test Stand Controls

An automatic closed loop control system consisting of an analog computer, digital sequencer, and the stand mounted electrohydraulic valves was available for control of test firing events when required. Figure 68 is a partial view of the LPRF control room showing the analog computer. The sequencer has capabilities for sequencing operation of up to 40 relay channels in 1-millisecond increments over a time interval of 2000 seconds. This system was used to interrogate designated parameters at specific time intervals to provide a go/no-go indication for the test either to proceed or advance to a sequenced shutdown. Analog control of up to ten functions using various control references such as flowrate, chamber pressure, mixture ratio, etc. was possible with the computer.
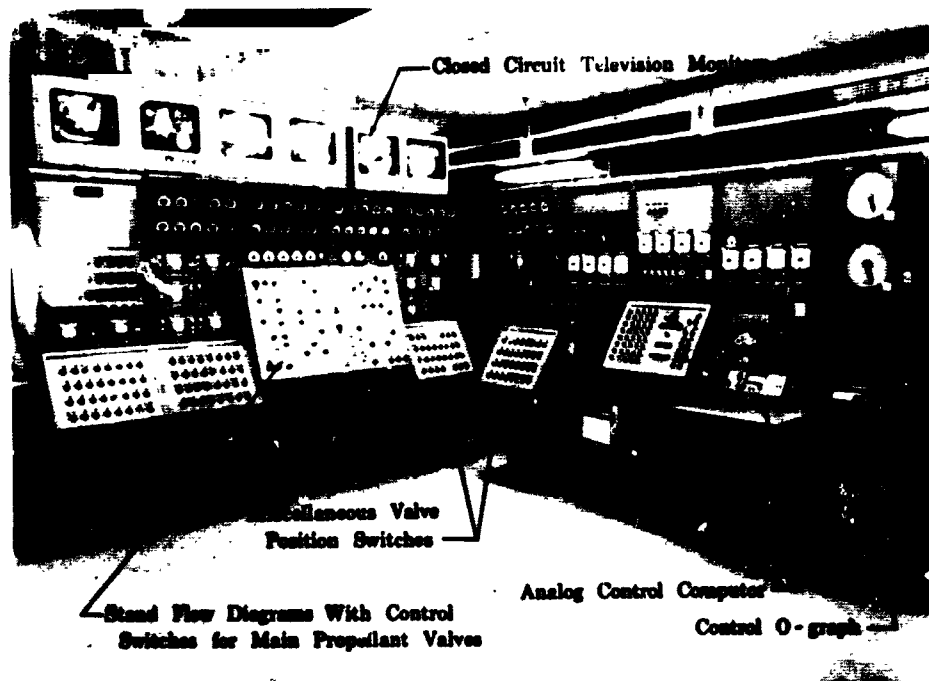
Figure 68.   LPRF Control Room   FD 19756

Control sequencing for each of the various types of tests was established during cold flow tests using the actual fuel (methane), but with liquid nitrogen substituted for the oxidizer. For uncooled sea level tests, the control sequence started with position control opening ramps of both the fuel and oxidizer valves using a timing sequence which provided simultaneous increases in the fuel and oxidizer pressures in the injector manifolds. Both valves remained in the open position until a flow of liquid oxidizer was established at the injector. At this time they were switched to a flow control mode. The initial position control mode was used in order to eliminate upsets that would be encountered in a flow control mode as the injector cooled down and the flow changed from gaseous to liquid phase.

110

In cooled pressure-fed thrust chamber tests, jacket coolant flow was established at the steady-state level before propellants were supplied to the injector. Cold flow tests were conducted with the objective of determining a sequence that would initiate injector flow after stable coolant flow was attained, but before the cooling jacket containe ' a significant amount of liquid. The avoidance of a significant amount of liquid was necessary to minimize the reduction or hesitation of coolant flow encountered when the rapid application of heat flux produced a rapid expansion of the coolant within the jacket. The coolant inlet valve was operated to control flowrate automatically and the coolant discharge valve was operated to maintain jacket exit pressure at a preset level automatically. In supplementary cooled tests, the injector fuel valve received its flow from the jacket discharge line, which was being controlled at a constant pressure. Therefore, it was possible to operate this valve in the same manner as if the fuel were supplied from a constant pressure tank. The injector propellant control scheme used for cooled tests was almost identical to that described for the uncooled tests.

For engine tests all control functions were accomplished by the engine control system. The test stand sequencer system was used only to schedule the actuation of the engine solenoid valves and to provide automatic go/no-go interrogations of critical parameters for safety shutdown systems. Mixture ratio and chamber pressure excursions were manually controlled from the control room using electro-mechanical drives to adjust the settings of the engine controls.

The go/no-go interrogations consisted of either continuous or intermittent sampling of critical parameters to determine if the test could be continued safely or if it should be advanced to shutdown. These checks, examples of which are given below, are used on all firing tests to assure safety on the test stand.

1. To verify ignition early in each test, the continuity of a weighted wire hanging in the center of the exhaust nozzle was checked. The time required for the wire to burn through was known and therefore provided a repeatable verification of timely ignition.

2. After stable operation had been attained, a continuous interrogation was initiated to ensure that chamber pressure was above the minimum level which would result if severe test rig damage or a facility malfunction occurred.

3. Continuous monitoring of the electrical continuity of a leak detection system that was used to provide an instal.* indication of leaks in the test stand or test rig fluorine plumbing. The system consisted of insulated wire wrapped around all lines and valves. If fluorine leaked through to the wiring, it caused a reaction of the insulation and either burn-through or shorting of the wire.

111

4. For simulated altitude tests a check of maximum diffuser pressure was used to ensure that the exhaust pressure did not exceed the incipient separation level of tne 40:1 area ratio nozzles (3 psia).

5. During the engine tests, a system was used to advance the test in the event that turbine inlet temperatures exceeded 850°R.

A number of purges were used to prevent contamination of the test article prior to test and to ensure clearing of propellants at shutdown. In general, most purges were controlled by electrically or hydraulically actuated valves that were sequenced off during the starting transient and were opened as the run valves were closed. Maintaining a continuous flow through the oxidizer injector to prevent aspiration of combustion products into the oxidizer manifold was found to be critical, and therefore a different purge method was employed at that location. A high flow helium purge (regulator pressure set at approximately 60% of the steady-state manifold pressure) was used. This purge remained on throughout the test and relied on a redundant check valve system to prevent backflow. This approach permitted continuous high volumetric purge flow through the oxidizer injector during normal test transients and assured continuous readiness in the event of unexpected emergency shutdowns.

(4) Data Acquisition

The LPRF central data acquisition system (figure 69) is capable of recording the outputs of up to 135 measurement channels from either of the four firing bays. Excellent recording accuracy and response are available through a 100-channel low-level input analog-to-digital converter. The converter feeds a magnetic tape system at commutated rates up to 80 scans per second for each of the entire 100 channels. This provides a data sample from each channel every 0.0125 second.

Figure 69. LPRF Data Recording Equipment FD 19757A

112

The records from the digital recorder were used for performance determination. Two 18 channel oscillographs and 14 channels of direct-inking strip charts are also available and were used primarily for monitoring during tests and analysis of transient behavior. A separate system including amplifiers, transducers and a high-speed 14-track tape recorder provides high-frequency data collection capability up to 20,000 cycles per second.

The locations of the instrumentation and the recording methods used for each of the various test configurations are shown on figures 64 through 67. Figure 70 shows engine mounted instrumentation used in addition to that shown on figure 67 for the supply system. Continuous remote test observation was possible through the use of six closed-circuit television channels with individual monitors; color film coverage was provided by three high speed cameras.

b. Oxidizer Pump Seal Test Rig

The initial durability and leakage rate test of the flox seal package was made using a liquid flox seal test rig fabricated and used previously for the fluorine pump dynamic seal investigation conducted in the Contract NASw-754 hydrogen-fluorine propulsion system research program (Reference A-1) · The rig was identical in all respects to a modified oxidizer pump, except that the impeller and inducer were eliminated and the forged housings were simplified accordingly. A drive adapter used in place of the gearbox housing acted as a mount between the pump and the drive unit and provided rear shaft bearing support identical to that in the turbopump assembly. The bearings were cooled by liquid nitrogen which was introduced at the rear roller bearing and was routed to the ball bearing mounted behind the pump dynamic seals. The schematic for the rig test arrangement is presented in figure 71; it consisted of a liquid nitrogen container, in which the test rig and a flox condensing coil were submerged, a 5 hp motor, and a variable speed drive.

A photograph of a test rig installed in the apparatus is presented in figure 72. This semi-portable arrangement was installed in the pump test position at the LPRF for the test. Gaseous flox was supplied, under pressure, from a special portable fluorine evaporator. The flox had previously been prepared in this container by evaporating liquid fluorine and liquid oxygen separately and using the method of gaseous partial pressures to establish the 82.6% concentration in the container. Flox pressure at the seal was controlled by a remotely operated valve in the gaseous flox supply line. Seal leakage was calculated from the pressure decay rate of the flox in the evaporator tubes.

113

Instrumentation List

No.(1)	Parameter	Recording and Readout Mode(2)			
		Digital Recorder	O-Graph	Strip Chart	Meter
1	Flox Pump Inlet Pressure	1			
2	Flox Pump Inlet Temperature			1	
3	Flox Pump Discharge Pressure				
4	Flox Pump Inlet Pressure				
5	Flox Injector Differential Pressure		1		
6	Flox Injector Inlet Temperature				
7	Flox Inlet Valve Position				
8	Flox Inlet Valve Body Pressure				
9	Flox Seal Cavity Pressure			1	
10	Seal Dam Helium Cavity Pressure			1	
11	Fuel Seal Cavity Pressure			1	
12	Flox Pump Bearing Temperature				
13	Flox Pump Housing Temperature				
14	Flox Pump Speed				
15	Flox Mixture Ratio Trimmer Position				1
16	Flox Injector Purge Pressure				
17	Methane Pump Inlet Pressure		1		
18	Methane Pump Inlet Temperature			1	
19	Methane Pump Interstage Pressure			1	
20	Methane Pump Interstage Temperature				
21	Methane Pump Discharge Pressure				
22	Methane Jacket Inlet Pressure				
23	Methane Jacket Inlet Temperature				
24	Methane Jacket Discharge Pressure				
25	Methane Jacket Discharge Temperature				
26	Methane Turbine Inlet Pressure		1		
27	Methane Turbine Inlet Temperature	1			
28	Methane Turbine Discharge Pressure	1			
29	Methane Turbine Discharge Temperature	1			
30	Fuel Injector Manifold Pressure	1	1		
31	Fuel Inlet Valve Position				
32	Interstage Valve Position				
33	Interstage Valve Body Pressure				
34	Interstage Valve Boost Cavity Pressure				
35	Discharge Valve Position	1			
36	Discharge Valve Body Pressure	1			
37	Discharge Valve Boost Cavity Pressure	1			
38	Fuel Pump Housing Temperature	1			
39	Gearbox Internal Pressure	1			
40	Thrust Control Servo Chamber Pressure		1		
41	Thrust Control Body Pressure		1		
42	Thrust Control Trimmer Position	1			1
43	Chamber Pressure at Thrust Control	1			
44	Chamber Pressure (Injector Face Static)	2	1	1	

(1) Numbers refer to locations shown on schematic.
(2) Numbers indicate quantity of records of parameters, either redundant or at different locations

FD 25693A

FD 23765D
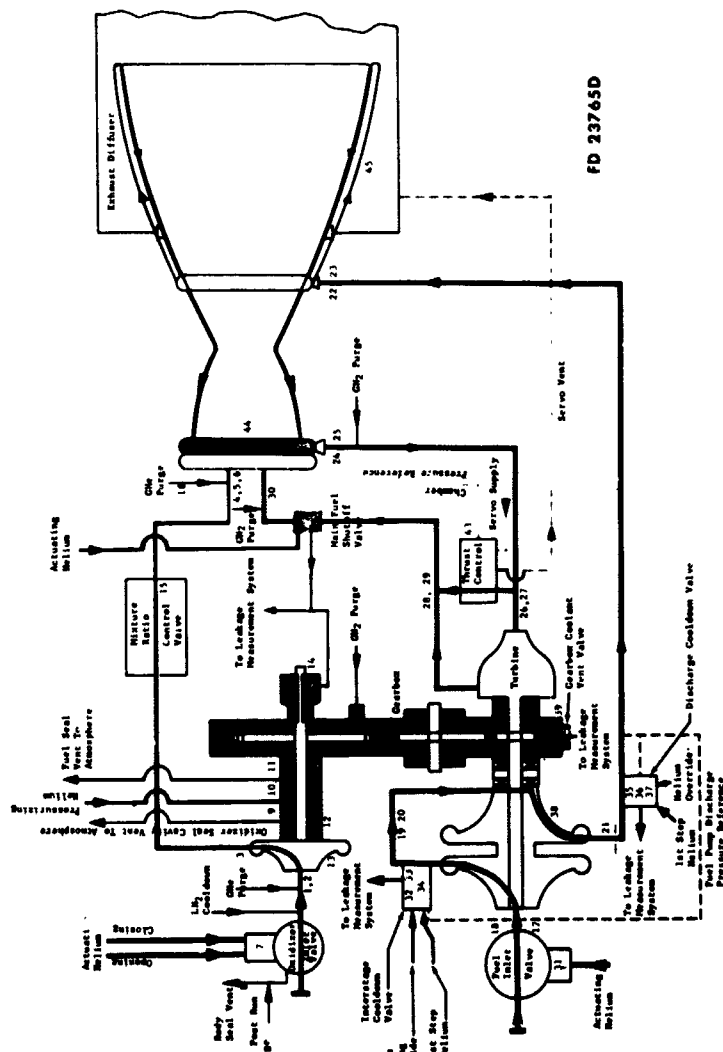
Figure 70. Flox/Methane Engine Instrumentation Locations

114
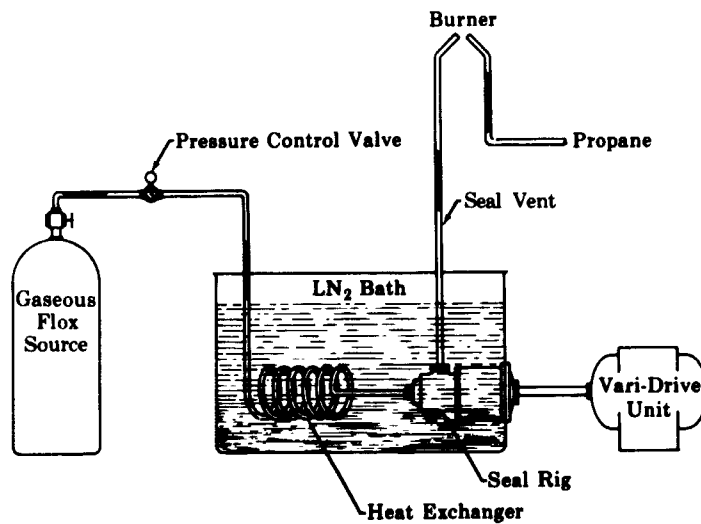
Figure 71. Flox Seal Test Schematic   FD 7394A
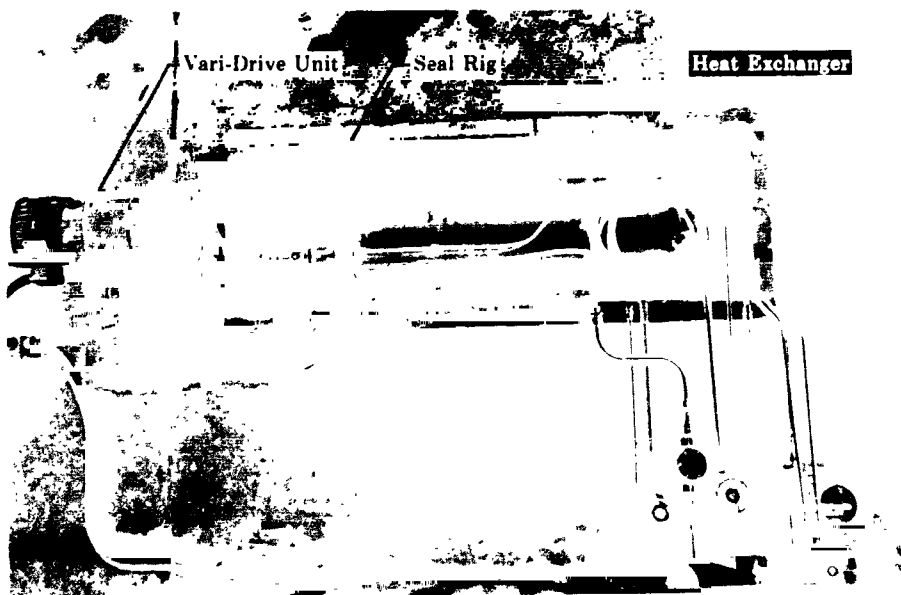
Figure 72. Liquid Flox Seal Test Apparatus   FD 7393

2. FLOX PUMP TEST LOOP

Liquid flox pump tests were conducted at the "I" Site of the NASA Lewis Research Center Plumbrook Station. The pressure and flow capabilities of the system were suitable for testing of modified RL10 oxidizer pumps, which made it possible to accomplish the pump testing required for the program without constructing new facilities. The drive adapter used in the seal rig tests was also used to mount the oxidizer pumps for these tests.

115

The propellant system of the facility is shown schematically in figure 73. It consists of a closed liquid fluorine loop incorporating the pump, a liquid nitrogen heat exchanger, a liquid fluorine accumulator, and necessary shutoff and control valves. Liquid nitrogen troughs are provided to cool all horizontal runs of fluorine piping.

The closed loop has the advantage of permitting pump tests to be accomplished with a minimum amount of liquid fluorine or flox. The total capacity of the system is approximately 500 pounds.

Automatic closed loop controls available at the facility permitted complete programing of pertinent pump parameters to obtain standard pump performance data. Typical operation of the RL10 oxidizer pump included a controlled speed ramp to operating conditions and automatically controlled flow excursions at constant controlled inlet total pressures. Tests were limited to static pump inlet pressures at or above ambient pressure to preclude the possibility of leakage into the system.
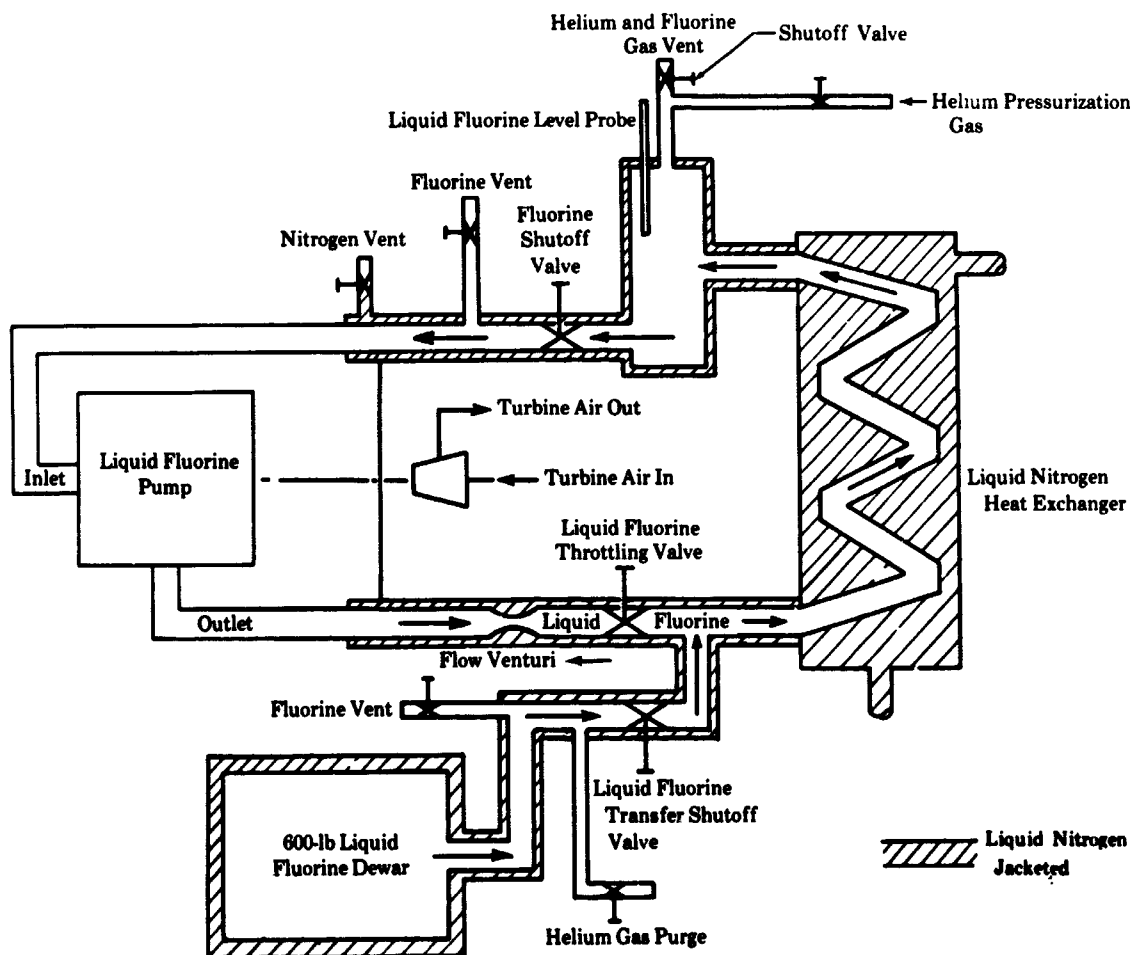
Figure 73.   NASA Liquid Fluorine Pump Loop Facility   *FD 13724A*

116

Data acquisition systems available to "I" Site include a low-level input analog-to-digital converter system with magnetic tape recording as well as several types of direct inking recorders and oscillographs necessary for test monitoring purposes. In testing of the RL10 oxidizer pump, all pertinent parameters were monitored on low-speed recorders during the entire period that flox was in the pump. The analog-to-digital data system was used only periodically to obtain performance data at selected points.

B. PROPELLANT HANDLING

1. FLOX

As noted above, all large scale liquid fluorine and flox operations at the Florida Research and Development Center are conducted at the LPRF. Handling of the propellants at the LPRF is accomplished remotely from the control room, which is located about 300 feet east of the test stands. Except for the supplier's delivery vehicles, which are equipped with manual valves, all fluorine systems are equipped with remotely operated valves. Liquid fluorine and liquid flox are stored in roadable Dewars similar to the delivery vessels, but equipped with remote-operated valves. The facility itself is west of all other test facilities and takes advantage of the prevailing easterly winds to carry fluorine vapors or reaction products away from inhabited areas.

The oxidizer in this program was liquid flox with a nominal fluorine concentration of 82.6 percent. The same procedures used for operation with liquid fluorine were used in handling the flox mixtures.

Detailed descriptions of fluorine handling procedures used by Pratt & Whitney Aircraft are presented in References A-1 and A-2. Rigorous standards of materials selection, fabrication, cleaning, passivation, and leak detection are followed for fluorine test facility design and operations. Metals of proved compatibility and durability (such as nickel, aluminum, copper and series 300 stainless steels) are used. During system design, mechanical joints are eliminated and full penetration welds used wherever possible. Facility valves are of the top-entry solid body type, having copper braid rings and Teflon chevron stem packings arranged as shown in Figure 74. Test stand fluorine systems are cleaned upon initial installation and after modifications involving cutting and welding. Cleaning is accomplished by flushing the system with an acidic solvent followed by flushing with demineralized water and vacuum drying. After cleaning, the system is passivated using gaseous fluorine at a pressure of approximately 200 psig. Mechanically assembled subsystems and components, such as instrumentation transducers, are individually passivated before installation. Prior to the first test of each series, the facility is passivated for 1 hour using gaseous fluorine at 15 psig. During this passivation a complete sniff check is made on all fluorine joints and valve stems.

Teflon "V" Rings

Coppe Braid Packing

Packing Column
Retainer

Vent Plugged

Copper Lantern
Ring

Packing Column

Valve Body with Ends
Prepared for Welding
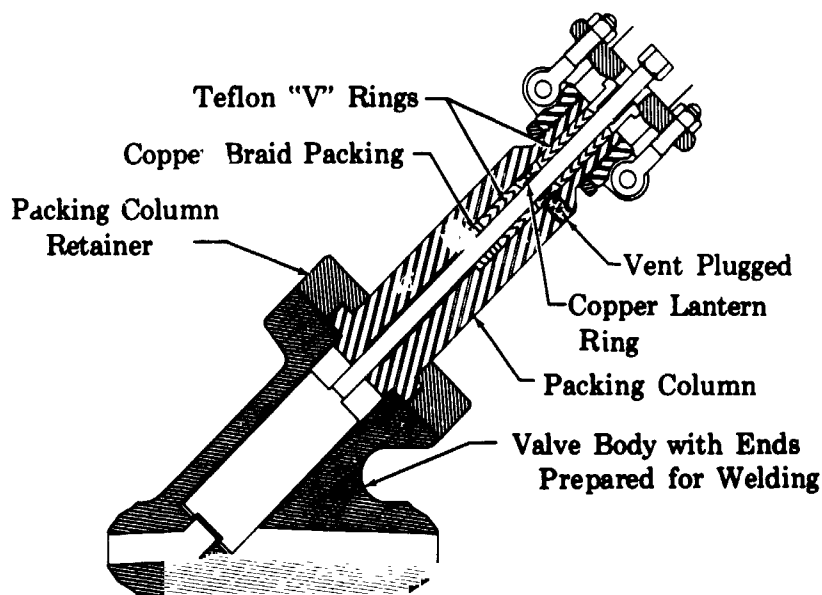
Figure 74. Liquid Fluorine Facility Valve   FD 25686

More than 288,000 pounds of liquid fluorine have been consumed at the LPRF in over 545 rocket chamber firings and in numerous valve and pump seal tests. While there have been several incidents involving fluorine leakage or reactions, there have been no serious personnel injuries and only minimal facility damage has been encountered.

Liquid flox was prepared in a nitrogen-jacketed roadable dewar by adding liquid oxygen and liquid fluorine while the dewar was mounted on load cells. The weight of each constituent added was determined from total dewar weight monitored and recorded in the control room. The concentration established by weighing was then verified by chemical analyses. Samples for analysis were taken after the entire flox batch was transferred to the oxidizer run tank and recirculated back to the roadable vessel twice to ensure a uniform mixture. Accurate samples were obtained by trapping liquid flox in a nitrogen-jacketed chamber. After trapping the liquid sample, the nitrogen flow to the jacket was secured, a valve to an evacuated bottle was opened, and the sample was permitted to warm up and evaporate until the system came to equilibrium.

Flox concentration of the vaporized sample was determined by laboratory analysis using the wet chemistry mercury absorption technique. This method of analysis is one of the oldest direct techniques for the determination of fluorine concentration. It is based upon the rapid absorption of fluorine gas by elemental mercury to reduce the pressure of a gaseous sample. The quantity of fluorine absorbed is determined by measurement of the pressure and volume of the sample before and after absorption.

The highly accurate mercury-absorption apparatus developed and used at the Florida Research and Development Center is shown schematically in figure 75. It uses a fluorine compatible pressure transducer to automatically record the pressure of the sample within a constant volume system. In operation, a portion of the vaporized flox sample was transferred into the evacuated reaction chamber. The reference initial pressure was established at this point and the recorder was set at 100%. A measured quantity of mercury was then allowed to flow into the reaction chamber. The pressure immediately decayed as the fluorine was absorbed by the mercury. A magnetic stirrer for the mercury was provided to disperse the inert interface of mercury fluoride which forms on the mercury surface, and thereby to assure complete absorption. When complete absorption was indicated (by a leveling of the pressure trace on the recorder), the reaction flask was opened to an evacuated expansion coil having a volume equal to the volume of the mercury added; thus the system was returned to its original volume. The pressure recorder then indicated directly the percentage of sample that was not absorbed. With this apparatus, duplicate analyses of samples in the range of 63-93% fluorine have shown a repeatability of 0.23%.
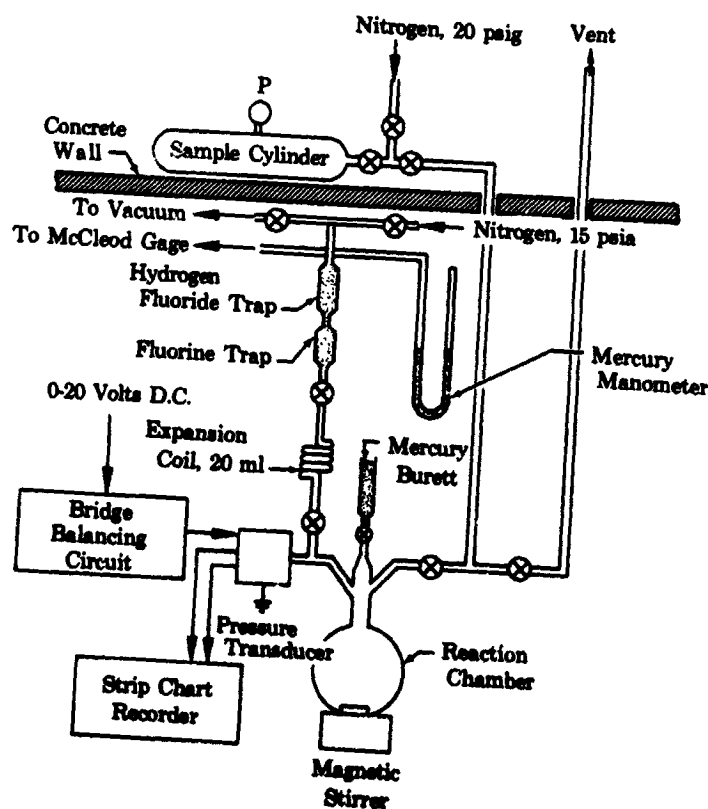
Figure 75. Schematic Diagram of Mercury Absorption Apparatus

FD 19753

119

A gas chromatograph system (Reference A-2) has been developed and was operational during the latter phases of this program; however, it was not used as a primary check of flox concentration because of the excellent results obtained with the simpler mercury absorption system.

2. METHANE

Methane was purchased as both a gas in high pressure cylinders and as a liquid in vacuum jacketed roadable dewars. Methane presented no unusual handling problems and was routinely handled using the methods commonly used for flammable gases and cryogenic liquids.

Methane is non-corrosive and almost any commercially available metal can be used. In the systems used by Pratt & Whitney Aircraft, the most common materials were stainless steel and copper for containers and lines, and soft aluminum or Teflon coated stainless steel in seals. Some non-metallic materials can be used in methane depending on the use and required length of service; however, methane is a strong solvent and non-metallic materials are usually deteriorated by the solvent action.

C. REFERENCES

A-1. "Research on A Hydrogen-Fluorine Propulsion System — Final Report," Pratt & Whitney Aircraft FR-1585, NASA CR-72074, Contract NASw-754, 21 October 1966. CONFIDENTIAL (Title Unclassified).

A-2. "Investigation of Light Hydrocarbon Fuels With Fluorine-Oxygen Mixture as Liquid Rocket Propellants — Final Report," Pratt & Whitney Aircraft FR-2227, NASA CR-72147, Contract NAS3-6296, 15 September 1967.

APPENDIX B
DATA REDUCTION AND PERFORMANCE CALCULATIONS
A. DATA ACQUISITION

The low-level input digital recording system at the Liquid Propellant Research Facility was used during tests to obtain magnetic tape records of all measured parameters at a scanning interval of 0.0125 seconds. A high-speed IBM System 360-Model 65 digital computer was used to reduce the recorded data to engineering units and to calculate the time based averages that are used for steady-state performance determination. ..Iaximum, minimum, and 3σ levels of the recorded data within the period of the average are printed out concurrently with the average to provide a convenient reference for critical review of parameter stability. Oscillograph, strip chart, and scan-to-scan digital data are also reviewed to ensure parameter stability.

B. PERFORMANCE ANALYSIS

Performance parameters not directly measured and the methods used for their determination are described in the following paragraphs.

1. THRUST

a. Uncooled Thrust Chamber Test

Vacuum thrust for the uncooled thrust chambers tested at sea level conditions was determined from measured thrust using the relation:

$$F_{vac} = F_{meas} + P_a A_e \qquad \text{(B-1)}$$

b. Cooled Thrust Chamber and Engine Tests

The supersonic diffuser described in Appendix A was used to simulate altitude conditions in all tests of the 40:1 expansion ratio cooled thrust chambers. The altitude test thrust chambers were mounted so that a portion of the expansion nozzle projected into the diffuser (figure 76). A low leakage slip seal was provided at the diffuser entrance to allow free axial nozzle translation. In determining the vacuum thrust for tests in the altitude system, the last term in equation (B-1) was modified to include the pressure forces encountered, resulting in the expression:

$$F_{vac} = F_{meas} + P_a A_s + P_{diff} (A_e - A_s) \qquad \text{(B-2)}$$
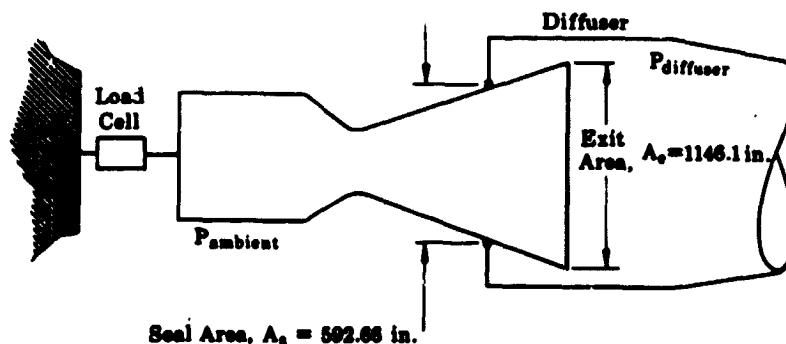
Figure 76. *Schematic Diagram of Chamber-Diffuser Installation*   FD 2560a

2. THRUST CHAMBER THROAT TOTAL PRESSURE

Thrust chamber throat total pressure was determined by correcting injector face static pressure measurements for momentum losses. The momentum loss was determined for each data point using a stepwise procedure programed for solution by digital computer.

To establish conditions at the initial station in the thrust chamber (see figure 77) it was assumed that injected propellants were mixed but unburned. The measured injector face static pressure and perfect gas relationships were then used to define properties at this station.
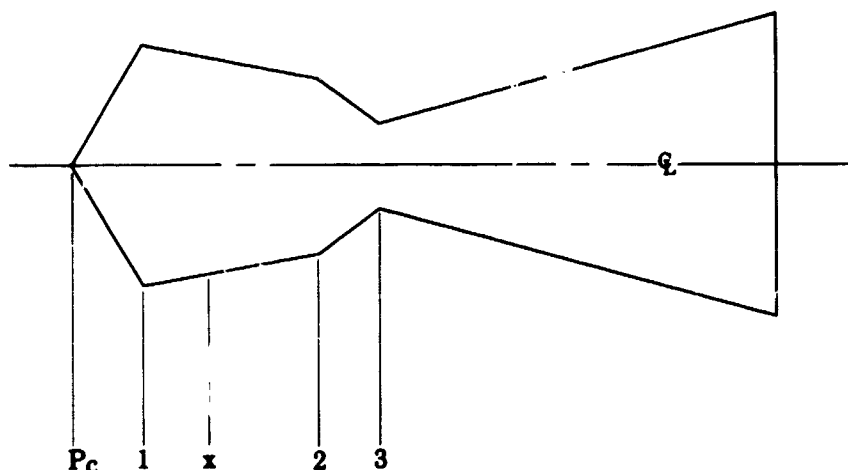
Figure 77. Stations Used in Momentum Loss Calculation FD 25687

In order to proceed from station 1 to station 2 where combustion is assumed to be complete, Rayleigh flow relations were used because the losses due to friction are negligible. The following relations hold between station 1 and any station x:

Conservation of mass:

$$\frac{\dot{w}_p}{A} = \rho_1 V_1 = \rho_x V_x \tag{B-3}$$

Conservation of momentum:

$$P_1 + \frac{\dot{w}_p V_1}{A_1 g} = P_x + \frac{\dot{w}_p V_x}{A_x g} \tag{B-4}$$

Conservation of energy:

$$h_1 + \frac{V_1^2}{2gJ} + Q = h_x + \frac{V_x^2}{2gJ} \tag{B-5}$$

The properties of the reacting fluid at location x are found through the simultaneous solution of the above three equations and the equations of state (assuming chemical equilibrium at station x):

$$P_1 = \rho_1 R_1 T_1 \tag{B-6}$$

$$P_x = \rho_x R_x T_x \tag{B-7}$$

Iterative calculations based on equations derived from the above, a Mach number balance against total temperature ratio, and thermodynamic properties following complete combustion were used to determine the fluid properties at each succeeding increment of x between stations 1 and 2. The constant flow area requirement implicit in these relations was satisfied for the converging RL10 chamber contour through the division of axial length between stations 1 and 2 into quarter inch increments for which the area change was very small.

At station 2 combustion was assumed to be complete and the total pressure at that point was determined. It is assumed that all combustion occurs upstream of station 2 and, therefore, the combustion chamber throat total pressure is identical to the station 2 total pressure.

3. PERFORMANCE PARAMETERS

Vacuum thrust and combustion chamber throat total pressure (P_t) determined as outlined in paragraphs 1 and 2 above are used to calculate the normal thrust chamber and engine performance parameters:

Vacuum Specific Impulse

$$I_{vac} = \frac{F_{vac}}{\dot{w}_o + \dot{w}_f} \tag{B-8}$$

Characteristic Exhaust Velocity

$$c^*_{(P_c)} = \frac{P_t A_t g}{\dot{w}_o + \dot{w}_f} \tag{B-9}$$

Vacuum Thrust Coefficient

$$C_{Fvac} = \frac{F_{vac}}{P_t A_t} = \frac{I_{vac} g}{c^*} \tag{B-10}$$

For the low expansion ratio uncooled sea level tests, characteristic exhaust velocity was also calculated from the measured thrust, using a theoretical thrust coefficient (C'_{Fvac}) and a calculated stream thrust coefficient C_s, which is equivalent to thrust coefficient efficiency when there are no kinetic losses.

$$c^*_{(F)} = \frac{F_{vac} g}{C_s C'_{Fvac} \dot{w}_p} \tag{B-11}$$

The stream thrust coefficient was calculated using the method of characteristics and including the effects of wall friction (Reference B-1). For the 15° half-angle area ratio of 3.266 nozzles used, the calculated value of C_s was 0.9758. Good correlation was obtained between c* values based on thrust and chamber pressure, which confirmed the validity of the method used to calculate throat total pressure, and thereby provided confidence in altitude test results.

4. PERFORMANCE EFFICIENCIES

Performance efficiencies were determined using full shifting equilibrium performance values, calculated with thermochemical data published by the Joint Army-Navy-Airforce (JANAF) Thermochemical Panel, as the reference Because propellant performance is a function of chamber pressure, mixture ratio, and propellant inlet energy, bivariant curve fits of the theoretical data were stored as permanent data in the computer program employed for performance calculations.

Theoretical Vacuum Specific Impulse

$$I'_{vac} = f_1 \left[P_t, r, \Delta hi \right] \qquad (B-12)$$

and

Theoretical Characteristic Exhaust Velocity

$$c^{*'} = f_2 \left[P_t, r, \Delta hi \right] \qquad (B-13)$$

Where Δhi was used to correct for the deviation of the actual inlet conditions from the reference normal boiling point liquid inlet state. These curve fits were then used to provide the theoretical performance for the efficiency determinations:

Ideal Specific Impulse Efficiency

$$\eta I_{vac} = I_{vac}/I'_{vac} \qquad (B-14)$$

Characteristic Exhaust Velocity Efficiency

$$\eta c^*_{(P_c)} = c^*_{(P_c)}/c^{*'} \qquad (B-15)$$

$$\eta c^*_{(F)} = c^*_{(F)}/c^{*'} \qquad (B-16)$$

Vacuum Thrust Coefficient Efficiency

$$\eta C_{F_{vac}} = \left[\frac{I_{vac}g}{c^*} \right] \left[\frac{c^{*'}}{I'_{vac} g} \right] = \frac{\eta I_{vac}}{\eta c^*} \qquad (B-17)$$

In calculating efficiencies, allowances for heat rejection to the thrust chamber walls were made by applying suitable corrections to measured performance values. The nature of the required heat rejection correction is dependent upon the cooling mode as described in the following paragraphs.

a. Regenerative Cooling (Engines and Pressure-Fed Thrust Chambers)

Specific impulse can be expressed as:

$$I = \frac{V_{pe}}{g} \qquad (B-18)$$

where V_{pe} is the propellant velocity at the nozzle exit, and the chamber/ nozzle steady-flow energy equation may be written as:

$$\frac{\dot{w}_o \, h_{o_i}}{\dot{w}_p} + \frac{\dot{w}_f \, h_{f_{ji}}}{\dot{w}_p} + Q + \frac{V_{pi}^2}{2gJ} = h_{pe} + \frac{V_{pe}^2}{2gJ} \qquad \text{(B-19)}$$

For regenerative cooling the heat transferred from the combustion products to the chamber walls is identical in magnitude to the heat gained by the fuel in cooling the jacket and there is no net loss to the system, so the value of the Q term in equation B-19 is zero, i.e., no correction is required.

The expression for characteristic exhaust velocity may be written as:

$$\text{(B-20)}$$

$$c^* = \frac{\sqrt{g \, k_{p_t} \, R_{p_t} \, T_{p_t}}}{k_{p_t} \sqrt{\left[\dfrac{2}{k_{p_t} + 1}\right]^{\left[\dfrac{k_{p_t} + 1}{k_{p_t}}\right]}}}$$

The ratio of propellant specific heats (k_p) and the gas constant (R_p) are weak functions of the propellant combustion temperature (T_p) over the heat rejection range of interest and can be assumed constant for a given mixture ratio and chamber pressure. The combustion temperature is affected by the temperature of the propellants at the injection point and therefore by any heat transfer to the propellants within the system between the inlet and the injector. There is no appreciable heat transfer to the oxidizer, but there is significant heating of the fuel which is the jacket coolant.

Characteristic exhaust velocity is a parameter that is based upon combustion product properties in the combustion chamber, i.e., the volume between the injector and the throat. As in the discussion above for effects on specific impulse, the heat transferred to the fuel coolant in the combustion chamber (upstream of the throat) is equal to the heat lost by the combustion gases, and there is no net effect of chamber heat transfer on characteristic velocity. However, the heat transferred to the fuel in cooling the expansion nozzle contributes to an increase in the inlet energy state of the propellant that is not obtained within the limits of the combustion chamber and therefore must be accounted for.

The change in combustion temperature resulting from heat addition to the fuel may be represented as:

$$T'_p - T_p = \frac{Q_n}{(C_p)_p} \qquad \text{(B-21)}$$

where Q_n is the heat transferred from the combustion products between the throat and the nozzle exit. It was not always possible to instrument chambers to determine coolant temperature rise at the throat, and therefore the correction was calculated as a constant percent of the overall heat transfer to the jacket. The percentage was based upon coolant temperature profile data obtained in instrumented chambers used for the pressure-fed chamber tests, which indicated that 80 percent of the coolant enthalpy change occurred between the coolant inlet manifold and the thrust chamber throat. Thrust chambers used in the engine tests did not incorporate enough instrumentation to provide an accurate determination of the nozzle heat transfer. The data does, however, tend to substantiate that obtained in the pressure-fed tests.

Using the 80% value,

$$Q_n = -0.8 \; \frac{\dot{w}_f \; (\Delta h_{j_c})}{\dot{w}_p} \tag{B-22}$$

and, combining equations (B-21) and (B-22)

$$T'_p = T_p - \frac{0.8 \; \dot{w}_f \; (\Delta h_{j_c})}{\dot{w}_p \; (C_p)_p} \tag{B-23}$$

Referring to equation (B-20), the corrected c^* is then

$$c^*_{corr} = c^*_{meas} \sqrt{T'_p / T_p} \tag{B-24}$$

or in a form more adaptable for calculations

$$c^*_{corr} = c^*_{meas} \left(\frac{c^{*'}_{corr}}{c^{*'}} \right) \tag{B-25}$$

Where $c^{*'}$ is determined from the curve fit for c^* (equation B-13) using the standard inlet conditions ($\Delta h_i = 0$) and $c^{*'}_{corr}$ is determined at standard inlet conditions using $\Delta h_i = Q_n$.

b. Supplementary Cooled Pressure-Fed Thrust Chambers

For the overcooled mode, where a portion of the coolant is dumped overboard ($\dot{w}_{f_{jd}}$), the steady-flow energy equation as it applies to the entire thrust chamber becomes

$$\frac{\dot{w}_o h_{o_i}}{\dot{w}_p} + \frac{(\dot{w}_{f_{jc}} - \dot{w}_{f_{jd}}) h_{f_{j_i}}}{\dot{w}_p} + Q + \frac{V_{p_i}^2}{2gJ} = h_e + \frac{V_{p_e}^2}{2gJ} \tag{B-26}$$

where $\dot{w}_{f_{jc}} - \dot{w}_{f_{jd}}$ is the injector fuel flow. In this instance only the heat transferred to the injector flow by the combustion gases is recovered as energy in the injected propellants, i.e., there is a net Q loss equal to:

$$Q = \dot{w}_{f_{jd}} \left[h_{j_o} - h_{j_i} \right] \tag{B-27}$$

126

The value of specific impulse calculated from the chamber inlet condition must be corrected for the heat lost in the dumped coolant. Again, the correction was determined in practice by using curve fit reference theoretical performance that accounted for heat rejection. The calculation was:

$$I_{vac_{corr}} = I_{vac_{meas}} \left(\frac{I_{vac_{corr}}'}{I_{vac}'} \right) \tag{B-28}$$

where the prime values were determined in the same manner as detailed for the c* calculation.

Heat transfer elements to be considered for c* efficiency determination in the overcooled mode include the energy picked up by the injected fuel $(\dot{w}_{f_{jc}} - \dot{w}_{f_{jd}})$ in the nozzle, minus the energy transferred to that portion of the chamber coolant flow which is dumped overboard, $w_{f_{jd}}$. Considering that 80 percent of heat transfer takes place between the coolant inlet and the throat, it can be shown that:

$$Q = -0.8 \; \frac{\dot{w}_{f_{jc}} (\Delta h_{j_c})}{\dot{w}_p} + \frac{\dot{w}_{f_{jd}} (\Delta h_{j_c})}{\dot{w}_p} \tag{B-29}$$

and therefore:

$$T'_p = T_p - 0.8 \; \frac{\dot{w}_{f_{jc}} (\Delta h_{j_c})}{\dot{w}_p (C_p)_p} + \frac{\dot{w}_{f_{jd}} (\Delta h_{j_c})}{\dot{w}_p (C_p)_p} \tag{B-30}$$

The corrected value of characteristic velocity is then calculated using equation B-25.

c. Separately Cooled Rigs

In the separately cooled pressure-fed rigs, gaseous injector fuel was supplied from a separate source and all of the thrust chamber coolant was dumped overboard. The increased energy of the gaseous fuel (from the liquid base conditions) was accounted for in the reference performance values through the curve fits depicted by equations B-12 and B-13. The heat loss corrections to measured data were similar to those used for the overcooled chambers. In the steady flow energy equation Q is the heat transferred to the dumped coolant (per pound of propellant).

$$\frac{\dot{w}_o h_o}{\dot{w}_p} + \frac{\dot{w}_f h_{f_i}}{\dot{w}_p} + Q + \frac{V_{pi}^2}{2gJ} = h_{pe} + \frac{V_{pe}^2}{2gJ} \tag{B-31}$$

$$Q = - \; \frac{\dot{w}_{j_c} (h_{c_{jd}} - h_{c_{ji}})}{\dot{w}_p} \tag{B-32}$$

Again, as in the case of the overcooled chambers, the value of specific impulse can be corrected for heat lost in the dumped coolant by using equation B-28.

Also considering that 80 percent of the heat transfer occurs in the nozzle, the value of heat transfer in the combustion chamber is

$$Q_c = \frac{0.2 \, \dot{w}_{jc} \, (h_{c_{jd}} - h_{c_{ji}})}{\dot{w}_p} \qquad (B\text{-}33)$$

The heat lost to the coolant reduces the combustion temperature, therefore

$$T_p{}' = T_p - Q_c / (C_p)_p \qquad (B\text{-}34)$$

and the corrected value of characteristic velocity is calculated using the method of equation B-25.

d. Uncooled Pressure-Fed Rigs

For the uncooled mode, the steady flow energy equation as it applies to the entire thrust chamber becomes

$$h_{p_i} + \frac{V_{pi}^2}{2gJ} + Q = h_{pe} + \frac{V_{pe}^2}{2gJ} \qquad (B\text{-}35)$$

where Q is the heat transferred from the combustion products to the heat sink chamber/nozzle walls and therefore lost to the exhaust stream. Specific impulse must be adjusted for the total flow of heat from the combustion products to the chamber-nozzle walls, which was calculated using heat transfer rates obtained from experimentally determined heat flux profiles. Corrected specific impulse was then obtained using equation B-28.

The heat transferred to the chamber walls upstream of the throat reduces the combustion temperature, and therefore must be accounted for with a correction to c^*. The heat transferred was calculated from the experimental heat flux profile, and c^* was corrected using equation B-25.

The use of a correction for thermal growth of the copper chambers was considered. However at the heat flux levels measured in these tests, the thermal growth of the 0.75 inch thick copper chambers during the short duration firings was negligible and corrections were not necessary.

C. EXPERIMENTAL DATA ERROR ANALYSIS

To validate the experimental performance data, a statistical error analysis was made for a typical engine demonstration test. These results are also applicable to performance data obtained in injector/chamber rig tests for which almost identical pressure, flowrate, and temperature instrumentation were used.

Estimates of performance data uncertainty were obtained by combining the precision and bias estimates for the individual parameters using a statistical variation analysis (Reference B-2). Basically, the precision error of a function may be estimated by combining the precision errors of the independent variables in that function in the following manner:

128

$$S_{\phi}^{2} = \sum_{i=1}^{n} \left(\frac{\partial \phi}{\partial x_{i}}\right)^{2} \left(Sx_{i}\right)^{2}$$

where:

S_{ϕ} = estimate of the precision error for the parameter (would be 1-σ precision for infinite sample)

$\dfrac{\partial \phi}{\partial x_{i}}$ = the partial derivative of the function with respect to the ith variable

$S_{x_{i}}$ = the precision error estimate value associated with the ith variable.

For example, in calculating characteristic exhaust velocity based on chamber pressure

$$c^{*}_{(P_{c})} = \frac{A_{t} g P_{t}}{\dot{w}_{p}}$$

the precision error estimate, $S_{c^{*}_{(Pc)}}$, is given by:

$$(Sc^{*}_{P_{c}})^{2} = \left(\frac{\partial c^{*}_{P_{c}}}{\partial A_{t}}\right)^{2} (S_{A_{t}})^{2} + \left(\frac{\partial c^{*}_{P_{c}}}{\partial P_{c}}\right)^{2} (S_{P_{c}})^{2} +$$

$$\left(\frac{\partial c^{*}_{P_{c}}}{\partial \dot{w}_{p}}\right)^{2} (S_{\dot{w}_{p}})^{2}$$

where:

$$\left(\frac{\partial c^{*}_{P_{c}}}{\partial A_{t}}\right) = \frac{g_{o} P_{c}}{\dot{w}_{p}}$$

$$\left(\frac{\partial c^{*}_{P_{c}}}{\partial P_{c}}\right) = \frac{A_{t} g_{o}}{\dot{w}_{p}}$$

$$\left(\frac{\partial c^{*}_{P_{c}}}{\partial \dot{w}_{p}}\right) = \frac{A_{t} g_{o} P_{c}}{(\dot{w}_{p})^{2}}$$

The bias limit associated with each function is estimated from identical equations, but substituting the bias limit of each parameter for the precision error. Using the methods suggested by the ICRPG Experimental Measurements Committee (Reference B-3), the uncertainty of each parameter was calculated from

$$U = \pm [B + 2S]$$

where B is the bias limit and S is the precision. The 2S value of the uncertainty, U, indicates that 95% confidence interval estimate is used to represent the precision portion of uncertainty. U therefore represents the limits around the true value beyond which no data would reasonably be expected to fall.

The uncertainty estimates for the engine performance parameters are given in table XVI. The uncertainty estimates presented are somewhat pessimistic because, while they reflect the increased accuracy from redundant measurements, they do not reflect the improvement obtained by time averaging.

TABLE XVI. EXPERIMENTAL ERROR ANALYSIS–ENGINE TEST NO. E-7

Parameter	Units	Nominal	Bias Limit (% of Nominal)	Precision 2S-95% Confidence (% of Nominal)	Uncertainty (% of Nominal)
P_c	$lb_f/in.^2$	238.4	0.150	0.500	0.650
F_{vac}	lb_f	11764	0.121	0.249	0.370
$\dot{w}_o$	lb_m/sec	25.54	0.954	0.805	1.759
$\dot{w}_f$	lb_m/sec	5.73	0.914	0.800	1.714
$\dot{w}_p$	lb_m/sec	31.57	0.796	0.679	1.470
I_{vac}	$lb_f\text{-}sec/lb_m$	376.3	0.804	0.716	1.580
c^*	ft/sec	6670	0.856	1.004	1.860
$C_{F vac}$	—	1.77	0.539	0.786	1.125

D. LIST OF SYMBOLS

Symbol	Parameter	Units
A	Area	in^2
C_F	Thrust Coefficient	—
C_p	Constant Pressure Specific Heat	$Btu/lb_m\text{-}°R$
C_s	Stream Thrust Coefficient	—
c^*	Characteristic Exhaust Velocity	ft/sec
F	Thrust	lb_f
f	Function of —	—
g	Gravitational Constant (32.174)	$lb_m\text{-}ft/lb_f\text{-}sec^2$
h	Enthalpy	Btu/lb_m
I	Specific Impulse	$lb_f\text{-}sec/lb_m$
J	Energy Conversion Constant (778)	$ft\text{-}lb_f/Btu$
k	Specific Heat Ratio	—
P	Pressure	lb_f/in^2
Q	Heat Added to Combustion Stream	Btu/lb_m
R	Gas Constant	$ft\text{-}lb_f/lb_m\text{-}°R$
r	Mixture Ratio, $\dot{w}_o/\dot{w}_f$	—
T	Temperature	$°R$
V	Velocity	ft/sec
$\dot{w}$	Flowrate	lb_m/sec
Δ	Difference	—
η	Efficiency	Percent
ρ	Density	lb_m/ft^3

Subscript Symbol

a	Ambient
c	Jacket Coolant
ch	Chamber
corr	Corrected for Heat Transfer
d	Dump
diff	Diffuser
e	Exit
F	Thrust
f	Fuel

Subscript
Symbol   **(Continued)**

i	Inlet
j	Cooling Jacket
meas	Measured
n	Nozzle
o	Oxidizer
p	Propellant Total
P_c	Chamber Pressure
s	Seal
t	Throat Total
vac	Vacuum
'	Theoretical

E. REFERENCES

B-1. "Digital Computer Programs for Rocket Nozzle Design and Analysis — Volume II — Bell Nozzle Design," Pratt & Whitney Aircraft FR-1021, prepared under Contract NAS9-2487, 26 June 1964.

B-2. Colbert, D. L., "Use of Partial Derivatives in Variation Analysis," Pratt & Whitney Aircraft FR-1993, 30 September 1966.

B-3. "ICRPG Handbook for Estimating the Uncertainty in Measurements Made With Liquid Propellant Rocket Engine Systems," CPIA Publication No. 180 prepared by Pratt & Whitney Aircraft for the ICRPG Performance Standardization Working Group, May 1969.

APPENDIX C

ENGINE CYCLE ANALYSIS

A. INTRODUCTION

As noted in the introduction to this report (Section II), studies were conducted to establish the theoretical feasibility of operating a modified RL10A-1 engine with flox/methane before the contract program described herein was undertaken. The results of those studies indicated that the system would be power-limited to a maximum chamber pressure of 250 psia, and component modifications were made based on the assumption of operation at that level. Before and during engine demonstration testing, additional cycle studies were conducted, using experimental data that became available, to establish details of the system. Such studies were made for the initial build and final build of the engine and are presented here for reference in the form of cycle balance sheets, or schematic diagrams upon which the operating parameters for components and fluid conditions at important points in the cycle are noted.

B. INITIAL ENGINE BUILD

Steady-state cycle balances for the initial engine build were completed based on extrapolation of heat transfer data obtained in the limited pressure-fed thrust chamber testing that was accomplished, fuel pump performance estimated from existing data for pump operation with hydrogen and propane, and oxidizer pump data obtained in component tests. Various combinations of component configurations were investigated, and a final arrangement, selected to maximize excess turbine power (bypass flow) while retaining system stability and providing flexibility for rebalancing the cycle as additional data were acquired, was established.

The cycle balance sheet showing the pretest cycle balance for build No. 1 of engine FX-153 is presented in figure 78. As discussed in Section V of this report, because of the significantly lower head rise requirements of methane compared to hydrogen, reductions in either the fuel pump diameter or speed were necessary. Some speed reductions were achieved through the use of RL10A-4 gearing, which provided a 2.118:1 ratio instead of the 2.5:1 ratio that is standard for the RL10A-1 engine. The rest of the head rise reduction was achieved by reducing the impeller diameters.

133

OXIDIZER PUMP

RPM	9,407
ΔP:	451.7
ΔT:	0.8
η:	70.03
HP:	44.6
D:	4.826

K: 10.77

P: 50.0
T: 153.7
ẇₒ: 30.33

P: 461.7
T: 153.9

OXIDIZER
CONTROL VALVE

P: 285.9
T: 153.8

OXIDIZER PUMP

SV-4

r: 5.75
Pcs: 260.0
Pct: 253.0

P: 354.8
r: 812.5

P: 742.7
T: 854.6

P: 808.9
T: 213.6

SV-8

P: 704.8
T: 854.6

P: 368.6

TURBINE

THRUST
CONTROL

SV-10

P: 50.0
T: 200.0
ẇf: 5.54

FUEL PUMP

ΔPORI: 27.8

SV-2

P: 308.9
T: 213.6

SV-6

FUEL PUMP

RPM:	19,926
ΔP:	758.9
ΔT:	13.6
η:	31.48
HP:	135.3
D:	4.25

TURBINE

w:	4.30
RPM:	19,926
P_T/P:	1.91
η:	47.71
HP:	182.2
A_{cd}:	0.471
w_T/w_f:	0.815

NOTES:
1. Fuel leakage: 0.26 lb/sec (includes SV-10, SV-6, and SV-8 leakage and gearbox coolant).
2. Gear train horsepower loss; 5% of oxidizer pump required horsepower.
3. All pressures in psia.
4. All temperatures in °R.
5. All flowrates in lb/sec.
6. All dimensions in inch units.
7. All efficiencies in percent.

Figure 78. Pretest Cycle Balance for Engine Build No. 1; r = 5.75

FD 25782

Becau.se regenerative cooling with a bulk-boiling coolant creates a potential for unstable operation, it was considered necessary to maintain the methane in the cooling jacket above its critical pressure with a downstream restriction. The restriction could have been incorporated in the 1st-stage turbine stator, but an orifice at the jacket discharge was used so that the turbine inlet area could be maximized. This was done to increase the mixture ratio range capability. Figure 79 shows that for an engine trimmed for r = 5.75, as the mixture ratio is decreased the required fuel pump discharge pressure increases. This causes a decrease in the amount of methane flow that may bypass the turbine or, as shown in figure 79, an increase in the turbine-to-chamber flow ratio*. If the restriction were obtained with a low fixed turbine area, the system would be power-limited at mixture ratios below 4.64. The point shown at a mixture ratio of 4.5 indicates that by removing the orifice, the fuel pump discharge pressure could be reduced by approximately 60 psia. This would then permit a reduction of almost 4% in the required power and allow extension of the lower operating mixture ratio limit without changes to the turbopump assembly.

Data from cold flow tests of the first engine build with the cycle showed that the modified pump would be operating in a regime of the head/flow curve having a positive slope. As discussed in Section V, operation in such a regime is potentially unstable. Therefore, the engine system was altered prior to the first firing by installing an orifice at the fuel pump discharge. The cycle balance with the fuel pump orifice installed is shown in figure 80.

* *Although the curves of figure 79 were calculated for the case with the orifice in the system, they would show essentially the same values if the turbine area were sized to maintain the same jacket pressure.*
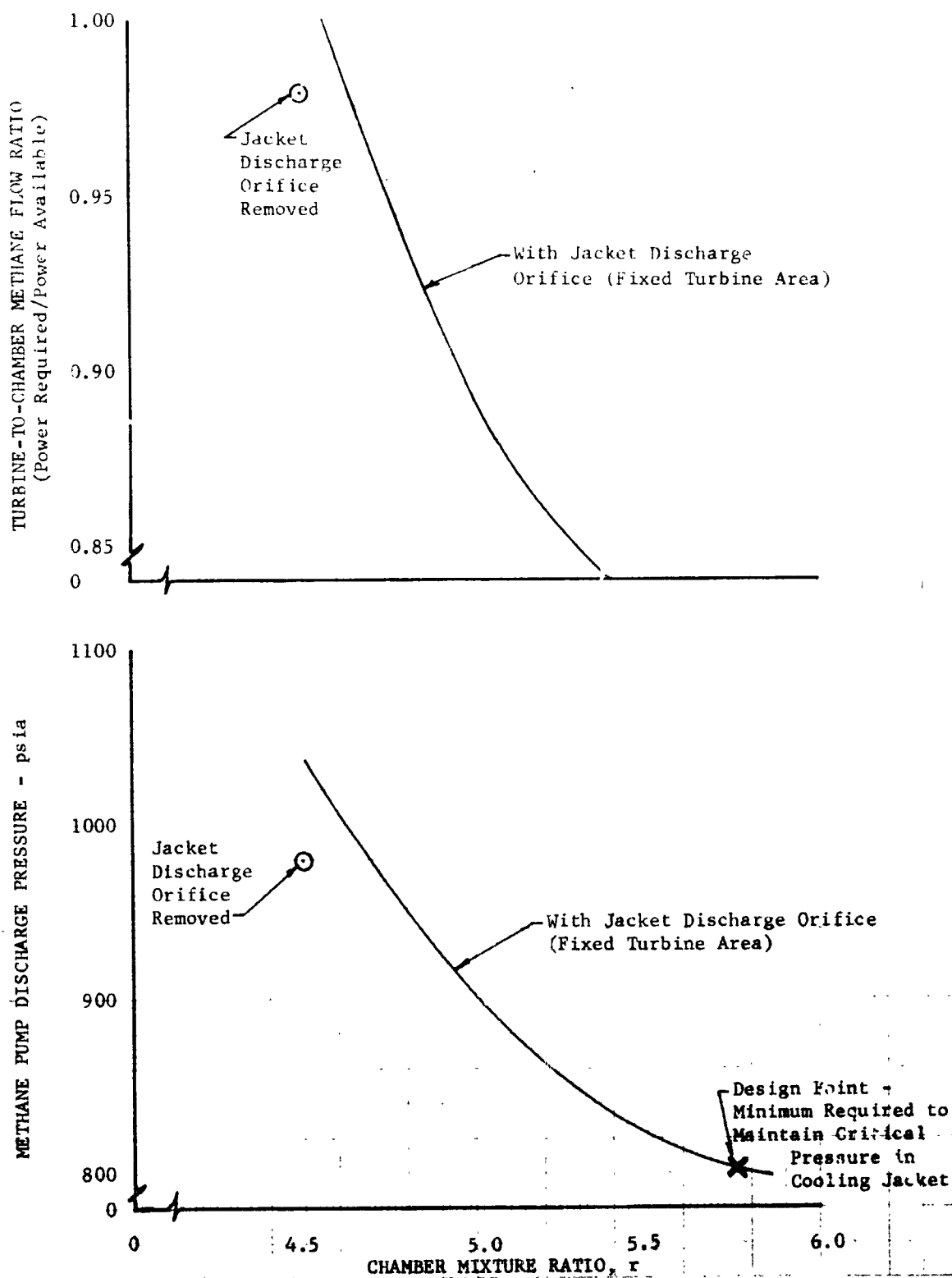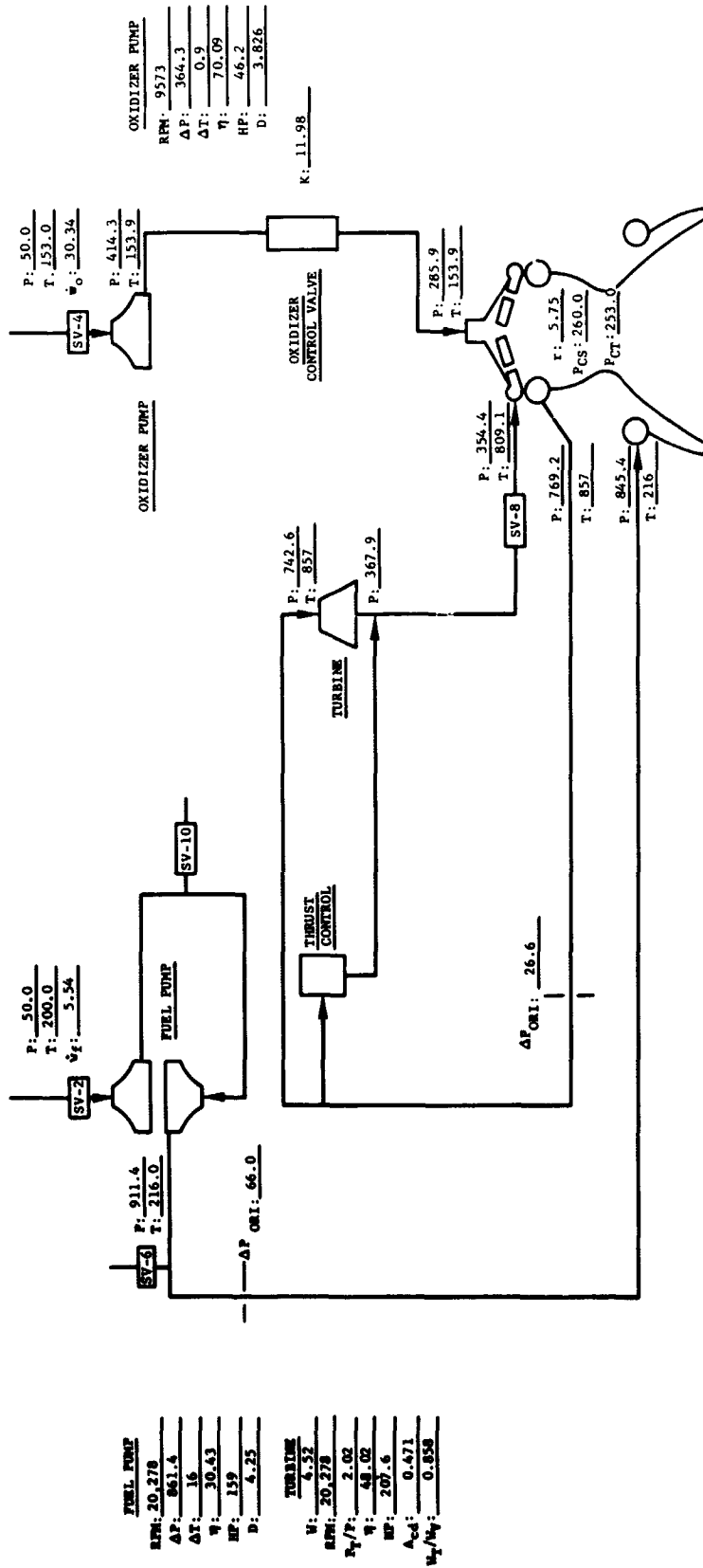
Figure 79. Variation in Cycle Paramet   with Mixture Ratio

DF 61661

136

Figure 80. Final Cycle Balance for Engine Build No. 1; r = 5.75

FD 24025

C. FINAL ENGINE BUILD

Component head rise and efficiency data obtained during engine tests E-1 through E-3 were used to recalculate a cycle balance for the final engine build (build No. 4). However, during the first test of the build, the turbine area increased because welds made to reduce the stator vane trailing edge gap failed. Recalculated cycle balance points for the actual turbine area and with a smaller fuel pump discharge orifice installed to compensate for the area change (i.e., for tests No. E-7 through E-9, see Section III) are presented in figures 81 through 83 for mixture ratios of 4.75, 5.25, and 5.75 at a chamber pressure of 250 psia. The components represented in these schematics were those used in the tests of the final engine build. The high fuel pump discharge restriction that was installed to compensate for the turbine change caused a considerable incr‪ in the required power. Therefore, these balances are for a highly compromised engine configuration.

The cycle balance at a mixture ratio of 5.75 (figure 83) indicates that a cooling jacket discharge pressure below the critical pressure of methane (673 psia). As mentioned above, operation at subcritical coolant pressures could result in unstable bulk boiling. The possibility of boiling instability is avoided in this case because the jacket inlet pressure is above critical, and the fuel is heated to above its critical temperature before the pressure is reduced below the critical value. Because of the failure of the turbine area modification, the jacket inlet pressure was below the critical value for 9.2 seconds during test No. E-4. No signs of instability were found and no chamber damage was noted after that test. Several other periods of subcritical operation were encountered in tests No. E-7, E-8, and E-9 after some chamber damage had previously been incurred. No signs of instability were noted, but because of the damage existing at the beginning of those tests, it cannot be determined whether any tube-to-tube fluctuations existed that could have contributed to increasing the damage.

Figure 84 shows the maximum chamber pressure that could have been achieved during build No. 4 if the turbine area had not increased and the fuel pump discharge orifice had been left at the size originally installed for dynamic stability purposes. The maximum chamber pressure limits shown in figure 84 for mixture ratios below 5.0 are limited by cycle power (zero turbine bypass flow). At higher mixture ratios, the maximum chamber pressure is restricted by the 1100-psi burst strength of the second-stage fuel pump housing. If this restriction were removed, sufficient cycle power would be available to attain a chamber pressure of 297 psia at a mixture of 5.75.

138

Figure 81. Cycle Balance for Final Configuration of Build No. 4; r = 4.75

Figure 82. Cycle Balance for Final Configuration of Build No. 4; r = 5.25

FD 25759

140

Figure 83. Cycle Balance for Final Configuration of Build No. 4; r = 5.75

FD 25758

141

Figure 84. Maximum Chamber Pressure for Pretest   DF 69118
            Configuration of Build No. 4

APPENDIX D

TEST SUMMARY

This appendix is presented in two parts: part I which consists of tables summarizing all important tests conducted during the program, and part II, which provides a detailed history of engine system testing.

The tables in part I are arranged according to type of test as indicated below. With the exception of the oxidizer pump tests, all testing was conducted at Pratt & Whitney Aircraft's Fiorida Research and Development Center. (See Appendix A.)

In part II, the engine system tests are discussed chronologically by engine build. The presentation here is intended to supplement the engine testing description given in Section III. Whereas results were summarized for the earlier ﹏ction, the testing program is discussed in sufficient detail in part II to explain the logic for, and limitations under which each of the engine system changes were made.

PART I - TEST SUMMARIES

Table XVII.   Flox/Methane Uncooled Pressure-Fed Thrust Chamber Tests

Table XVIII.   Flox/Methane Cooled Pressure-Fed Thrust Chamber Tests

Table XIX.   Flox/Methane Engine Demonstration Tests

Table XX.   Oxidizer Pump and Seal Rig Tests (pump tests conducted at "I" Site — Plumbrook Station, NASA Lewis Research Center)

TABLE XVII. FLOX/METHANE UNCOOLED PRESSURE-FED THRUST CHAMBER TESTS

Test No.	Duration, sec	Injector S/N	Remarks
1-USL	2.5	HK 713	Satisfactory start transient; ignition indicated within 50 msec; 1 sec of steady-state operating data obtained for performance calculations.
2-USL	1.95	HK 713	Satisfactory start transient; ignition indicated within 50 msec; test terminated after 1.95 sec due to reaction in injector oxidizer manifold caused oy purge valve malfunction; no steady-state data obtained.
3-USL	2.5	HK 707	Start transient unsatisfactory due to depletion of flox in run tank; no steady-state data obtained.
4-USL	2.5	HK 707	Satisfactory start transient; ignition indicated within 50 msec; approximately 1 sec of steady-state operating data obtained for performance calculations.
5-USL	2.5	HK 707	Approximately 0.75 sec of steady-state operating data obtained for performance calculations.
6-USL	2.5	HK 707	Approximately 1.5 sec of steady-state operating data obtained for performance calculations.
7-USL	1.33	HK 707	Satisfactory start transient; test terminated after 1.33 sec due to depletion of flox in supply tank; no steady-state data obtained.
8-USL	4.0	HK 707	Ignition within 50 msec; approximately 1.5 sec of steady-state operating data obtained for performance calculations.
9-USL	4.0	HK 707	Approximately 2.75 sec of steady-state operating data obtained for performance calculations.
10-USL	4.0	HK 707	Approximately 0.75 sec of steady-state operating data obtained for performance calculations.
11-USL	4.0	HK 707	Approximately 2.0 sec of steady-state operating data obtained for performance calculations.
12-USL	4.0	HK 707	Approximately 1.75 sec of steady-state operating data obtained for performance calculations.
13-USL	4.0	HK 707	Approximately 2.25 sec of steady-state operating data obtained for performance calculations.
14-USL	4.0	1F 764	Approximately 1.25 sec of steady-state operating data obtained for performance determination; burning of oxidizer spud tip on one outer row element.
15-USL	4.0	1F 764	Approximately 0.5 sec of steady-state operating data obtained for performance determination, no additional spud burning evident on damaged outer row spud.
16-USL	4.0	1F 764	Approximately 1 sec of steady-state operating data obtained for performance determination.
17-USL	4.0	1F 764	Approximately 1 sec of steady-state operating data obtained for performance determination.
18-USL	4.0	1F 764	Approximately 0.75 sec of steady-state operating data obtained for performance determination.
19-USL	4.0	RY 14	Approximately 0.75 sec of steady-state operating data obtained for performance determination; large number of swirlers missing and four oxidizer injection elements burned flush with the oxidizer support plate; temporary injector repairs accomplished on site.
20-USL	1.6	RY 14	Satisfactory start transient; test terminated after 1.6 sec by flourine leak indication at injector backplate; 0.25 sec of steady-state operating data obtained for performance determination.

144

TABLE XVIII. FLOX/METHANE COOLED PRESSURE-FED THRUST CHAMBER TESTS

Test No.	Test Duration Seconds	Cooling Mode	Injector S/N	Chamber S/N	Remarks
1-CA	2.5	Supplemental	IF 763-1	KD 115	Test terminated prematurely by false signal from fluorine leak detector system; damage occurred to injector outer row spuds and some swirlers; silver braze in tube transition area of chamber slight washing.
2-CA	5.7	Supplemental	IF 763-1	KD 115	Test terminated prematurely by low hydraulic pressure sensing system; damage to injector spuds and swirlers occurred in outer row; many chamber tubes burned in combustion area, apparently during start transient.
3-CA	6.4	Separate	IF 763-2	HF 318	Start transient satisfactory; cooling tubes failed in nozzle; some injector spud tips eroded, but no swirlers lost.

TABLE XIX. FLOX/METHANE ENGINE DEMONSTRATION TESTS

Test No.	Engine Build No.	Test Duration, sec	Remarks
E-1	1	43.4	Engine acceleration satisfactory but system control response slower than that of oxygen/hydrogen engine. Chamber pressure and mixture ratio low during steady-state operation because of cooling tube damage caused by coolant flow slowdown during start transient. Injector and chamber severely damaged after shutdown due to failure of oxidizer valve to close as programed.
E-2	2	5.1	Engine acceleration and control improved, but coolant flow slowdown still encountered, with resulting coolant tube failures. Test terminated prematurely by low chamber pressure advance system. Extensive injector oxidizer spud erosion noted in post-test inspection.
E-3	3	17.0	Engine started with open turbine bypass to eliminate thrust control contribution to coolant flow slowdown during start transient. Acceleration satisfactory with minimum thrust overshoot, but coolant slowdown not eliminated. Extensive tube damage experienced.
E-4	4	13.8	Scheduled opening oxidizer flow control valve used, chamber coolant jacket volume reduced. Engine started with open thrust control. Scheduled oxidizer valve produced satisfactory acceleration with almost linear chamber pressure increase. Only minor coolant slowdown noted, but combination of low mixture ratio and open thrust control allowed the oxidizer control valve to unseat. Engine decelerated slowly due to high oxidizer restriction.
E-5	4	24.3	Engine started in same manner as previous test but with thrust control sequenced into system at time of peak rpm. Oxidizer control valve again unseated, causing system to decelerate. Sufficient data obtained to establish that turbine flow area had increased, apparently at the start of test E-4, to cause low mixture ratio operation.
E-6	4	4.0	High ΔP orifice installed at fuel pump exit to compensate for turbine area increase. Acceleration time was increased and thrust control was sequenced into system before peak rpm. With the high residual jacket heat, this produced turbopump overspeed resulting in rupture of 1st-stage fuel pump housing. Post-test pressure checks revealed minor leaks in thrust chamber tubes.
E-7	4	61.5	First-stage fuel pump housing replaced. Thrust control activation time moved to coincide with point of peak rpm. Engine operated at chamber pressure above 225 psia for 5.5 seconds. Mixture ratio still low and pump speed decreased as residual jacket heat was dissipated. Engine stabilized at 200-psia chamber pressure for over 40 seconds with floating oxidizer control valve. Chamber leaks increased; fuel leakage through tube openings approximately 15% of total fuel flow.
E-8	4	5.0	Engine started with active thrust control because of power loss caused by tube leakage. Line added around oxidizer control valve to bypass approximately 25% of flox for increased mixture ratio. Feedback loop set up between thrust control, oxidizer control valve, and bypass line produced 1-Hz cycling of engine between 200- and 250-psia chamber pressure. Mixture ratio exceeded 6, causing high turbine temperature shutdown. No change in hardware condition noted after test.
E-9	4	11.6	Engine started with closed thrust control to prevent instability found in test E-8. System stabilized at approximately 230 psia. Low level of flox in run tank allowed helium ingestion, with subsequent loss in oxidizer head rise. System restabilized at 200 psia with floating oxidizer control valve. Test terminated in anticipation of flox depletion. Program scope did not allow further testing.

TABLE XX. OXIDIZER PUMP AND SEAL RIG TESTS

Test No.	Type of Test	Rig No.	Test Duration Min.	Remarks
SR-1	Seal Rig	————	31.8	Rig test to evaluate shaft seal material combinations for use in the flox pump. Used Kentanium K-162B nosepiece and mating ring for primary seal. Secondary seal was Kentanium K-162B mating ring on a solid alumina split ring. Leakage and wear rates satisfactory.
P-1	Pump*	C71Y002	34.0	Pump checkout test. Primary seal mating ring found to have thin radial crack, but seal performance during test was consistent. Made four flow excursions at rated speed (9950 rpm). All data satisfactory.
P-2	Pump*	C71Y002	5.0	Satisfactory checkout test of final pump configuration.
P-3	Pump*	C71Y001	5.0	Satisfactory checkout test of backup pump.

* *Pump tests conducted at "I" Site, NASA-Lewis Research Center Plumbrook Station.*

PART II — ENGINE TEST HISTORY

The major occurrences during engine systems testing and the component changes incorporated for the tests listed in table XIX are presented below by engine build.

A. ENGINE BUILD NO. 1

1. BUILD SUMMARY

The first test of engine FX-153 was conducted primarily to check out the minor modifications made to the test facility to convert from pressure-fed thrust chamber testing to integrated engine system testing. During the 43.4-second test (designated E-1), several important items were verified:

1. Sufficient starting power was available to provide rapid turbopump acceleration.

2. The turbopump components operated very nearly as predicted.

3. The control system was adequate.

4. The purge procedures were adequate to prevent damage to the injector swirlers.

Several problems that limited the duration of nominal chamber pressure operation were encountered. Also, a malfunction of the oxidizer inlet shutoff valve at shutdown resulted in severe damage to the chamber and injector.

2. TEST HARDWARE

Modified RL10A-3 thrust chamber S/N JP 97 was used in build No. 1 of engine FX-153. As described in Section IV, modifications to this chamber included installation of cooling fins in the long tube transition region and twisted copper inserts in the chamber region. The modified turbopump and control components used are discussed in Sections V and VI, respectively. Because test No. E-1 was primarily a facility checkout test, injector S/N IF 764, which was recognized as nonoptimum from a performance standpoint, was used. This injector, previously used in tests No. 14-USL through 18-USL, incorporated thin stainless steel swirlers in the intermediate rows of oxidizer elements. It was selected for the checkout engine to provide a stringent check of swirler durability. Experience during the chamber/injector pressure-fed rig tests had shown that the start and shutdown procedures required to prevent damage to this type swirler were more critical than with the thick nickel swirlers that had been used in pressure-fed tests before the engine was assembled.

3. TEST DISCUSSION

Important occurrences in test No. E-1 can best be illustrated by reference to figure 85. Turbopump rotation started 1.3 sec after the main fuel shutoff valve was opened; this was approximately 1 sec longer than in hydrogen fueled RL10 engines. As the engine accelerated, the oxidizer flowrate was restricted to a low value by the mixture ratio control valve; when the oxidizer pump pressure rise reached 140 psi the poppet opened and allowed full oxidizer flow. This point is shown by the rapid rise in chamber pressure at 2.7 sec. The 1.4-sec interval between the start of rotation and the opening of this valve was approximately 10 times that encountered in an oxygen-hydrogen RL10 transient. However, the engine did reach design speed, which proved that sufficient power was available in the cycle.

Although the thrust control reset system reacted to limit the acceleration, the chamber pressure overshot to a peak value of 330 psia (at approximately 3.3 sec). This overshoot was greater than normal and reflected an apparent slower reaction of the engine system with flox methane than with oxygen/hydrogen. Also, the action of the thrust control bypass piston indicated a tendency toward sticking. When the thrust control acted, a slight overcorrection reduced the chamber pressure to 220 psia (at 4.5 sec), followed by a slight overacceleration to 280 psia (at 4.9 sec).

The system appeared to be controlling at 260 psia chamber pressure at 5.7 sec, when the oxidizer pump discharge pressure suddenly decreased without a change in turbopump speed. When this occurred, the thrust control sensed the lower chamber pressure and accelerated the turbopump in an attempt to increase the flow. The oxidizer pump did not recover for approximately 3 sec. During this time, the turbopump started to decelerate and the system restabilized at 175 psia chamber pressure and a mixture ratio of 3.0 for the remainder of the test. The extent of the speed reduction was greater than could be expected from the increase in required power as the oxidizer pump recovered; post-test data examination indicated a loss of turbine flow when turbopump speed started to decrease.

The loss of turbine flow is indicative of leaks in the cooling tubes; however it was impossible to recognize the occurrence of leaks while the test was in progress. The exact time of failure was difficult to establish even in post-test data analysis, because all conditions were transient up to the time it occurred. The data indicated that some tube leakage was definitely occurring as early as 8.0 sec.
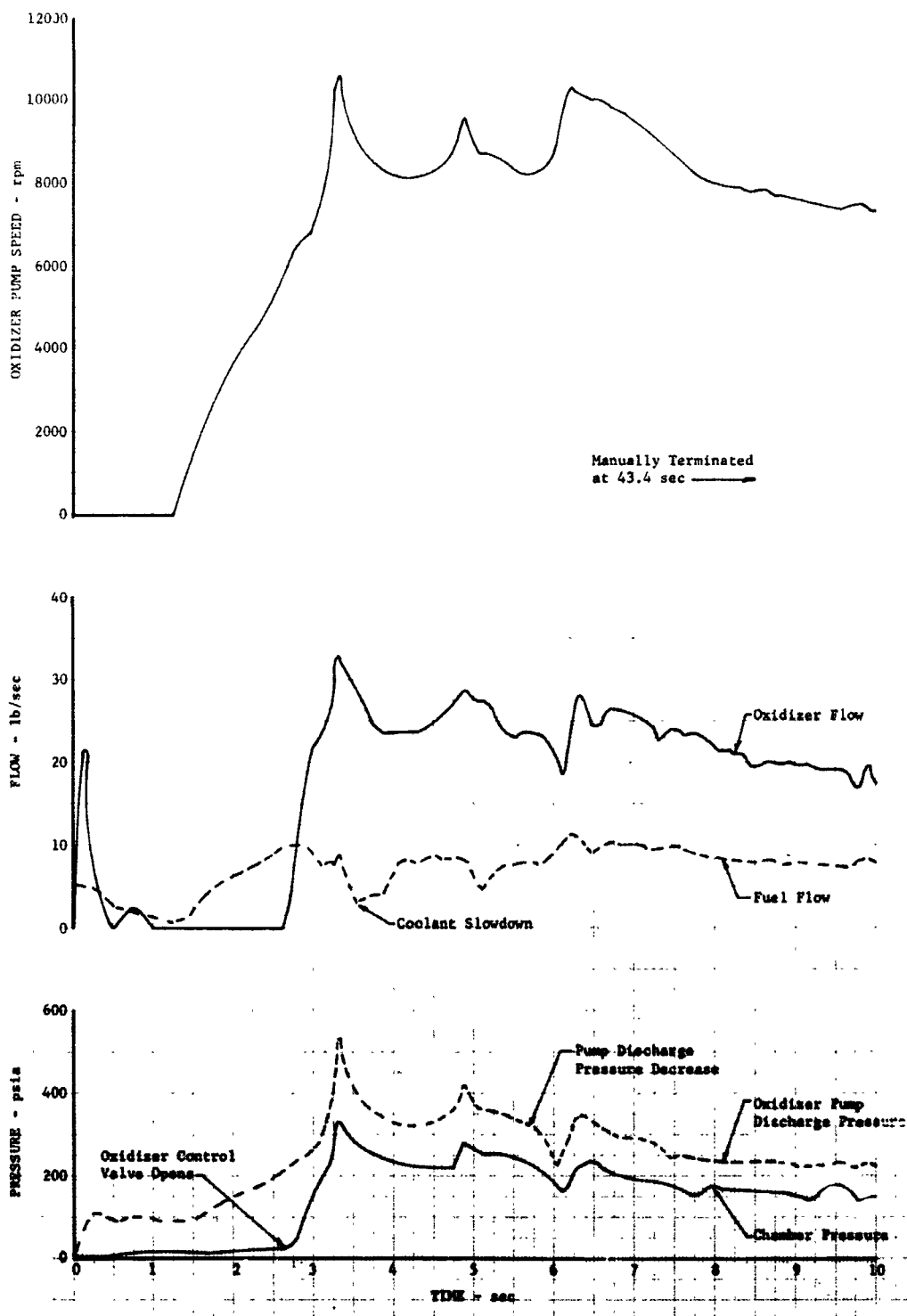
149

Figure 85. *Starting Transient for Engine Test No. E-1*   *DF 68963*

When test E-1 was terminated by the engineer in charge, the oxidizer inlet shutoff valve failed to close for 50 sec after fuel shutoff. As a result, approximately 10 gallons of flox were dumped into the hot chamber. Motion picture coverage of the test was terminated approximately 20 sec after shutdown, and up to that time no damage was visible; however, extensive chamber and injector damage was found at post-test inspection. The extent of the post-test damage prevented determination of the location of the tube failures that occurred during the firing, but analysis of characteristic velocity data showed that they were upstream of the throat. There was no nozzle damage except at the bottom of the engine, where it was obvious that there had been a stream of liquid oxidizer.

The adequacy of the injector purge sequence established for engine testing was verified by the injector condition following the test. Although the Rigimesh faceplate and oxidizer spudplate were severely damaged, all but one of the oxidizer swirlers were intact. That one was located at the bottom of the injector in a position where the whole spud and a portion of the spudplate were damaged by reaction during the post-test oxidizer flow.

In the following paragraphs, each problem encountered in the test is listed and its effect on the rest of the system is examined. System changes made to prevent recurrence of the problems are also discussed.

a. Slow Turbopump Rotation

A delayed start in turbopump rotation is usually the result of high static torque. As normal test procedure, the static torque is checked before and after each test or cold flow. The pre- and post-test torques measured for this test were within acceptable limits for RL10 engines and were very close to those measured between cold flows. Because post-test checks of the assembled turbopump revealed no irregularities, the most probable explanation for the temporary high torque was that moisture in the system had condensed and frozen during pump cooldown. Therefore, purge flowrates were increased for the next test. The explanation was not entirely satisfactory because all systems were protected by continuous gaseous nitrogen purges and, during the 48 hours preceding the test, the moisture content of the purge gas was less than 1 ppm.

b. Slow Response to Thrust Control

Slow response to the thrust control which may have contributed to the coolant tube damage was caused primarily by slower system response than that of an oxygen/hydrogen RL10 engine. The thrust control piston action was somewhat sluggish (as if it were sticking) but still within acceptable oxygen/hydrogen RL10 limits. For the second engine build, the thrust control sensitivity was increased by increasing the servo supply flow. (Refer to Section VI for control description.)

c. Thrust Chamber Damage

Coolant tube leakage started at some time during the first 8 seconds of the test. The exact time of failure cannot be unequivocally established; however, the sharp decrease in turbopump speed at 6.2 seconds could be symptomatic of the onset. The jacket would have had to be relatively intact for the fuel turbopump to reaccelerate as it did at 4.3 and 5.7 sec. It was thus reasoned that the tubes were weakened or eroded during the early portion of the transient, and that they failed during the last period of high turbopump speed. Post-test chamber damage, resulting from flox introduction through the oxidizer valve that did not close, prevented identification of the area in which the failure started, but it was encouraging to note that all regions predicted to have low tube wall margins were relatively intact.

It was conjectured that the cause of failure was related to the sudden expansion of the methane within the jacket during the first chamber pressure spike. This expansion caused a temporary coolant flow slowdown, thereby reducing cooling. Some extent of coolant flow slowdown is typical of the RL10 starting transient with hydrogen, and with methane the large density change at vaporization (Reference D-1) increases the duration of the effect. In test No. E-1, the problem was aggravated by the delay of turbopump rotation, which increased the amount of high-density methane within the jacket prior to start.

For the second test, oxidizer starting flow was increased to provide more heat during start, thus reducing the amount of low-temperature methane within the jacket. In addition, the oxidizer flow control valve cracking pressure was increased. This was done to allow the fuel system to reach a higher pressure before the high heat flux occurred.

d. Oxidizer Pump Head Reduction

The temporary decrease in oxidizer pump outlet pressure that started at 5.7 sec was an effect resembling inlet cavitation. However the net positive suction pressure at the time of the occurrence was 40 psi and satisfactory operation of the pump at this level had been previously demonstrated. The likelihood that the phenomenon was true cavitation was therefore small. Gas ingestion at the inlet could have caused the behavior noted, and the inlet purge system or flox vaporization in the inlet instrumentation taps would have been possible sources of gas. For later tests the purge shutoff valves were moved closer to the engine to minimize the line volume between them and the check valves at the engine connections, and the inlet instrumentation transducers were also more closely coupled. This problem did not recur.

e. Oxidizer Shutoff Valve

The oxidizer shutoff valve failed to close until 50 sec after the shutdown

signal, although the helium pressure that actuates the valve was vented as sequenced. In post-test bench tests, the valve demonstrated a tendency to stick, but the resistance that caused sluggish action did not appear to be enough to prevent closing. As in the case of the high static turbopump torque, these factors indicated condensed moisture in the system; the purge system was therefore modified. Also, a separate helium supply was added to provide a positive closing pressure to the actuating bellows.

B. ENGINE BUILD NO. 2

1. BUILD SUMMARY

Engine FX-153 was assembled a second time using an optimized injector and with all component modifications deemed necessary based on the results of test No. E-1 incorporated. The test of build 2, No. E-2, was terminated at 5.1 seconds when chamber pressure decreased below a level considered reasonable. It was determined that the chamber pressure decrease was caused by injector deterioration that resulted because of chamber damage.

2. TEST HARDWARE

The same control and turbopump components used in build 1 of Engine FX-153 were used in build No. 2. The thrust chamber, S/N JP 88, incorporated the same modifications as those of the chamber for the first build, plus instrumentation consisting of twelve coolant bulk temperature thermocouples. Details of instrumentation installation are discussed in Section IV.

Modified RL10A-3 injector S/N 3K 2945 was used in this build. The modifications to this injector, detailed in Section IV, included installation of thick nickel swirlers in all oxidizer elements and incorporation of a reduced porosity (60 scfm) Rigimesh fuel faceplate with 0.012-inch fuel gaps.

3. TEST DISCUSSION

The following discussion includes a review of the test occurrences and the changes produced by the modifications made between tests. As in the discussion of test No. E-1, reference to a time plot of the primary engine parameters (figure 86) facilitates understanding of the important test events.
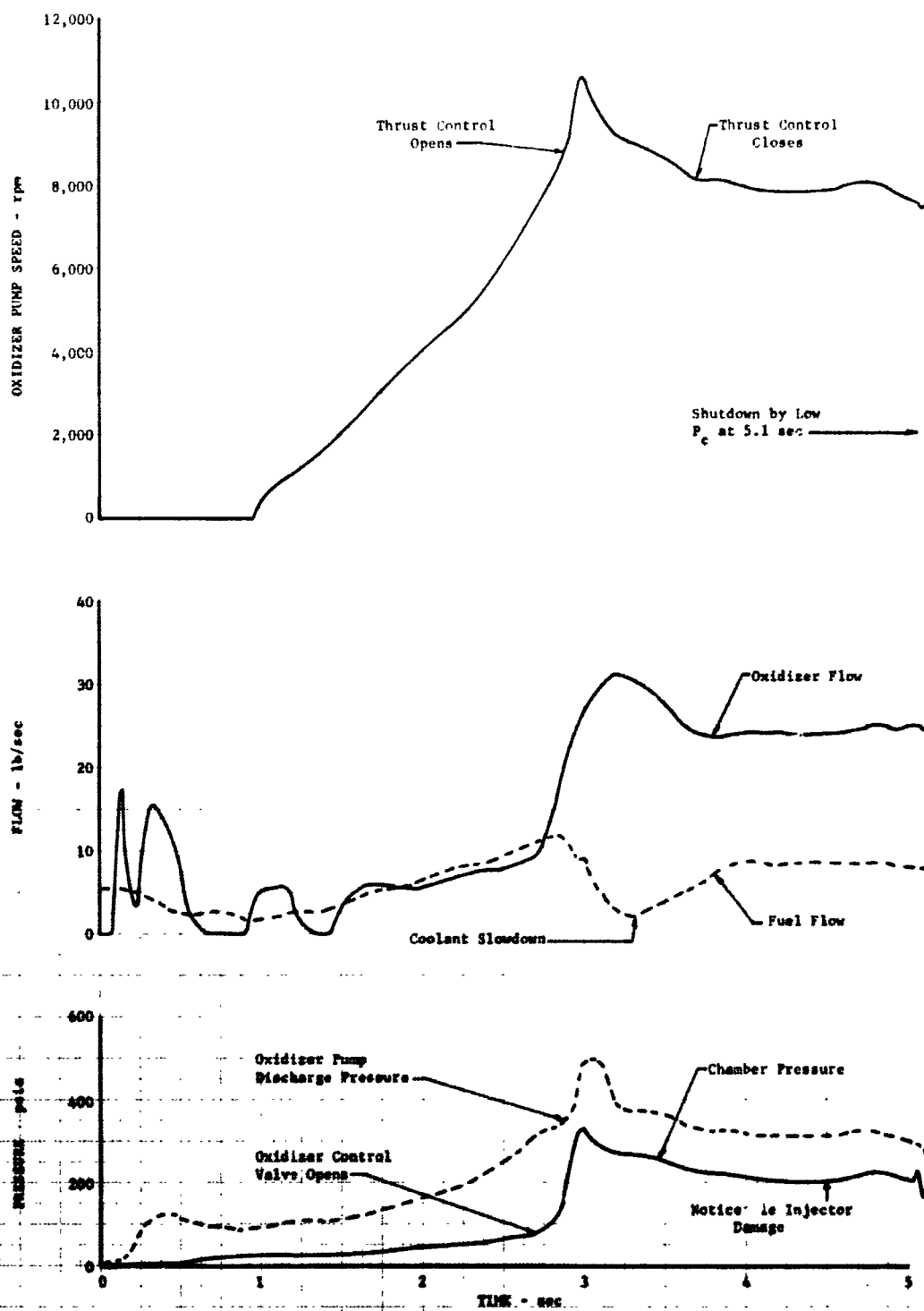
Figure 86. Starting Transient for Engine Test No. E-2

DF 68960

Turbopump rotation started at 0.9 seconds (compared to 1.3 seconds for test No. E-1). The chamber pressure level resulting because of the increased flox bypass flow was approximately 30 psi for the first 1.7 seconds, with a gradual increase to 80 psi over the next 1.0 second. At 2.7 seconds, there was a rapid chamber pressure increase as the oxidizer control valve opened. Although the thrust control reset system reacted to control the system overacceleration by opening the turbine bypass at 2.9 seconds (220 psia chamber pressure), chamber pressure peaked at 330 psia at 3.0 seconds. The thrust control closed the turbine bypass at 3.7 seconds when the chamber pressure had reduced to 230 psia. At this time the turbopump deceleration had almost ceased but speed did not begin to increase for approximately 0.8 second. The limited response to thrust control action indicated that some chamber tube damage had occurred by 3.7 seconds and that fuel was being diverted into the chamber from the jacket, and not reaching the turbine. Post test chamber inspection revealed that approximately 60% of the tubes were burned in the chamber area. Analysis of the conditions occurring in the chamber established that the failure resulted from the reduced coolant velocities during the coolant slowdown.

At 4.5 seconds the pump reaccelerated. An apparent increase in fuel flow area at this time reflected initiation of injector damage. The fuel flow area change was followed by an increase in the oxidizer area, and from this sequence it was surmised that the injector failure mode was oxidizer spud erosion. The rapid spud erosion was most probably the result of reduced cooling because a large portion of the fuel was leaking through damaged chamber tubes, and low flow, coupled with high methane temperatures, did not provide adequate injector cooling. At the time of failure, the injector mixture ratio was 6.58 and the methane temperature was 800°R.

4. RESULTS OF SYSTEM CONTROL CHANGES

a. Increased Oxidizer Starting Flow

After test No. E-1, the oxidizer control valve was modified to increase the starting flowrate. This was done to increase the heat transfer during the acceleration period, so that the coolant flow slowdown, which occurred at the point of rapid chamber pressure increase, would be diminished. The increased bypass flow did increase the chamber pressure during this period (30 psia compared to 15 psia), but the accompanying heat transfer increase was insufficient to reduce the coolant slowdown. One of the most important differences created by this change was a decrease in oxidizer system cooldown time. The greater starting flowrate promoted more rapid cooldown and caused liquid flox to reach the injector before the oxidizer control valve opened. At the low oxidizer volumetric flowrate, injector differential pressure was at a low value and, while the low differential pressure did not cause any problem during this test, it was a potentially dangerous condition in that methane or products of combustion could have been aspirated into

the oxidizer cavity. For the third engine build the bypass flowrate was reduced to the level used in the first test.

b. Increased Oxidizer Control Valve Cracking Pressure

For the first test the oxidizer control valve poppet was set to open at an oxidizer pump differential pressure of 140 psi. This was increased to 190 psi for the second test so that the fuel system would be at a higher pressure when the main oxidizer flow started. This change produced the desired result and also appeared to slow the transition from bypass to main oxidizer flow. This delay was desirable to reduce the coolant slowdown caused by a rapid change in heat flux, and the higher cracking pressure value was retained for the next test.

c. Thrust Control Servo Flow Increase

The thrust control servo supply and body vent orifice sizes were increased to increase the servo supply flowrate and thereby improve control sensitivity. This modification produced the desired result as evidenced by the reduced chamber pressure undershoot in test No. E-2. The thrust control was left in this configuration.

C. ENGINE BUILD NO. 3

1. BUILD SUMMARY

Review of transient data from the first two firings showed that the secondary slowdown caused by thrust control action was largely responsible for chamber damage. Therefore, the starting sequence was modified for test No. E-3 to maintain the thrust control bypass open and the control locked out of the loop until the turbopump had accelerated and steady-state conditions were attained. This control scheme worked essentially as expected and the system accelerated to the predicted chamber pressure of approximately 230 psia with minimum overshoot. Unfortunately, other changes occurred which produced an even more severe coolant slowdown than previously encountered. The resulting coolant slowdown resulted in chamber damage which limited the steady-state chamber pressure and mixture ratio, and the test was manually terminated after 17 seconds.

2. TEST HARDWARE

With the exception of the oxidizer pump, thrust chamber, and injector, all components used on engine FX-153 for test No. E-3 were the same as those used for the previous two tests. Oxidizer pump S/N C71Y002, which was previously used, was replaced with an identical unit, S/N C71Y001, because during the storage period between engine builds a small crack developed in its secondary flox seal. (See Section V.) Modifications to the injector (S/N AAF11) and thrust chamber (S/N JP 42) used are discussed in detail in Section IV. Briefly, the injector incorporated a solid nickel

spudplate with nickel swirlers in all oxidizer elements. Chamber modifications were similar to those used in the previous engine tests, the major change being the use of 11-inch long blocking inserts in the injector ends of the long tubes. This change was incorporated to increase the chamber cooling margin in the event of additional coolant slowdowns.

A minor modification to limit the thrust control bypass area was also incorporated. The bypass piston travel was limited so that the maximum bypass area would be 10% greater than required for 250-psia operation at the maximum excess power point. As mentioned, it was predicted that this bypass area would provide a chamber pressure of 230 psia at the starting mixture ratio of 5.4.

3. TEST DISCUSSION

During test No. E-3, a coolant slowdown during the start transient was again encountered. However, because of the changes in starting procedure, the slowdown was entirely due to coolant expansion caused by the rapid increase in heat flux. With the slower acceleration rate created by the open thrust control, a substantially larger amount of fuel entered the cooling jacket prior to the automatic opening of the oxidizer flow control valve and introduction of full oxidizer flow into the thrust chamber. Thus at the time when the oxidizer valve opened, producing a step increase in heat flux, the density of the coolant within the jacket was significantly higher than on previous tests and the surge due to expansion was much greater than those previously experienced.

Figure 87 shows the behavior of the important engine parameters during the start transient. The correspondence of the opening of the oxidizer control valve and the reduction in measured fuel flow are quite obvious. Following a slight overacceleration at 2.7 seconds, the engine stabilized at approximately 225 psia chamber pressure for nearly 0.6 second. It was established, based upon analysis of test data, that some chamber damage had definitely occurred by 3.5 seconds. However, due to the transient behavior of the fuel flow before this time, it was impossible to determine exactly when the damage started to occur. With fuel leakage through damaged chamber tubes, turbine power decreased and the engine stabilized at a chamber pressure of 180 psia for the remainder of the test. When attempts to increase the chamber pressure failed, the test was terminated by the engineer in charge.

Post-test inspection revealed that about 25% of the tubes had developed leaks in the chamber region. Most of the damaged tubes appeared to have pressure type ruptures typical of overheating, although a few tubes showed indications of injector flow impingement. All other components were in excellent condition.
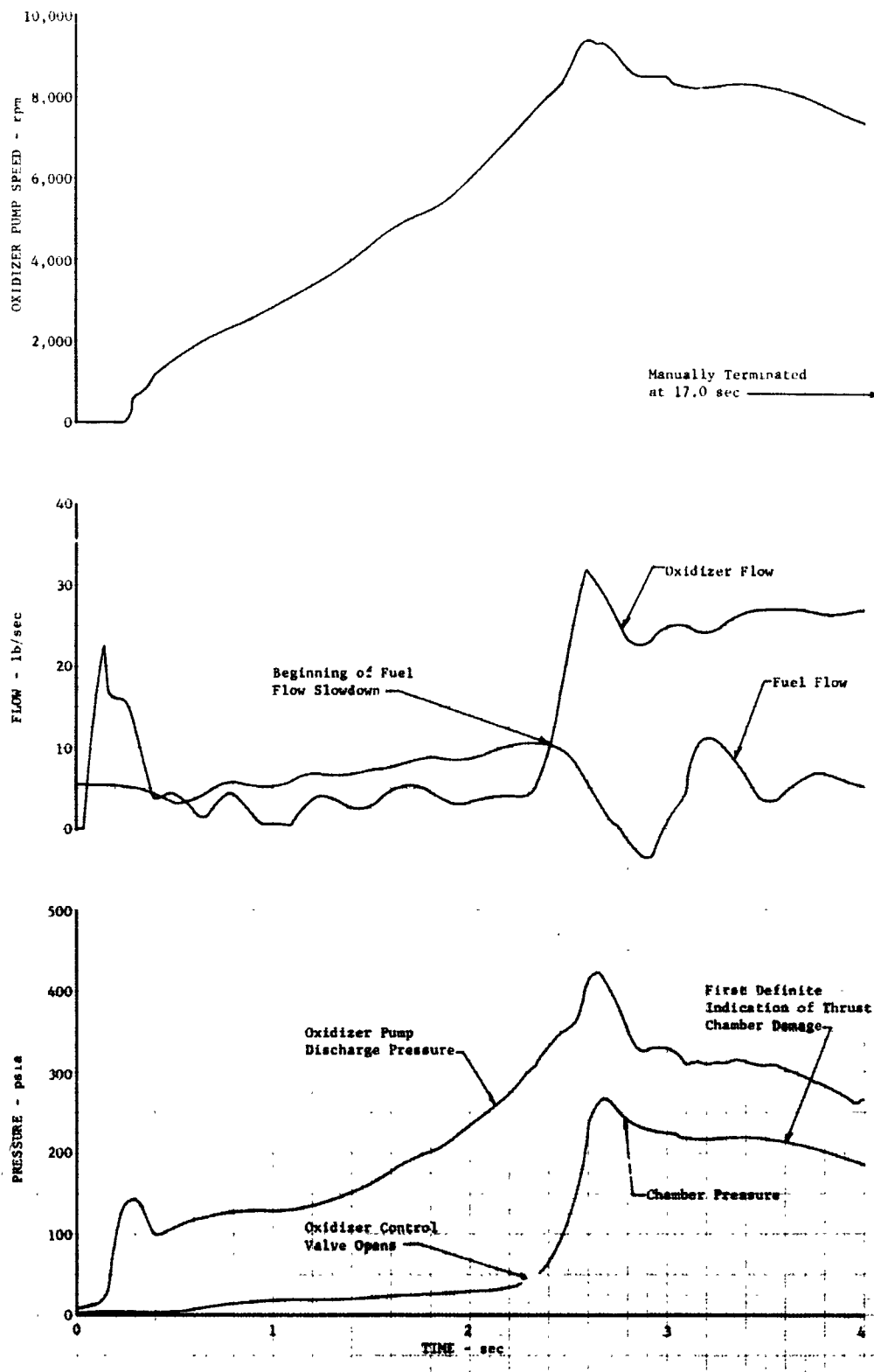
157

Figure 87. Starting Transient for Engine Test No. E-3   DF 68961

158

One significant difference in this test compared to previous engine firings was the almost immediate start of turbopump rotation. In tests Nos. E-1 and E-2 there was a period of approximately 1 second between the opening of the propellant valves and the start of turbopump rotation. In test No. E-3 rotation began at approximately 0.25 seconds after start. (See figure 86.) The 0.25-second time to turbopump rotation was a more representative value for the RL10 engine; the greater delay in the first two tests was traced to insufficient clearance between the oxidizer spur gear hub and the gearbox housing of pump, S/N C71Y002. The low clearance caused binding when a rearward shaft loading was applied, and was evidenced by galling of the housing surface. The binding was not revealed by static torque checks, which are made with essentially no axial load. However, the pressure resulting from the initiation of oxidizer flow provided sufficient loading to cause rubbing. Standard inspection and component tests at engine disassembly after test No. E-2 did not reveal the galling; it was detected only when a complete oxidizer pump teardown was made to inspect the seal area. (See Section V.)

D. ENGINE BUILD NO. 4

1. BUILD SUMMARY

The engine feasibility demonstration was completed with six firing tests conducted on engine build No. 4. Although extended periods of steady-state operation at the design chamber pressure of 250 psia were not achieved, the problems which prevented the attainment of this goal during this last test series were relatively minor. A mismatching of components created by a change in the turbine flow area during the first test of the series (test No. E-4) was the primary cause. Unfortunately, this was the last test series and the remaining scope of program effort was not adequate to permit disassembly of the engine for reoperation of the turbine and a subsequent reassembly. Various sequencing and propellant flow orifice changes were made to overcome the mismatch and these allowed a significant amount of engine data to be obtained.

The total firing duration accumulated in the six tests of build No. 4 was 120.2 seconds; approximately 65 seconds were accumulated at chamber pressures over 200 psia (17 seconds over 225 psia). With the exception of the change in the turbine flow area and some relatively minor damage sustained by the thrust chamber, all other engine components were in excellent condition at the conclusion of the test program. These results produced a high degree of confidence that satisfactory operation at the 250 psia chamber pressure design point could be achieved with further minor modifications to the existing components.

2. TEST HARDWARE

Build No. 4 was assembled using the same components employed in

159

build No. 3, with the exception of the thrust chamber and oxidizer control valve. Modifications were made to the thrust chamber and a substitute oxidizer control valve was incorporated to reduce the coolant surge encountered during the starting transients of previous tests.

The thrust chamber, S/N JP 88, was previously used in engine build No. 2. It was repaired, and two additional modifications were incorporated to increase the cooling margin in the chamber area and to reduce the contained volume in the tubes. These were: (1) installation of internal tube fins in the combustion chamber area, and (2) the insertion of filler rods in all nozzle tubes. Specific details are given in Section IV.

As previously mentioned, signs of possible injector impingement were noted on the thrust chamber walls after test No. E-3. To minimize any effects of oxidizer stream misdirection, twenty-five 0.010-in. diameter fuel holes were drilled near the outer circumference of the injector face in the suspect areas. In addition, all fuel annuli in the outer rows were electro-discharge-machined to increase the gaps in their outer semicircles from 0.015 to 0.020 in.

The satisfactory operation of all components during the initial part of test No. E-3 provided a representative base for predicting the effect of control variations on the engine starting transient. Data from that test verified that it was imperative to minimize the coolant surge resulting from rapid expansion of the methane contained in the chamber tubes at the initiation of rapid heat flux increase. Methods suggested to accomplish this were: (1) supply more heat to the coolant early in the acceleration period, and (2) reduce the rate of chamber pressure (heat flux) increase.

It was determined that both of these results could best be achieved with a scheduled gradual opening of the oxidizer control valve, rather than by delaying poppet action in the standard RL10 valve configuration. An oxidizer control valve previously modified for scheduled opening and used on a fluorine/hydrogen modified RL10A-3-3 engine (as discussed in Section VI) was available for use on build No. 4. This valve was designed to begin opening almost simultaneously with the opening of the oxidizer shutoff valve, providing an immediate source of heat. The valve ports were configured to provide a linear increase in oxidizer flowrate with pump discharge pressure rise. It was recognized that a high oxidizer pump discharge pressure would be required to seat the poppet if the existing spring were retained. However, cycle analysis indicated that sufficient pressure would be available to seat the valve at mixture ratios above approximately 4.5, and because a high spring rate was desirable to slow the chamber pressure starting ramp, it was decided to retain the existing spring. Based on extrapolations of data from test No. E-3, it was estimated that this valve characteristic would provide an almost linear increase in chamber pressure with time.

160

3. TEST DISCUSSION

a. Test No. E-4

With one exception, the starting sequence for this test was identical to that of test No. E-3, i.e., open thrust control to be manually actuated when the engine stabilized after the start transient. The change consisted of delaying the opening of the oxidizer inlet valve by 0.200 sec to obtain the fuel lead required to establish coolant flow into the jacket before the start of oxidizer flow through the scheduled control valve.

Engine behavior during the start transient is illustrated by the plot of important operating parameters presented in figure 88. The scheduled oxidizer control valve produced a relatively gradual rise in chamber pressure during the initial phase of the start, but the turbopump acceleration rate was greater than predicted and the chamber pressure increase became exponential rather than linear later in the transient. Some of the increased acceleration rate was attributed to the higher turbine inlet temperature maintained throughout the start transient as compared with test No. E-3. Turbine temperature histories for the two starts are compared in figure 89. The high temperature in test No. E-4 was the result of the increased residual heat provided by the greater mass of the cooling jacket (due to the filler inserts) and also by the scheduled oxidizer control valve which provided a higher oxidizer flow throughout the starting period. A fuel slowdown was noted at the point of maximum chamber pressure increase, but its magnitude was minor compared to that encountered in test No. E-3. This verified that a small jacket volume and an extended chamber pressure ramp were desirable to prevent chamber damage during the starting period.

The engine stabilized at the design chamber pressure of 250 psia for 1.5 seconds at a mixture ratio of 3.6, after which the turbopump slowly decelerated. The reduced speed resulted in an oxidizer pump discharge pressure too low to keep the spring-loaded oxidizer control valve in its full open position. (As discussed previously, it was predicted that the oxidizer control valve would not seat if the engine operated at a mixture ratio below 4.5.) As the valve closed from the full open position it created a higher flow restriction and, therefore, reduction in mixture ratio which further reduced speed. When the thrust control was activated at 5.5 seconds there was a temporary increase in rpm, but it was not sufficient to seat the oxidizer control valve and the system continued to decelerate. The test was manually terminated at 13.8 seconds.

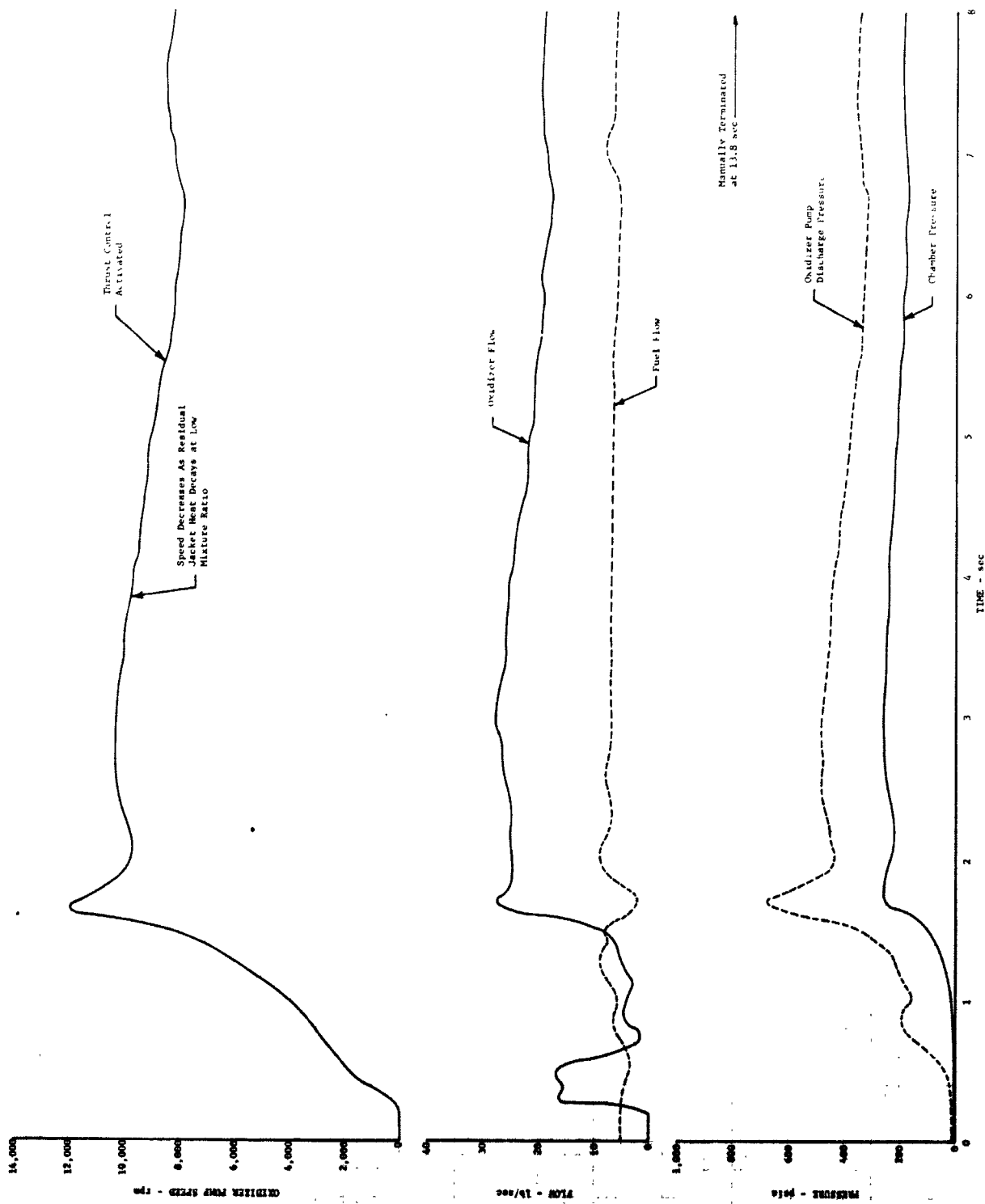There was no visible hardware damage following the test.

Figure 88. Starting Transient for Engine Test No. E-4
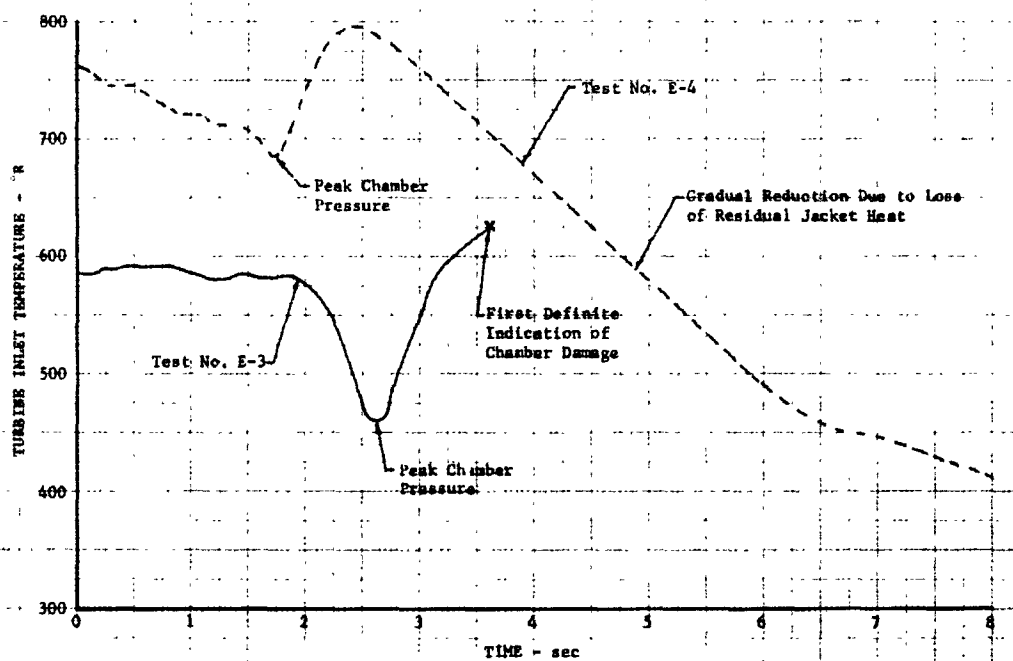
DF 68967

Figure 89. Effect of Engine Modifications on Starting Turbine Inlet Temperature

DF 68959

b. Test No. E-5

Preliminary control room analysis of the data from test No. E-4 indicated that the mixture ratio was lower than predicted because of delays in achieving complete opening of the oxidizer flow control valve. It was felt that if the thrust control bypass were sequenced closed at the correct time, turbopump speed could be maintained long enough for the oxidizer control valve to open fully, thereby permitting the engine to sustain operation at the desired chamber pressure. Therefore, prior to test No. E-5, three changes were made to ensure that the oxidizer control valve would be open before the turbopump experienced any significant speed reduction. The changes were: (1) the thrust control was sequenced into the system at the point of peak rpm, (2) the oxidizer control valve reference pressure cavity was connected to the altitude simulation system to decrease the back pressure, and (3) the oxidizer control valve setting was changed to increase the starting mixture ratio.

Start transient data for test No. E-5 are presented in figure 90. As was expected, no appreciable change in the initial part of the start transient was produced by the above mentioned changes. A comparison of figures 88

169

and 90 shows that the amount of turbopump deceleration following the initial starting overshoot was decreased, and the engine sustained the 250 psia chamber pressure level for a longer duration than in the previous test. The mixture ratio was still low and as the turbine inlet temperature approached its equilibrium value, the pump speed again decreased to a value too low to keep the oxidizer valve seated. As this occurred the chamber pressure decayed gradually and the test was manually terminated after 24.3 seconds.

No visual chamber or injector damage was found after this test; however, a detailed analysis of the data from this firing in combination with that from test No. E-4 indicated that the turbine flow area was greater than intended. For the reasons mentioned above, it was not possible to remove the engine from the test facility for inspection of the turbine, so it was necessary to proceed on the assumption that the turbine area had changed without establishing the mode of the failure. Ultimately, post-test inspection revealed that the change resulted from failure of welds made at the stator vane trailing edges where the vanes were deformed to reduce area.
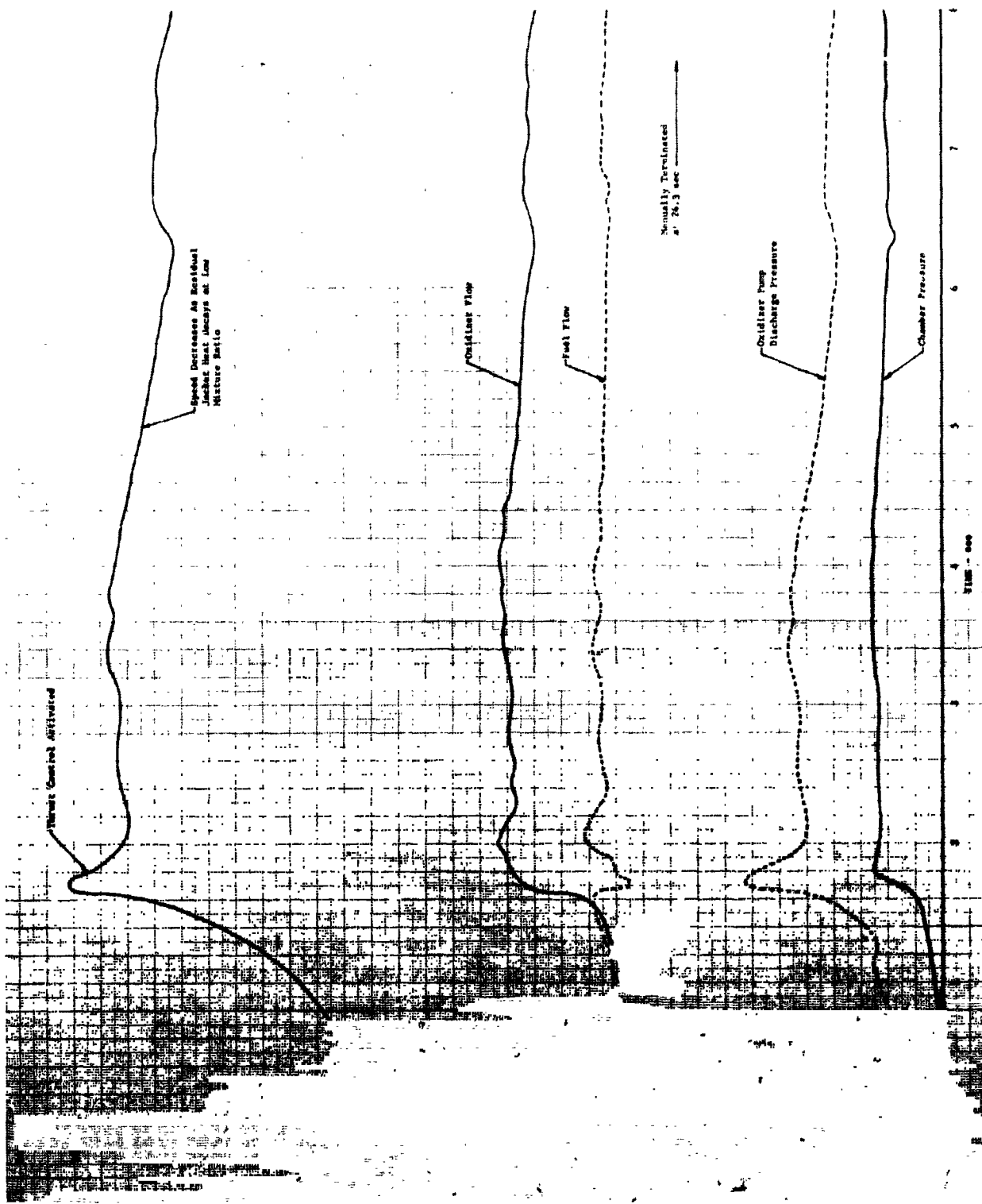
Figure 99. Starting Transient for Engine Test No. E-5

DF 6896A

c.   Tes' No. E-6

Because available funds did not permit removal of the engine from the test stand for turbine inspection, much less repair, it was necessary to devise another means of balancing the cycle to increase the mixture ratio and the turbopump speed. The method chosen was to increase the flow resistance in the fuel system. The most readily available way to accomplish this was to decrease the size of the fuel pump discharge orifice. In addition to providing a higher steady-state mixture ratio balance, a high flow restriction at this point has a stabilizing influence which was expected to reduce coolant slowdown.

Test No. E-6 was started with the same sequence used for the preceding test. The higher restriction at the fuel pump discharge resulted in a significant reduction in the turbopump acceleration rate, and, as shown in figure 91, the thrust control was sequenced into the system before the point of peak rpm was reached. When the thrust control was sequenced into the system, it sensed the low chamber pressure and closed the turbine bypass. The closed bypass coupled with the higher turbine inlet temperature (compared to tests No. E-1 and E-2, which were also started with an active thrust control) produced a speed overshoot before the thrust control could react. The resulting high fuel pump pressure caused a rupture of the first-stage fuel pump housing. At the time of rupture the 1st-stage discharge pressure was 900 psia, or above the 850 psia limit estimated from the calculated housing stress and the 0.2% yield strength of housing material at 200°R. Cycle power was reduced because of the housing failure and the test was automatically terminated at 4.0 seconds by a low chamber pressure stand safety system. Post-test inspection revealed a single crack emanating from the vicinity of the cutwater and extending in a circumferential direction approximately 180 degrees around the housing.

Some minor leaks in the chamber tubes, attributed to the reduction in coolant flow which occurred when the fuel pump ruptured, were detected after the test. These leaks were not visible and could only be located during pressure checks of the chamber. The pressure decay rate during these checks was very low, and calculations indicated that only about 1% of the fuel would bypass the turbine. This was not considered to be significant enough to affect engine operation, and testing was resumed after the fuel pump housing was replaced.
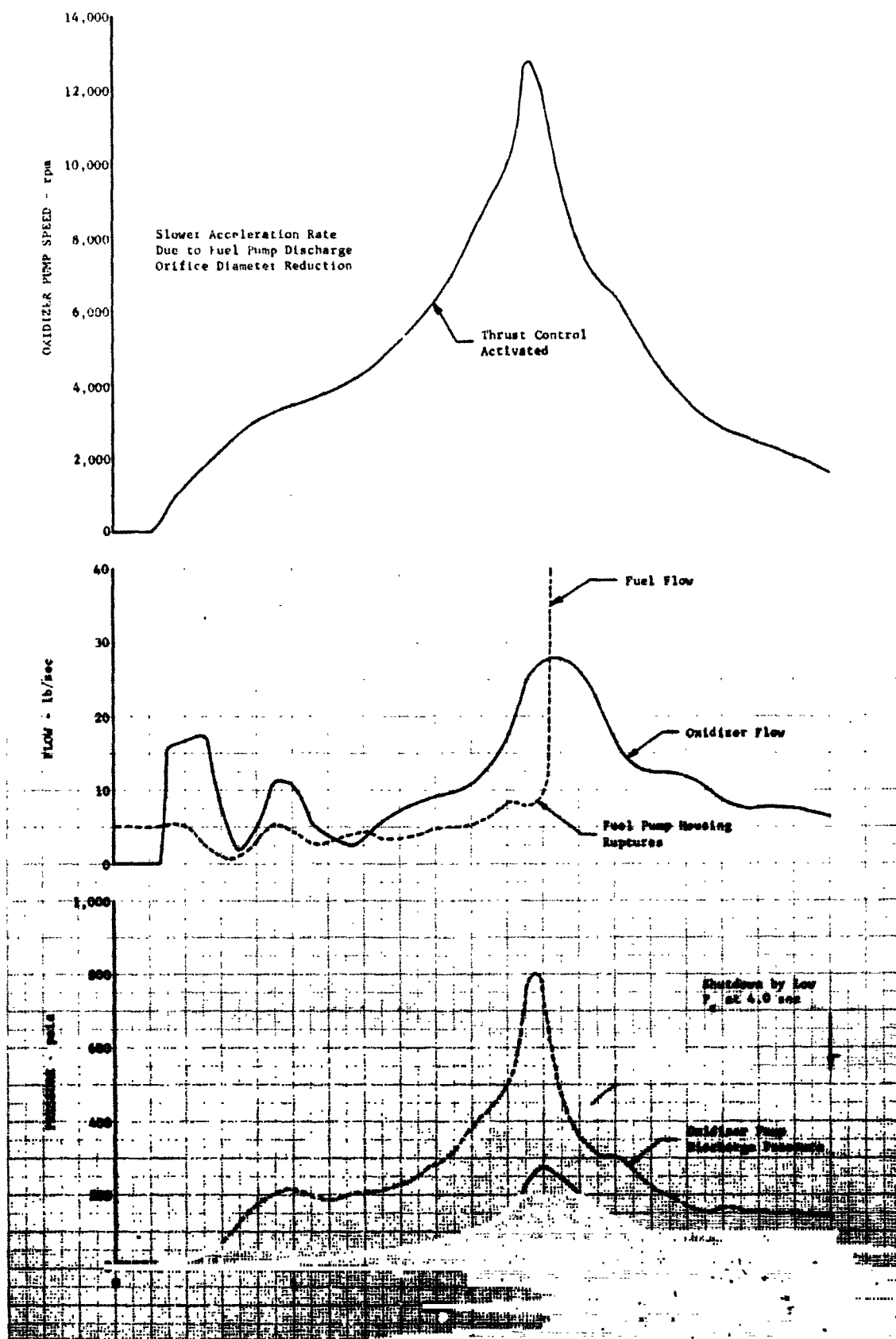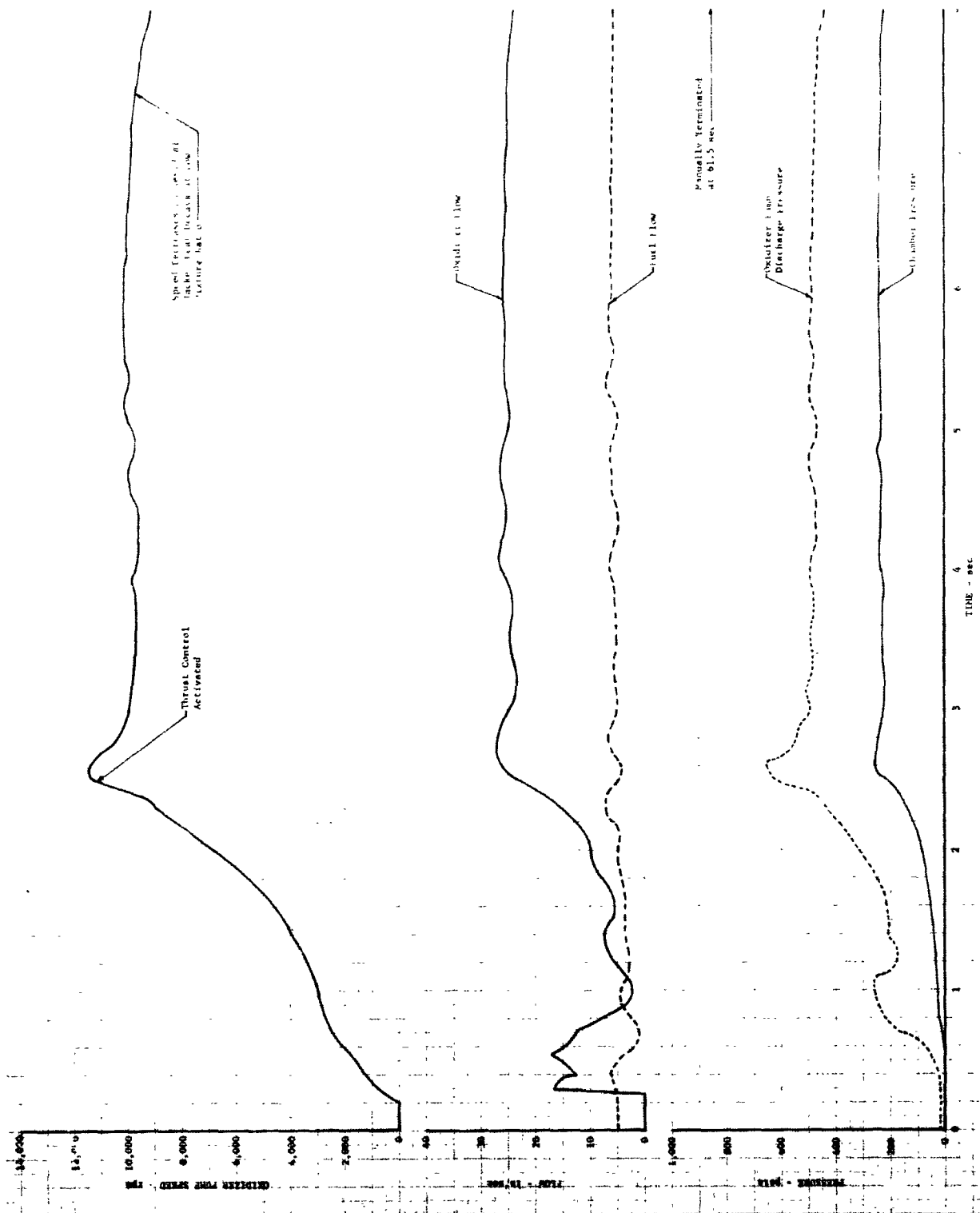
Figure 91. Starting Transient for Engine Test No. E-6

DF 68962

d. *Test No. E-7*

Analysis of the data from test No. E-6 showed that the reduced accelera-
tion rate resulting from the greater fuel pump discharge restriction delayed
the occurrence of peak rpm by approximately 0.7 second. For test No. E-7
the activation time of the thrust control was adjusted to compensate. This
reduced the amount of overshoot and eliminated the high fuel pump dis-
charge pressure experienced on the previous test. As shown in figure 92, the
engine stabilized at a chamber pressure of 235 psia, r=4.3, for approximately
5 seconds. This low mixture ratio again caused a decrease in rpm as turbine
inlet temperature decreased. The chamber pressure slowly decreased to
approximately 200 psia and stabilized at that point. The test was terminated
after 61.5 seconds.

Post-test inspection of the engine revealed that the chamber tube
leakage had increased to a point where approximately 15% of the fuel was
being injected through the damaged areas. Most of the damage was in the
form of pinhole leaks just upstream of the throat at a point near the end
of the chamber fins. A few additional pinhole leaks were noted in the
chamber region approximately 2 to 6 in. from the injector. The amount of
leakage represented a flow area of less than 0.1 in².

Because the thrust chamber leakage represented an area approximately
equal to the thrust control bypass area, calculations indicated that the cycle
would still have adequate power, and testing was continued.

Figure 92. Starting Transient for Engine Test No. E-7

DF 68966

169

e. *Test No. E-8*

To compensate for thrust chamber tube leakage the thrust control was maintained closed throughout the acceleration transient of test No. E-8. Also, in order to increase the mixture ratio with the reduced power available, it was necessary to reduce the flow resistance in the oxidizer system. This was accomplished by installing a bypass line around the oxidizer control valve; the line was sized to pass approximately 25% of the oxidizer flow.

During the starting transient the thrust control lead-lag system reacted to limit overshoot and opened the turbine bypass. When this occurred, the oxidizer control valve became unseated, producing an additional reduction in chamber pressure. The thrust control then reacted to increase the chamber pressure and the oxidizer control valve reseated. As shown in figure 93, the couple set up between these two valves resulted in a 1 Hz cycling of the engine between 200 and 250 psia chamber pressure. Experience in previous tests with this engine had shown that the cycle could not ordinarily recover after the oxidizer control valve became unseated, but in this instance the oxidizer bypass provided the extra power required for reacceleration. The upset to the system produced by the cycling resulted in an average mixture ratio above 6, with a corresponding turbine inlet temperature slightly above 1000°R. The test was automatically terminated at 5.0 seconds by the high turbine temperature abort system. No additional hardware deterioration was noted after the test.
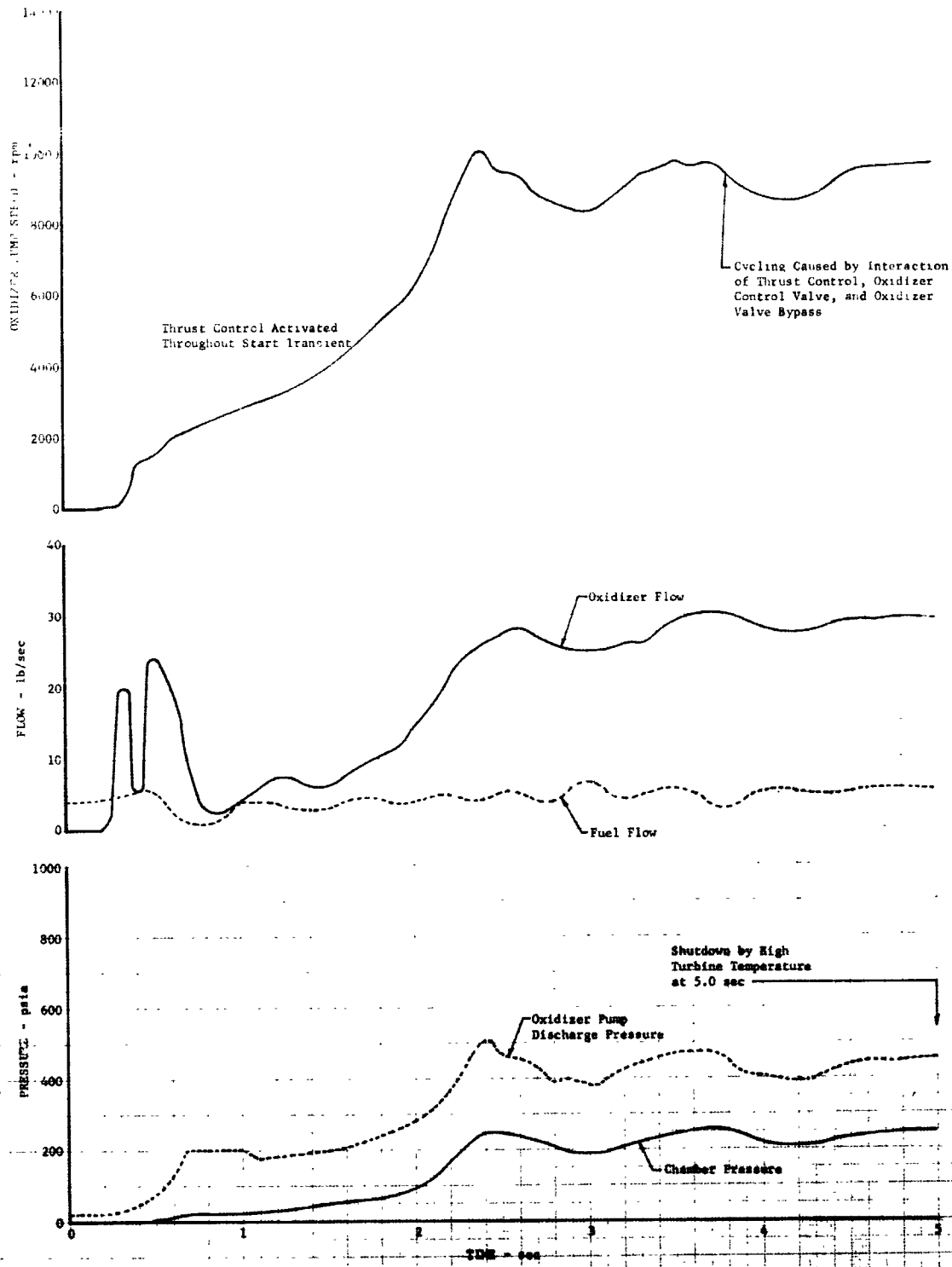
Figure 93. Starting Transient for Engine Test No. E-8

DF 68965

f. Test No. E-9

At the completion of test No. E-8, the planned program effort was essentially complete and the supplies o prepared propellants were nearly exhausted, but it was decided to attempt one final test to obtain as much data as possible with the hardware.

In order to avoid control instability, test No. E-9 was made with the thrust control reference bellows vented so that the turbine bypass would remain closed throughout the test. No overspeed problem was anticipated because of the power reduction caused by leakage through the damaged thrust char ⁱⁱ r tubes. The opening of the oxidizer inlet control valve was delayed a⸱ ⸱ᵛuₜ¹ᵒnal 0.2 second (total 0.4 second) to ensure that coolant flow through the damaged tubes was stabilized before oxidizer flow was initiated.

Figure 94 shows that the engine stabilized at a chamber pressure of approximately 230 psia, r=5.3, for approximately 3 seconds. At that time (5 seconds into the test), the oxidizer pump head rise dropped and the chamber pressure immediately decreased to approximately 200 psia without a decrease in pump rpm, indicating ingestion of pressurant gas from the nearly empty oxidizer tank. The chamber pressure remained at the 200 psia level and at 11.6 seconds the test was terminated by the engineer in charge.

E. REFERENCES

D-1. "Investigation of Light Hydrocarbon Fuels With Fluorine-Oxygen Mixture as Liquid Rocket Propellants — Final Report," Pratt & Whitney Aircraft FR-2872, NASA CR-72425, Contract NAS3-10294, 28 June 1968.
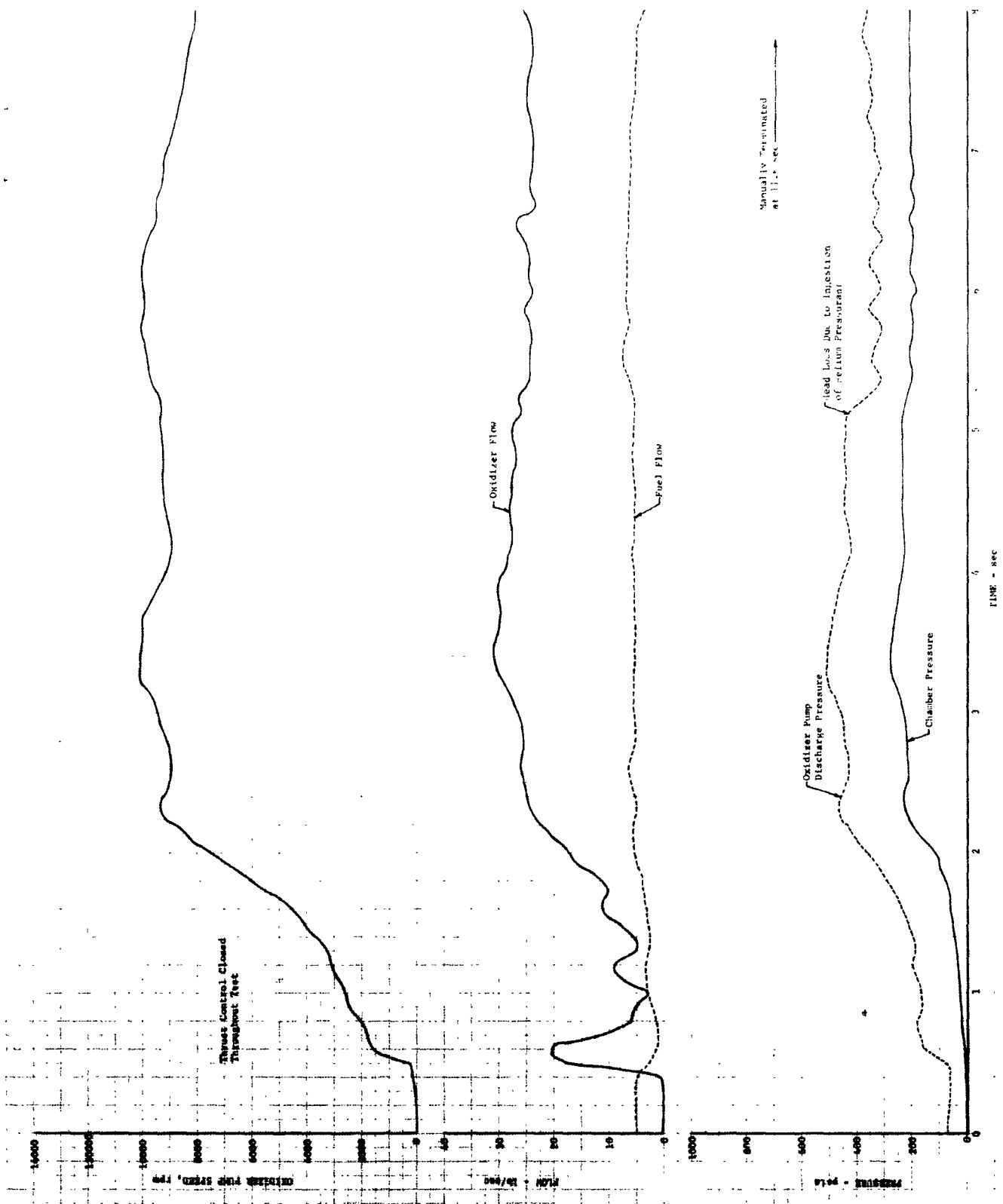
Figure 94. Starting Transient for Engine Test No. E-9

DF 68968

179

APPENDIX E

REFERENCES

1. "Investigation of Light Hydrocarbon Fuels With Flox Mixtures as Liquid Rocket Propellants — Final Report," Pratt & Whitney Aircraft FR-1443, NASA CR-54445, Contract NAS3-4195, 1 September 1965.

2. "Investigation of Light Hydrocarbon Fuels With Fluorine-Oxygen Mixture as Liquid Rocket Propellants — Final Report," Pratt & Whitney Aircraft FR-2227, NASA CR-72147, Contract NAS3-6296, 15 September 1967.

3. "Investigation of Light Hydrocarbon Fuels With Fluorine-Oxygen Mixture as Liquid Rocket Propellants — Final Report," Pratt & Whitney Aircraft FR-2872, NASA CR-72425, Contract NAS3-10294, 28 June 1968.

4. "Research on A Hydrogen-Fluorine Propulsion System — Final Report," Pratt & Whitney Aircraft FR-1585, NASA CR-72074, Contract NASw-754, 21 October 1966. CONFIDENTIAL (Title Unclassified).

5. Kinetic Flow Performance in Nozzles — Monthly Progress Report No. 5," United Aircraft Research Laboratories Report G-910666-5, Contract NAS3-11225, 24 October 1968.

6. Masters, A.I., "Idealized Models for Prediction and Correlation of Rocket Efficiencies," Pratt & Whitney Aircraft PDS-2364, 10 April 1967. CONFIDENTIAL (Title Unclassified).

7. Glickstein, M.R. and J.E. Jackson, "Two Dimensional Heat Flux Measurements in Uncooled Rocket Nozzles," *Bulletin of the 6th Liquid Propulsion Symposium*, Volume II, CPIA, 1964.

8. Bartz, D.R., "A Simple Equation for Rapid Estimation of Rocket Nozzle Convective Heat Transfer Coefficients," *Jet Propulsion*, January 1957.

9. "Design Report for RL10A-3 Rocket Engine," Pratt & Whitney Aircraft FR-324C, Contract NAS8-5626, 31 January 1964.

10. "Hydrogen-Fluorine Engine Evaluation — Final Report," Pratt & Whitney Aircraft FR-3030, NASA CR-72481, to be published.

APPENDIX F

NOMENCLATURE

Symbol	Description	Units
C_{Fvac}	Thrust coefficient at $P_a = 0$	—
C_s	Theoretical stream thrust coefficient (predicted aerodynamic efficiency accounting for friction and divergence losses)	—
c^*	Characteristic exhaust velocity	ft/sec
F_{vac}	Thrust at $P_a = 0$	lb_f
h	Film coefficient	Btu/in²-sec-°R
I_{vac}	Specific impulse at $P_a = 0$	$\dfrac{lb_f\text{-sec}}{lb_m}$
NPSH	Pump net positive suction head	ft
P_a	Ambient pressure	psia
P_c	Chamber pressure	psia
r	Mixture ratio (oxidizer-to-fuel) by weight	—
$\dot{w}$	Flowrate	lb_m/sec
Δ_h	Specific enthalpy rise	Btu/lb_m
ϵ_e	Nozzle exit-to-throat area ratio	—
η	Efficiency	%

Subscripts:

Bartz	Film coefficient calculated by Bartz closed form
c	Coolant
exp	Experimental value
(F)	Based on thrust
f	Fuel
o	Oxidizer
(P_c)	Based on chamber pressure
theo	Theoretical value